Dissertation

submitted to the

Combined Faculty of Natural Sciences and Mathematics

of the Ruperto Carola University Heidelberg, Germany

for the degree of

Doctor of Natural Sciences

Presented by

M.Sc. Christian Litke

born in Bad Soden, Germany

Oral examination: 15.12.2020

Role of epigenetic mechanisms in structural and functional plasticity in the CNS: focus on spinal sensitization

Referees: Jun.-Prof. Dr. Daniela Mauceri

Prof. Dr. Hilmar Bading

Prof. Dr. Stephan Frings

Dr. Radhika Puttagunta

Abstract

Neurons have a highly specialized morphology whose signal-regulated remodeling is key to their function in neuronal networks. Activity-dependent nuclear calcium signaling is a crucial regulator of gene transcription in hippocampal and spinal cord neurons and mediates gene expression by directly acting on transcription factors or by regulating epigenetic processes, such as the induction of DNA methyltransferases (DNMTs) or the nucleo-cytoplasmic shuttling of class IIa histone deacetylases (HDAC4, -5, -7, and -9). Epigenetic mechanisms regulate several neuroadaptive phenomena in hippocampal neurons including, among others, synaptic plasticity and memory formation. In the first part of this thesis we describe how the subcellular localization of HDAC4 controls the morphology of hippocampal neurons by modulating the expression of a factor critical for dendrite architecture.

Epigenetic regulators have also been suggested to mediate central sensitization in spinal cord neurons and the development of chronic pain. The transition from acute to chronic pain is considered a pathological manifestation of neuronal plasticity in nociceptive pathways and shares common molecular pathways with memory formation. However, if and how epigenetic gene regulatory events control also structural remodeling of spinal cord circuits, relevant for central sensitization, remains to be investigated. Here we characterized the impact of synaptic activity and chronic inflammatory pain on the expression and activity of DNMTs and HDACs in spinal cord neurons and found that the de novo methyltransferase Dnmt3a2 and HDAC4 were particularly affected. We demonstrate that activity-induced levels of Dnmt3a2 contribute to spinal sensitization and hypersensitivity in the CFA model of inflammatory pain by regulating the expression of pain- and plasticity-related genes. Moreover, we found that long-lasting, but not acute inflammatory pain, results in a nuclear export of HDAC4 in spinal cord neurons, which is accompanied by increased levels of histone 3 acetylation. Using recombinant adeno-associated virus-mediated expression of a nuclear localized dominant active mutant of HDAC4 in dorsal horn neurons, we demonstrated that nuclear HDAC4 blunts the development of mechanical hypersensitivity without affecting acute nociception. Next generation RNA-sequencing analysis produced a list of HDAC4-regulated candidate genes in the context of chronic inflammatory pain. The identified candidates include both well-known and novel mediators of chronic pain development and have been functionally tested *in vivo* with

gain of function and loss of function experiments. Our results identify HDAC4 and its target genes, as key epigenetic regulators of central sensitization in chronic inflammatory pain and as possible targets for pain therapies.

Zusammenfassung

Nervenzellen verfügen über eine hochspezialisierte Morphologie, deren signalregulierte Umstrukturierung entscheidend zu ihrer Funktion in neuronalen Netzwerken beiträgt. Aktivitätsabhängige nukleare Kalziumsignale regulieren die Gentranskription in Nervenzellen des Hippocampus, sowie des Rückenmarks, durch direkte Einwirkung auf Transkriptionsfaktoren oder durch die Steuerung epigenetischer Prozesse, wie der Induktion von DNA-Methyltransferasen (DNMTs) oder dem nukleo-zytoplasmatischen Transport von Histondeacetylasen der Klasse IIa (HDAC4, -5, -7 und -9). Epigenetische Mechanismen regulieren verschiedene neuroadaptive Phänomene in Nervenzellen des Hippocampus und spielen unter anderem eine entscheidende Rolle für die synaptische Plastizität und Gedächtnisbildung. Im ersten Teil dieser Arbeit beschreiben wir, wie die subzelluläre Lokalisation von HDAC4 die Morphologie von Nervenzellen des Hippocampus moduliert, indem sie die Expression eines für die Dendritenstruktur kritischen Faktors steuert.

Bisherige Untersuchungen legen nahe, dass epigenetische Prozesse ebenfalls zur zentralen Sensibilisierung von Rückenmarksneuronen und der Entwicklung chronischer Schmerzen beitragen. Der Übergang von akutem zu chronischem Schmerz beruht auf pathologischen Veränderungen neuronaler Plastizität in nozizeptiven Bahnen und unterliegt dabei zum Teil denselben molekularen Mechanismen, welche bei der Gedächtnisbildung eine Rolle spielen. Ob und wie genregulatorische epigenetische Ereignisse den für die zentrale Sensibilisierung relevanten strukturellen Umbau von Rückenmarkschaltkreisen steuern, muss jedoch noch untersucht werden. Wir haben den Einfluss synaptischer Aktivität, sowie chronisch entzündlicher Schmerzen auf die Expression und Aktivität von DNMTs und HDACs in Rückenmarksneuronen charakterisiert und festgestellt, dass die De-novo-Methyltransferase Dnmt3a2, sowie HDAC4 besonders betroffen sind. Wir zeigen, dass die aktivitätsinduzierte Expression von Dnmt3a2 zur zentralen Sensibilisierung und Überempfindlichkeit von Mäusen im entzündlichen Schmerzmodell beiträgt, indem sie die Transkription bestimmter Schmerz- und Plastizitäts-relevanter Gene beeinflusst. Darüber hinaus fanden wir heraus, dass langanhaltende, jedoch nicht akute entzündliche Schmerzen zu einem nuklearen Export von HDAC4 in Neuronen des Rückenmarks führen, was mit einer erhöhten Acetylierung der Histone einhergeht. Mit Hilfe einer stets nuklear lokalisierten aktiven Mutante von HDAC4, welche durch

rekombinante Adeno-assoziierten Viren in Hinterhornneuronen des Rückenmarks exprimiert wurde, konnten wir zeigen, dass nukleares HDAC4 die Entwicklung einer Sensibilisierung auf mechanische Reize im Schmerzmodell abmildert, ohne dabei die akute Schmerzwahrnehmung zu beeinträchtigen. Eine RNA-Sequenzierung ergab eine Liste HDAC4-regulierter Gene, die im Zusammenhang mit der Entstehung chronisch entzündlicher Schmerzen stehen. Die identifizierten Kandidatengene umfassen sowohl bekannte als auch neuartige Mediatoren der chronischen Schmerzentwicklung und wurden funktionell *in vivo* getestet. Unsere Untersuchungen identifizieren HDAC4 und dessen Zielgene als wichtige epigenetische Regulatoren der zentralen Sensibilisierung bei chronisch-entzündlichen Schmerzen und als mögliche Ziele für künftige Schmerztherapien.

Acknowledgements

I would like to express my deep gratitude to everyone who supported me during my doctoral thesis.

First, I want to thank Daniela Mauceri, my supervisor, mentor and friend who guided me throughout these exciting and challenging years of my life in the best possible way I can imagine. I highly appreciate the trust you put into me and thank you for accepting me as doctoral student in your lab. You constantly supported me ever since we met during my bachelor studies and taught me not only neuroscience but also helped me to develop my career and to grow as a person. Thank you also for creating an appreciative, warm and motivating atmosphere in our lab. I will surely miss our scientific discussions, Betriebsausflüge, Christmas market visits, or chitchat about the latest series on Netflix.

I also would like to thank Hilmar Bading for welcoming me aboard the Neuroscience Department and for his valuable scientific input and feedback throughout the years. Thank you for being member of my TAC and examiner of this thesis.

Thanks to Rohini Kuner for organizing a great SFB with lots of scientific events, giving me the opportunity to be part of a wonderful scientific community. It was an honor to have you in my TAC.

I would also like to thank Radhika Puttagunta and Stephan Frings for gladly accepting to be examiners of this thesis. It would not have been possible without your support.

A million thanks to Anna Hertle for her priceless contribution to this work and for teaching me microsurgical techniques or how to prepare spinal cord cultures. Thank you for your great support with the *in vivo* work and TVAs. Your positive attitude has always been a motivation.

Big thank you to Ana Oliveira for joining forces on the Dnmt-project; your great expertise and for always helping me out with numerous aliquots and good ideas.

I would like to thank Manuela Simonetti and Anke Tappe-Theodor for their constant valuable support and readiness to teach me important techniques for the *in vivo* work of this study and for providing helpful feedback on generated data.

I also thank Daria Bunina for her kind help with the analysis of generated RNAseq data.

Special thanks to Iris Bünzli-Ehret for providing countless hippocampal cultures over the years, as well as to Monika Schwab and Oliver Teubner for being the heart and soul of the lab and for their reliable technical support whenever needed.

Thanks to all my colleagues in the lab, past and present, who became my friends over the years. I am grateful for all the good times we had together in the lab, during lunch, coffee break, movie events, Pausenexpress, IZN retreats etc.

Thanks to my “pain buddy” Sara Ben Ayed who accompanied me almost throughout the entire time and through countless hours of surgeries in the IBF.
I am especially thankful to the members of our small group: Bahar Aksan, Annabelle Schlüter and Alexandra Merkel. It was a pleasure working with you. Thanks for your help and creating a joyful atmosphere. Our lab freezer is a silent witness of all the fun and good times we had together as a team.
Special thanks to Ann-Kristin Kenkel. I am honored to have supervised you and appreciate your valuable contribution to this work. I also thank all the other lab rotation and visiting students who joined our lab over the years.
Finally, I express my deepest gratitude to my parents and brother. Danke für Eure bedingungslose Unterstützung und Liebe. Dafür, dass Ihr immer an mich geglaubt habt und für den Stolz, den Ihr mir entgegenbringt. Ihr habt mir alles was ich brauchte, um dies zu erreichen mit auf den Weg gegeben. Danke für das großartige Leben, welches Ihr mir ermöglicht habt und für unsere schöne gemeinsame Zeit als Familie. Dieser Dank gilt selbstverständlich allen Familienmitgliedern und Freunden, welche mich immer auf meinem Werdegang unterstützt haben und fest an mich glauben.
Höchster Dank und Liebe geht an meine wundervolle Frau, die immer an meiner Seite steht und mit der ich mich gemeinsam über Erfolge freuen kann. Du gibst mir den nötigen Halt in den stressigsten und schwierigsten Situationen. Danke dafür. Ich liebe dich.

Table of contents

Abbreviations

ABC	ATP-binding cassette
AMPA	α-amino-3-hydroxy-5-methyl-4-isoxazolepropionic acid
ANOVA	analysis of variance
Ara-C	cytosine β-D-arabinofuranoside
ASIC	acid-sensing ion channel
ATP	adenosine triphosphate
BDNF	brain-derived neurotrophic factor
Bic	bicuculline
bp	base pair
BSA	bovine serum albumin
BSCB	blood-spinal cord-barrier
CaBP	calcium binding protein
CaM	calmodulin
CAMK	calcium/calmodulin-dependent protein kinase
CBP	CREB-binding protein
CeA	central amygdala
CFA	Complete Freund's Adjuvant
CGRP	calcitonin-gene related peptide
ChIP	chromatin immunoprecipitation
CoREST	co-repressor of repressor element-1 silencing transcription factor
Cox	cyclooxygenase
CREB	cAMP-responsive element-binding protein
CSF	cerebrospinal fluid
CtBP	C-terminal binding protein
DEG	differentially expressed gene
DIV	days *in vitro*
DM	dissociation medium
DNMT	DNA methyltransferase
DREAM	downstream regulatory element antagonist modulator
DRG	dorsal root ganglion
DTT	dithiothreitol
EAAT	excitatory amino acid transporter

ECL	enhanced chemiluminescence
eNMDAR	extrasynaptic N-methyl-D-aspartate receptor
EPSC	excitatory postsynaptic current
EPSP	excitatory postsynaptic potential
ERG	early response gene
EtOH	ethanol
FC	fold change
FDR	false discovery rate
FIGF	c-fos-induced growth factor
FIGF	fos-induced growth factor
GABA	gamma aminobutyric acid
GDB	gelatin buffer
GFP	green fluorescent protein
GM	growth medium
HAT	histone acetyl transferase
HDAC	histone deacetylase
HP1	heterochromatin protein 1
hrGFP	humanized Renilla reniformis GFP
HRP	horseradish peroxidase
HIAA	hydroxyindol acetate
i.p.	intraperitoneal
i.t.	intrathecal
IB4	isolectin B4
IBF	Interfakultäre Biomedizinische Forschungseinrichtung
ICC	immunocytochemistry
IEG	immediate early gene
IHC	immunohistochemistry
IL	interleukin
IZN	Interdisciplinary Center for Neurosciences
KYNA	kynurenic acid
Ky/Mg	kynurenic acid/MgCl2 solution
LTM	long-term memory
MAPK	mitogen activated protein kinase

MBP	methyl-CpG-binding protein
MeCP2	methyl-CpG-binding protein 2
MEF2	myocyte enhancer factor 2
MK801	dizocilpine
mRNA	messenger RNA
MRP4	multidrug resistance-associated protein 4
NAc	nucleus accumbens
NCoR	nuclear hormone receptor co-repressor
NES	nuclear export signal
NGF	nerve growth factor
NMDA	N-methyl-D-aspartate
NRM	nucleus raphe magnus
NRP	neuropilin
NSAID	non-steroidal anti-inflammatory drug
o/n	overnight
PAG	periaqueductal gray
PAGE	polyacrylamide gel electrophoresis
PBS	phosphate-buffered saline
PBST	PBS-Tween 20
PCR	polymerase chain reaction
PFA	paraformaldehyde
PIGF	placental growth factor
PKC	protein kinase C
QRT-PCR	quantitative reverse transcriptase PCR
rAAV	recombinant adeno-associated virus
RIPA	radioimmunoprecipitation assay
RNAi	RNA interference
ROS	reactive oxygen species
RT	room temperature
RTK	receptor tyrosine kinase
RVM	rostral ventral medulla
s.c.	subcutaneous
SBB	Sudan Black B

SCI	spinal cord injury
SDS	sodium dodecyl sulfate
SGG	salt-glucose-glycine solution
shRNA	short hairpin RNA
SIRT	sirtuin
SMRT	silencing mediator of retinoic acid and thyroid hormone receptor
TBOA	DL-threo-β-benzyloxyaspartate
TF	transcription factor
TM	transfection medium
TNF-a	tumor necrosis factor a
TrkA	tropomyosin receptor kinase A
TRP	transient receptor potential channel
TRPV1R	transient receptor potential vanilloid 1 receptor
TSS	transcription start site
TTX	tetrodotoxin
v/v	volume per volume
VEGF	vascular endothelial growth factor
VEGFR	vascular endothelial growth factor receptor
VGCC-L	L-type voltage-gated calcium channels
WDR	wide dynamic range neuron
wt	wildtype
XA	xanthurenic acid

List of Figures

List of Tables

1 Introduction

1.1 Neuronal activity and nuclear calcium-dependent adaptive processes

Neurons constantly undergo activity-dependent structural and functional changes in response to external and internal stimuli, allowing complex organisms to adjust to their environment. Neuronal plasticity relies on various inter- and intracellular signal transduction mechanisms, mediating short- or long-lasting adaptations. Long-term changes in synaptic plasticity and cellular morphology, affecting network connectivity, require regulation of gene transcription (McClung and Nestler, 2008, Yap and Greenberg, 2018)

1.1.1 Nuclear calcium signaling

A key regulator of gene transcription in neurons is nuclear calcium. Calcium can mediate the communication between synapses and the nucleus and is required for complex neuroadaptations, like neuronal survival, memory formation, addiction or the development of chronic pain (Bading, 2000, Bading, 2013, Zhang et al., 2009). Calcium ions enter the cytosol via different routes and reach the cell nucleus through nuclear pore complexes, triggering activation of transcription-regulating signaling pathways (Bading, 2013, Hardingham et al., 1997, Eder and Bading, 2007). The principle pathway for calcium entry is initiated by glutamatergic excitatory synaptic stimulation, of N-methyl-D-aspartate (NMDA), α-amino-3-hydroxy-5-methyl-4-isoxazolepropionic acid (AMPA) and kainate receptors (Bading, 2013). The resulting excitatory postsynaptic potential (EPSP) and membrane depolarization releases the magnesium block of synaptic NMDA receptors (NMDARs) and opens L-type voltage-gated calcium channels (VGCC-L), located in the somatic and perisomatic membrane, allowing calcium influx (Bading et al., 1995, Stuart and Sakmann, 1994, Westenbroek et al., 1990).

Upon calcium entry several signaling cascades in the cytoplasm and nucleus are initiated, mediating both transcriptional regulation of specific target genes and more widespread gene regulatory events (Bading, 2013).

The principal target of nuclear calcium signaling is the transcription factor (TF) cAMP-responsive element-binding protein (CREB), which mediates the transcription of many genes (Hardingham et al., 2001, Hardingham et al., 1997). Upon nuclear calcium entry, CREB is activated by phosphorylation at its serine residue 133 via calcium/calmodulin-dependent protein kinase IV (CaMKIV), a serine/threonine kinase (Chow et al., 2005, Soderling, 1999), allowing recruitment of its co-activator CREB-binding protein (CBP) to specific promoters (Chawla et al., 1998, Hardingham et al., 1999). CBP also depends on phosphorylation regulated by nuclear calcium and CaMKIV (Impey et al., 2002). CREB-CBP interaction induces transcription of a number of immediate early genes (IEGs) that often act as TFs themselves, regulating a variety of secondary response genes (Hardingham et al., 1997, Zhang et al., 2009). Other transcriptional regulatory mechanisms mediated by nuclear calcium include the inactivation of the transcriptional repressor DREAM (downstream regulatory element antagonist modulator) (Carrion et al., 1999, Mellström and Naranjo, 2001), or the nuclear export of the cell death-promoting forkhead transcription factor FOXO3A (Burgering and Kops, 2002).

Nuclear calcium also regulates gene transcription on a more global level via several pathways, involving epigenetic mechanisms. CREB and other TFs like c-Jun recruit CBP to the DNA (Cruzalegui et al., 1999, Goldman et al., 1997), where it stimulates a loosening of the chromatin structure through its intrinsic histone acetylation HAT activity, promoting RNA polymerase II-mediated gene transcription (Orphanides and Reinberg, 2000, Vo and Goodman, 2001). Via calcium/calmodulin-dependent protein kinase II (CaMKII)–mediated signaling, nuclear calcium acts on methyl-CpG-binding protein 2 (MeCP2), a transcription factor with a known role in chromatin remodeling and neuronal network formation (Cohen et al., 2011, Skene et al., 2010). Other nuclear calcium dependent epigenetic processes that provide an additional level of transcriptional control are the induction of DNA methyltransferases (Oliveira et al., 2012) and the nucleo-cytoplasmic shuttling of class IIa HDACs (Chawla et al., 2003, Schlumm et al., 2013). Both epigenetic mechanisms stand in the focus of this thesis and will be covered in more detail.

In sum, nuclear calcium is a very potent and versatile regulator of gene transcription in neurons that mediates a number of functional neuroadaptations, including acquired neuroprotection (Papadia et al., 2005, Zhang et al., 2009), memory formation and consolidation (Kang et al., 2001, Limback-Stokin et al., 2004, Weislogel et al., 2013), as well as central sensitization during the development of chronic pain (Simonetti et al., 2013). All these functional adaptations have in common that they rely on structural plasticity and changes in neuronal morphology.

1.1.2 Neuronal morphology and VEGFD

The morphology of a neuron is constituted by the complex geometry of its dendritic tree and defines the cells ability to receive and integrate incoming neuronal signals, which in turn determines the output (Cline and Haas, 2008, Jan and Jan, 2003). The cell type-specific morphology of dendrites is already determined during development by intrinsic genetic programs and intra-cellular mechanisms (Corty et al., 2009, Goldberg, 2004). However, the geometry of the dendritic arbor is constantly shaped by electrical neuronal activity (Chen and Ghosh, 2005, Zhang and Poo, 2001). Adaptations in length and branching of the dendritic arbor impact the performance of a single nerve cell but also alter the proficiency of the entire neuronal network, finally impacting complex cognitive abilities of the organism and changing its behavior. This concept is underpinned by mathematical network modelling (Häusser et al., 2000, Segev and London, 2000) and gets further supported by morphological studies of the brain, linking neurological diseases associated with mental retardation, like Rett syndrome, (Kaufmann and Moser, 2000) or neurodegenerative diseases, like Alzheimer's disease (Dickstein et al., 2007), to a simplification of dendritic architecture. Several molecular pathways, including nuclear calcium-dependent CaMKIV signaling (Chow et al., 2005), have been associated with the regulation of dendritic architecture and remodeling of spines (Marie et al., 2005, Redmond et al., 2002). In hippocampal neurons, it has been shown that expression of the calmodulin binding-peptide CaMBP4 (Wang et al., 1995), blocking nuclear calcium signaling by inactivating the nuclear calcium/CaM complex (Zhang et al., 2007, Papadia et al., 2005), has severe effects on the length and complexity of the dendritic arbor, by interfering with the transcription of CBP-dependent genes (Mauceri et al., 2011).

This effect could also be observed after overexpression of CaMKIVK75E, a catalytically inactive mutant of CaMKIV (Anderson et al., 1997, Mauceri et al., 2011).

Further investigations revealed vascular endothelial growth factor D (VEGFD) as the key nuclear calcium-dependent mediator of the observed structural changes (Mauceri et al., 2011, Mauceri et al., 2015, Zhang et al., 2009). VEGFD, also termed *c-fos*-induced growth factor (FIGF), is a secreted protein and has been originally described as an inducer of mitogenesis in the fibroblasts of mice (Orlandini et al., 1996). It belongs to the VEGF-family, including VEGF (also known as VEGFA), placental growth factor (PIGF), VEGFB, VEGFC, VEGFD, and VEGFE, all of which share a common, conserved VEGF homology domain (VHD) (McDonald and Hendrickson, 1993, Stacker and Achen, 2018) (Figure 1). VEGFD and its family members are known for their regulatory role in angiogenesis and lymphangiogenesis, the sprouting of new capillaries and lymphatic vessels, during development and in healthy tissue (Lohela et al., 2009).

VEGFD has also been implicated in the pathogenesis of several human diseases, including cancer, where it can enhance the formation of tumor lymphatics, by supporting the growth of tumors and metastasis formation (Stacker et al., 2001), as well as in pulmonary- and cardiovascular diseases, ocular indications, lymphedema, inflammation and obesity (Stacker and Achen, 2018). VEGFD, and its closest homologue VEGFC (Stacker et al., 1999), are expressed in a range of tissues during development and in the adult organism, including the heart, lungs, and liver (Avantaggiato et al., 1998, Kukk et al., 1996), showing an enrichment in endothelial cells (Stacker 2018). However, recent studies found VEGFD also in the nervous system, including hippocampus and cortex, with expression levels sometimes even higher in neurons than in endothelial cells (Lein et al., 2007, Mauceri et al., 2011, Uhlén et al., 2015, Saunders et al., 2018a, Zeisel et al., 2018). Moreover, VEGF and VEGFC have known functions in neurogenesis (Cao et al., 2004, Le Bras et al., 2006). As secreted factors, VEGFs act by binding as ligand to specific receptors. Vascular endothelial growth factor receptors (VEGFR) are a family of membrane bound RTKs, that undergo dimerization and autophosphorylation at their intracellular tyrosine residues upon ligand binding, thereby initiating signaling cascades via certain kinases, including MAPKs (Lee et al., 1996). All identified VEGFRs, including VEGFR-1 (Flt-1), VEGFR-2 (KDR or Flk-1), VEGFR-3 (Flt-4), and their co-receptors

neuropilin (NRP)-1 and 2 (Ferrara et al., 2003), are broadly expressed in endothelial cells but are also found in neurons (Le Bras et al., 2006). In humans, VEGFD and VEGFC both signal via VEGFR-2 and -3, whereas murine VEGFD can only activate VEGFR-3 (Baldwin et al., 2001). VEGFR-2 additionally interacts with VEGF, VEGFB and VEGFE. VEGFR-1 instead, binds VEGF, VEGFB, and PIGF (Takahashi and Shibuya, 2005) (Figure 1).

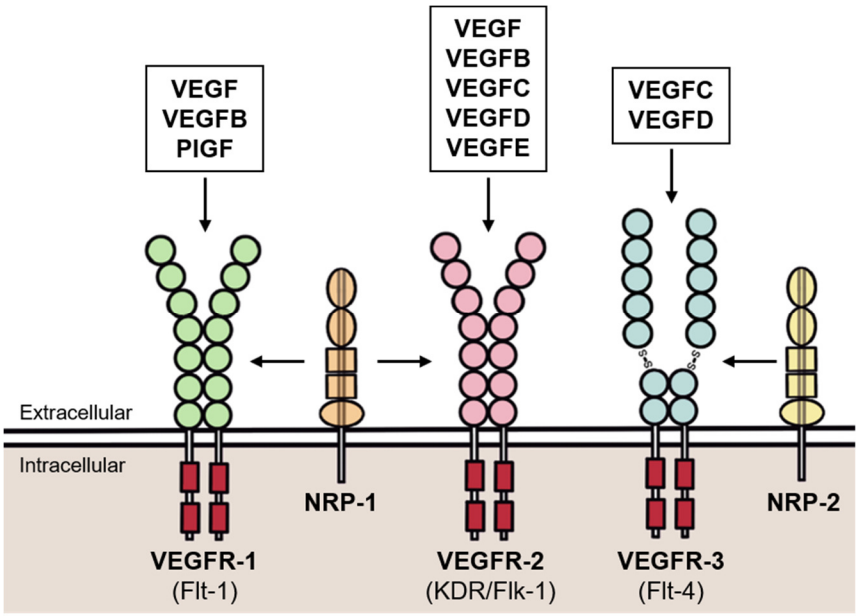

Figure 1: The vascular endothelial growth factor family and their receptors.
Schematic diagram illustrating the interactions of vascular endothelial growth factor receptors (VEGFRs) with members of the VEGF family and neuropilin (NRP) co-receptors. Murine VEGFD activates only VEGFR-3 (Flt-4). VEGF receptors consist of immunoglobulin-like domains in the extracellular space, a transmembrane domain, and intracellular tyrosine kinase domains that undergo dimerization upon ligand binding, initiating downstream signaling cascades. (Modified from (Stacker and Achen, 2018)).

Mauceri et al. demonstrated that the expression of VEGFD in hippocampal neurons is regulated by basal neuronal activity and nuclear calcium-CaMKIV signaling (Mauceri et al., 2011). Even though a promoter analysis suggested no involvement of the principal CaMKIV-signaling target CREB in the regulation of VEGFD expression, RNA interference experiments as well as expression of the adenovirus protein E1A, an inhibitor of CBP activity (Arany et al., 1995, Bannister and Kouzarides, 1995), could show that transcription of *vegfd* is regulated by the CREB co-activator CBP (Mauceri et al., 2011). Moreover, it was shown that VEGFD expression depends on

the cell's capacity to buffer nuclear calcium (Mauceri et al., 2015). Several calcium binding proteins (CaBPs), like parvalbumin, act as calcium buffers and regulate intracellular calcium signaling by affecting the spatiotemporal characteristics of nuclear calcium transients (Schwaller, 2009). Nuclear targeted parvalbumin, interfered with CREB/CBP-dependent transcription and the expression of VEGFD (Mauceri et al., 2015).

Previous studies have linked reduced levels of VEGFD expression in hippocampal neurons, *in vitro* and *in vivo*, to a decrease in the length and complexity of the dendritic arbor (Mauceri et al., 2011, Mauceri et al., 2015). VEGFD could be identified as key regulator for the maintenance of dendritic morphology and cognitive functioning, by targeting its expression with RNA interference (Mauceri et al., 2011). It has been shown that in mice, VEGFD regulates dendritic arborization via an autocrine mechanism, activating VEGFR-3 and p38 MAP kinase signaling in hippocampal neurons (Mauceri et al., 2011). Furthermore, multielectrode array (MEA) and patch-clamp recordings showed that silencing of VEGFD is linked to a decrease in the network activity of hippocampal neurons, indicated by reduced spike frequencies and neuronal excitability. Moreover, a decrease in the number of AMPA receptors and membrane capacitance could be detected, indicative of a reduced membrane surface area, which is in accordance with the observed reduction in dendritic arborization of shVEGFD-expressing neurons (Mauceri et al., 2011). Mice with reduced VEGFD expression levels in their hippocampus showed impairments in spatial memory performance and fear-induced memory formation (Mauceri et al., 2011). The crucial regulatory role of VEGFD for complex cognitive functions could further be confirmed by Hemstedt et al. showing that nuclear calcium-VEGFD signaling is required for fear memory consolidation and extinction in mice (Hemstedt et al., 2017).

1.1.3 Neuronal morphology in health and disease

Many neurodegenerative disorders, including ALS (amyotrophic lateral sclerosis), Huntington's-, Alzheimer's, or Parkinson's disease are associated with a decline of the neuronal architecture, loss of synaptic connectivity and impairments in gene regulation (Fogarty et al., 2017, Burke and O'Malley, 2013, Perl, 2010, Reiner et al., 2011). Many acute and chronic neurologic diseases have been linked to an overactivation of excitatory amino acid receptors, a pathological event named excitotoxicity, resulting in cell death (Dong et al., 2009). Excitotoxicity can be triggered by hypoxia or ischemia, inducing uncontrolled glutamate release into the extracellular space, or by direct NMDA exposure, finally leading to an excessive entry of calcium into the cells via synaptic but also extrasynaptic NMDA receptors (eNMDAR) (Bading, 2013, Bading, 2017, Hardingham and Bading, 2010, Parsons and Raymond, 2014). Whereas synaptic NMDAR signaling is known to promote synaptic plasticity and neuroprotective effects, activation of NMDARs located in the extrasynaptic membrane counteracts nuclear calcium signaling by inducing transcriptional shut-off of CREB-dependent gene transcription, ultimately leading to degeneration and cell death (Hardingham and Bading, 2010, Hardingham et al., 2002).

Bath application of glutamate in cultured neurons, activating extrasynaptic NMDARs (Hardingham et al., 2002), has also been shown to act on epigenetic mechanisms by regulating the subcellular localization of class IIa HDACs. It has been suggested that activation of eNMDARs antagonizes pro-survival transcriptional pathways, by promoting nuclear accumulation of HDAC4 and -5 (Chawla et al., 2003). Recently, NMDA-mediated excitotoxicity, inducing the death of retinal ganglion cells (RGCs) and capillary damage *in vivo*, could be linked to a downregulation of VEGFD expression in neurons. (Schlüter et al., 2020). The rapid shut-off of VEGFD expression by eNMDAR activation has further been confirmed in cultured hippocampal neurons and in cortical neurons of mice subjected to the middle cerebral artery occlusion (MCAO) model of stroke (Mauceri et al., 2020). In both studies, VEGFD-supplementation strategies were successful in preserving neuronal structures from excitotoxic damage and promoted functional recovery (Mauceri et al., 2020, Schlüter et al., 2020).

In conclusion, neuronal morphology depends on synaptic activity and nuclear calcium-regulated gene transcription, which can be affected by physiological as well as pathophysiological events. Further, VEGFD has emerged as a crucial dendrite maintenance factor in neurons, playing a central role for cognitive functions and during disease (Mauceri et al., 2020, Mauceri et al., 2011, Mauceri et al., 2015, Schlüter et al., 2020, Hemstedt et al., 2017).

In the first part of this thesis, we investigate the effects of a synaptic activity- and nuclear calcium-regulated epigenetic mechanism, the nucleo-cytoplasmic shuttling of class IIa HDACs, on the morphology of hippocampal neurons and highlight the key role of VEGFD in the regulation of dendritic structures.

1.2 Epigenetics

1.2.1 Epigenetic modifications and chromatin remodeling

The term *epigenetics* has first been introduced by Conrad Waddington in 1942, broadly referring to all biological processes that modulate the transition from a genotype to a certain phenotype (Waddington, 2012). Today's research understands epigenetics as the study of epigenetic traits, which are defined as "a stably heritable phenotype resulting from changes in a chromosome without alterations in the DNA sequence." (Berger et al., 2009). Several epigenetic mechanisms have been identified that regulate gene transcription by chemically modifying the DNA or histone proteins of the nucleosome (Dupont et al., 2009, Wolffe and Guschin, 2000). These modifications can be preserved during cell division and even be inherited between generations, under certain circumstances (Berger et al., 2009, Dean et al., 2003, van Otterdijk and Michels, 2016). Nowadays, epigenetic modifications are more and more recognized as not static but highly dynamic and reversible processes, especially in neurons (Marshall and Bredy, 2016, Sweatt, 2013). A central aspect of epigenetic gene regulation is chromatin remodeling, since many epigenetic modifications influence the condensation pattern of chromatin, changing the access of transcription factors to the DNA (Li et al., 2007). In eukaryotic cells, DNA is packed around small, positively charged histone proteins in the nucleus, forming nucleosomes, the principal building block of chromatin (Zlatanova et al., 1998) (Figure 2).

A nucleosome consists of 146 base pairs (bp) of DNA wrapped around an octamer of histones, containing two copies of each core protein H2A, H2B, H3 and H4. Linker histones H1 and H5 provide a connection at the entry and exit sites of a nucleosome, allowing the formation of higher-order structures like the 10-nm and 30-nm chromatin fiber, which get further coiled into the chromatids of a chromosome (Zlatanova et al., 1998).

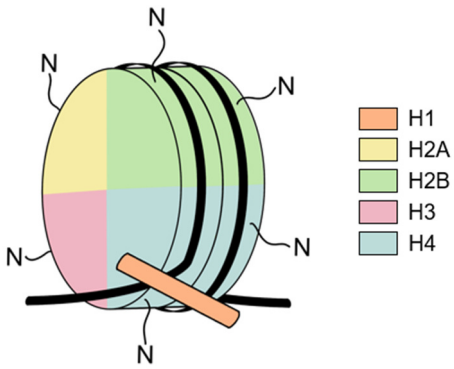

Figure 2: Nucleosome structure.
Schematic illustration of a nucleosome, the basic structural unit of DNA packaging in eukaryotes. 146 bp of DNA are wrapped around an octamer of two copies of each core histone protein H2A, H2B, H3 and H4. Linker histone H1 binds the DNA at the entry and exit sites of the nucleosome. N-terminal ends of histone core proteins represent the major sites for post-translational modifications. (Modified from (Morgan and Morgan, 2007)).

Epigenetic modifications, modulating chromatin structure and gene expression, can be achieved via covalent modifications of DNA itself (Griffith and Mahler, 1969), or by a variety of posttranslational modifications of the histone proteins. The epigenetic players mediating these changes are categorized as writers, readers, and erasers (Gillette and Hill, 2015, Biswas and Rao, 2018). Writers catalyze the addition of various chemical modifications to histones and DNA, whereas readers are proteins that contain specialized domains, such as the bromo- or chromodomain, necessary to recognize and interpret specific epigenetic marks. Finally, erasers are enzymes that remove the modifications introduced by the writers (Gillette and Hill, 2015, Biswas and Rao, 2018). The primary epigenetic modification of DNA is the conversion of cytosine into 5-methylcytosine by methylation at CpG sites, catalyzed and maintained by DNA methyltransferases (DNMTs) (Okano et al., 1999, Smith et al., 1992). Methylation of DNA has generally been associated with transcriptional repression and plays a role in genetic imprinting by silencing alleles in the germline, important for transgenerational inheritance (SanMiguel and Bartolomei, 2018).

However, recent studies show that DNA methylation is a highly complex process, also able to induce gene transcription, depending on the genomic location of the epigenetic mark (Suzuki and Bird, 2008).

Posttranslational modifications of histones, including acetylation, methylation, phosphorylation, ubiquitylation and sumoylation can occur throughout the protein sequence and are mediated by a variety of enzymes. However, the most frequently modified sites are specific amino acid residues located at the N-terminal tails of the histone core proteins (Kouzarides, 2007, Marmorstein and Trievel, 2009).

One of the best characterized histone modifications is the acetylation of lysine residues of histones H3(-K9;-K14; K18; -K23) and H4(-K5; -K8; -K12; -K16), which is generally associated with transcriptional activation (Dupont et al., 2009).

1.2.2 Histone acetylation and HDACs

Histone acetylation and deacetylation is a steadily balanced and highly regulated process. Histone acetyltransferases (HATs) catalyze the transfer of acetyl groups, derived from acetyl-coenzyme A to the ε-amino groups of lysine residues, while histone deacetylases (HDACs) reverse the reaction (Peserico and Simone, 2011, Racey and Byvoet, 1971).

Deacetylated lysine moieties contain a positively charged ε-amino group, which facilitates binding to the negatively charged phosphate groups of the DNA backbone, promoting chromatin condensation (Fang, 2005) (Figure 3). Hypoacetylated histones are associated with transcriptional repression (Lee and Workman, 2007), yet some genes are activated by HDACs activity (Nusinzon and Horvath, 2005). On the other side, HATs change the positively charged $-NH_3^+$ group into a neutral amide, resulting in relaxation of the chromatin structure, favoring TF binding and gene transcription (Grunstein, 1997, McGhee and Felsenfeld, 1980) (Figure 3). However, an opening of the chromatin structure by acetylation can also lead to the interaction with other chromatin remodeling enzymes (Berger, 2007).

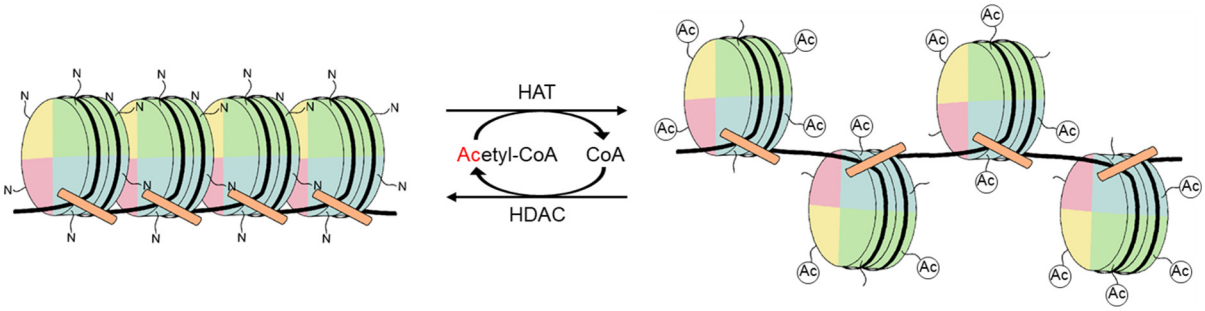

Figure 3: Histone acetylation/deacetylation regulates chromatin structure.
Schematic illustration of histone acetylation of lysine residues at the N-terminal ends of histone core proteins, leading to a relaxation of the chromatin structure by decreasing the binding affinity between histones and DNA. Acetylation is catalyzed by histone acetyltransferases (HATs) using acetyl coenzyme A (Acetyl-CoA) as donor of the acetyl group. Histone deacetylases (HDACs) revert the process by removing the acetyl groups. (Modified from (Eslaminejad et al., 2013)).

In this thesis, emphasis is placed on histone deacetylases and their regulatory effects in gene transcription. In mammals eighteen HDACs have been identified, which are divided into four classes based on their catalytic domain and mechanism of action, (class I; -II; -III and -IV) (Thiagalingam et al., 2003). All HDACs of classes I, II and IV are referred to as the classical HDAC family. They share a conserved deacetylase domain and require divalent zinc ions to catalyze their reaction (Finnin et al., 1999). HDACs of class III are termed sirtuins (SIRT1 – SIRT7) and belong to the SIR2-like family of NAD^+-dependent deacetylases, differing in their mechanism of action from the classical family (Haigis and Guarente, 2006). The classical HDAC members are categorized according to structural and functional properties and their homology to different yeast enzymes (Figure 4).

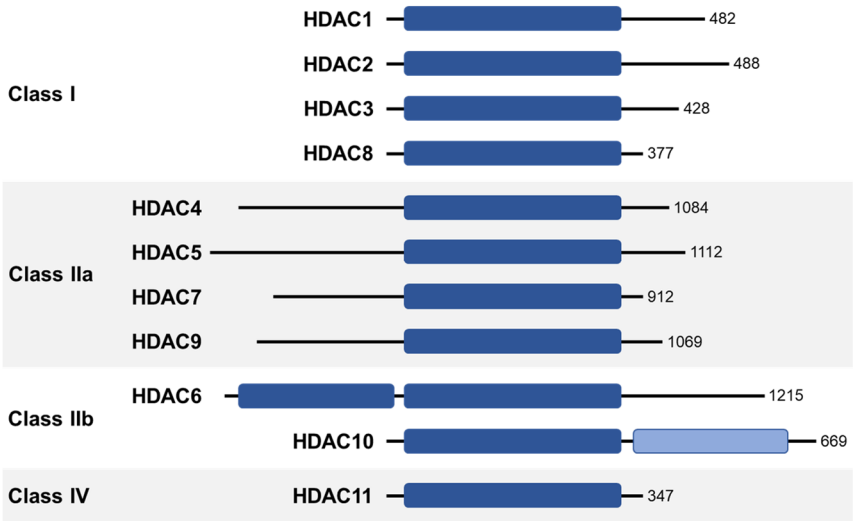

Figure 4: Classes of classical HDAC family members.

Eleven members of the classical HDAC family in mammals are divided into four classes based on their sequence and domain structure. Class II HDACs are homologues of the yeast protein HDA1 and subdivided into class IIa and IIb. HDACs of class IIa are characterized by a prolonged N-terminal region, regulating nucleo-cytoplasmic shuttling. Class IIb HDACs possess a second deacetylation domain, which is truncated and non-functional in HDAC10. Class I HDACs are homolog to the yeast protein RPD3. HDAC11 was associated with class I but got categorized as distinct member of class IV, due to unique sequence properties. (Modified from (Haberland et al., 2009)).

HDAC1, -2, -3 and -8 of class I are defined by their homology to RPD3. They are ubiquitously expressed and primarily localized in the nucleus, where they are often part of complex transcriptional repressor complexes. HDAC1 and -2 are part of the HDAC-co-repressor of repressor element-1 silencing transcription factor (CoREST) complex, which regulates neuronal gene expression and silences neuronal genes in non-neuronal tissues (Huang et al., 1999, You et al., 2001). HDAC3 is known for its interaction with the two co-repressors SMRT (silencing mediator of retinoic acid and thyroid hormone receptor) and NCoR (nuclear hormone receptor co-repressor), both required as integral component for HDAC3 deacetylation activity. The SMRT/NCoR-HDAC3 complex regulates the expression of genes important for development, metabolomic homeostasis, and during inflammation (Mottis et al., 2013).
HDAC1 and -2 are recruited by the transcriptional repression domain of MeCP2, linking DNA methylation of CpG residues and histone deacetylation (Tucker, 2001).
HDAC11, originally categorized as a member of class I, became a distinct member of class IV, following profound sequence analyses (Gregoretti et al., 2004). It is mainly localized in the nucleus and expressed in the brain, heart, skeletal muscle and liver. Not much is known about its function, besides its role in the repression of immunological targets like interleukin 10 (IL-10) (Gao et al., 2002).
Class II HDACs (HDAC4; -5; -6; -7; -9 and -10) are homologues of the yeast protein HDA1 (histone deacetylase 1) (Martin et al., 2007). Their expression patterns are tissue-specific and developmental stage-dependent. During development they have been shown to play an essential role for the differentiation of neuronal progenitor cells and dendritogenesis (Ajamian et al., 2003, Ageta-Ishihara et al., 2013, Gu et al., 2018, Sugo et al., 2010). Class II HDACs are further subdivided into class IIa (HDAC4; -5; -7 and -9) and class IIb (HDAC6 and -10), based on their domain organization. Class IIb is characterized by a second deacetylase (DAC) domain (Martin et al., 2007).

The focus of this study, however, lies on class IIa HDACs, which possess a large N-terminal domain that interacts with numerous non-histone proteins and regulates HDACs subcellular localization and activity (Martin et al., 2007) (Figure 5).

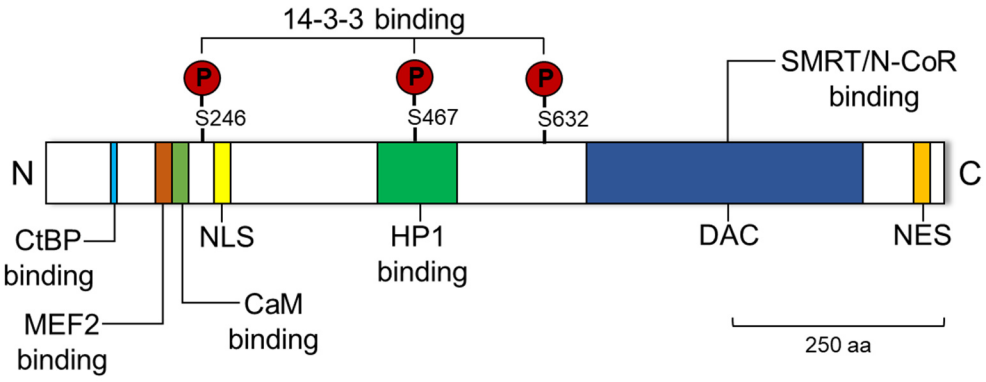

Figure 5: HDAC4 protein domains and its interaction partners.
HDAC4 targets distinct gene promoters by interacting with the transcription factor MEF2 via its N-terminal domain. Binding of the calcium sensor calmodulin (CaM) can displace HDAC4 from MEF2. Interactions with co-repressors CtBP and HP1 at the N-terminal domain and with the SMRT/N-CoR co-repressor complex at the C-terminal deacetylation (DAC) domain, mediate transcriptional repressive activity of HDAC4. Phosphorylation of HDAC4 at its serine residues S246, S467, and S632 facilitates binding of the chaperone 14-3-3 and promotes the nuclear export of HDAC4. CaM (calmodulin); CtBP (C-terminal binding protein); DAC (deacetylation domain); HP1 (heterochromatin protein 1); MEF2 (myocyte enhancer factor 2); N-CoR (nuclear hormone receptor co-repressor); NES (nuclear export signal); NLS (nuclear localization signal); SMRT (silencing mediator of retinoic acid and thyroid hormone receptor). (Modified from (Wang et al., 2014, Verdin et al., 2003)).

1.2.2.3 Nucleo-cytoplasmic shuttling of class IIa HDACs

The nucleo-cytoplasmic shuttling of class IIa HDACs is a complex process, which is primarily regulated by protein kinases and phosphatases (Paroni et al., 2008, Parra and Verdin, 2010, Zhao et al., 2001), and has best been described for HDAC4, which is standing in the focus of this study (**Fehler! Verweisquelle konnte nicht gefunden werden.**). HDAC4 is highly expressed in the rodent hippocampus and forebrain regions, as well as in heart and skeletal muscles (Broide et al., 2007, Grozinger et al., 1999). Its nuclear export is mediated by the phosphorylation of three serine residues (S246, S467, and S632), which can be catalyzed by CaM-Kinases (Backs et al., 2006), present in the nucleus of hippocampal neurons (Parra and Verdin, 2010). However, the subcellular shuttling of class IIa HDACs is very cell type specific and

the exact mechanisms are still not understood. While CaMKII has been shown to specifically regulate the export of HDAC4 in cardiomyocytes (Backs et al., 2006), HDAC4 subcellular localization was only partially affected by CaMKII in hippocampal neurons (Chawla et al., 2003), suggesting the involvement of other kinases, including CaMKI and -IV, as well as ERK-MAP kinases (Chawla et al., 2003, Zhao et al., 2001, Zhou et al., 2000). Phosphorylation of HDAC4 facilitates binding of the chaperone protein 14-3-3 (Grozinger and Schreiber, 2000), which activates the nuclear export signal (NES) of HDAC4 at its C-terminus and promotes translocation to the cytosol through a CRM1 (exportin 1)-dependent mechanism (McKinsey et al., 2001, Wang and Yang, 2001). In contrast, nuclear import is regulated by an arginine-lysine rich tripartite nuclear localization signal (NLS), located in the N-terminus of HDAC4, which interacts with importin-α, mediating the transport across the nuclear envelope (Grozinger and Schreiber, 2000, Wang and Yang, 2001). Nuclear import is triggered by dephosphorylation of HDAC4 in the cytosol, which can be catalyzed by the serine/threonine protein phosphatase 2A (PP2A), revealing its intrinsic NLS (Liu et al., 2005, Paroni et al., 2008).

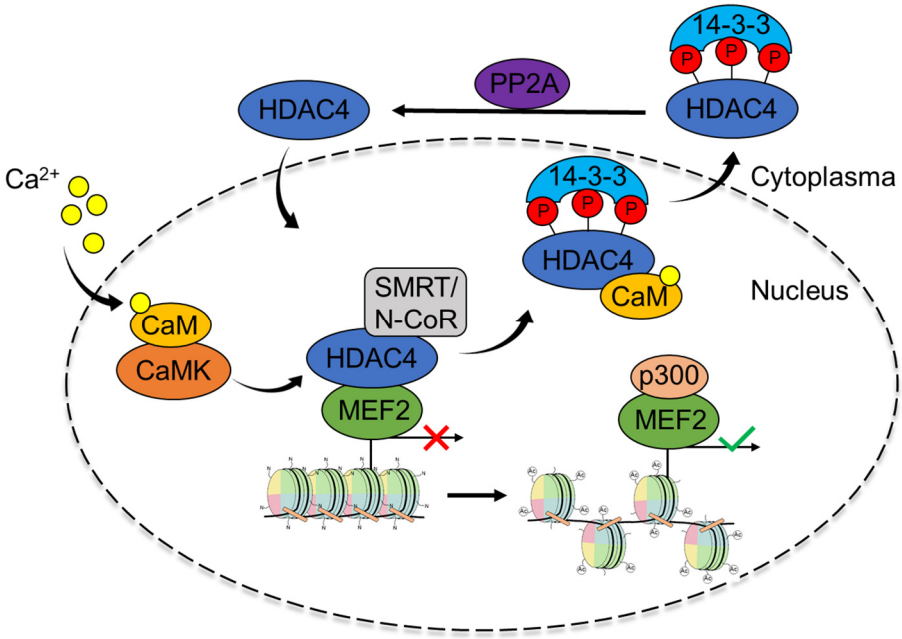

Figure 6: Nucleo-cytoplasmic shuttling of HDAC4.
Nuclear export of HDAC4 is initiated by phosphorylation of three serine residues by Ca^{2+}/Calmodulin dependent kinase (CaMK) activity. Following phosphorylation, 14-3-3 proteins bind and activate the nuclear export signal of HDAC4, promoting its translocation to the cytosol. Dephosphorylation in the cytoplasma by phosphatases (e.g. PP2A) unmasks the nuclear localization sequence of HDAC4 and triggers its nuclear import. Nuclear HDAC4 can bind to the transcription factor MEF2 and recruits the co-repressor complex SMRT/N-CoR to MEF2-specific promoters, inhibiting gene transcription.

Calmodulin (CaM) competes with HDAC4-MEF2 interaction and supports HDAC4 nuclear export. Cytolsolic HDAC4 promotes binding of MEF2 to the co-activator p300, stimulating gene expression. (Modified from (Backs et al., 2006)).

1.2.2.4 Transcriptional regulation by HDACs

The exact molecular mechanisms, by which HDAC4 and other class IIa HDACs contribute to transcriptional control, are not completely understood. In fact, studies have shown that in vertebrae the deacetylation domain of class IIa HDACs is not functional due to a histidine mutation of a tyrosine residue within the DAC domain, which is critical for its function (Lahm et al., 2007, Schuetz et al., 2008). However, genome-wide transcriptional profiling and experiments using the activity-dependent synthetic promoter E-SARE (Kawashima et al., 2013) have shown that nuclear HDAC4 silences the expression of several early response genes (ERGs), including *c-fos*, *arc* and *npas4*, by inhibiting TFs, which rely on neuronal excitation, on gene promoters (Zhu et al., 2019). It has also been shown that deacetylation can be achieved by recruiting the SMRT/NCoR-HDAC3 co-repressor complex to the C-terminal deacetylation domain of class IIa HDACs (Fischle et al., 2001, Fischle et al., 2002, Guenther et al., 2001). A well-studied example of how class IIa HDACs regulate gene expression, is the interaction between HDAC4 and the transcription factor MEF2 (myocyte enhancer factor 2). MEF2 is known for its regulatory function in cellular differentiation, determining for example the fiber type of skeletal muscles (Bassel-Duby and Olson, 2006), and is highly expressed in muscle tissue and neurons (McKinsey et al., 2002). MEF2-regulates gene transcription by recruiting class IIa HDACs via their N-terminal domain. Class IIa HDACs, in turn, affect the chromatin state of the MEF2-targeted promoter region by recruiting the SMRT/NCoR-HDAC3 co-repressor complex, attached to their C-terminus, to the DNA: In addition, the N-terminal domain of class IIa HDACs contains binding sites for transcriptional co-repressors C-terminal binding protein (CtBP) (Zhang et al., 2001) and heterochromatin protein 1 (HP1) (Martin et al., 2007, Zhang et al., 2002), promoting transcriptional repression (Figure 5).

The interaction with MEF2 also affects the subcellular localization of class IIa HDACs in neurons. In hippocampal neurons it has been shown that the nucleo-cytoplasmic shuttling of HDAC4 and other class IIa HDACs depends on synaptic activity and nuclear calcium signaling (Chawla et al., 2003, Schlumm et al., 2013).

Following synaptic activity, CaM-activated kinases stimulate the nuclear export of HDACs (**Fehler! Verweisquelle konnte nicht gefunden werden.**). In addition, HDAC4 and -5 contain binding sites for CaM, competing with MEF2 interaction. While MEF2 is bound to DNA and anchors the HDACs to the nucleus, binding of CaM, instead of MEF2, promotes the nuclear export of class IIa HDACs (Berger et al., 2003, Youn et al., 2000).

Under basal conditions, class IIa HDACs are predominantly localized in the cytoplasm (Darcy et al., 2010, Schlumm et al., 2013). Silencing of neuronal activity by the sodium channel blocker tetrodotoxin (TTX) (Hardingham et al., 2001), or blockade of calcium signaling by CaMBP4, preventing the activation of nuclear calcium/calmodulin complex's downstream targets (Wang et al., 1995), has been shown to result in HDACs nuclear accumulation (Schlumm et al., 2013, Sando et al., 2012). Moreover, activation of extrasynaptic NMDA receptors, could be linked with nuclear accumulation of HDAC4 in cultured hippocampal neurons (Chawla et al., 2003), as well as in retinal ganglion cells, by using an excitotoxicity-triggered *in vivo* model of neurodegeneration (Schlüter et al., 2019).

In addition, a constitutively nuclear localized mutant of HDAC4, named HDAC4 3SA, has been developed, which cannot be transported to the cytosol due to alanine substitutions of three serine residues (S246, S467, and S632), whose phosphorylation is required for its nuclear export (Grozinger and Schreiber, 2000, McKinsey et al., 2001). Nuclear accumulation of HDAC4 by overexpression of HDAC4 3SA in hippocampal neurons has been shown to impact the transcription of many activity and nuclear calcium-regulated genes with important functions for cognitive abilities, like memory formation and consolidation, as well as, neuroprotection and even the development of chronic pain (Kim et al., 2012b, Schlumm et al., 2013, Simonetti et al., 2013, Zhu et al., 2019). HDAC4 subcellular localization and activity have also been shown to regulate the expression of synaptic proteins, thereby changing the shape of synapses, modulating neuronal transmission and even cell survival (Sando et al., 2012).

The nucleo-cytoplamsic shuttling of HDAC4 in neurons could be linked with CaMKII-dependent formation of long-term memories (LTM) in *C. elegans* (Wang et al., 2011a) and dynamic changes in the subcellular localization of HDAC4 and -5 are essential for spatiotemporal control of transcriptional programs during memory formation in mice (Zhu et al., 2019).

A loss of HDAC4 has been associated with neurodegeneration (Chen and Cepko, 2009, Sando et al., 2012), and a null knockout of HDAC4 in mice is even lethal within two weeks after birth (Vega et al., 2004). However, these results have been challenged by studies, relying on conditional deletion of HDAC4 in the nervous system (Price et al., 2013).
Mutations in the human HDAC4 locus have also been linked to mental retardation and the brachydactyly syndrome (Williams et al., 2010). In addition, many neuronal pathologies, like stroke, Alzheimer's or Parkinson's disease, display nuclear accumulation of HDAC4 (Kassis et al., 2015, Shen et al., 2016, Wu et al., 2016, Yuan et al., 2016, Li et al., 2012). Changes in the subcellular localization of HDAC4 could also be observed in retinal ganglion cells, in a model of excitotoxicity *in vivo* (Schlüter et al., 2019). Moreover, HDAC4 has been implicated in various types of cancer and pharmacological treatments with different HDAC inhibitors have proven their therapeutical value (Drummond et al., 2005). However, prominent HDAC inhibitors like suberoylanilide hydroxamic acid (SAHA), trichostatin A (TSA), or sodium butyrate act in an unspecific way and inhibit either all HDACs at once or whole HDAC classes (Eckschlager et al., 2017), making such treatments susceptible for various side effects.

Taken together, HDAC4 has been shown to play a central role in the physiology and pathophysiology of many neurological processes, but a detailed understanding of its regulatory effects in neurons is still missing. In this study we are focusing on the subcellular localization of class IIa HDACs and investigate their regulatory effects on structural and functional properties of neurons and their networks.

1.2.3 DNA methylation and DNMTs

DNA methylation has long been considered a stable and irreversible epigenetic mark and inhibitor of gene transcription. However, recent studies identified DNA methylation, particularly in neurons, as a highly dynamic process that is critical for activity-induced neuroadaptive changes (Tognini et al., 2015, Riccio, 2010, Luo et al., 2018). A synaptic activity and nuclear calcium-dependent epigenetic process, which has been described in hippocampal neurons, is the induction of the immediate early gene Dnmt3a2 (Oliveira et al., 2012). DNA methyltransferases (DNMTs) are a family

of enzymes that catalyze the transfer of methyl group from S-adenyl methionine (SAM) to the fifth carbon of a cytosine residue of the DNA (Moore et al., 2013). DNMT activity is essential for the differentiation of cells during development (Holliday and Pugh, 1975). It also plays a regulatory role in postmitotic cells of the mammalian CNS (Feng et al., 2005, Goto et al., 1994) and has been linked to the formation of memories (Miller and Sweatt, 2007, Monsey et al., 2011). Traditionally, DNA-methylation has been associated with a repressed chromatin state and transcriptional inhibition, which can be achieved by two different mechanisms (Klose and Bird, 2006). First, methylation of cytosine bases can lead to the dissociation of transcription factors from their DNA binding sites (Watt and Molloy, 1988) and secondly, it allows binding of methyl-CpG-binding proteins (MBPs), like MeCP2, that have been shown to recruit transcriptional co-repressor complexes, which, in turn, silence transcription in the targeted promoter region (Jones et al., 1998, Nan et al., 1998).

However, several studies have shown that, depending on the genomic location of the epigenetic modification, DNA methylation and also binding of MeCP2 can result in gene activation, instead (Chahrour et al., 2008, Chen et al., 2003, Suzuki and Bird, 2008). Interestingly, in hippocampal neurons it has been demonstrated that MeCP2 activity regulates gene transcription in a synaptic activity and nuclear calcium-dependent manner, requiring CaMKII-mediated phosphorylation at its serine residue 421 (Buchthal et al., 2012).

In mammals several DNMTs have been identified which can be distinguished by their preferred DNA substrate. Dnmt1 maintains already established methylation patterns during cell division by copying them on the new DNA strand, whereas the *de novo* methyltransferases Dnmt3a and Dnmt3b catalyze cytosine methylation at previously unmethylated CpG sites (Klose and Bird, 2006). A fourth member, DNMT2, has been identified, which displays a weak enzymatic activity and does not affect DNA methylation patterns (Okano et al., 1998). Instead it has been linked with the methylation of small RNA molecules (Goll et al., 2006). The DNMT-related protein Dnmt3L, which does not possess an active catalytical domain, has been shown to modulate the methylation activity of Dnmt3a and Dnmt3b (Suetake et al., 2004).

The gene locus of Dnmt3a encodes two alternative transcript variants, *dnmt3a1* and *dnmt3a2* (Chen et al., 2002). Dnmt3a2 lacks 219 (mouse) or 223 (human) amino acid residues at its N-terminal domain due to transcription from an intronic promoter

region. While Dnmt3a1 is predominantly localized in regions of heterochromatin, Dnmt3a2 has been associated with actively transcribed euchromatin (Chen et al., 2002). Moreover, in contrast to Dnmt3a1, the expression of Dnmt3a2 is regulated by neuronal activity and partially dependent on nuclear calcium signaling (Oliveira et al., 2012).

Experiments regulating the expression of Dnmt3a2 in the adult mouse hippocampus have shown that Dnmt3a2 is a central epigenetic regulator controlling important cognitive abilities, like the formation and extinction of fear memories, by mediating the expression of plasticity related genes, including *arc* and *c-fos* (Oliveira, 2016, Oliveira et al., 2012).

It has been recently demonstrated that increased levels of Dnmt3a2 within selected neurons of the mouse dentate gyrus, can enhance memory performance by supporting the formation of neuronal engrams during memory consolidation and retrieval (Gulmez Karaca et al., 2020).

Moreover, changes in the expression and activity of Dnmt3a2 have been linked to complex behaviors in drug addiction, which are mediated by the mesolimbic brain reward system (Cannella et al., 2018). Dopaminergic signaling in primary striatal cultures, as well as activation of the nucleus accumbens (NAc)-shell, upon administration of cocaine, have been shown to selectively induce the expression of Dnmt3a2, but not that of DNM3a1 (Cannella et al., 2018). In addition, Dnmt3a2 expression regulated the induction of plasticity-related immediate early genes, important for the establishment of long-lasting drug cue memories (Cannella et al., 2018).

The role of epigenetic mechanisms in the regulation of neuro-adaptive processes such as synaptic plasticity and memory is thus well established (Haggarty and Tsai, 2011, Zovkic et al., 2013).

In the field of pain research, the phenomenon of central sensitization, critical for the induction and maintenance of hypersensitivity in chronic pain, has been shown to share relevant mechanisms of neuronal plasticity with memory formation (Rahn et al., 2013). Over the past decade, epigenetic processes gained increasing attention in the search for novel strategies to treat pathological pain conditions. Indeed, several epigenetic mechanisms have been linked to the transition from acute to chronic pain (Denk and McMahon, 2012, Geranton and Tochiki, 2015, Buchheit et al., 2012). This

includes changes in the pattern of DNA methylation and histone acetylation in different animal models of chronic pain (Wang et al., 2011b, Khangura et al., 2017).
Dnmt3a-activity has already been shown to regulate the development and maintenance of bone cancer pain, as well as neuropathic pain in a mouse model of chronic constriction injury (CCI) (Miao et al., 2017, Shao et al., 2017). Yet, the specific role of synaptic activity-regulated Dnmt3a2, critical for plasticity and neuro-adaptive processes, has not been investigated in chronic pain.
In the course of this doctoral thesis, we investigated the expression of Dnmt3a2 and its consequences in mouse models of acute and persistent inflammatory pain.

1.3 From nociception to chronic pain

Pain is a complex sensory experience and plays an important physiological function for our well-being. It is defined as “an unpleasant sensory and emotional experience, which is associated with actual or potential tissue damage, or described in terms of such damage” (IASP Task Force on Taxonomy, 1994, p. 209). Nociception describes the “neural process of encoding and processing noxious stimuli” (Loeser and Treede, 2008), which is required to sense and experience pain. Physiological pain and nociception are required to protect the body from potential tissue damage, by triggering an adequate behavioral response to noxious stimuli, like heat, cold, mechanical pressure, or chemical irritants (Julius and Basbaum, 2001, Woolf and Ma, 2007).
For example, tissue damage from a sunburned skin, leads to a temporary sensitization of the stimulated pain pathways, which is characterized by two phenomena: allodynia, meaning usually innocuous stimuli elicit pain, and hyperalgesia, where normally painful stimuli are perceived with higher intensity (Basbaum et al., 2009). Under physiological conditions, this hypersensitivity resolves over time and the excitability of the nociceptive systems returns to pre-injury states, after the injury-induced inflammation has passed and the wound is healed (Basbaum et al., 2009).
However, under certain circumstances, like an ongoing inflammation, a nerve lesion by accident, or a disease that affects the somatosensory nervous system, like cancer or diabetes, pain can become pathological and persists long after the acute injury is gone. In humans, pathological pain is considered chronic when present for more than

six months, but the time scales of underlying mechanisms and events can be very different in-between individuals.

Chronic pain is considered a debilitating condition that affects up to 20% of the world's population and is responsible for enormous socioeconomic costs every year (Breivik et al., 2006). Because of its pronounced emotional component, chronic pain is strongly interconnected with psychological diseases like depression and the use of antidepressant drugs for the treatment of chronic pain is well established (Sheng et al., 2017, Descalzi et al., 2017). However, progress in the pharmacological treatment of chronic pain has been very limited over the past decades (Denk and McMahon, 2012).

The underlying mechanisms for the transition from acute to chronic pain are complex and involve maladaptive changes in the peripheral and central nervous system. (Woolf and Salter, 2000, Basbaum et al., 2009). In order to understand pain hypersensitivity and to develop novel therapeutic interventions, it is key to study the cells and molecular pathways that underlie pain sensation.

1.3.1 Nociception

Noxious stimuli that reach certain thresholds are detected in the periphery by nociceptors, a subpopulation of primary afferent nerve fibers (Basbaum et al., 2009). Their somas are located in the dorsal root ganglia (DRGs) close to the spinal cord, and possess a peripheral branch to innervate the skin and viscera, as well as a central branch that projects incoming signals to second order neurons in the dorsal horn of the spinal cord, or directly to the brain stem via ascending pathways (Figure 7).

1.3.2 Nociceptors

Nociceptors are classified by their degree of myelination and axon diameter, determining their conduction velocity and therefore functional properties in the pain processing pathways (Meyer et al., 2006). Their predominant excitatory neurotransmitter is glutamate (Julius and Basbaum, 2001). One major class of nociceptors are medium-diameter Aδ-fibers, which are thinly myelinated and mediate an acute, well-localized "sharp" pain sensation, with a relatively fast conduction velocity of 5 – 30 m/s (Basbaum et al., 2009). They differ from large diameter and

rapid conducting Aβ-fibers (30 – 100 m/s) of the somatosensory system, which respond, under normal conditions, to innocuous mechanical stimulation, important for our sense of touch. The other major class of nociceptors is made of small diameter, unmyelinated C-fibers, with a slow conduction speed of 0.2 – 2 m/s. They convey the sensation of a “second”, poorly localized and rather long-lasting pain (Basbaum et al., 2009).

Nociceptors are further subdivided based on their threshold modalities and according to their expression of receptors that convey sensitivity to different stimuli. Aδ nociceptors of type I are characterized by a high thermal threshold (>50°C) and respond to mechanical, as well as chemical stimuli, whereas type II Aδ-fibers possess a lower heat threshold (>43°C) but a much higher mechanical threshold instead (Basbaum et al., 2009). The unmyelinated C-fibers are a heterogenous group of nociceptors (Snider and McMahon, 1998). Like the myelinated afferents, most of the C-fibers are polymodal and respond to both heat and mechanical stimuli (Perl, 2007). These afferents are named mechano-heat-sensitive (CMH) fibers. A subpopulation of C-fibers which can be triggered by heat but not by mechanical pressure, under naïve conditions, is termed “silent nociceptors”. They become mechanically sensitive upon inflammation and are thought to play a role for the transition from acute to chronic pain (Schmidt et al., 1995). C-fibers can be further subdivided by their expression of certain peptides into peptidergic and non-peptidergic nociceptors. The peptidergic population releases neuropeptides like substance P or CGRP (calcitonin-gene related peptide) and expresses the tropomyosin receptor kinase A (TrkA), a high affinity receptor for the neurotrophic peptide NGF (nerve growth factor), which in turn plays a role in inflammatory pain (Mizumura and Murase, 2015, Basbaum et al., 2009). Non-peptidergic C-fibers are characterized by the expression of the receptor tyrosine kinase RET, which mediates signaling of the glial cell line-derived neurotrophic factor ligands, neurturin (NRTN) and artemin (ARTN) (Basbaum et al., 2009). Many non-peptidergic C-fibers bind to isolectin B4 (IB4), which can be used for selective immunohistological stainings. They are also characterized by the expression of the ligand-gated ion channel $P2X_3$, which transduces ATP-evoked nociceptive signals in inflamed tissues (Basbaum et al., 2009, North, 2004).

In order to detect various external stimuli, polymodal nociceptors rely on a diversity of signal transduction mechanisms. Several transient receptor potential (TRP) channels

have been identified, which are expressed by primary afferents and play an important role in the detection of nociceptive signals (Julius and Basbaum, 2001). TRPV1 is a prominent member of the TRP vanilloid family and confers sensitivity to heat (>43°C) (Basbaum et al., 2009). It is also activated by the vanilloid capsaicin (8-methyl-*N*-vanillyl-6-nonenamide), the active component of chili peppers, allowing the entry of sodium and calcium ions into the cell (Caterina et al., 1997, Julius and Basbaum, 2001). Several other TRP channels are important for non-painful somatosensation as well, including TRPV3 and TRPV4 for the detection of warmth (34 – 42°C), or TRPM8, a TRP-channel of the melastatin family, for the sensation of cold (< 25°C). TRPA1 (ankyrin family) on the other side, has been shown to respond to several chemicals and noxious cold (<17°C) (Basbaum et al., 2009). Harmful mechanical stimuli are transduced by nociceptors expressing the voltage-gated sodium channels $Na_v1.7$ and $Na_v1.8$, whereas acids can be sensed by voltage-insensitive sodium channels termed ASICs (Acid-sensing ion channels) (Zimmermann et al., 2007, Lingueglia, 2007).

The latest approach to classify the different types of nociceptors, besides measuring their electrophysiological properties, is by single-cell RNA sequencing analysis, where nociceptive neurons have been distinguished based on their expression profiles of molecular marker proteins (Usoskin et al., 2015).

1.3.3 The spinal cord

The spinal cord extends from the medulla oblongata of the brainstem down to the lumbar region of the vertebral column. It is surrounded and protected by the bones of the vertebral column as well as by three layers of meninges, the dura mater, arachnoid mater and pia mater. Cerebrospinal fluid (CSF) circulates through the subarachnoid space, between the arachnoid mater and pia mater, as well as through the central canal of the spinal cord. It provides additional mechanical protection and regulates homeostasis of the interstitial environment of the CNS (Telano and Baker, 2020).

Depending on the innervated body region, spinal nerves enter and leave the spinal cord at different levels, determining the segments of the spinal cord. The mouse spinal cord is, similar to most mammals, divided into 34 segments: eight cervical (C1 – 8), thirteen thoracic (T1 – 13), six lumbar (L1 – 6), four sacral (S1 – 4), and

three coccygeal (Co1 – 3) segments (Harrison et al., 2013, Watson and Kayalioglu, 2009). The spinal segments are named by the vertebrae through which the nerve roots pass the spinal column. However, in the adult animal the location of the spinal segments does not correspond to the vertebral segments, because the backbone is growing faster than the spinal cord during development. Therefore, the roots of the spinal nerves bridge an increasing distance towards the caudal vertebrae, as they still pass through their original intervertebral foramen (Ashwell, 2009). The spinal cord segments innervating the upper and lower limbs show a cervical and lumbar enlargement because of the increased number of neurons processing incoming and outcoming signals (Watson and Kayalioglu, 2009). While efferent nerve fibers of motor neurons leave the spinal cord via the ventral horn, all primary afferent nerve fibers project to the dorsal horn, which acts as a hub for the somatosensory information from the periphery (Basbaum et al., 2009).

1.3.4 The dorsal horn

The dorsal horn is organized into six laminae with distinct anatomical and functional properties (Julius and Basbaum, 2001, Watson and Kayalioglu, 2009), which are targeted by the primary afferents in a strictly organized manner (Figure 7). Myelinated Aδ- and unmyelinated, peptidergic C-fiber nociceptors terminate into the superficial laminae I and outer lamina II (lamina II_o), where they synapse to large projection neurons (lamina I) and interneurons (lamina II_o). Nonpeptidergic nociceptors project to interneurons of the inner lamina II (lamina II_i). Aδ-fibers target another class of projection neurons in the deep lamina V, so called wide-dynamic range neurons (WDR). This type of projection neurons receives also innocuous input from mechanosensory Aβ-fibers (Abraira and Ginty, 2013, Todd, 2010, Basbaum et al., 2009). In addition, Aβ-fibers synapse onto excitatory interneurons located in the inner lamina II, which are characterized by the expression of protein kinase c-gamma (PKCγ) (Neumann et al., 2008), as well as onto other interneurons in laminae III and IV (Basbaum et al., 2009).

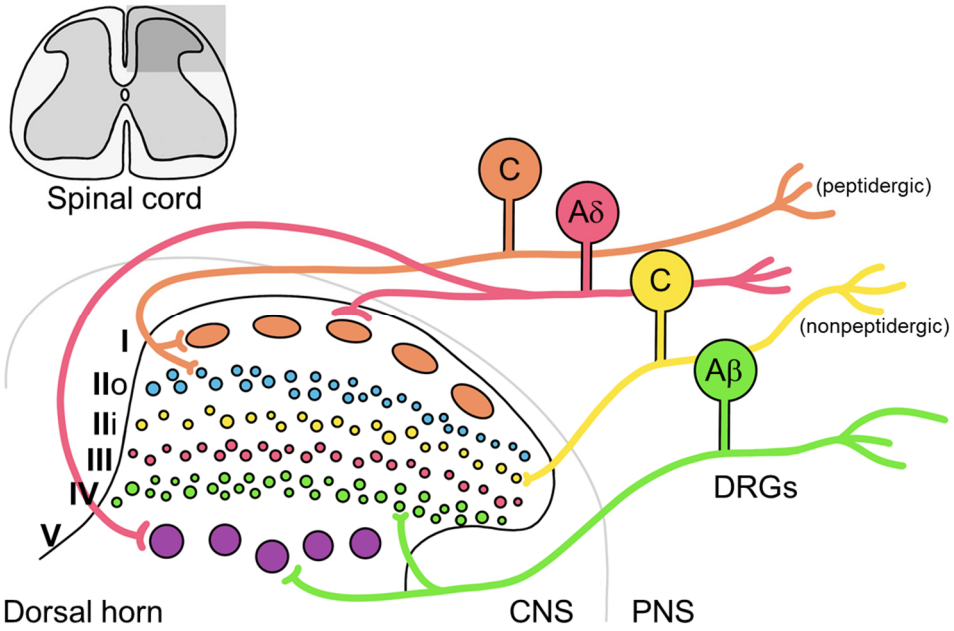

Figure 7: Primary sensory afferents and dorsal horn laminae.

Primary afferent neurons innervate the periphery and are located in dorsal root ganglia (DRGs). They project incoming signals to the spinal cord dorsal horn with a specific termination pattern. Myelinated Aδ- and unmyelinated, peptidergic C-fiber nociceptors synapse to large projection neurons in lamina I and interneurons in the outer lamina II (II_o). Nonpeptidergic C-fibers project to interneurons of the inner lamina II (II_i). Aδ-fibers also target wide-dynamic range projection neurons (WDR) in lamina V. Innocuous input is carried by myelinated Aβ-fibers synapsing to $PKC\gamma^+$ interneurons at the ventral border of laminae II_i/III, as well as onto other interneurons in laminae III/IV, and WDR projection neurons in lamina V. (Modified from (Basbaum et al., 2009)).

The circuitry and cell composition of the dorsal horn is very complex and a complete understanding of all discrete neuronal subpopulation, their organization and function, is still missing. Interneurons are critical for the processing of incoming sensory information and represent a very heterogenous group of neurons. Based on expression-analyses of transcription factors during development, a vast variety of either excitatory or inhibitory interneurons, transmitting glutamate, glycine or gamma aminobutyric acid (GABA), have been identified (Cheng et al., 2005, Todd, 2010, Cheng et al., 2017). The processed information is sent to subcortical and cortical regions of the brain by projection neurons in lamina I and V, via different ascending white matter tracts. The spinothalamic tract is important for sensory discrimination of noxious stimuli and transmits nociceptive input to the somatosensory cortex via the thalamus, providing information about pain intensity and localization (Basbaum et al.,

2009). In contrast, projections via the spinoreticulothalamic and spinoparabrachial tract target the cingulate and insular cortex via connections in the parabrachial nucleus of the brainstem, as well as in the amygdala. These regions of the brain have all been associated with the processing of aversive and emotional aspects of the pain experience (Basbaum et al., 2009, Todd, 2010). However, there is no specific pain-processing central area in the brain. It is rather an interplay of multiple, distributed brain regions, which contribute to a complex pain experience (Basbaum et al., 2009, Apkarian et al., 2005). The ascending nociceptive pathways are also interconnected with neurons of the rostral ventral medulla (RVM) in the brain stem and periaqueductal gray (PAG) of the midbrain, which initiate a descending feedback system that regulates in turn the output of nociceptive signals at the level of the spinal cord (Basbaum et al., 2009, Kuner and Flor, 2017).

1.3.5 Peripheral sensitization

Injuries to the skin, or nerve damages, often associated with diseases like diabetes, arthritis, or even cancer, can alter the functional properties of peripheral nerves, leading to an increased excitability (Basbaum et al., 2009). Peripheral sensitization is initiated by the release of inflammatory compounds by activated nociceptors and several non-neuronal cells that either reside or infiltrate the affected tissue, changing the chemical environment of the nerve endings (Basbaum et al., 2009). This “inflammatory soup” consists of extracellular adenosine triphosphate (ATP), protons, neurotransmitters, peptides, like substance P, CGRP, or bradykinin; neurothrophins, including NGF, as well as of numerous cytokines (Basbaum et al., 2009). In particular, interleukin 1β (IL-1β) and 6 (IL-6), as well as tumor necrosis factor α (TNF-α) contribute to hypersensitivity by recruiting and triggering the release of even more algesic compounds, including prostaglandins that potentiate the inflammatory response (Rittner et al., 2008). Several receptors, like TrkA or TRPV1, expressed on the surface of the nociceptors, interact with the inflammatory components, resulting in an acute functional potentiation of the receptors by the activation of intracellular signaling cascades, finally leading to thermal and mechanical hypersensitivity by reducing the receptor activation thresholds (Basbaum et al., 2009). Even long-lasting changes in the expression of pro-inflammatory proteins and nociceptive receptors, including substance P, TRPV1, or voltage-gated sodium channels, can be triggered

by neurothrophins, like NGF, that get transported to the nucleus of the nociceptors (Chao, 2003, Ji et al., 2002).

In order to counteract hyperalgesia and inflammatory pain, non-steroidal anti-inflammatory drugs (NSAIDs), like aspirin or ibuprofen, are frequently used to inhibit the synthesis of pro-inflammatory components like prostaglandins, by inhibiting the enzymes cyclooxygenase 1 and 2 (Cox-1 and Cox-2) (Zarghi and Arfaei, 2011, Basbaum et al., 2009). Inflammatory autoimmune diseases, like rheumatoid arthritis, have also been treated by blocking the activity of NGF or TNF-α via the application of neutralizing antibodies (Atzeni et al., 2005).

1.3.6 Central sensitization

Long-lasting or repetitive noxious stimuli can lead to a hyperexcitability of neurons of the central nervous system, resulting in allodynia and hyperalgesia even long after the initiating stimulus is gone (Latremoliere and Woolf, 2009). The underlying phenomenon is termed central sensitization and comprises several complex mechanisms that convey the transition from acute to pathological, chronic pain (Latremoliere and Woolf, 2009, Woolf and Salter, 2000, Basbaum et al., 2009, Woolf, 1983). The principal mechanisms involve the loss of inhibitory input (disinhibition), glial-neuronal interactions, as well as changes in NMDAR-mediated synaptic transmission (Basbaum et al., 2009).

1.3.6.1 Disinhibition

GABAergic and glycinergic interneurons located in the spinal cord dorsal horn constantly regulate incoming sensory information by tonic inhibition and prevent spontaneous firing of nociceptors in the absence of painful stimuli (Basbaum et al., 2009, Sandkühler, 2009). In contrast, disinhibition is associated with hypersensitivity and has been observed following peripheral injury, or upon pharmacological inhibition of GABA or glycine receptors in the spinal cord (Sivilotti and Woolf, 1994, Yaksh, 1989). In animal models of neuropathic pain, reduced levels of inhibitory postsynaptic currents have been measured in neurons of the dorsal horn. However, the underlying mechanisms are still not fully understood but a possible involvement of nerve injury-induced cell-death of GABAergic interneurons is discussed (Moore et al., 2002, Polgár et al., 2005). Disinhibition of glycinergic signaling has also been shown to

mediate thermal and mechanical hypersensitivity in rodent models of tissue injury, involving the release of the prostaglandin PGE_2 in the spinal cord (Harvey et al., 2004). Upon binding to the prostaglandin E_2 receptor 2 (EP_2), which is expressed by excitatory interneurons and projection neurons of the superficial spinal cord, PGE_2 blocks inhibitory glycine receptor signaling, by cAMP-PKA-mediated phosphorylation of the GlyRα3 subunit (Basbaum et al., 2009).

1.3.6.2 Neuronal-glial interactions

Also glial cells, especially microglia and astrocytes, have been shown to mediate central sensitization, following injury or disease (Basbaum et al., 2009). Microglia are specialized macrophages of the CNS and reside in the grey matter of the spinal cord. Upon peripheral nerve injury, microglia rapidly accumulate around affected nerve terminals in the spinal cord, where they release a variety of signaling molecules, including cytokines (IL-1β, IL-6, and TNF-α), neurotrophins, like the brain-derived neurotrophic factor (BDNF), and reactive oxygen species (ROS), leading to a sensitization of the neurons by various mechanisms, including dishinhibiton (Basbaum et al., 2009, Larson, 2008, Coull et al., 2005, Latremoliere and Woolf, 2009). Notably, microglia were also found activated in the brainstem after peripheral nerve damage, where they interfere with the inhibitory, descending feedback system of supraspinal nuclei (Ren and Dubner, 2008, Porreca et al., 2002). Interestingly, nociceptive activity of afferent fibers, following peripheral inflammation, does not trigger microglial activation. Instead, physical damage of the peripheral nerve, as in neuropathic pain models, is required for the release of signaling molecules, including ATP, which can activate microglia via purinergic receptors (Tsuda et al., 2003). In turn, ATP-activated microglia release BDNF, which can bind to TrkB receptors on the surface of projection neurons in lamina I, thereby eliciting disinhibition by influencing the chloride ion gradient, resulting in a shift from GABA-mediated hyperpolarization towards depolarization in affected neurons (Basbaum et al., 2009, Coull et al., 2005).
On the other side, astrocytes have also been shown to play a role in spinal sensitization (Ren and Dubner, 2008). They can be activated in the spinal cord upon peripheral tissue or nerve damage, where they interfere with the intercellular glutamate signaling (Sung et al., 2003, Chiang et al., 2007). In contrast to microglia, astroglial activation is delayed but more persistent, suggesting an involvement of

astroglia in the maintenance of chronic pain, rather than the induction of central sensitization (Basbaum et al., 2009, Ren and Dubner, 2008).

1.3.6.3 Glutamatergic signaling

Glutamate/NMDA receptor-mediated signaling is another key mechanism for the establishment of central sensitization and development of chronic pain. An acute activation of nociceptors results in the release of glutamate at central terminals in the dorsal horn. Glutamate primarily activates AMPA and kainate receptors at the synapse of second order neurons, triggering excitatory postsynaptic currents (EPSCs), which eventually lead to the generation of action potentials, sending nociceptive information to supraspinal regions in the brain (Basbaum et al., 2009). During a short or mild activation of the nociceptors, NMDA receptors stay silent due to a voltage-dependent block of the ion-channel by magnesium. However, in the setting of an injury, increased levels of glutamate are released, resulting in a stronger depolarization of the postsynaptic membrane, which is sufficient to unblock quiescent NMDA receptors, allowing elevated entry of Ca^{2+} ions into the cell (Mayer et al., 1984, Latremoliere and Woolf, 2009). Increased levels of calcium activate several downstream signaling cascades leading to a strengthening of the synaptic connections, which in turn enhances the excitability of dorsal horn neurons, driving hyperalgesia (Latremoliere and Woolf, 2009, Basbaum et al., 2009).

Moreover, innocuous stimuli in the surrounding area of the primary injury site also contribute to central sensitization by eliciting so called secondary hyperalgesia via heterosynaptic facilitation. Thereby, unconventional circuits for the transmission of nociceptive signals are established by the input of Aβ-fibers, which usually respond to light touch, resulting in allodynia (Basbaum et al., 2009, Campbell et al., 1988).

Whereas the early phase of central sensitization relies on glutamate-mediated strengthening of synaptic inputs and changes in the properties and trafficking of ion channels in the membrane (Basbaum et al., 2009, Carvalho et al., 2000, Chen and Roche, 2007), the maintenance and establishment of long-lasting central sensitization, characteristic for chronic pain, relies on changes in gene transcription and structural alterations (Latremoliere and Woolf, 2009, Woolf and Salter, 2000).

1.3.7 Structural plasticity and chronic pain

Several studies have linked structural changes at various anatomical scales of the nociceptive system to the development and maintenance of chronic pain (Kuner, 2010).

Region-specific morphological changes in the brain, mainly decreases in gray matter volume, have been reported in chronic pain patients, as well as rodent models, and are associated with frequent nociceptive stimulation (Kuner, 2010, Seminowicz et al., 2010, Rodriguez-Raecke et al., 2009). Cell atrophy of interneurons can result in the loss of descending inhibitory feedback, whereas proliferation of microglia and astrocytes may influence nociceptive processing by the release of modulatory substances (Kuner, 2010).

Activity-dependent changes of structural plasticity can also result in aberrant connectivity of nociceptive pathways. Several neuropathies and chronic diseases have been associated with degeneration, sprouting or hypertrophy of axons in peripheral tissues (Kuner, 2010, Ceyhan et al., 2009). Recently, it has been shown that sensorimotor training after spinal cord injury (SCI) is effective in ameliorating neuropathic pain by reducing the density of nociceptive fibers in a mouse model of SCI (Sliwinski et al., 2018).

Another level of structural plasticity is that of activity-dependent changes in size and density of dendritic spines, altering the strength of synaptic transmission (Kuner, 2010). SCI-induced neuropathic pain has been associated with increased formation, redistribution and elaboration of dendritic spines in neurons of spinal laminae IV and V (Tan et al., 2008). Inhibition of the small GTP-binding protein Rac1, a regulator of cytoskeleton reorganization and dendritic spine morphology (Nakayama et al., 2000), attenuated SCI-induced hyperexcitability of dorsal horn neurons and ameliorated pain hypersensitivity (Tan et al., 2008). In the CFA model of inflammatory pain, the synaptic scaffolding protein Homer1a has been shown to protect against the development of inflammatory hypersensitivity, without interfering with physiological nociception, by reducing the density of spines in dorsal horn laminae IV and V neurons (Tappe et al., 2006).

Gene-chip analysis, following CFA-mediated paw inflammation, revealed a nuclear calcium-dependent pool of pain- and plasticity- related genes in the spinal cord (Simonetti et al., 2013), including *ptgs2* (COX-2), a critical mediator of inflammatory hypersensitivity (Vardeh et al., 2009) and the complement factor C1q-c, whose

dependencies on nuclear calcium signaling have already been demonstrated in hippocampal neurons (Schlumm et al., 2013, Zhang et al., 2009). C1q-c has been shown to ameliorate inflammatory pain-induced hypersensitivity by pruning the density of dendritic spines in dorsal horn neurons (Simonetti et al., 2013).

Taken together, nociceptive activity-induced structural adaptations in the central and peripheral nervous system play a critical role in the modulation of pain processing and for the development and maintenance of chronic pain.

1.4 Hypothesis and aims

In a model of persistent inflammatory pain, changes in gene transcription and structural alterations, have been shown to depend on nuclear calcium signaling (Simonetti et al., 2013). Nociceptive activity triggers nuclear calcium transients in neurons of the dorsal horn, resulting in nuclear calcium-regulated downstream events like the phosphorylation and activation of CREB and MeCP2 (Ma et al., 2001, Ji and Rupp, 1997, Géranton et al., 2007). In contrast, inhibition of nuclear calcium signaling interferes with the development of long-term inflammatory hypersensitivity, without affecting basal or acute pain sensitivity (Simonetti et al., 2013).

As pointed out at the beginning, nuclear calcium regulates gene transcription, important for neuroadaptive phenomena, also by mediating epigenetic mechanisms, such as the subcellular shuttling of class IIa HDACs and the induction of Dnmt3a2 (Oliveira et al., 2012, Schlumm et al., 2013). In recent years, several epigenetic processes, including histone acetylation and DNA methylation, have been linked to central sensitization and the transition from acute to chronic pain (Buchheit et al., 2012, Denk and McMahon, 2012). However, a detailed understanding of the underlying molecular mechanisms and genes, regulating structural and functional changes, is still missing.

Previous studies relied on rather unspecific pharmacological inhibition of HDACs, without discriminating between different HDAC members, or investigated the role of DNMTs in pain without differentiating between the synaptic activity-dependent isoform Dnmt3a2 and activity-independent isoform Dnmt3a1.

In this study, we investigate the effects of long-lasting and acute inflammatory pain on the expression and activity of nuclear calcium-regulated epigenetic regulators

(class IIa HDACs and Dnmt3a2) and evaluate if and how changes in the epigenetic processes contribute to central sensitization by altering the transcription of plasticity and pain-related genes.

In the first part of this thesis, we focus our attention on the subcellular localization of HDAC4, a class IIa member, in cultured hippocampal neurons and investigate its role in the regulation of dendritic structures and neuronal morphology.

In part two, we assess changes in the expression of the activity-dependent *de novo* DNA methyltransferase Dnmt3a2 in a mouse model of persistent inflammatory pain and assess its consequences for the transcription of pain- and plasticity-related genes and behavioral hypersensitivity.

Finally, we investigate the expression and nucleo-cytoplasmic shuttling of HDACs and its consequences on histone acetylation in cultured neurons of the spinal cord, as well as in dorsal horn neurons *in vivo*, using different mouse models of inflammatory pain. We then manipulate the subcellular localization of HDAC4 in central neurons of the spinal cord and evaluate changes in histone acetylation, gene transcription, neuronal morphology, and pain behavior.

2 Materials and methods

2.1 Animal work

All animal procedures in this study were carried out in accordance with the local animal welfare committee (Regierungspräsidium, Karlsruhe, Germany) and were designed in line with the EU Directive 2010/63/EU and guidelines of the “National Centre for the Replacement, Refinement and Reduction of Animals in Research”.
Adult male C57BL/6N wild-type mice between 8 to 14 weeks old (Charles River, Sulzfeld, Germany) were used throughout all experiments. Animals were housed in small groups under ambient humidity and light conditions on a 12 h light-dark cycle and had ad libitum access to food and water. To ensure optimal conditions for housing and behavioral testing, temperature (23°C ± 1°C) and humidity (45-65%), were constantly controlled. All surgical procedures were performed within approved rooms of the IBF and IZN and suitable equipment. All animals were assigned to the different experimental groups randomly.

2.1.1 In vivo injections of rAAV

First, mice were anesthetized via intraperitoneal injection using a mix of fentanyl (50 µg/kg), medetomidine (5 mg/kg), and midazolam (500 µg/kg) (in 0.9% saline). The depth of anesthesia was constantly monitored (absence of pain reflexes) and, if necessary, adjusted by additional administration of a one-third dose of the anesthetic mixture. Eyes were protected from dehydration using eye ointment. To relieve possible postoperative pain shortly after awakening, carprofen (5 mg/kg) was administered subcutaneously (s.c.) during anesthesia. The back of the mice got shaved and the skin got disinfected with 70% ethanol. Subsequently laminectomy was performed, starting with a small incision in the skin of the back (< 0.5 cm length). The superficial muscle layer was removed, exposing the spinal column and the intervertebral membrane between the spinal segments L3 and L5 was opened. Using a microprocessor-controlled minipump and a 35 gauge beveled “NanoFil” needle (World Precision Instruments), 500 nl of a 2:1 mixture of rAAV stocks with 20% mannitol were injected into the parenchyma of the spinal cord dorsal horn of the L3-L5 segments on each side (total of two injections per mouse) at a flow rate of 50 nl/min. After total volume release, the needle rested for 5 min at the injection site

to minimize leakage of the injection solution. The wound got closed using sutures and a local anesthetic (lidocaine) was applied on the back of the animals.
Anesthesia was antagonized after completion of all surgical measures by subcutaneous administration of a mixture of atipamezole (750 µg/kg), flumazenil (500 µg/kg) and naloxone (1.2 mg/kg) and hind limb function was tested to exclude any nerve damage. Postoperative pain was further counteracted by a single injection of buprenorphine (100 µg/kg, s.c.), one hour after the animals woke up. Mice were kept on a warming plate (39°C) for recovery and to prevent hypothermia. Animals were allowed to recover for at least three weeks after surgery before any further analysis, which also ensured optimal target gene expression.

2.1.2 Intrathecal injections

Intrathecal injections were performed according to established protocols (Njoo et al., 2014). Animals were placed individually in a chamber and anesthesia was induced with 3% isoflurane (in O_2) until no signs of righting reflexes could be observed. Mice were placed in front of a nose cone for continued isoflurane administration (1.5% in O_2) during the procedure. The lower back of the animal was shaved and wiped with 70% EtOH to facilitate a better visualization during needle insertion. 10 µl of injection solution got prepared using a 0.3 ml insulin syringe with a 30 G needle (BD Medical). The spinous process of the L6 vertebra was located and the spinal column was fixed around this area by gentle pressure before the needle was carefully inserted between the groove of vertebrae L5 and L6. As a sign for a successful entry of the intradural space, a tail flick could be observed. The needle position was carefully secured with one hand, while the injection solution was slowly released. After injection, mice were placed in their cages to recover from anesthesia.
Intrathecal injections were used to deliver siRNAs (see 2.5) and probenecid (*p*-(di-*n*-propylsulfamyl) benzoic acid) (Sigma), a pharmacological inhibitor of the OAT1 channel. For stock solution 50 mg probenecid were dissolved in a total volume of 5 ml (10 µg/µl), consisting of 4 ml saline (0.9%), 850 µl Tris (1 M, pH 8.0), 150 µl NaOH (2 M), and 210 µl HCl (2 M). For intrathecal injection a total volume of 10 µl containing 16 µg of probenecid were applied per mouse. Solvent solution without probenecid was used as control. Probenecid concentration was chosen according to literature values (Salzer et al., 2001) and adjusted to the mouse CSF volume.

2.1.3 Animal pain models

2.1.3.1 Complete Freund's Adjuvant (CFA) model

For the induction of long-lasting inflammatory pain, 20 µl of CFA (Sigma Aldrich, F5881-10ml), containing 20 µg of heat killed *Mycobacteria* (strain H37Ra, ATCC 25177), were injected subcutaneously into the plantar surface of the hind paw, directly behind the walking pads and in parallel to the skin surface. (Stösser et al., 2010). This leads to the attraction of macrophages and other immune cells to the injection site, eliciting an immune response that lasts for up to two weeks. An equivalent volume of 0.9% saline was injected as control. All intraplantar injections were performed under isoflurane anesthesia.

2.1.3.2 Capsaicin model

Acute inflammatory pain was induced by injecting 20 µl of 0.03% capsaicin solution (in PBS; Tocris, cat. no. 0462) into the plantar surface of the hind paw. Capsaicin is a natural agonist of the TRPV1 (Transient Receptor Potential Vanilloid 1) receptor, exciting a subset of primary afferent neurons (Caterina et al., 1997). For non-behavioral experiments, animals were anesthetized using isoflurane and 0.9% saline injections were performed as control. For behavioral measurements, animals were anesthetized using ether to ensure a short wake-up phase (<1 min) after anesthesia, allowing measurements of short-lasting nocifensive behaviors during a conscious state.

2.1.3.3 Formalin model

For the formalin test, 20 µl of a 1% formalin solution (in saline) were injected subcutaneously into the plantar surface of one hind paw. This induces nocifensive behaviors, which can be divided into two phases. During Phase I (up to 10 min), peripheral nerve endings are activated leading to acute nocifensive behaviors, such as shaking and licking of the affected paw. The second phase, which lasts up to 1 h after formalin injection, is characterized by the development of acute nociceptive hypersensitivity, which is thought to be based on plasticity-dependent changes in the central nervous system as well as ongoing nociceptor activation (Coderre et al., 1990, Hunskaar and Hole, 1987, Tjolsen et al., 1992). Similar to the capsaicin model,

mice were anesthetized using ether to ensure a short wake-up time of less than 1 min.

2.1.4 Pain behavioral tests

All behavioral tests were conducted by the same experimenter in awake and unrestrained animals during the light phase and the experimenter was blinded to the identity of the treatments that mice received. Animals were acclimatized for 1 h per day to the testing environment for three consecutive days prior to behavioral measurements and on the day of testing. At the end of behavioral tests, animals were sacrificed, and relevant tissue was processed for further analysis (e.g. to confirm viral expression using fluorescence microscopy).

2.1.4.1 Mechanical sensitivity (von Frey test)

To evaluate changes in mechanical sensitivity after treatments, animals were placed in plexiglass boxes on an elevated metal grid (IITC Life Science) and responses to paw pressure were determined by applying a series of von Frey filaments (Ugo Basile, Aesthesio™, Precise Tactile Sensory Evaluator) with ascending forces (0.008 g; 0.02 g; 0.04 g; 0.07 g; 0.16 g; 0.4 g; 0.6 g; 1 g; 1.4 g; 2 g) to the plantar surface of the hind paws. The applied force, which is determined by the length and diameter of each filament, remains constant due to bending of the filament once the designated force is reached. In total, each filament was applied five times to each paw in increasing order, starting with the filament producing the lowest force. To avoid repeated stimulus-induced sensitization, testing of both paws alternated between animals, and single paws did not get re-stimulated before all other mice have been tested. Up to 12 animals were tested in parallel. To assess mechanical sensitivity, all filaments were applied, and the number of withdrawals was recorded. Withdrawal frequency was calculated as a percentage of withdrawals out of the total number of von Frey applications per filament. Baseline sensitivity for all filaments and animals was tested before surgery or any other intervention.

2.1.4.2 Thermal sensitivity (Hargreaves test)

Thermal hypersensitivity was assessed according to the Hargreaves' method using a plantar test analgesia meter (IITC Life Science). Mice were placed in plexiglass chambers on a glass platform (20.5 cm high) and a focused, radiant heat light source was applied to the plantar surface of each hind paw using a mirror. The glass floor was constantly heated to 29°C, minimizing the possibility of delayed responses to the heat source. Latency to the withdrawal of the paw was measured in seconds using an automated 15 s cut-off to avoid tissue damage. Start, stop and reset of the test were performed manually using the pushbutton on the test head. Light intensity was adjusted to give a latency of 6 – 8 s in naïve animals (intensity=50%). Paws of mice were randomly tested to avoid a habituation effect and a delay of at least 1 min in-between measurements per paw and animal, was obeyed. Thermal sensitivity was always assessed after mechanical sensitivity and basal mean latencies were determined before any intervention.

2.1.4.3 Acute sensitivity

Following capsaicin or formalin injections into the hind paw under ether anesthesia animals were placed in an empty plexiglass chamber. Immediately after waking, the duration of all nocifensive behaviors, such as licking, shaking or flicking of the injected paw, were measured in seconds over a time period of 5 min after injection of capsaicin and over a time period of 60 min, divided into 5 min intervals, after formalin injections.

2.2 Gene expression analysis

2.2.1 RNA extraction and cDNA synthesis

Animals were sacrificed and fresh spinal cord tissue (L3-L5) was quickly harvested and rapidly frozen in liquid nitrogen. In the case of viral-injected mice, only infected tissue was dissected for further analysis using, whenever possible, Green Fluorescent Protein (GFP) fluorescence as guidance. For *in vitro* experiments, cultured cells were harvested in lysis buffer from 35 mm dishes using a cell scraper (Corning Life Sciences). Total RNA was extracted from the dorsal part of the spinal cord, or from cultured hippocampal or spinal cord neurons, using the "RNeasy Mini

Kit" (Qiagen) including an optional DNase I treatment at room temperature for 15 min according to manufacturer's instructions. Extracted RNA was reverse transcribed into first strand cDNA using the "High Capacity cDNA Reverse Transcription Kit" (Applied Biosystems). PCR was performed in a thermal cycler (C100TM, Bio-Rad) using the following program:

Table 1: PCR program used for cDNA synthesis

Program step	Temperature	Duration
Annealing	25°C	10 min
Annealing/Elongation	37°C	120 min
Denaturation	85°C	5 s
Storage	4°C	∞

2.2.2 qPCR

Quantitative reverse transcriptase PCR (QRT-PCR) was done on a StepOne plus real-time PCR system using TaqMan® gene expression assays (Applied Biosystems) for the indicated genes (Table 2). Expression of target genes was normalized against the expression of *gusb* and/or *gapdh*, which were used as endogenous control genes.

Table 2: List of TaqMan probes used for QRT-PCR

Gene	Gene name	Assay ID
arc	activity regulated cytoskeletal-associated protein	Mm00479619_g1
bdnf	brain derived neurotrophic factor	Mm00432069_m1
c1qc	complement component 1, q subcomponent, C	Mm00776126_m1
cfos	FBJ osteosarcoma oncogene	Mm00487425_m1
cxcr4	chemokine (C-X-C motif) receptor 4	Mm01292123_m1
dnmt3a1	DNA methyltransferase 3A1	Mm00432870_m1
dnmt3a2	DNA methyltransferase 3A2	Mm00463987_m1
fez1	fasciculation and elongation protein zeta 1	Mm00805945_m1
flt4	FMS-like tyrosine kinase 4	Mm01292618_m1
gapdh	glyceraldehyde-3-phosphate dehydrogenase	Mm99999915_g1

gusb	glucuronidase beta	Mm00446953_m1
h19	H19, imprinted maternally expressed transcript	Mm01156721_g1
kdr	kinase insert domain protein receptor	Mm00440099_m1
lrg1	leucine-rich alpha-2-glycoprotein 1	Mm01278767_m1
msln	mesothelin	Mm00450770_m1
nov	nephroblastoma overexpressed gene	Mm00456855_m1
prx	periaxin	Mm00479826_m1
ptgs2	prostaglandin-endoperoxide synthase 2	Mm00478374_m1
slc22a6	solute carrier family 22, member 6 (OAT1)	Mm00456258_m1
slc26a7	solute carrier family 26, member 7 (SUT2)	Mm00524162_m1
vegf	vascular endothelial growth factor A	Mm01281449_m1
vegfc	vascular endothelial growth factor C	Mm01202432_m1
vegfd	vascular endothelial growth factor D	Mm00438965_m1

2.2.3 RNA sequencing analysis

Total RNA was isolated from infected dorsal horn tissue of mice, intra-spinally injected with rAAV-lacZ, -HDAC4 wt, or -HDAC4 3SA. Three samples of each condition were collected and 0.3 µg of total RNA from each sample was used for RNAseq. Differential gene expression analysis was performed by GATC Biotech (Inview Transcriptome Discover, GATC Biotech AG, Constance, Germany). Briefly, a cDNA library was generated by purification and fragmentation of poly-A containing mRNA molecules. Strand-specific cDNA was synthesized with random primers and ligated to adapters, used for adapter-specific PCR amplification. Sequencing was performed with a “Genome Sequencer Illumina HiSeq 4000” using 50 bp single end reads in FastQ format with at least 30 million reads (±3%). Gene expression was analyzed using the Bowtie, TopHat, Cufflinks, Cuffmerge, Cuffdiff software suite (Trapnell et al., 2010, Langmead et al., 2009, Trapnell et al., 2009). TopHat identifies the potential exon-exon splice junctions of aligned sequences and Cufflinks quantifies the transcripts from the pre-processed RNAseq alignment assembly. Then, Cuffmerge merges the identified transcript pieces to full length transcripts and annotates them. Finally, merged transcripts from three samples per condition are compared using Cuffdiff to determine the differential expression levels at transcript level including a measure of significance between conditions.

Mus musculus, mm10/GRCm38, Ensembl reference genome was used for the alignment. For the annotations of genes, the v85 Ensembl database was taken as a reference. The cutoff for determining significant differentially expressed genes (DEGs) was set to $P_{adjusted}<0.05$ (false discovery rate adjusted P-value). DEGs with a log2 foldchange > 0.5 were considered up-regulated and down-regulated with a log2 foldchange < -0.5.

Gene ontology analysis of DEGs, within the selected cutoff in LacZ-expressing mice, was performed using the PANTHER overrepresentation test (released 2020-04-07) and database (released 2020-02-21) (Mi et al., 2013). Fisher's exact test with FDR correction was chosen and the background database was restricted to the pool of genes annotated in our RNA sequencing analysis.

2.3 Expression constructs

All plasmids and viral expression constructs in this work were kindly provided by Dr. Daniela Mauceri, Dr. Ana Oliveira, Dr. Anna Hertle, and further collaborators.

Expression vectors used for co-transfection with hrGFP (lacZ, HDAC4 wt, HDAC4 3SA, HDAC3 and HDAC11) or production of viral expression constructs were all epitope-tagged at their C-terminal end and under the control of the cytomegalovirus (CMV) enhancer/chicken β-actin (CBA) promoter (lacZ, HDAC3 and HDAC11) or human synapsin (hSyn) promoter (HDAC4 wt, and HDAC4 3SA) as previously described (Mauceri et al., 2011, Schlumm et al., 2013). LacZ, HDAC4 wt and HDAC4 3SA carry a flag tag while HDAC3 and HDAC11 constructs contain a HA tag.

Expression vectors generated for shRNA-mediated in vivo knockdown of chosen target genes were all under the control of the U6 promoter and carried a GFP-tag under the control of the CBA promoter (shDnmt3a2, shControl, shOAT1-1, shOAT1-2, shUNC). The rAAV-shControl and rAAV-shDnmt3a2 viruses used in this work have been previously extensively characterized *in vitro* and *in vivo* for their specificity and efficacy (Oliveira et al., 2012, Oliveira et al., 2016). The Dnmt3a2-targeting shRNA sequence recognizes the 5'UTR sequence unique to Dnmt3a2 (CCCGGACGGGCAGCTATTTACAGAGCCTCGAGGCTCTGTAAATAGCTGCCCGTTTTTTGAAGCTT).

The shControl sequence is CGACTACCGTTGTTATAGGTGTTGATATCCGCACCTA TAACAACGGTAGTTTTT TTCCAA (Oliveira et al., 2012).
The following small interfering RNA (siRNA) sense-strand sequences from Qiagen were used to generate rAAV-shRNA plasmids: CCCAGACAATTAAATAAATTT (shOAT1-1; SI01420804), ATCCTAGTGAATGGCATAATA (shOAT1-2; SI01420797). A scrambled version, which does not target any sequence was designed as control (shUNC).
For overexpression of OAT1, the template sequence derived from the human gene encoding OAT1 (*slc22a6*) and was obtained from Prof. Geckle. The sequence was sub-cloned into a construct driving the expression of the transgene under the CMV/CBA promoter followed by a HA-tag at the C-terminal end.

2.4 rAAV production

The method used to construct, package, and purify recombinant adeno-associated viruses (rAAVs) has previously been described in detail (McClure et al., 2011). Briefly, rAAVs of serotype 1/2 were produced by co-transfecting HEK293 cells using standard calcium phosphate precipitation. HEK293 cells were cultured in Dulbecco's Modified Eagle Medium (DMEM, Life Technologies) containing high concentrations of glucose (4.5 g/l) and supplemented with 10% fetal bovine serum (FBS), 5 units/ml penicillin and 5 mg/ml streptomycin (Sigma). Prior to cell transfection, culture medium was replaced with fresh modified Dulbecco medium (Iscove's Modified Dulbecco's Medium, Life Technologies) containing 5% FBS without antibiotics. Packaging of rAAVs was carried out with helper plasmids pFD6, pRV1, and pH21 together with the respective pAAV-construct (shDnmt3a2, shControl, shUNC, shOAT1-1, shOAT1-2, or OAT1, lacZ, HDAC4 wt, or HDAC4 3SA). Following transfection, the medium was again replaced with fresh DMEM containing 10% FBS and antibiotics. Cells were collected at low speed centrifugation, resuspended in 150 mM NaCl-10mM Tris-HCl (pH 8.5) and lysed by incubation with 0.5% sodium deoxycholate followed by freeze-thaw cycles. Recombinant AAVs were purified using heparin affinity columns (HiTrap Heparin HP, GE Healthcare). rAAVs stocks were concentrated using Amicon Ultra-4 centrifugal filter devices (Millipore).
Recombinant AAVs were intra-spinally injected *in vivo* (see 2.1.1) or used to infect hippocampal and spinal cord primary cultures (see 2.6).

2.5 siRNAs

Small interfering RNA (siRNA) sequences targeting OAT1 (*slc22a6*) or negative control siRNA (Cat. no.: 1022076) from Qiagen were intrathecally delivered using the *in vivo*-jetPEI® transfection reagent (Polyplus transfection) according to the manufacturer's description. Equal parts of the siRNA sequences (Table 3) were combined at a stock concentration of 20 µM and used to prepare the siRNA/PEI complex solution. Solution A, containing a 1:1 dilution of 10% glucose solution with mixed siRNAs (5 µM final [c]), was mixed with solution B, containing a 1:1 dilution of 10% glucose solution with 0.12 µl of PEI reagent per 1 µg of siRNA, and incubated for 15 min at RT before use. 10 µl of solution were intrathecally delivered once per day for three consecutive injections, before behavioral assessment.

Table 3: List of siRNAs

siRNA	Target sequence	Catalog No.
Mm_Slc22a6_1	AAGGAACTGACTCTAAACAAA	SI01420783
Mm_Slc22a6_2	TCGGAAGGTGCTGATCTTGAA	SI01420790
Mm_Slc22a6_3	ATCCTAGTGAATGGCATAATA	SI01420797
Mm_Slc22a6_4	CCCAGACAATTAAATAAATTT	SI01420804

2.6 Neuronal cultures and treatments

Primary cultures were prepared from newborn C57BL/6J mice. Pups were quickly decapitated and kept in cold phosphate-buffered saline (PBS). Isolation and culturing of hippocampal neurons was performed by Iris Bünzli-Ehret according to established protocols (Bading and Greenberg, 1991, Bading et al., 1993, Zhang et al., 2011a). In parallel, spinal cord cultures were prepared as follows: 5 ml Kynurenic acid/$MgCl_2$ solution (Ky/Mg) and 68.8 µl NaOH (0.2 M) were added to 45 ml of dissociation medium (DM) and stored at RT. Pubs were transferred into a dish containing DM (+Ky/Mg) and the complete spinal cord was quickly removed and cleaned from meningeal tissue. Spinal cords were transferred into a sterile round-bottomed tube containing pre-warmed (37°C) enzyme solution (22.5 mg L-cysteine (Sigma Aldrich) and 500 U papain (CellSystems GmbH) in 50 ml DM (+Ky/Mg)) and incubated, two times for 20 min at 37°C in a water bath, while slowly and constantly stirring. The

tissue got washed three times with 2 ml DM (+Ky/Mg) for 1 min each and subsequently incubated two times for 5 min in inhibitor solution (1% trypsin inhibitor (Sigma Aldrich) in DM (+Ky/Mg)) at 37°C to stop the enzymatic reaction. Tissue was then washed three times for 1 min in 2 ml of growth medium (GM) and dissociated three times in 2 ml GM by triturating the tissue with a pipette (2x 50 and 1x 20 repetitions). In-between dissociation steps, the cell suspension was allowed to rest for 5 min. The complete cell suspension was finally diluted with pre-warmed "OptiMEM"/glucose solution (Invitrogen), to obtain a final concentration of 0.75 x 10^6 cells/ml. Depending on the experimental setup, cells were plated on poly-D-lysine and laminin-coated 35 mm dishes with or without glass coverslips or 4-well plates. 2.5 h after plating, growth medium was replaced. In order to inhibit proliferation of non-neuronal cells, 2.8 µM cytosine β-D-arabinofuranoside (Ara-C, Sigma Aldrich) was added into the culturing medium after three days *in vitro* (DIV) for hippocampal cells and after 4 DIV for spinal cord neurons.

DNA transfections were performed on DIV 8 using "Lipofectamine 2000" (Invitrogen) for 2.5 h at 37°C (Wiegert et al., 2007) before it was replaced with transfection medium (TM). TM consisted of a salt-glucose-glycine (SGG) solution supplemented with 10% minimum essential medium (Life Technologies) plus sodium selenite (2.9 µM), insulin (72 µM), transferrin (7.2 µM), and penicillin-streptomycin (0.5%). Cells which were not used for transfection received a full medium change to TM, instead. Experiments were done at DIV 10, if not stated otherwise, and fixed or harvested for further analysis according to experimental time points. All drug treatments of cultured neurons were performed at 37°C and 5% CO_2. Control cells were treated with respective vehicle only.

Neurons used for morphometric analysis were co-transfected with 0.3 µg/ml hrGFP and 1.5 µg/ml of the respective plasmid DNA (lacZ, HDAC4 wt, HDAC4 3SA, HDAC3, or HDAC11). In order to develop a mature and rich network of processes, morphology of cultured neurons was not analyzed until DIV 13, except for cells in Figure 12A-C, which were already analyzed at DIV 10.

Transfected cells in Figure 12Figure 13 were treated with 100 ng/ml recombinant mouse VEGFD (R&D Systems GmbH) or 100 ng/ml recombinant mouse VEGFC (Biocat) over a period of three days until analysis.

Hippocampal neurons used to determine the subcellular localization of endogenous HDAC4 were either treated with 20 µM NMDA (*N*-methyl-*D*-aspartate), 50 µM TBOA (*DL*-threo-β-benzyloxyaspartate), and/or 10 µM dizocilpine (MK 801) for 1 hour.
Cultured spinal cord neurons used to characterize the subcellular shuttling and expression of endogenous HDACs were treated with 50 µM bicuculline (Bic) at DIV 13/14 over a time period of 0.5 h, 2 h, or 8 h, inducing synaptic activity by antagonizing $GABA_A$ receptors (disinhibition).
Hippocampal and spinal cord cultures used for QRT-PCR analysis were infected with respective rAAV-constructs on DIV 3 and maintained at 37°C, 5% CO_2 for one additional week prior to harvesting for RNA extraction (DIV 10).

Table 4: Cell culture media

Reagent	Final concentration
Dissociation medium (DM)	
Na_2SO_4	82 mM
$MgCl_2$	5.85 mM
K_2SO_4	30 mM
$CaCl_2$	0.25 mM
HEPES	1 mM
Glucose	20 mM
Phenol red (in H_2O)	0.2% (v/v)
Ky/Mg solution	
Kynurenic acid	10 mM
$MgCl_2$	100 mM
HEPES	5 mM
Phenol red	0.5% (v/v)
NaOH (in H_2O)	12.5 mM
Growth medium (GM)	
Rat serum	1% (v/v)
B-27 supplement (Invitrogen)	2% (v/v)
Penicillin/Streptomycin	0.5% (v/v)

L-glutamine (in “Neurobasal A” medium) (Invitrogen)	0.5 mM
Salt glucose glycine solution (SGG)	
NaCl	114 mM
$NaHCO_3$	26 mM
KCl	5.3 mM
$MgCl_2$	1 mM
$CaCl_2$	2 mM
HEPES	10 mM
Glycine	1 mM
Glucose	30 mM
Sodium pyruvate	0.5 mM
Phenol red (in H_2O)	0.2% (v/v)

All reagents are from Sigma Aldrich, if not stated otherwise. Culturing media were sterile filtered and stored at 4°C.

2.7 Immunocytochemistry (ICC)

Following transfection and/or treatments, cells were fixed for 20 min at RT with 4% paraformaldehyde (PFA), 4% sucrose in PBS (pH 7.4). Cells were washed three times with PBS and antibodies were diluted in GDB (0.1% gelatin, 0.3% Triton X-100, 15 mM Na_2HPO_4, 400 mM NaCl), whereby gelatin prevents unspecific binding of the antibodies, while Triton X-100 is used for permeabilization of the cells. Subsequently cells were incubated for 3 h in primary antibodies and 1 h in secondary antibodies. In between and after the incubation with antibodies cells were washed using HPO_4/NaCl buffer (20 mM Na_2HPO_4 and 500 mM NaCl). Nuclei were visualized using Hoechst staining (1:6000). Coverslips were mounted with Mowiol 4-88 (Calbiochem) on regular glass microscopy slides.

Table 5: Primary antibodies (Immunocytochemistry)

Antibody	Species	Type	Dilution	Product code
AcH3	rabbit	IgG; monoclonal	1:200	#9649 (Cell Signaling)
Flag-M2	mouse	IgG; monoclonal	1:200	F3165 (Sigma Aldrich)
HA	rabbit	IgG; polyclonal	1:200	sc-805 (Santa Cruz)
HDAC1	rabbit	IgG; polyclonal	1:200	PA1-860 (Thermo Scientific)
HDAC3	rabbit	IgG; polyclonal	1:200	#2632 (Cell Signaling)
HDAC4	rabbit	IgG; monoclonal	1:200	#7628 (Cell Signaling)
HDAC5	rabbit	IgG; monoclonal	1:200	#20458 (Cell Signaling)
HDAC7	rabbit	IgG; polyclonal	1:200	H2662 (Sigma Aldrich)
HDAC9	rabbit	IgG; polyclonal	1:200	ab18970 (Abcam)
HDAC10	rabbit	IgG; polyclonal	1:200	ab53096 (Abcam)
HDAC11	rabbit	IgG; polyclonal	1:200	ab18973 (Abcam)
NeuN	mouse	IgG; monoclonal	1:500	MAB377 (Merck)
OAT1	rabbit	IgG; polyclonal	1:200	ab135924 (Abcam)

Table 6: Secondary antibodies (Immunocytochemistry)

Antibody	Dilution	Product code
Alexa Fluor® 488 goat anti-rabbit IgG (H+L)	1:400	#A-11008 (Life Technologies)
Alexa Fluor® 594 goat anti-mouse IgG (H+L)	1:400	#A-11005 (Life Technologies)
Alexa Fluor® 633 goat anti-rabbit IgG (H+L)	1:400	#A-21070 (Life Technologies)

2.8 Immunohistochemistry (IHC)

Animals were euthanized, according to experimental timepoints, with an overdose of Narcoren (300 mg/kg, i.p.) and transcardially perfused with PBS followed by 10% formalin (Sigma Aldrich). Spinal cords and dorsal root ganglia (DRG) were isolated and post-fixed for 2 h in 10% formalin. Subsequently, tissues were incubated in 30% sucrose (in PBS) at 4°C overnight for cryoprotection. Samples were embedded into Tissue Freezing Medium® (Thermo Scientific) and 20 µm sections of the lumbar

spinal cord segments L3-L5, and respective DRG, were cut at -15°C using a Leica C1950 or Thermo NX70 Cryostat. Serial sections were mounted on Superfrost Plus Adhesion Microscope Slides™ (Thermo Scientific). All animals from one experimental group were processed at the same time and slides were stored at -20°C until further use. For immunohistochemical staining, slides were dried for 20 min at 50°C and sections were encircled with a hydrophobic barrier using a “PAP pen” (Science Services). Sections were subsequently blocked and permeabilized using 10% normal goat serum (NGS) or normal donkey serum (NDS) in 2x GDB (0.2% gelatin, 0.6% Triton X-100, 30 mM Na_2HPO_4, 800 mM NaCl) for 1.5 h at RT. Slides were washed three times for 10 min at RT with 1% Triton X-100 (in PBS). Antibodies were diluted, according to their host species, in respective blocking solution, and sections were incubated overnight at 4°C in a moist chamber with primary antibodies. Slides were washed again, as described before, and sections were incubated for 1.5 h at RT with secondary antibodies (diluted in blocking solution). Slides were again washed and optionally incubated with 0.1% “Sudan Black B” (SBB) (Sigma Aldrich), a lipophilic dye, in 70% ethanol (EtOH) for 10 min at RT in order to sequester autofluorescent signals (Schnell et al., 1999). Slides were washed in PBS and Hoechst 33258 was used for visualization of nuclei. Coverslips were mounted with Mowiol 4-88 (Calbiochem).

Table 7: Primary antibodies (Immunohistochemistry)

Antibody	Species	Type	Dilution	Product code
AcH3	rabbit	IgG; monoclonal	1:1000	#9649 (Cell Signaling)
Flag-M2	mouse	IgG; monoclonal	1:200	F3165 (Sigma Aldrich)
HA	rabbit	IgG; polyclonal	1:200	sc-805 (Santa Cruz)
HDAC1	rabbit	IgG; polyclonal	1:200	PA1-860 (Thermo)
HDAC4	rabbit	IgG; monoclonal	1:500	#7628 (Cell Signaling)
HDAC6	rabbit	IgG; polyclonal	1:200	ab1440 (Abcam)
HDAC7	rabbit	IgG; polyclonal	1:500	H2662 (Sigma Aldrich)
HDAC9	rabbit	IgG; polyclonal	1:500	ab18970 (Abcam)
HDAC10	rabbit	IgG; polyclonal	1:200	ab53096 (Abcam)
NeuN	mouse	IgG; monoclonal	1:1000	MAB377 (Merck)
OAT1	rabbit	IgG; polyclonal	1:500	ab135924 (Abcam)

Table 8: Secondary antibodies (Immunohistochemistry)

Antibody	Dilution	Product code
Alexa Fluor® 488 goat anti-mouse IgG (H+L)	1:1000	#A-11001 (Life Technologies)
Alexa Fluor® 594 goat anti-mouse IgG (H+L)	1:1000	#A-11005 (Life Technologies)
Alexa Fluor® 488 goat anti-rabbit IgG (H+L)	1:1000	#A-11008 (Life Technologies)
Alexa Fluor® 594 goat anti-rabbit IgG (H+L)	1:1000	#A-11037 (Life Technologies)

2.9 Immunoblot analysis

To analyze target gene expression at protein level, animals were sacrificed using CO_2 and spinal cords were quickly isolated. Fresh tissue was rinsed in cold PBS, and the dorsal part of lumbar spinal cord segments L3-5 was dissected and homogenized in radioimmunoprecipitation assay (RIPA) buffer (150 mM NaCl, 1%Triton X-100, 0.57% sodium deoxycholate, 0.1% SDS, 50 mM Tris, pH 8, 1x Complete™ cocktail of protease inhibitors (Roche)). Homogenate was centrifuged and protein concentration was determined with a colorimetric protein assay (Bio Rad) based on the Bradford method using BSA as standard. Homogenates were mixed with 2x Laemmli sample buffer (160 mM Tris HCl, pH 6.8, 4% SDS, 30% glycerol, 0.02% bromophenol blue) and 1% dithiothreitol (DTT), as a reducing agent to cleave disulfide bridges, and heated for 5 min at 95°C in order to disrupt secondary and tertiary protein structures. For *in vitro* experiments, cultured cells were directly harvested in 2x Laemmli sample buffer (+1% DTT) from 35 mm dishes using a cell scraper (Corning Life Sciences) before incubation at 95°C for 5 min.

For SDS-PAGE 25 µg of each spinal cord protein sample, and 20 µl of culture tissue lysates, were loaded on a gel comprising a stacking gel (3.75% acrylamide) and a resolving gel with either 15% acrylamide for proteins with a molecular weight <50 kDa, or 7% for molecular weights >50 kDa. Discontinuous gel electrophoresis was performed at constant amperage (30 mA for stacking and 100 mA for separation) in running buffer (19 mM glycine, 2.5mM Tris, 0.01% SDS). Proteins were transferred on nitrocellulose membranes (Amersham™ 0.45 µm, GE

Healthcare) in transfer buffer (15 mM glycine, 2 mM Tris, 0.01% SDS, 20% methanol) at a constant voltage of 18 V for 2.5 h for proteins with a molecular weight >100 kDa, and for 1.5 h for molecular weights <100 kDa. Ponceau staining (SERVA) was performed to visualize proteins and membranes were subsequently blocked in 5% milk powder in PBST (1xPBS, 0.1% Tween 20 (Sigma Aldrich)) for 1 h at RT on a shaker. Membranes were incubated o/n with primary antibodies at 4°C, shaking. The next day, membranes were washed three times for 10 min with PBST and incubated with HRP-conjugated secondary antibodies for 45 min at RT on a shaker. Membranes were again washed and detected with enhanced chemiluminescence (ECL) solution (Clarity™, Bio Rad) and the "ChemiDoc™ Imaging System" (Bio Rad). For protein expression analysis of spinal cord dorsal horn tissue and neuronal cultures, relative protein band densities were measured using ImageJ/Fiji. Backgrounds of all images were subtracted. Relative protein band densities were calculated by normalizing to the loading control (β-actin or tubulin). For each time point, relative protein levels of treated samples were further normalized to relative protein levels of the control.

Table 9: Primary antibodies (Immunoblot analysis)

Antibody	Species	Type	Dilution	Product code
AcH3	rabbit	IgG; monoclonal	1:2000 (BSA)	#9649 (Cell Signaling)
β-actin	mouse	IgG; monoclonal	1:2000 (BSA)	sc-47778 (Santa Cruz)
c-fos	rabbit	IgG; polyclonal	1:2000 (Milk)	sc-52 (Santa Cruz)
Histone3	rabbit	IgG, polyclonal	1:4000 (BSA)	06-755 (Sigma Aldrich)
HA	mouse	IgG, polyclonal	1:1000 (Milk)	MMS-101R (Covance)
HDAC1	rabbit	IgG; polyclonal	1:2000 (Milk)	PA1-860 (Thermo)
HDAC3	rabbit	IgG; polyclonal	1:1000 (BSA)	#2632 (Cell Signaling)
HDAC4	rabbit	IgG; monoclonal	1:6000 (BSA)	#7628 (Cell Signaling)
HDAC5	rabbit	IgG; monoclonal	1:1000 (BSA)	#20458 (Cell Signaling)
HDAC6	rabbit	IgG; polyclonal	1:1000 (Milk)	ab1440 (Abcam)
HDAC7	rabbit	IgG; polyclonal	1:2000 (BSA)	H2662 (Sigma Aldrich)
HDAC9	rabbit	IgG; polyclonal	1:4000 (Milk)	ab18970 (Abcam)
HDAC10	rabbit	IgG; polyclonal	1:1000 (BSA)	ab53096 (Abcam)
HDAC11	rabbit	IgG; polyclonal	1:200 (BSA)	ab18973 (Abcam)

OAT1	rabbit	IgG; polyclonal	1:2000 (BSA)	ab135924 (Abcam)
Tubulin	mouse	IgG; monoclonal	1:400,000 (Milk)	T9026 (Merck)

Table 10: Secondary antibodies (Immunoblot analysis)

Antibody	Dilution	Product code
Peroxidase AffiniPure goat anti-mouse IgG (H+L)	1:5000	115-035-003 (Jackson Immuno Research)
Peroxidase AffiniPure goat anti-rabbit IgG (H+L)	1:5000	111-035-144 (Jackson Immuno Research)

2.10 Golgi-Cox staining

Golgi-Cox staining was performed using the "FD Rapid GolgiStain™ Kit" (FD Neurotechnologies), according to manufacturer's instructions and based on the principles of the method described by Ramón-Moliner (Ramón-Moliner, 1970). Fresh unfixed spinal cord tissue of animals expressing either lacZ, HDAC4 wt, or HDAC4 3SA, after intraspinal delivery of rAAV constructs for a minimum of three weeks, was quickly removed and washed in PBS. Subsequently, tissues were placed in pre-incubated impregnation solution (Solution A+B), containing potassium (di)chromate and mercuric chloride, for 12 days at RT and protected from light. During that time impregnation solution was replaced once after 24 hours of initial incubation. Next, tissues were transferred into solution C and incubated for four days, while replacing solution C once after 24 hours. Spinal cords were embedded into Tissue Freezing Medium® (Thermo Scientific), frozen in dry ice and 160 µm thick tissue sections were cut using a Thermo NX70 Cryostat at -22°C. Sections were mounted on gelatinized glass slides (#7802, Lab Scientific Inc.) carrying droplets of solution C. Excessive amounts of tissue freezing medium and solution C were carefully removed and slides were dried at RT o/n helping to prevent detachment of the sections during the staining procedure. The following day, slides were rinsed 2x 4 min in cold water and placed in staining solution D+E for 10 min, while gently shaking. After another washing step in water, sections were sequentially dehydrated in ethanol with increasing concentrations (50%, 75%, 95%, 100%) for 4 min, each. Sections were cleared in xylene (Sigma Aldrich) for 12 min and subsequently

mounted with glass coverslips using “Eukitt® Quick-hardening mounting medium” (Sigma Aldrich). Slides were stored at RT in the dark until further analysis.

2.11 Data Analyses

2.11.1 Morphometric analyses

Primary hippocampal and spinal cord cultured neurons used for morphometric analyses, were analyzed two or five days after transfection, as indicated in results, using a Leica TCS SP2 or SP8 laser-scanning confocal microscope.

Golgi-stained tissue sections of the lumbar spinal cord were examined using a Nikon Eclipse Ni-E upright automated microscope with a Nikon DS-Ri2 camera. Dorsal horn neurons located within lamina V with at least three primary dendrites, completely impregnated and a cell body diameter bigger than 20 µm (Simonetti et al., 2013, Cao et al., 2017) were included in the analysis. Even though these criteria do not imply a physiological characterization of analyzed neurons, they were thought to control for the vast morphological diversity of spinal cord dorsal horn neurons. Per condition (rAAV-lacZ, -HDAC4 wt, -HDAC4 3SA) 23-31 neurons from four independent experiments, identified in this manner, were included into analyses. For morphometric analyses, total dendritic length and complexity of single neurons were calculated using Fiji-software (Schindelin et al., 2012). A z-stack acquisition was imported, calibrated and manually traced using the simple neurite tracer plugin (Longair et al., 2011). Total dendritic length was determined as the sum of the lengths of all dendrites. For three-dimensional Sholl analysis (Sholl, 1953), the shell interval was set to 5 µm using a plugin available for Fiji. Total number of intersections was defined by the sum of all intersections between the traced dendrites and the shells used for Sholl analysis up to a radius of 185 µm. In primary hippocampal cultured neurons, dendritic spine density over randomly chosen 20 µm dendrite portions was manually computed.

All analyses were performed blind. Number of analyzed neurons for each experimental condition and number of independent experiments are indicated in the respective figure legend.

2.11.2 Quantification of nuclear signal in neuronal cultures

Cells treated with 50 µM Bic or either with 20 µM NMDA, 50 µM TBOA, and/or 10 µM MK 801, were fixed and immunostained with antibodies directed against HDAC1, -3, -4, -5, -7, -9, -10, -11 or AcH3. Nuclei were visualized using Hoechst. Up to eight random images of each condition were acquired using a Nikon Ni-E upright fluorescence microscope or Leica DM IRBE inverted fluorescence microscope with a 40x objective. Fluorescent intensities of nuclear antibody signals were measured in ImageJ using the Hoechst channel to define the nuclei as region of interest. Measured intensity values were normalized to vehicle-treated controls. Representative images were acquired using a Leica TCS SP2 or SP8 laser-scanning confocal microscope.

2.11.3 Quantification of cell death rate

Cell death rate of cultured spinal cord neurons, co-transfected with hrGFP and either lacZ, HDAC4 wt or HDAC4 3SA, was determined by manually counting the number of collapsed or disintegrated nuclei of transfected neurons over the total number of transfected cells, using a Leica DM IRBE inverted fluorescence microscope with a 40x objective.

2.11.4 Quantification of nuclear signal in spinal cord neurons

Tissue sections of the lumbar spinal cord segments L3-L5 of mice treated with either CFA or saline were immunostained with antibodies directed against HDAC4, -7, -9, AcH3, or OAT1. Nuclei were co-labelled with Hoechst and NeuN as neuronal marker. Up to ten images of the dorsal horn area were acquired per condition using a Leica DM IRBE inverted fluorescence microscope with a 20x objective. Fluorescent intensities of nuclear antibody signals within neurons of the dorsal horn were measured in ImageJ using the Hoechst and NeuN channel to define the nuclei of neuronal cells as region of interest. Measured intensity values were normalized to saline-injected controls.

2.11.5 Statistical analyses

Statistical analyses were performed using Prism 6 software (GraphPad Software Inc.). Results were considered to be statistically significant for significance levels of $p<0.05$ (*), $p<0.01$ (**), $p<0.001$ (***), or $p<0.0001$ (****). Performed statistical tests are indicated in the figure legends. Two-tailed Student's t-test was used for the comparison of two conditions depending on the same variable. One-way ANOVA was used for comparisons of more than two conditions depending on the same variable, followed by Dunnett's post hoc test for comparison to control and by Tukey's post hoc test for comparisons in-between conditions. Experiments depending on two independent variables, like behavioral tests, were analyzed using two-way ANOVA with repeated measures followed by Dunnett's post hoc test for comparisons to basal values and Tukey's post hoc test for comparisons between conditions. Multiple t-tests were used instead, when comparing only two conditions. All data are presented as means ± SEM or SD, as indicated in the figure legends.

3 Results

3.1 Histone deacetylase 4 shapes neuronal morphology

3.1.1 Subcellular localization of HDAC4 affects neuronal morphology

Nuclear calcium signaling regulates changes in neuronal morphology, as well as the subcellular localization of class IIa HDACs (Schlumm et al., 2013, Mauceri et al., 2011, Mauceri et al., 2015). We investigated if both events are functionally linked. As model system, we used primary neuronal hippocampal cultures. We focused our work on HDAC4, a member of class IIa HDACs (Figure 4), which is abundantly expressed in hippocampal neurons (Broide et al., 2007) and which shuttles in a synaptic activity and nuclear calcium dependent manner between cytosol and nucleus (Chawla et al., 2003, Schlumm et al., 2013). To test whether HDAC4 subcellular shuttling is impacting neuronal structure, we made use of the constitutively nuclear-localized dominant active mutant of HDAC4 (HDAC4 3SA), which has been characterized previously (Schlumm et al., 2013, Chawla et al., 2003). HDAC4 3SA cannot shuttle between the nucleus and the cytoplasm, due to substitutions of three critical phosphorylation sites important for its nuclear export (Figure 5).

Hippocampal cultures were transfected with plasmids driving the expression of either HDAC4 3SA, HDAC4 wildtype (HDAC4 wt), leading to an overexpression of HDAC4 in addition to the endogenous gene, or lacZ, encoding for the bacterial enzyme β-galactosidase, as control. All constructs carried a flag tag, allowing immuno-detection to verify their subcellular localization. Co-transfection with hrGFP was performed to visualize the entire dendritic architecture of transfected neurons (Mauceri et al., 2011). In line with previous observations, HDAC4 wt showed a predominantly cytoplasmic distribution (Schlumm et al., 2013), whereas HDAC4 3SA was only present in the nucleus, as expected (Figure 8A). LacZ was equally distributed in both compartments. Morphometric analysis showed that the size and complexity of the dendritic tree was severely declined in neurons expressing the nuclear HDAC4 mutant compared to cells expressing either HDAC4 wt or lacZ (Figure 8A). No significant change in total dendritic length could be detected between lacZ and HDAC4 wt expressing neurons. However, dendritic length was significantly reduced

in HDAC4 3SA expressing neurons in comparison to both controls (lacZ, 3779 µm ± 243 µm; HDAC4 wt, 4037 µm ± 264 µm; HDAC4 3SA, 2138 µm ± 115 µm) (Figure 8B). Sholl analysis (Sholl, 1953) was performed to estimate dendritic complexity and showed a reduced number of intersections in neurons expressing HDAC4 3SA compared to both controls (lacZ, 583 ± 35; HDAC4 wt, 537 ± 44; HDAC4 3SA, 324 ± 19) (Figure 8C-D). In contrast, spine density was not affected by the nuclear localized HDAC4 mutant (Figure 8E-F).

These data show that nuclear accumulation of HDAC4 affects the dendritic architecture of cultured hippocampal neurons.

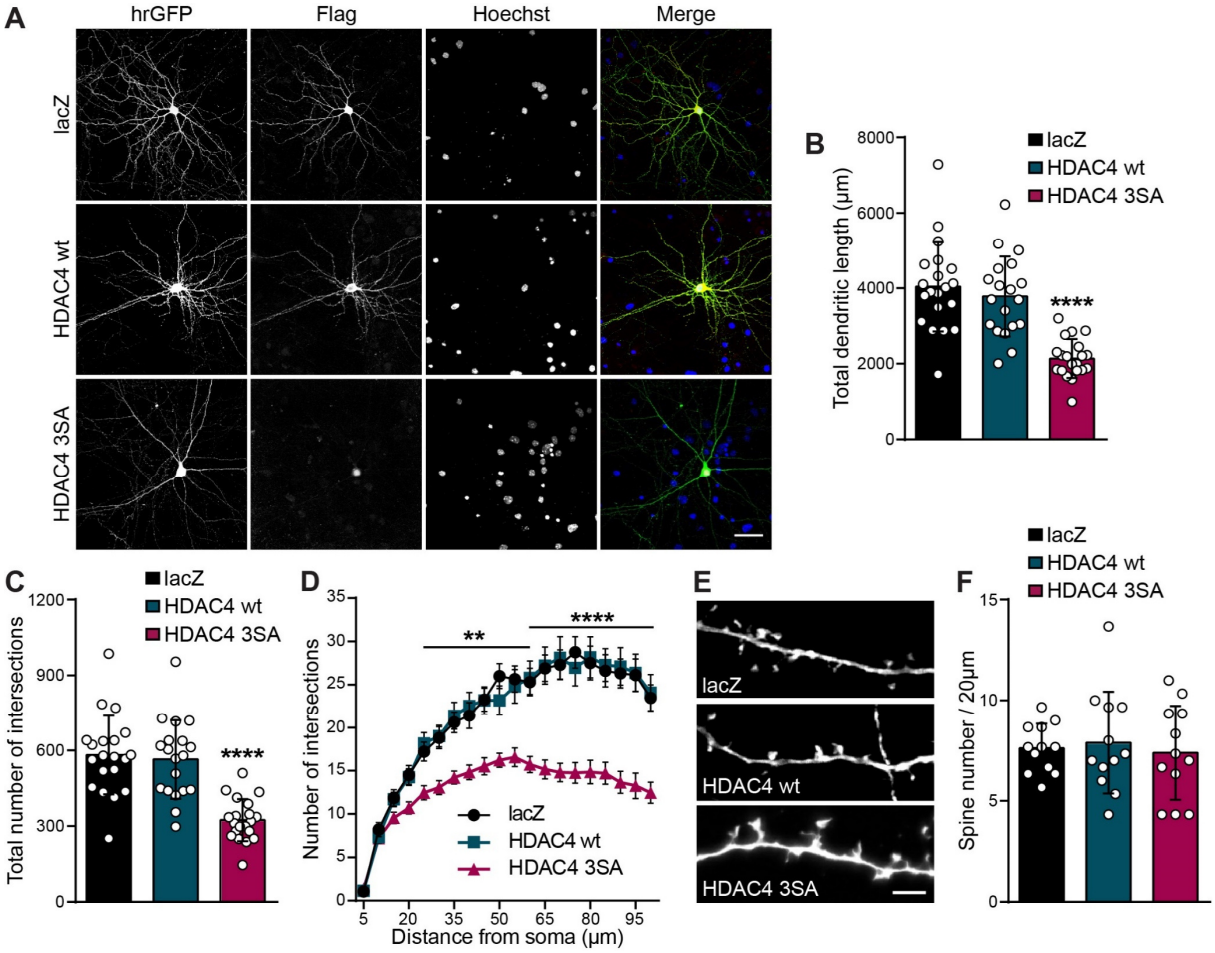

Figure 8: HDAC4 nuclear accumulation impairs neuronal morphology.

(A) Representative images of cultured hippocampal neurons at DIV 13, co-transfected with hrGFP and flag-tagged constructs lacZ, HDAC4 wt, or HDAC4 3SA for 5 days. hrGFP fluorescence reveals complete dendritic architecture and immunolabeling of flag tags shows the subcellular localization of transgenes. Nuclei were labelled with Hoechst. Scale bar is 40 µm. (B) Quantification of the total dendritic length of hippocampal neurons transfected as indicated. (C) Total number of intersections derived from Sholl analysis (D). (E) Representative images of dendritic spines of transfected hippocampal neurons and quantification of spine density (F). Scale bar is 5 µm. In total, 20 neurons

(lacZ and HDAC4 3SA) and 19 neurons (HDAC4 wt) from five independent experiments (n=5) were analyzed for each construct (B-D). For spine density analysis 12 neurons from three independent experiments (n=3) were analyzed for each construct (F). Statistically significant differences were determined by one-way ANOVA (B-C, F) and two-way ANOVA (D), followed by Tukey's post hoc test. ****, $p < 0.0001$; **, $p < 0.01$. In bar graphs, each point represents a value derived from one neuron. Graphs represent mean ± S.D.

3.1.2 Activation of eNMDARs triggers HDAC4 nuclear accumulation

Endogenous HDAC4 in hippocampal neurons is predominantly localized in the cytoplasm (Schlumm et al., 2013, Darcy et al., 2010, Sando et al., 2012). However, deprivation of synaptic activity (Sando et al., 2012, Schlumm et al., 2013), as well as several neuronal pathologies, like stroke, Alzheimer's or Parkinson's disease, result in a nuclear accumulation of HDAC4 (Kassis et al., 2015, Shen et al., 2016, Wu et al., 2016, Yuan et al., 2016, Li et al., 2012). Those neurodegenerative diseases have all been commonly associated with the noxious downstream signaling triggered by activation of extrasynaptic *N*-methyl-*D*-aspartate receptors (eNMDARs), (Hardingham et al., 2002, Parsons and Raymond, 2014, Bading, 2017, Hardingham and Bading, 2010) and just recently, changes in the subcellular localization of HDACs have been linked to excitotoxicity-triggered degeneration of retinal ganglion cells in mice (Schlüter et al., 2019).

We investigated if activation of eNMDARs in hippocampal neurons triggers nuclear accumulation of HDAC4, thereby affecting neuronal morphology (Figure 8). We exposed hippocampal cultures to bath application of NMDA, resulting in a direct activation of eNMDARs (Hardingham et al., 2002), or treated the cells with the glutamate re-uptake inhibitor *DL*-threo-β-benzyloxyaspartate (TBOA), triggering eNMDAR stimulation by blocking the clearance of glutamate from the extrasynaptic space via neighboring cells expressing excitatory amino acid transporters (EAATs) (Hardingham et al., 2002). Both NMDA and TBOA treatments led to nuclear accumulation of endogenous HDAC4 (Figure 9). Co-administration of dizocilpine (MK801), an open-channel, noncompetitive antagonist of NMDA receptors, prevented this effect. In contrast, cells treated only with MK801, which would block preferentially the synaptic NMDARs, showed increased nuclear HDAC4 levels, which is in line with previous observations describing a nuclear accumulation due to deprivation of basal synaptic activity (Schlumm et al., 2013, Sando et al., 2012).

Taken together, our results indicate that activation of eNMDARs promotes re-localization of HDAC4 from the cytoplasm towards the nucleus.

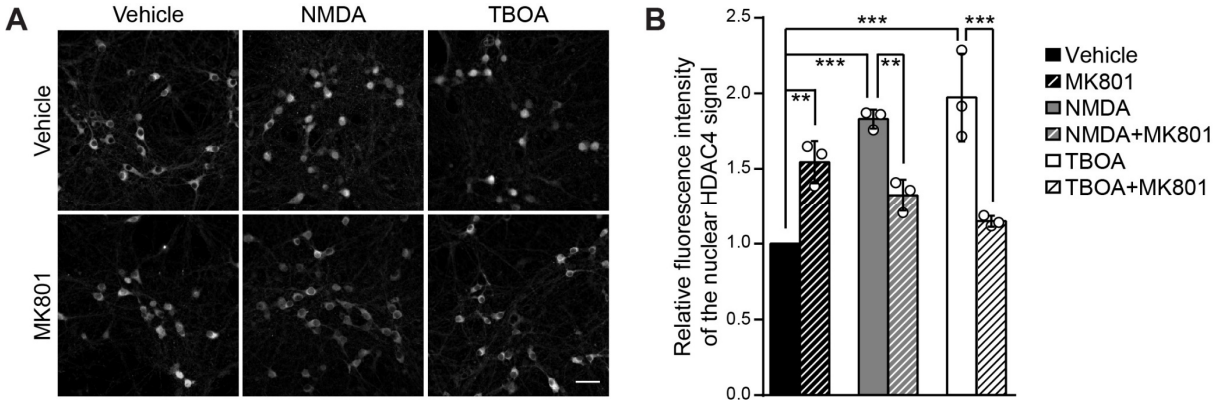

Figure 9: Activation of eNMDARs triggers HDAC4 nuclear accumulation.
(A) Representative images of cultured hippocampal neurons immunostained for endogenous HDAC4. Cells were either treated for 1 h with NMDA (20 µM), TBOA (50 µM), and/or MK801 (10 µM), as indicated. Controls remained untreated (vehicle). Scale bar is 40 µm. (B) Quantification of the reactive fluorescent intensity of the nuclear HDAC4 signal normalized to respective untreated control. For each condition, three independent experiments were analyzed (n=3). Statistically significant differences were determined by one-way ANOVA followed by Tukey's post hoc test. ***, $p < 0.001$; **, $p < 0.01$. Each point represents the mean value derived from one experiment. Graphs represent mean ± S.D.

3.1.3 Other classes of HDACs do not regulate dendritic morphology

Next, we tested whether other classes of the HDACs family could also affect neuronal morphology. Therefore, we overexpressed HDAC3 (class I) and HDAC11 (class IV) using transfection of primary hippocampal cultures with epitope-tagged expression constructs for HDAC3 and -11. LacZ-expression was used as control and all cells were additionally co-transfected with hrGFP to visualize the complete neuronal structure (Figure 10A). Morphometric analyses showed no effects of HDAC3 or -11 on the total dendritic length (lacZ, 2499 µm ± 144 µm; HDAC3, 2681 µm ± 134 µm; HDAC11, 2838 µm ± 115 µm) (Figure 10B) and complexity (total number of intersections: lacZ, 389 µm ± 21 µm; HDAC3, 424 µm ± 21 µm; HDAC11, 450 µm ± 20 µm) (Figure 10C-D) of mature neurons. These results indicate a specific role for class IIa HDAC4 in regulating dendrite architecture.

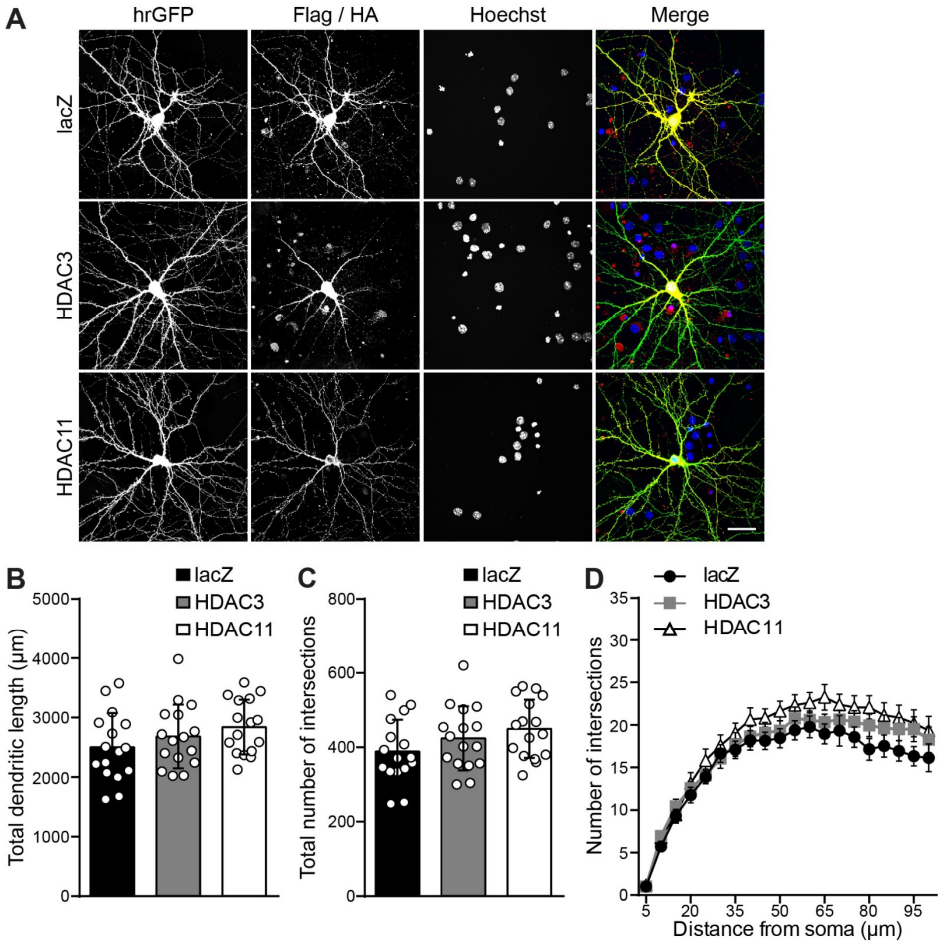

Figure 10: HDAC3 and 11 do not regulate dendritic morphology.
(A) Representative images of cultured hippocampal neurons at DIV 13, co-transfected with hrGFP and HA-tagged constructs HDAC3 and HDAC11, or lacZ (flag-tagged) for 5 days. hrGFP fluorescence reveals complete dendritic architecture and immunolabeling of epitope tags shows the subcellular localization of transgenes. Nuclei were labelled with Hoechst. Scale bar is 40 µm. (B) Quantification of the total dendritic length of hippocampal neurons transfected as indicated. (C) Total number of intersections derived from Sholl analysis (D). In total, 16 neurons from four independent experiments (n=4) were analyzed for each construct. Statistically significant differences were determined by one-way ANOVA (B-C) and two-way ANOVA (D), followed by Tukey's post hoc test. In bar graphs, each point represents a value derived from one neuron. Graphs represent mean ± S.D.

3.1.4 HDAC4 regulates the expression of VEGFD

Vascular endothelial growth factor D (VEGFD) has been previously described as key regulator of neuronal structure (Hemstedt et al., 2017, Mauceri et al., 2011, Mauceri et al., 2015). Its expression is controlled by nuclear calcium signaling and depends on the calcium buffering capacity of the nucleus (Mauceri et al., 2011, Mauceri et al., 2015). Moreover, it was recently shown how activation of extrasynaptic NMDARs leads to a decrease of VEGFD expression (Mauceri et al., 2020, Schlüter et al., 2020). We investigated if changes in the localization of HDAC4 would affect VEGFD expression. Primary hippocampal cultures were infected on DIV 3 either with rAAV-lacZ, rAAV-HDAC4 wt, or rAAV-HDAC4 3SA (performed by Dr. Daniela Mauceri) (Figure 11A). Uninfected cells were used as additional control. At DIV 10, neurons were harvested, and total RNA extracted (performed by Dr. Daniela Mauceri). Quantitative reverse transcriptase PCR (QRT-PCR) showed that expression levels of *vegfd* were indeed significantly reduced in neurons expressing the nuclear HDAC4 mutant, compared to neurons infected with the other constructs or uninfected controls (*vegfd*: rAAV-HDAC4 3SA, 0.77 ± 0.04; rAAV-HDAC4 wt, 1 ± 0.04; rAAV-lacZ, 1.13 ± 0.13) (Figure 11A). Moreover, subcellular localization of HDAC4 had no effect on the expression of other VEGF family members (*vegf* and *vegfc*), nor on relevant signaling receptors, VEGFR2 (*kdr*) and VEGFR3 (*flt4*). In an additional control experiment cells were either infected with rAAV-HDAC3, rAAV-HDAC11, or remained uninfected (Figure 11B). QRT-PCR revealed that mRNA levels of *vegfd* remained unaltered by the overexpression of class I and IV HDAC members (HDAC3 and HDAC11, respectively). At the same time, expression levels of *cxcr4*, a known molecular target of HDAC3 (Kim et al., 2010), were significantly reduced by overexpression of HDAC3, but not by HDAC11. To a similar extent, we found the expression of the previously identified target of HDAC11, *fez1* (Bryant et al., 2017), to be decreased in both HDAC11 and HDAC3 expressing cultures. These results suggest that HDAC4 contributes to the regulation of expression of the morphological regulator *vegfd* in hippocampal neurons.

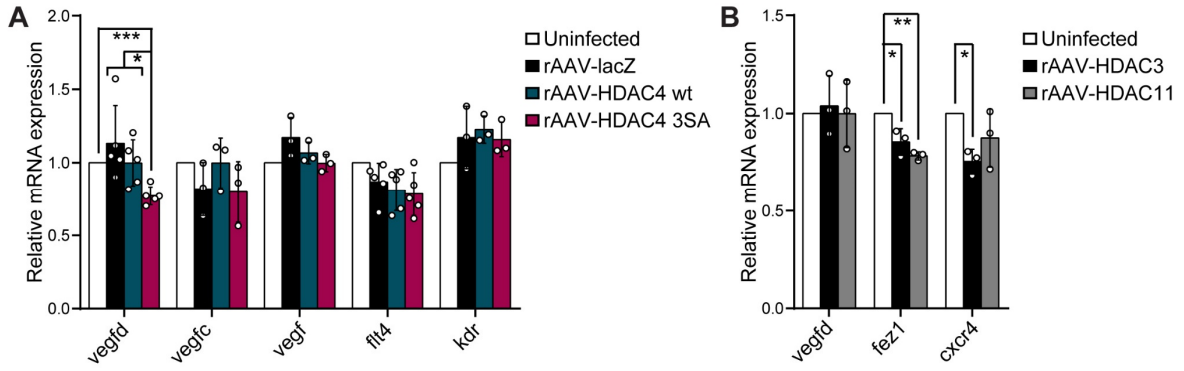

Figure 11: HDAC4 regulates the expression of VEGFD.
(A) QRT-PCR analysis of *vegfd* (n=5), *vegfc* (n=3), *vegf* (n=3), *flt4* (n=5), and *kdr* (n=3) mRNA levels in uninfected hippocampal neurons and in cells infected with rAAV-lacZ, rAAV-HDAC4 wt, or rAAV-HDAC4 3SA. (B) QRT-PCR analysis of *vegfd* (n=3), *fez1* (n=3), and *cxcr4* (n=3) mRNA levels in uninfected hippocampal neurons and in cells infected with rAAV-HDAC3 or rAAV-HDAC11. Expression values were normalized to uninfected controls. Statistically significant differences were determined by one-way ANOVA followed by Tukey's post hoc test. Graphs represent mean ± S.D. (Neuronal infections and QRT-PCR analysis in panel (A) were performed by Dr. Daniela Mauceri).

3.1.5 VEGFD prevents dendritic impairment and restores structural integrity

Given that nuclear accumulation of HDAC4 in neurons results in both, simplification of dendritic morphology (Figure 8) and downregulation of *vegfd* expression (Figure 11), we tested if supplementation of VEGFD in cells expressing the nuclear HDAC4 mutant could rescue neuronal morphology. Therefore, we made use of an expression construct encoding for VEGFD, which has been previously characterized (Mauceri et al., 2011, Hemstedt et al., 2017). Indeed, co-overexpression of VEGFD in hippocampal neurons could successfully compensate for downregulation of *vegfd* and prevent the loss of structural integrity due to HDAC4 3SA expression, without altering the morphology of control cells, expressing lacZ or HDAC4 wt (Litke et al., 2018) (data not shown; experiment was conducted and analyzed by Dr. Daniela Mauceri).

To investigate whether VEGFD is also able to restore dendritic structures after they have already been impaired by nuclear HDAC4, hippocampal neurons were transfected with expression vectors for lacZ, HDAC4 wt or HDAC4 3SA, and neuronal morphology was analyzed after two days of expression of the transgenes (at DIV 10), instead after five days of expression (DIV 13), as in previous

experiments. Morphometric analyses revealed that two days of HDAC4 3SA-expression were sufficient to significantly compromise dendritic architecture, compared to control neurons (total dendritic length: lacZ, 2617 µm ± 189 µm; HDAC4 wt, 2692 µm ± 188 µm; HDAC4 3SA, 1667 µm ± 106 µm (Figure 12A); total number of intersections: lacZ, 394 ± 28; HDAC4 wt, 421 ± 32; HDAC4 3SA, 252 ± 16 (Figure 12B-C). 100 ng/ml of recombinant VEGFD (rVEGFD) were applied to the culturing medium at DIV 10, two days after expression of the transgenes, when damage was already done (Figure 12A-C). Dendritic trees of cells were analyzed at DIV 13. Similar to previous results (Figure 8), HDAC4 3SA expressing neurons displayed reduced total dendritic length (lacZ, 2095 µm ± 134 µm; HDAC4 wt, 2399 µm ± 245 µm; HDAC4 3SA, 1194 µm ± 88 µm; Figure 12D-E) and a lower degree of structural complexity (total number of intersections: lacZ, 335 ± 24; HDAC4 wt, 384 ± 43; HDAC4 3SA, 185 ± 15; Figure 12F-G), compared to controls. In contrast, rVEGFD treatment successfully restored length and complexity in mutant expressing neurons, while, in accordance to previous observations (Mauceri et al., 2011, Mauceri et al., 2015, Hemstedt et al., 2017), it had no effect on control conditions (total dendritic length: lacZ + rVEGFD, 2320 µm ± 168 µm; HDAC4 wt + rVEGFD, 2138 µm ± 123 µm; HDAC4 3SA + rVEGFD, 1822 µm ± 116 µm; total number of intersections: lacZ + rVEGFD, 363 ± 29; HDAC4 wt + rVEGFD, 336 ± 20; HDAC4 3SA + rVEGFD, 280 ± 18) (Figure 12E-G). In summary, VEGFD-supplementation can prevent an impairment of the dendritic tree and even restore dendritic arborization after it has been compromised by nuclear HDAC4.

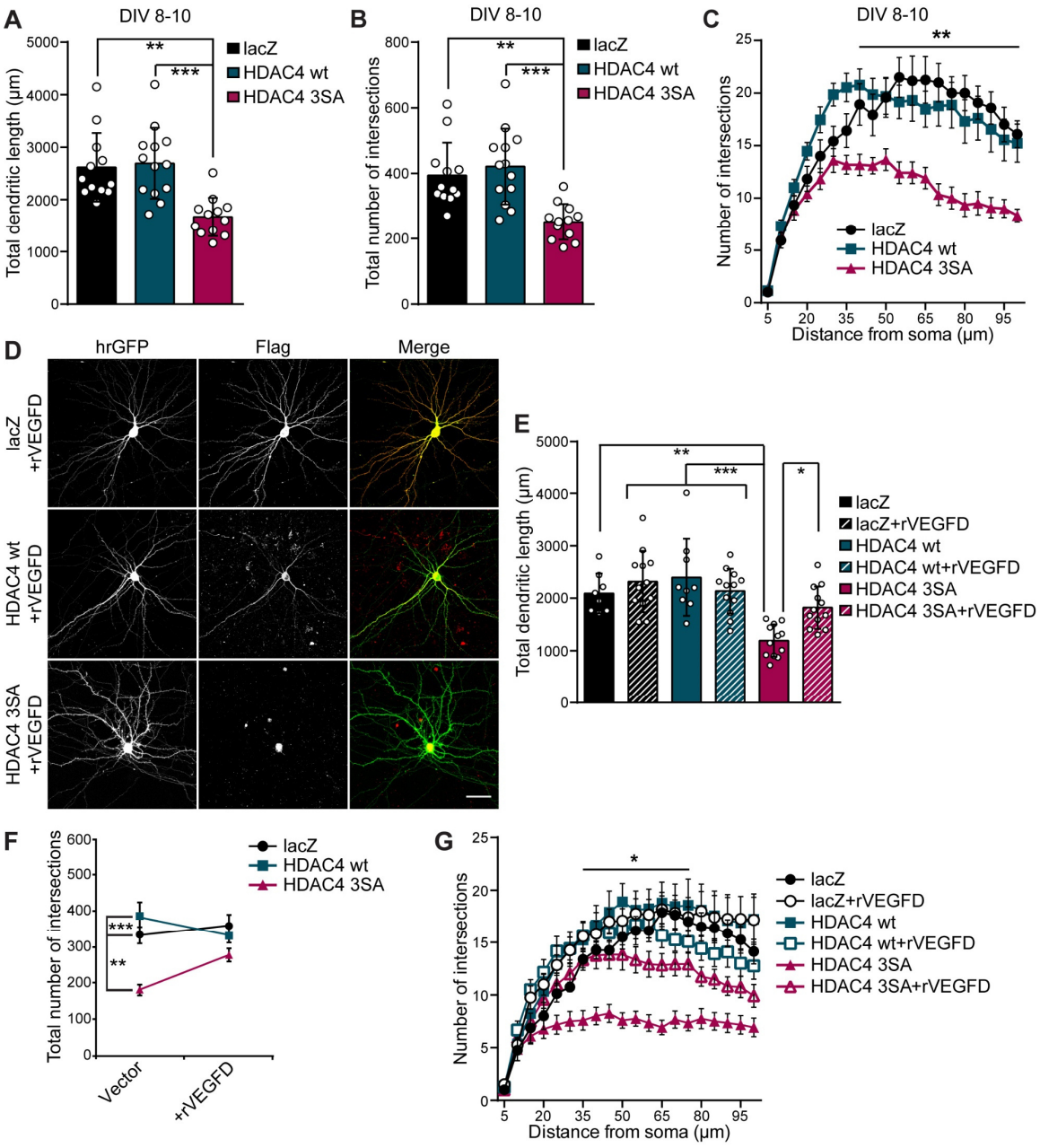

Figure 12: VEGFD prevents dendritic impairment and restores structural integrity.

(A) Quantification of the total dendritic length of hippocampal neurons at DIV 10. Cells were co-transfected with hrGFP and flag-tagged constructs lacZ, HDAC4 wt, or HDAC4 3SA at DIV 8. (B) Quantification of total number of intersections derived from Sholl analysis (C) at DIV 10, transfected as indicated. (D) Representative images of cultured hippocampal neurons at DIV 13, transfected as in A, and treated or not with rVEGFD (100 ng/ml) for three days. hrGFP fluorescence reveals complete dendritic architecture and flag tags were immunostained with Alexa 594. Scale bar is 40 µm. (E) Quantification of the total dendritic length of hippocampal neurons transfected as indicated, with or without treatment with rVEGFD for three days. (F) Quantification of total number of intersections at DIV 13, derived from Sholl analysis (G), in hippocampal neurons transfected as indicated, with or without treatment with rVEGFD for three days. For analyses at DIV 10, 12 (lacZ and HDAC4 3SA) and

13 neurons (HDAC4 wt) from three independent experiments (n=3) were analyzed for each construct (A-C). At DIV 13, 8 (lacZ), 9 (HDAC4 wt), and 12 neurons (lacZ + rVEGFD; HDAC4 wt + rVEGFD; HDAC4 3SA; HDAC4 3SA + rVEGFD) from three independent experiments (n=3) were analyzed for each construct (E-G). Statistically significant differences were determined by one-way ANOVA (A-B, E-F) and two-way ANOVA (C, G), followed by Tukey's post hoc test. ***, $p < 0.001$; **, $p < 0.01$; *, $p < 0.05$. In bar graphs, each point represents a value derived from one neuron. Graphs represent mean ± S.D.

3.1.6 VEGFC cannot restore dendritic morphology

VEGFC is the closest homologue of VEGFD and belongs to the same family of growth factors. Both are secreted factors and activate the same tyrosine kinase receptors (VEGFR2 and -3) (Yamazaki and Morita, 2006).

Although expression of HDAC4 3SA did not significantly affect expression levels of *vegfc* (Figure 11), we tested in a control experiment, whether application of recombinant VEGFC (rVEGFC) would have an ameliorating effect on dendritic morphology in HDAC4 mutant expressing cells. Using the same experimental strategy, 100 ng/ml of rVEGFC were added to the culturing medium for three days *in vitro*. Total dendritic length of all neurons expressing HDAC4 3SA, with or without rVEGFC treatment, was severely impaired in comparison to lacZ or HDAC4 wt transfected cells (lacZ, 2797 µm ± 211 µm; HDAC4 wt, 2676 µm ± 150 µm; HDAC4 3SA, 1593 µm ± 101 µm; lacZ + rVEGFC, 2944 µm ± 150 µm; HDAC4 wt + rVEGFC, 2726 µm ± 151 µm; HDAC4 3SA + rVEGFC, 1546 µm ± 105 µm) (Figure 13A-B). Furthermore, supplementation of VEGFC could not restore the complexity of dendritic trees (total number of intersections: lacZ, 421 ± 29; HDAC4 wt, 404 ± 24; HDAC4 3SA, 230 ± 15; lacZ + rVEGFC, 451 ± 22; HDAC4 wt + rVEGFC, 424 ± 22; HDAC4 3SA + rVEGFC, 233 ± 16) (Figure 13C-D). Thus, in contrast to VEGFD, VEGFC cannot rescue neuronal morphology of cells affected by nuclear-localized HDAC4.

In summary, our experiments showed that nuclear accumulation of HDAC4, which can be triggered in neurons by activation of eNMDARs, leads to a downregulation of *vegfd*, compromising dendritic arbor integrity in hippocampal neurons. Supplementation of VEGFD, but not VEGFC, can counteract these detrimental effects and even restore neuronal morphology after dendritic structures have been

destroyed. The presented results have been published in *The Journal of Biological Chemistry* (Litke et al., 2018).

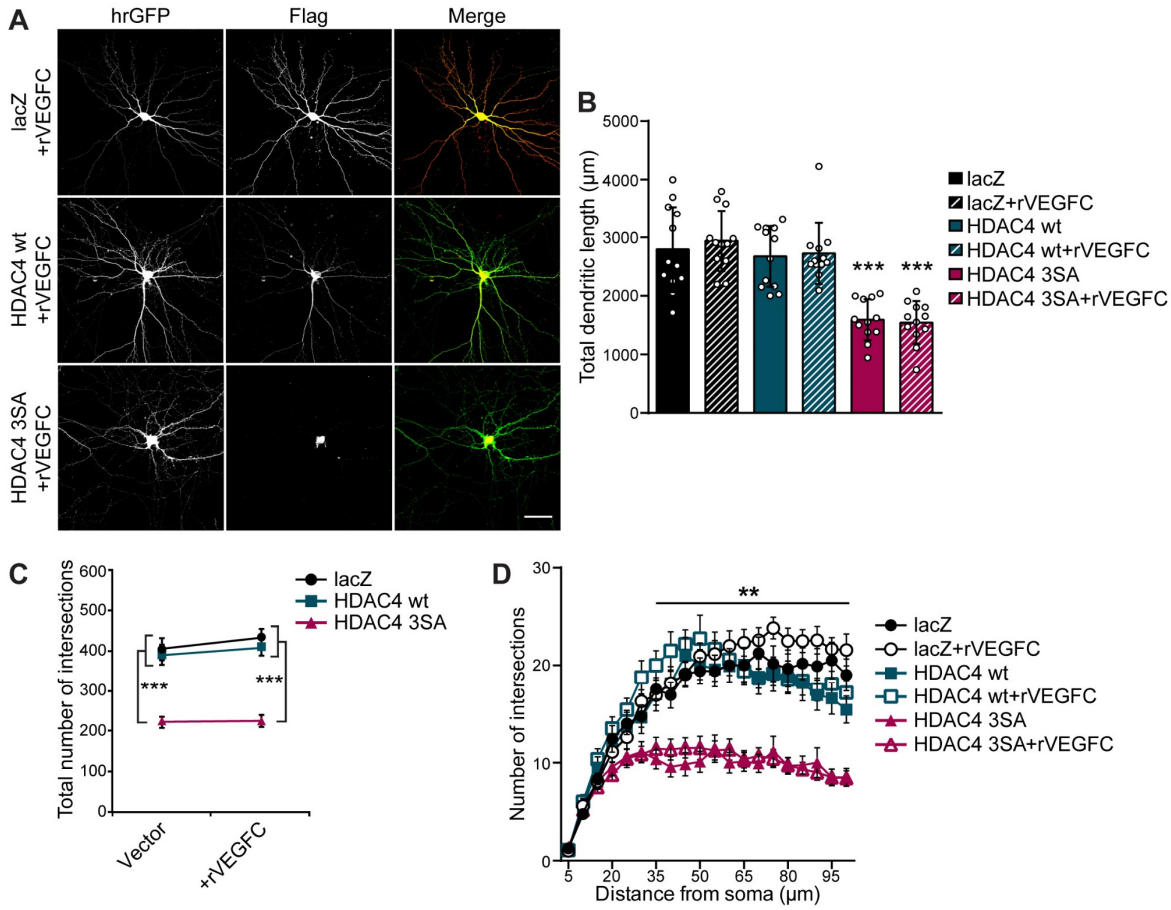

Figure 13: VEGFC cannot restore morphology of HDAC4 3SA expressing neurons.
(A) Representative images of cultured hippocampal neurons at DIV 13, co-transfected with hrGFP and flag-tagged constructs lacZ, HDAC4 wt, or HDAC4 3SA at DIV 8, and treated or not with rVEGFC (100 ng/ml) for three days. hrGFP fluorescence reveals complete dendritic architecture and flag tags were immunostained with Alexa 594. Scale bar is 40 µm. (B) Quantification of the total dendritic length of hippocampal neurons transfected as indicated, with or without treatment with rVEGFC for three days. (C) Quantification of the total number of intersections at DIV 13, derived from Sholl analysis (D), in hippocampal neurons transfected as indicated, with or without treatment with rVEGFC for three days. In total, 12 neurons from three independent experiments (n=3) were analyzed for each construct. Statistically significant differences were determined by one-way ANOVA (B-C) and two-way ANOVA (D), followed by Tukey's post hoc test. ***, $p < 0.001$; **, $p < 0.01$. In bar graphs, each point represents a value derived from one neuron. Graphs represent mean ± S.D.

3.2 De novo DNA methyltransferases in chronic inflammatory pain

The other nuclear calcium-regulated epigenetic process investigated in this study, besides nucleo-cytoplasmic shuttling of class IIa HDACs, is the synaptic activity-dependent induction of the immediate early gene *dnmt3a2*. Dnmt3a2 plays an important regulatory role for several cognitive abilities by inducing the expression of plasticity related genes (Oliveira, 2016, Oliveira et al., 2012). Just recently it has been demonstrated that in the dentate gyrus, expression levels of Dnmt3a2 within selected neuronal ensembles, play a crucial role for memory consolidation and retrieval (Gulmez Karaca et al., 2020). Moreover, Dnmt3a2 expression is induced by dopaminergic signaling in primary striatal cultures as well as in neurons of the NAc-shell upon cocaine administration (Cannella et al., 2018).

Activity and nuclear calcium-dependent adaptive processes, have also been described in neurons of the spinal cord where they play a role in central sensitization and the development of chronic pain, by mediating maladaptive changes in central nociceptive pathways (Bading, 2013, Basbaum et al., 2009, Woolf and Salter, 2000). In the CFA model of inflammatory pain, it has been shown that nociceptive activity triggers nuclear calcium transients in neurons of the dorsal horn, controlling changes in gene transcription that mediate long-lasting hypersensitivity in mice (Simonetti et al., 2013).

In this part of the study, which has been published in *Molecular Pain* (Litke et al., 2019), we investigate if and how the synaptic activity-regulated de novo DNA methyltransferase Dnmt3a2 is linked to the development of chronic inflammatory pain.

3.2.1 Dnmt3a2 regulates gene transcription in inflammatory pain

To investigate whether Dnmt3a2 expression is also regulated by nociceptive activity in cells of the spinal cord, we measured its expression levels over time in lumbar segments (L3-5) of the dorsal horn in mice after intraplantar injection of CFA (1 h; 3 h; 6 h) into the hind paw. QRT-PCR analysis, performed and analyzed by Dr. Ana Oliveira, showed that inflammatory pain results in a significant upregulation of *dnmt3a2*, whereas the expression of its alternative transcript *dnmt3a1* was not affected (data not shown). This observation is in line with previous findings, indicating that transcription of *dnmt3a1* is not dependent on synaptic activity in neurons

(Oliveira et al., 2012, Cannella et al., 2018). Moreover, several immediate early genes, reportedly regulated by Dnmt3a2 expression in neurons, including *c-fos*, *bdnf*, and *arc* (Oliveira, 2016, Oliveira et al., 2012), were also induced in the spinal cord dorsal horn upon intraplantar CFA injection. Furthermore, in agreement with previous findings (Simonetti et al., 2013), we found mRNA levels of *ptgs2*, a critical inflammatory mediator, encoding the prostaglandin synthase cyclooxygenase 2 (Cox-2), significantly induced after three hours and still at 48 hours upon CFA injection. In contrast, expression of immediate early genes *c-fos, bdnf* and *arc* was transiently induced between one to six hours post-CFA injection (data not shown).

Our findings that nociceptive activity induces expression levels of Dnmt3a2 in the spinal cord together with its known ability to regulate plasticity-dependent processes in neurons suggest that Dnmt3a2 is involved in the development of central sensitization. To test our hypothesis, we targeted transcription of *dnmt3a2* using viral-mediated RNA interference (RNAi). Recombinant viral vectors encoding short hairpin RNAs (shRNAs), either targeting mouse *dnmt3a2* mRNA (rAAV-shDnmt3a2) or without any target sequence in the mouse genome (rAAV-shControl), were stereotactically delivered into the lumbar spinal parenchyma of segments L3 to L5. This method is a robust experimental strategy previously successfully used for long-lasting, stable gene delivery without damage (Simonetti et al., 2013, South et al., 2003, Lu et al., 2015).

Both rAAV-vectors contained an additional expression cassette for GFP allowing detection of the delivered expression constructs and were provided by Dr. Ana Oliveira (Figure 14A). The efficacy of rAAV-shDnmt3a2 to decrease mRNA levels of Dnmt3a2 has been extensively tested and validated *in* vitro and *in vivo* (Oliveira, 2016, Oliveira et al., 2012, Cannella et al., 2018). We could further confirm the efficacy of rAAV-shDnmt3a2 in primary cultured spinal cord neurons, infected with either rAAV-shDnmt3a2 or -shControl, demonstrating a reduction of *dnmt3a2* mRNA levels at resting conditions. Moreover, after depolarization with potassium chloride (KCl) solution induction of *dnmt3a2* was significantly decreased in rAAV-shDnmt3a2 infected cells (data not shown; experiment was performed by Dr. Daniela Mauceri). Three weeks after intraspinal delivery of constructs, the GFP signal of rAAV-shDnmt3a2 and -shControl could be detected in the spinal cord dorsal horn (Figure 14B). This indicates correct targeting of the injection and successful infection of cells with viral particles (Figure 14B).

To test whether RNAi-mediated knockdown of *dnmt3a2* interferes with the upregulation of CFA-induced genes, mice intra-spinally injected with either rAAV-shDnmt3a2 or -shControl, received intraplantar CFA injections, after a recovery-period of three weeks, allowing the shRNA to be effective. Three hours after CFA injection, dorsal horn tissue of the lumbar spinal cord was quickly isolated for QRT-PCR and mRNA levels of *c-fos*, *bdnf*, *arc*, and *ptgs2* were determined (in collaboration with Dr. Ana Oliveira). In agreement with previous results, animals expressing the shControl showed a significant induction of all analyzed immediate early genes, as well as the pain-effector gene *ptgs2* (Figure 14C). However, mice expressing shDnmt3a2, did not display a significant induction of *c-fos* and *bdnf*, anymore, whereas expression of *arc* was still induced upon CFA injection (Figure 14C). Interestingly, the induction of *ptgs2*, a crucial mediator of the inflammatory pain signaling cascade (Vardeh et al., 2009, Svensson and Yaksh, 2002), was blocked in animals receiving *in vivo* knockdown of *dnmt3a2*, compared to control mice. These data suggest that Dnmt3a2 is required for activity-dependent gene transcription in the spinal cord, where it can regulate the expression of inflammatory pain-related genes.

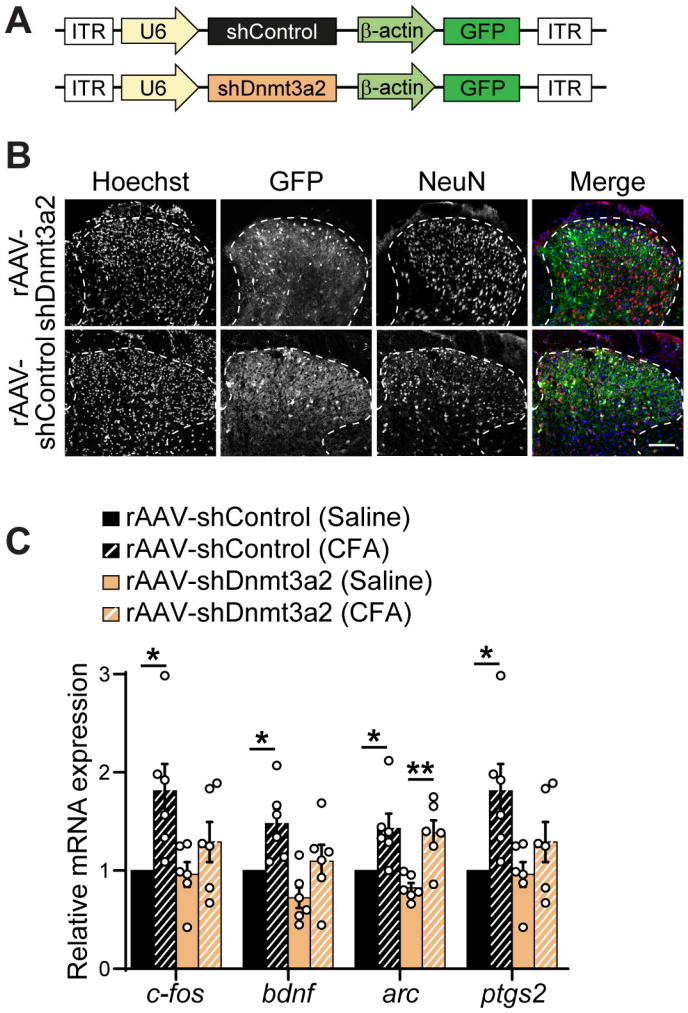

Figure 14: Dnmt3a2 regulates gene transcription in chronic inflammatory pain.
(A) Schematic representation of the rAAVs used for *in vivo* RNA interference-dependent knockdown. (B) Representative images of transverse spinal cord slices after intraspinal rAAV injection, revealing localization of GFP-tagged constructs in the dorsal horn (green). Immunolabeling of neuronal marker (NeuN) protein is shown in red and nuclei were labelled with Hoechst (blue). Scale bar is 100 µm. (C) QRT-PCR analysis of *c-fos*, *bdnf*, *arc*, and *ptgs2* mRNA levels in the dorsal spinal cord of mice intraspinally injected with rAAV-shControl or rAAV-shDnmt3a2 three hours after intraplantar injection of saline or CFA as indicated. N=6 animals per condition. Expression values were normalized to saline injected animals expressing shControl. Statistically significant differences were determined by one-way ANOVA followed by Bonferroni's post hoc test. **, $p < 0.01$; *, $p < 0.05$. In bar graphs, each point represents a value derived from one animal. Graphs represent mean ± SEM. (QRT-PCR analysis in (C) was performed by Dr. Ana Oliveira).

3.2.2 Dnmt3a2 mediates pain hypersensitivity

In vivo-knockdown of *dnmt3a2* in the spinal cord dorsal horn blocked the induction of genes associated with inflammatory pain (Figure 14). Therefore, we investigated whether Dnmt3a2 expression affects pain behavior in mice. We employed the capsaicin model of acute- and the CFA model of chronic inflammatory pain. Mice intra-spinally injected with rAAV-shDnmt3a2 or -shControl received, after a recovery period of three weeks, plantar injections of either capsaicin or CFA into one of the hind paws. Capsaicin triggers activation of TRPV1-expressing nociceptors leading to acute nocifensive behaviors, like shaking or flicking of the paw, lasting for several minutes (Gregory et al., 2013, Hunskaar et al., 1985, O'Neill et al., 2012), whereas CFA causes a complex painful inflammatory reaction in the afflicted paw, lasting for weeks (Iadarola et al., 1988, Ren and Dubner, 1999) (see also Figure 19). Both experimental groups showed no significant difference in their responses to the acute pain stimulus, expressed as the cumulative durations of nocifensive behaviors within five minutes after capsaicin injection (rAAV-shDnmt3a2: 24.74 s ± 2.05 s; rAAV-shControl: 26.42 s ± 1.71 s; Figure 15A). This suggests that expression levels of *dnmt3a2* do not affect acute nociception during inflammatory pain.

Using the CFA model of chronic inflammatory pain, thermal and mechanical sensitivity were assessed in collaboration with the group of Prof. Rohini Kuner, applying the Hargreaves' method and von Frey test, respectively. Both experimental groups, rAAV-shDnmt3a2 and -shControl injected mice, displayed similar response latencies to thermal heat stimulation at basal levels (before CFA injection) indicating that Dnmt3a2 expression levels do not affect basal nociception (Figure 15B). After intraplantar CFA injection, all animals developed thermal hyperalgesia lasting for the entire observation period of ten days. However, starting two days post-CFA, mice expressing shDnmt3a2, displayed a significantly prolonged response latency to thermal heat stimulation, indicating decreased thermal hyperalgesia (Figure 15B). Measurements at the contralateral side, where paws were injected with saline instead of CFA, revealed no signs of thermal hyperalgesia nor any differences in the response latencies between both experimental groups (Figure 15C).

To test mechanical sensitivity, von Frey filaments ranging from 0.07-1 g were applied to both hind paws and total number of responses to the different filaments at a given time was determined. Both experimental groups developed mechanical hypersensitivity post CFA injection, persistent over time (Figure 15D). However, mice

intra-spinally injected with rAAV-shDnmt3a2, displayed a significant reduction in the sum of responses to filament stimuli. This effect became evident after one day and was still present ten days after intraplantar CFA injection (Figure 15D). Basal response frequency to von Frey filaments was not significantly affected by intraspinal injection of rAAV-shDnmt3a2 (Figure 15F), which is in line with the results of thermal pain assessment. Differences in the number of responses to mechanical stimulation was most prominent 24 hours after CFA injection and applied forces of 0.16 g and 0.4 g (Figure 15G). Response frequency to light touch filaments (0.07 g) was significantly reduced in mice expressing rAAV-shDnmt3a2, starting one day after CFA injection (Figure 15H), suggesting that lowered expression levels of *dnmt3a2* ameliorate allodynia. Response frequencies of the contralateral side were not significantly affected by Dnmt3a2 expression (Figure 15E).

Taken together, our results indicate that in the dorsal horn of the spinal cord, Dnmt3a2 expression is required for the development of long-lasting thermal, as well as mechanical hypersensitivity in mice, whereas basal and acute nociception is not affected (Litke et al., 2019).

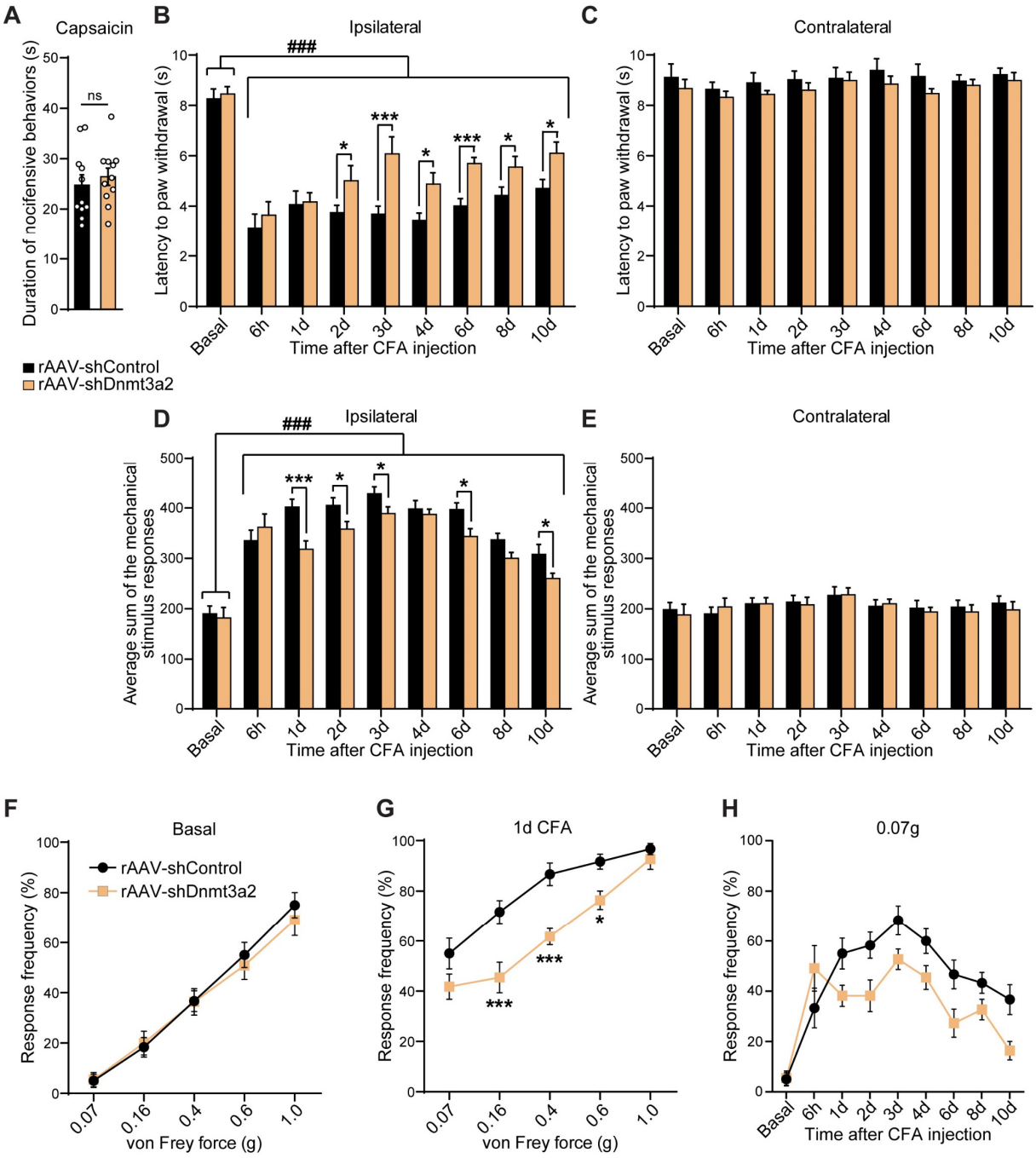

Figure 15: Dnmt3a2 mediates hypersensitivity in persistent inflammatory pain.

(A) Analysis of acute nocifensive behavior following intraplantar injection of capsaicin in mice intra-spinally injected with rAAV-shControl or rAAV-shDnmt3a2 as indicated. (B-C) Analysis of paw withdrawal latency to determine thermal response thresholds following intraplantar CFA (ipsilateral) or saline (contralateral) injection at indicated timepoints in mice intra-spinally injected with rAAV-shControl or rAAV-shDnmt3a2. (D-E) Analysis of mechanical hypersensitivity following intraplantar CFA (ipsilateral) or saline (contralateral) injection at indicated timepoints in mice intra-spinally injected with rAAV-shControl or rAAV-shDnmt3a2 by measuring the sum of stimulus responses of the paw to von Frey filaments (0.07-1 g). (F-G) Analysis of basal (F) mechanical sensitivity to von Frey filaments of increasing forces and one day after intraplantar CFA injection (G). (H) Analysis of paw withdrawal

frequency following stimulation with the 0.07 g (light touch) von Frey filament at indicated timepoints after intraplantar CFA injection. In (A) eleven animals (n=11) were analyzed per experimental group and eleven to twelve (n=11-12) mice per experimental group in (B-H). Statistically significant differences were determined by two-tailed Student's t-test (A) or two-way ANOVA with repeated measures followed by Dunnett's post hoc test for comparisons to basal values and multiple t-tests for comparisons between rAAV-shControl and rAAV-shDnmt3a2 (B-H). ***, $p < 0.001$; **, $p < 0.01$; *, $p < 0.05$; ###, $p < 0.0001$. Asterisks (*) refer to statistical comparisons between rAAV-shControl and rAAV-shDnmt3a2 and hashtags (#) to comparisons relative to basal values (B-H). In bar graphs, each point represents a value derived from one animal (A). Graphs represent mean ± SEM. (Von Frey and Hargreave's test (B-H) were performed by the group of Prof. Rohini Kuner).

3.3 The role of histone deacetylases in inflammatory pain

The previous study on neuronal activity-dependent Dnmt3a2 expression in the spinal cord dorsal horn demonstrates that epigenetic regulatory processes play a key role in the development of spinal sensitization. This concept is further supported by many studies that have linked epigenetic mechanisms to the development and maintenance of chronic pain states (Denk and McMahon, 2012). Besides DNA methylation, changes in the acetylation of histones have been observed in various pain models and pharmacological inhibition of HDACs has been used to treat inflammatory pain in pre-clinical studies (Zhang et al., 2011b, Bai et al., 2010, Crow et al., 2013, Chiechio et al., 2009, Shakespear et al., 2011). However, these studies rely on unspecific inhibition of HDACs, not discriminating between different HDAC members or classes. Therefore, the role of specific HDACs in the modulation of central sensitization remains unclear.

Especially HDAC members of class IIa, with their ability to shuttle between the nucleus and cytoplasm in a synaptic activity and nuclear calcium-dependent manner, have recently emerged as key regulators of several neuroadaptive phenomena (Kim et al., 2012b, Crow et al., 2013, Renthal et al., 2007). In particular, the subcellular localization of HDAC4 has been shown to regulate the transcription of synaptic activity and nuclear calcium-dependent genes (Schlumm et al., 2013) and plays a critical role for synaptic plasticity as well as dendritic morphology in hippocampal neurons (Sando et al., 2012, Litke et al., 2018). HDAC4 is also essential for cognitive abilities like memory formation (Sando et al., 2012, Zhu et al., 2019, Wang et al., 2011a). Given that memory formation and central sensitization share common

molecular mechanisms (Crow et al., 2013, Rahn et al., 2013, Bading, 2013), we sought to investigate possible effects of nociceptive activity on the nucleo-cytoplasmic shuttling and activity of class IIa HDACs in neurons of the spinal cord. In turn, we evaluated if and how changes in their subcellular localization, contribute to central sensitization by changing the transcription of plasticity and pain-related genes.

3.3.1 Synaptic activity-mediated nuclear export of HDAC4

Previous studies in hippocampal neurons have shown that the nucleo-cytoplasmic shuttling of class IIa HDACs is regulated by synaptic activity and nuclear calcium-signaling (Chawla et al., 2003, Schlumm et al., 2013, Litke et al., 2018). Here, we investigated whether synaptic activity modulates HDACs subcellular shuttling in neurons of the spinal cord.

The protocol to culture primary spinal cord neurons was established in our lab by Dr. Anna Hertle. Spinal cord neurons were treated with the $GABA_A$-receptor antagonist bicuculline (Bic) over a period of 0.5 h, 2 h, or 8 h to elicit bursts of action potential firing (Schlumm et al., 2013, Nowak et al., 1982). Cells were fixed and the nuclear content of HDAC1; -3; -4; -5; -7; -9: -10 and -11 was quantified in neurons. Under basal conditions, HDACs were equally distributed between the cytosol and the nucleus (Figure 16A), or primarily localized in the nucleus (HDAC1 and -3; data not shown).

In line with previous experiments using hippocampal neurons (Schlumm et al., 2013), members of class I (HDAC1 and 3), class IIb (HDAC10), and class IV (HDAC11) did not change their subcellular distribution upon induction of synaptic activity (Figure 16B). Surprisingly, amongst members of class IIa, only HDAC4 displayed a significant reduction of its nuclear signal in spinal cord neurons following two and eight hours after stimulation compared to control (HDAC4: 0.77 ± 0.09 (0.5 h); 0.55 ± 0.09 (2 h); 0.56 ± 0.06 (8 h); Figure 16A, C). Thus, our data show that synaptic activity triggers specifically nuclear export of HDAC4 in cultured spinal cord neurons.

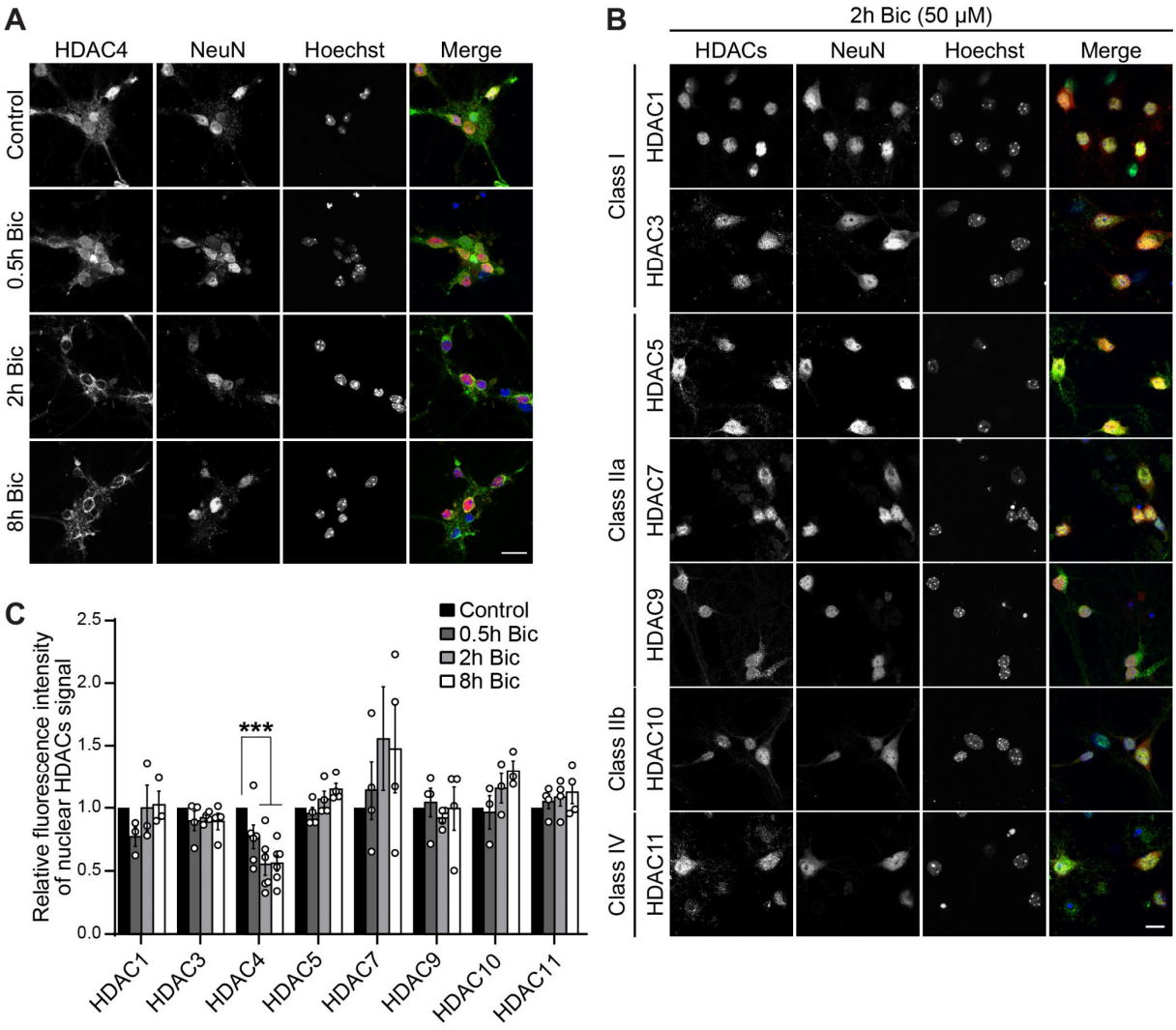

Figure 16: Synaptic activity triggers HDAC4 nuclear export in spinal cord neurons.

(A) Representative images of DIV10/11 cultured primary spinal cord neurons immunostained for endogenous HDAC4 (green). Cells were treated with 50 µM bicuculline (Bic) for either 0.5; 2, or 8 hours, as indicated. (B) Representative images of spinal cord cultures, treated as in (A), 2Nuclei were labelled with Hoechst (blue) and NeuN (red) as neuronal marker. Scale bar is 20 µm (A-B). (C) Quantification of the relative fluorescent intensity of the nuclear signal of HDACs normalized to respective controls. Each point represents the mean value derived from one independent experiment. Ca. 40 cells were analyzed per condition and experiment (n=3-6). Statistically significant differences were determined by one-way ANOVA followed by Dunnet's post hoc test. ***, $p < 0.001$. Graphs represent mean ± SEM.

3.3.2 HDACs expression in spinal cord neurons

In order to investigate whether the detected reduction of nuclear HDAC4 following stimulation could be ascribed to a reduction of expression, we next measured the protein expression levels of HDACs in spinal cord cultures following bicuculline treatment (Figure 17). No significant change in the expression of any tested HDAC member could be detected upon stimulation. However, we observed a strong transient induction of the immediate early gene c-fos, indicative of a successful stimulation of synaptic activity (*c-fos*: 1.06 ± 0.04 (0.5 h); 16.48 ± 1.78 (2 h); 10.02 ± 2.59 (8 h); Figure 17B).

In summary, the detected activity-dependent reduction of nuclear HDAC4 (Figure 16A, C) appears to be due to translocation of HDAC4 towards the cytosol, rather than to a decrease in its expression.

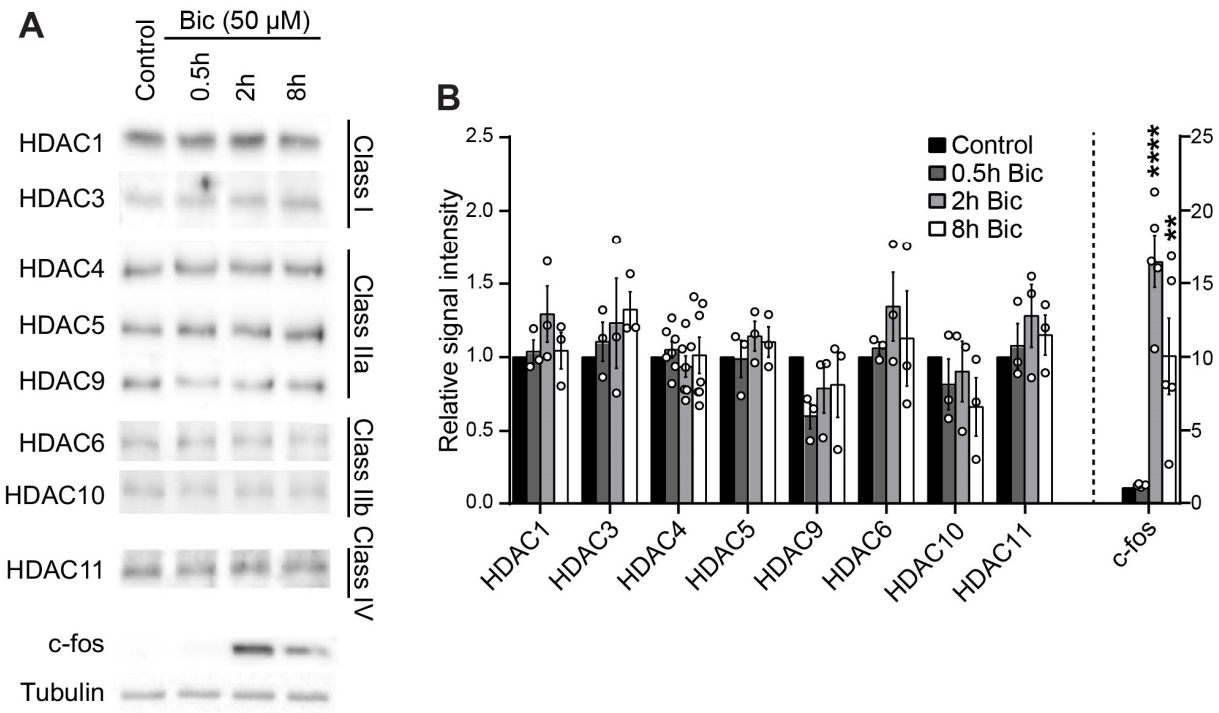

Figure 17: Synaptic activity does not affect HDACs expression in the spinal cord.

(A) Representative immunoblots of different HDACs, c-fos and tubulin from primary spinal cord cultured neurons treated with Bic (50 µM) for the indicated timepoints. (B) Quantification of relative protein levels of different HDACs and c-fos, as in (A), normalized to the signal intensity of tubulin and to controls. Each point represents the mean value derived from one independent experiment (n=3-7). Statistically significant differences were determined by one-way ANOVA followed by Dunnet's post hoc test. ****, $p < 0.0001$; **, $p < 0.01$. In bar graphs, each point represents the mean value derived from one independent experiment. Graphs represent mean ± SEM.

3.3.3 Histone H3 acetylation in spinal cord neurons

HDACs catalyze the removal of acetyl groups from lysine residues of histone and non-histone proteins and regulate gene transcription by changing the chromatin structure and modification of transcription factor activity (Peserico and Simone, 2011, Gallinari et al., 2007). The N-terminal lysine residue at position 9 of histone 3 (H3K9) is a prominent target of post-translational histone modification and associated with changes in gene transcription (Dupont et al., 2009).

Using immunocytochemistry and Western blot analyses, we determined levels of acetylated histone H3K9 (AcH3) in cultured spinal cord neurons treated with bicuculline (Figure 18). We found that synaptic activity increased AcH3, while total histone H3 levels remained constant over time (AcH3/H3-ratio: 1.22 ± 0.2 (0.5 h); 1.68 ± 0.19 (2 h); 1.65 ± 0.2 (8 h); Figure 18C-D). Using immunocytochemistry of spinal cord cultures, we determined that the activity-dependent induction of AcH3 was taking place in neurons (AcH3: 1.61 ± 0.11 (0.5 h); 2.31 ± 0.34 (2 h); 2.06 ± 0.32 (8 h); Figure 18A-B).

In summary, synaptic activity reduces levels of nuclear HDAC4 and promotes acetylation of histone H3 in cultured spinal cord neurons, suggesting that both events are functionally linked.

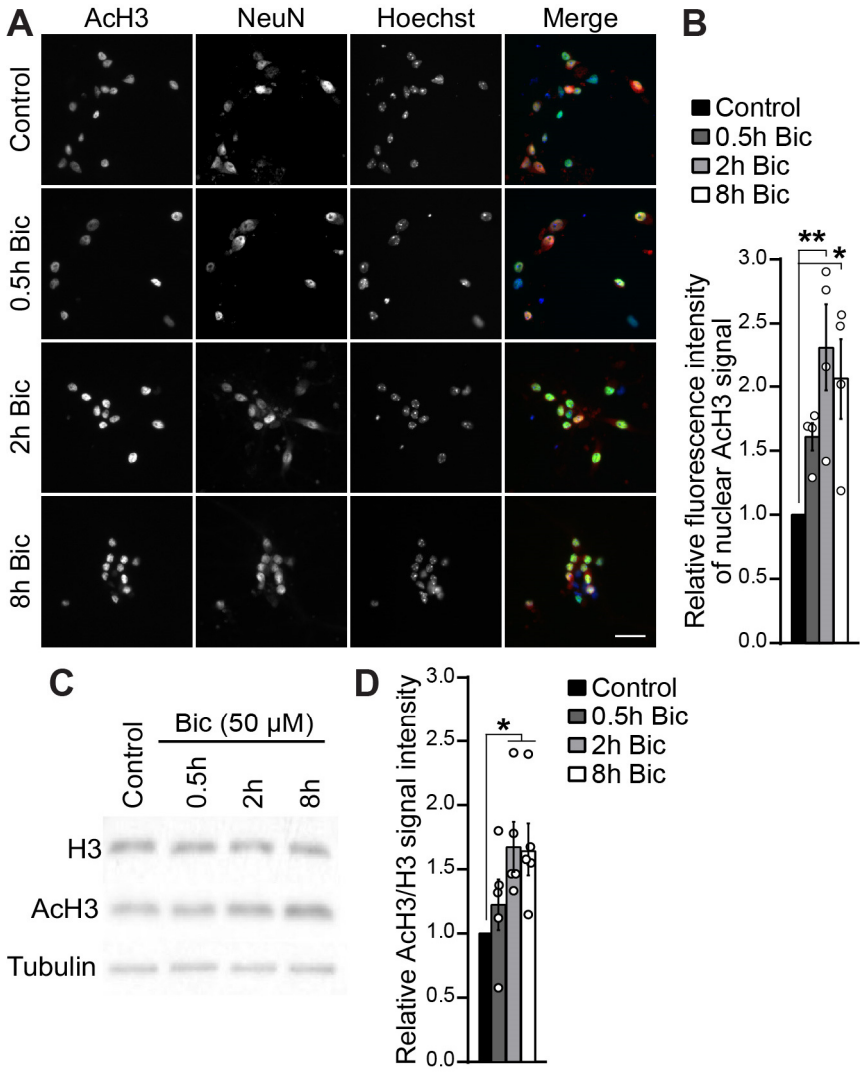

Figure 18: Synaptic activity triggers histone 3 acetylation in spinal cord neurons.

(A) Representative images of primary cultured spinal cord neurons at DIV10/11 immunostained for AcH3 (green). Cells were treated with Bic (50 µM) for the indicated time. Nuclei were labelled with Hoechst (blue) and NeuN (red) as neuronal marker. Scale bar is 40 µm. (B) Quantification of the relative fluorescent intensity of the nuclear signal of acetylated histone H3-Lys9 (AcH3) in spinal cord neurons, treated as indicated. Ca. 30 cells were analyzed per condition of each experiment (n=4). (C) Representative immunoblots of histone H3, acetylated histone H3-Lys9 (AcH3) and tubulin from spinal cord cultures treated with Bic (50 µM) for the indicated timepoints. (D) Quantification of the relative protein levels displayed in (C) (n=5-6). Graph shows the relative AcH3/H3 signal intensity-ratio, normalized to tubulin and controls. Statistically significant differences were determined by one-way ANOVA followed by Dunnett's post hoc test. **, $p < 0.01$; *, $p < 0.05$. In bar graphs, each point represents the mean value derived from one independent experiment. Graphs represent mean ± SEM.

3.3.4 Effects of inflammatory pain on HDAC4 and histone acetylation in dorsal horn neurons

Since synaptic activity in cultured spinal cord neurons induced nuclear export of HDAC4 and resulted in elevated levels of histone acetylation (Figure 16Figure 18), we investigated whether nociceptive activity had a similar effect in neurons of the spinal cord *in vivo*. We made use of the CFA model of long-lasting inflammatory pain in mice to induce persistent allodynia and hyperalgesia. The model is used to mimic the time course of chronic inflammatory pain conditions, such as rheumatoid arthritis or tendonitis (Gregory et al., 2013, Ren and Dubner, 1999). Hind paw diameter (medial-lateral axis) and thickness (dorso-ventral axis) were measured with a digital caliper after intraplantar injection of CFA or saline. As expected, both paw diameter and thickness were significantly increased 24 hours and seven days after injection of CFA, compared to saline injected contralateral paws (paw diameter: 24 h: 3.77 mm ± 0.12 mm (saline) vs. 4.92 mm ± 0.19 mm (CFA); 7 d: 3.7 mm ± 0.16 mm (saline) vs. 4.62 mm ± 0.15 mm (CFA); paw thickness: 24 h: 2.15 mm ± 0.15 mm (saline) vs. 3.65 mm ± 0.19 mm (CFA); 7 d: 2.27 mm ± 0.05 mm (saline) vs. 3.55 mm ± 0.15 mm (CFA); Figure 19A-C). The CFA-induced paw edema was associated with increased mechanical and thermal hypersensitivity, shown by an increase of the responses to von Frey mechanical stimulation (Figure 19D) and a reduction of the paw withdrawal latency to radiant heat (Figure 19E).

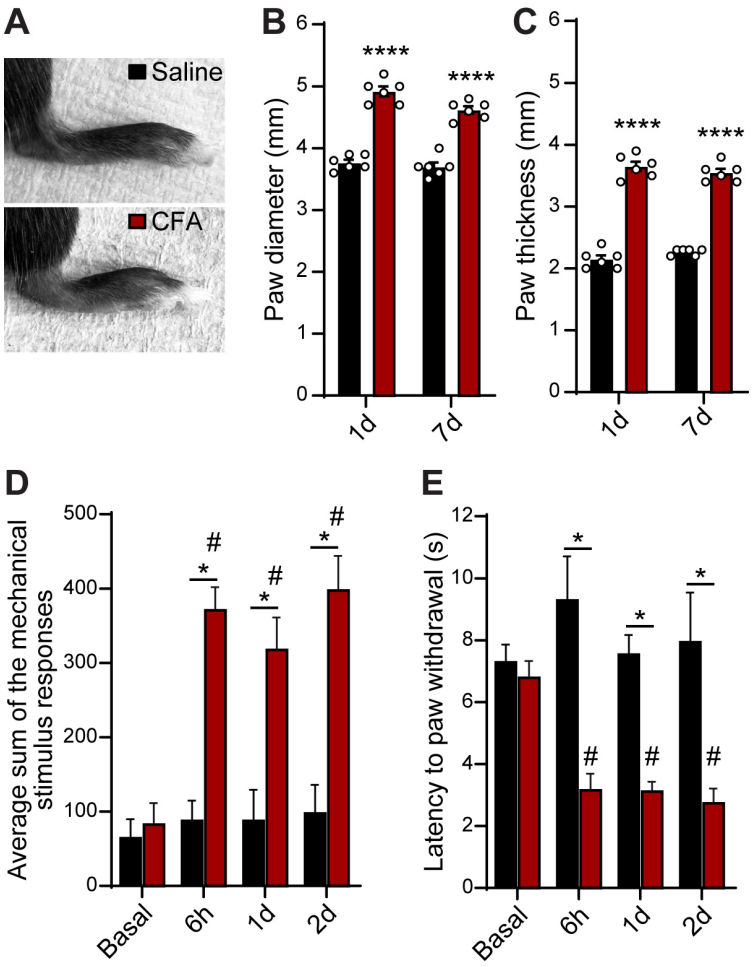

Figure 19: CFA model of inflammatory pain.

(A) Representative images of mouse hind paws 24 (B-C) Medial-lateral (diameter) and dorsal-ventral (thickness) dimensions of hind paws from mice, one or seven days after CFA or saline injections (n=6 mice per condition and timepoint). (D) Analysis of mechanical hypersensitivity following intraplantar injections of CFA or saline at indicated timepoints in wild type animals, by measuring the sum of stimulus responses of the paw to von Frey filaments (0.07-1.4 g). (E) Analysis of paw withdrawal latency to determine thermal response thresholds following intraplantar injections as in (D). Statistically significant differences were determined by two-tailed Student's t-test (B-C) or two-way ANOVA with repeated measures followed by Dunnett's post hoc test for comparisons to basal values and multiple t-tests for comparisons between saline and CFA (D-E). ****, $p < 0.0001$; *, $p < 0.05$; $^{\#}$, $p < 0.001$. In bar graphs, each point represents a value derived from one animal (B-C). Asterisks (*) refer to statistical comparisons between saline and CFA, and hashtags ($^{\#}$) to comparisons relative to basal values (B-E). Graphs represent mean ± SEM.

We then analyzed whether CFA-induced inflammatory pain affects the subcellular localization of class IIa HDACs or acetylation levels of histone H3 in dorsal horn neurons of the lumbar spinal cord segments L3-L5. Immunohistochemistry and WB analyses were performed 0.5 h, 2 h, 6 h, and 24 h after plantar injection of CFA and compared to saline injected mice. Under basal conditions, spinal cord sections revealed an equal subcellular distribution of endogenous class IIa HDACs (HDAC4, -7, and -9) in-between the nucleus and cytosol (Figure 20A), similar to cultured spinal cord neurons (Figure 16). Following CFA injection, nuclear HDAC4 signal was reduced over time in neurons of laminae I – V (Figure 20A-C). In line with previous observations in cultured spinal cord neurons, the nuclear export appeared to be specific for HDAC4 as other class IIa HDACs (HDAC7 and -9) did not change their subcellular localization (Figure 20A-B).

Expression analysis of HDAC1 (class I), HDAC4, -5, -9 (class IIa) and HDAC11 (class IV) in the dorsal part of the lumbar spinal cord showed no significant changes over time following CFA injection (Figure 20D-E), suggesting that the CFA-mediated reduction of nuclear HDAC4 is caused by a shift in its subcellular localization and not by changes in expression.

Similar to what observed using cultured spinal cord neurons, nuclear reduction of HDAC4 signal was accompanied by an increase of AcH3 levels in dorsal horn neurons (Figure 20C-E). The levels of total histone H3 remained constant over time (AcH3/H3-ratio: 1.88 ± 0.57 (0.5 h); 1.87 ± 0.53 (2 h); 2.28 ± 0.33 (6 h); 2.44 ± 0.37 (24 h); Figure 20E). As a control, we assessed the expression of c-fos, which we found significantly induced two hours after CFA application (c-fos: 1.58 ± 0.24 (0.5 h); 2.39 ± 0.28 (2 h); 1.31 ± 0.21 (6 h); 1.06 ± 0.2 (24 h); Figure 20F).

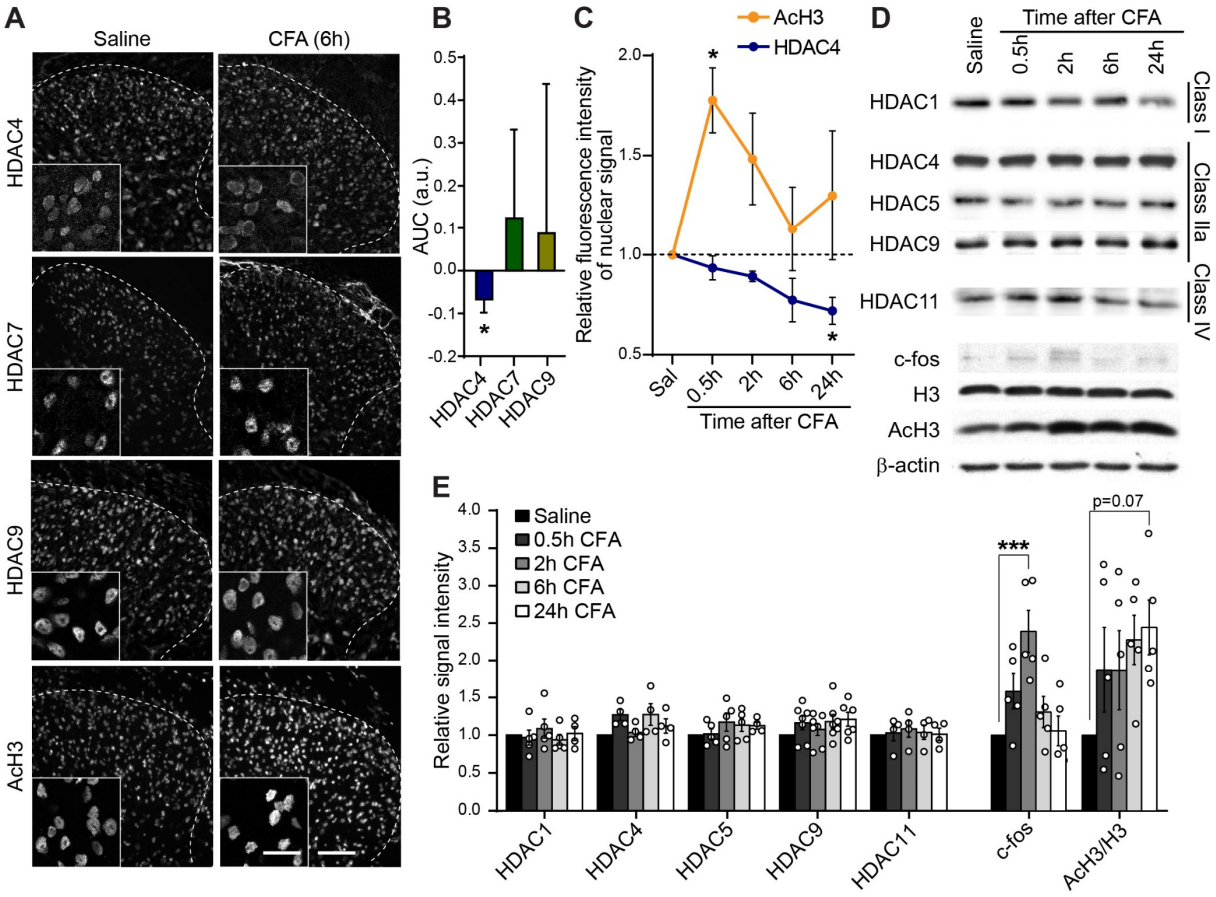

Figure 20: Inflammatory pain induces HDAC4 nuclear export in dorsal horn neurons.

(A) Representative images of dorsal horn sections of lumbar spinal segments L3-5 of mice at 6 h after saline or CFA injection, immunostained for HDAC4, -7, -9, or acetylated histone H3-Lys9 (AcH3), as indicated. Scale bar is 100 µm. Higher magnifications of the upper laminae are shown in panels at the lower-left corner with a scale bar of 20 µm. (B) Quantifications of the average nuclear fluorescence signal intensities of HDACs in neurons of the dorsal horn, displayed as integrals over a time course series (shown in C) and normalized to saline injected mice (n=4 mice per condition and timepoint). (C) Quantification of relative fluorescence intensities of the nuclear signal of AcH3 and HDAC4 in neurons of the dorsal horn (laminae I-V), following CFA injection for the indicated timepoint and normalized to saline controls (n=4 mice per condition and timepoint). (D) Representative immunoblots of different HDACs, c-fos, histone H3, AcH3, and β-actin from dorsal horn tissue of the lumbar spinal cord segments L3-5, following saline or CFA injection, as indicated. (E) Quantification of the relative protein levels displayed in (D), normalized to saline injected control mice. Acetylation of histone H3 is presented as signal intensity-ratio of AcH3 over H3 (n=4-7 mice per condition and timepoint). Statistically significant differences were determined by two-tailed Student's t-test (B) or one-way ANOVA followed by Dunnett's post hoc test (C, E). ***, $p < 0.001$; *, $p < 0.05$. In bar graphs, each point represents the mean value derived from one animal. Graphs represent mean ± SEM.

3.3.5 Acute pain and histone acetylation in dorsal horn neurons

Intraplantar injection of CFA results in a long-lasting inflammation of the injected tissue and reliably induces hypersensitivity (hyperalgesia and allodynia), characteristic of chronic pain (Gregory et al., 2013). Besides enhancing spontaneous and acute pain behaviors also changes in non-reflexive measures, like reduced weight bearing on the injected hind limb or decreased wheel running activity, have been described in the CFA model, covering further aspects of chronic pain (Cobos et al., 2012, Parvathy and Masocha, 2013, Pitzer et al., 2016). Moreover, CFA injections are frequently used to resemble chronic inflammatory conditions of humans like rheumatoid arthritis (Gregory et al., 2013).

In contrast, intraplantar injection of capsaicin leads to activation of TRPV1-containing nociceptors in the periphery and results in short-lasting, acute inflammatory pain (Gregory et al., 2013). Evoked nocifensive behaviors typically range from tens of seconds to a few minutes. In comparison to the CFA model of long-lasting inflammatory pain, capsaicin did not trigger the induction of c-fos in the lumbar dorsal horn of the spinal cord and did not change the acetylation of histone H3 (Figure 21).

Thus, our analyses suggest that persistent, but not acute, inflammatory pain induces nuclear export of HDAC4 in dorsal horn neurons of the spinal cord, elevating histone H3 acetylation.

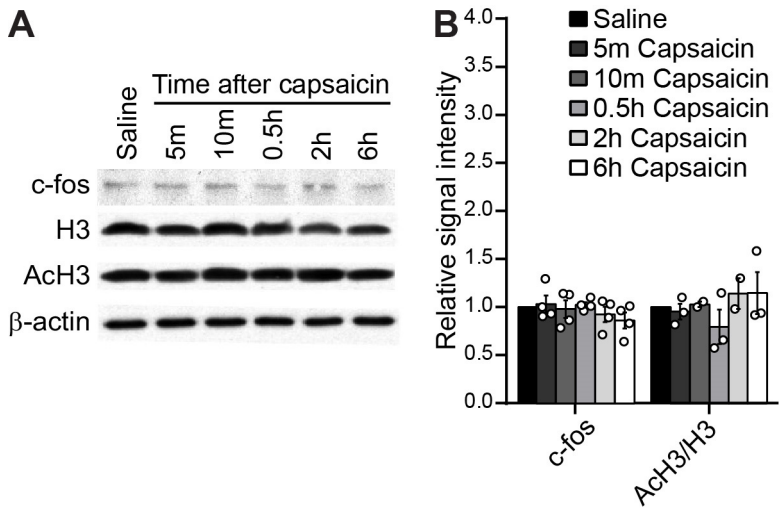

Figure 21: Acute pain does not affect histone 3 acetylation in the spinal cord.

(A) Representative immunoblots of c-fos, H3, AcH3, and β-actin from dorsal horn tissue of the lumbar spinal cord segments L3-5, following saline or capsaicin injection, as indicated. (B) Quantification of the relative protein levels displayed in (A), normalized to saline injected control mice. Acetylation of histone H3 is presented as signal intensity-ratio of AcH3 over H3 (n=2-4 mice per condition and

timepoint). No statistically significant differences were determined by one-way ANOVA followed by Dunnett's post hoc test. In bar graphs, each point represents the mean value derived from one animal. Graphs represent mean ± SEM.

3.3.6 Nuclear HDAC4 regulates histone acetylation and gene expression in spinal cord neurons *in vivo*

The reduction of nuclear HDAC4 in spinal cord neurons following prolonged inflammatory pain and its known ability to influence neuronal plasticity (Sando et al., 2012, Litke et al., 2018), indicate that the subcellular localization of HDAC4 might be involved in central sensitization. Thus, we made use of the constitutively nuclear-localized dominant-active mutant of HDAC4 (HDAC4 3SA) (Litke et al., 2018, Grozinger and Schreiber, 2000, Schlumm et al., 2013, Chawla et al., 2003). Expression constructs encoding HDAC4 3SA, HDAC4 wt, or lacZ were delivered to cultured spinal cord neurons or neurons of the dorsal horn *in vivo* (Figure 22A). When expressed in cultured spinal cord neurons, HDAC4 3SA could only be detected in the nucleus, as expected (Figure 22B). Control neurons expressing lacZ or HDAC4 wt showed a distribution of the transgenes throughout the entire cell revealed by co-expression of hrGFP (Figure 22B). To exclude possible toxic effects on cell viability due to overexpression of transgenes, we quantified the cell death rate in transfected cultured neurons. No significant changes between constructs could be determined, and transfected neurons showed a typical cell death rate of approximately 10% (lacZ: 10.13% ± 0.9%; HDAC4 wt: 12.33% ± 1.02%; HDAC4 3SA: 10.86% ± 1.27%; Figure 22C).

Persistent inflammatory pain triggers a reduction of nuclear HDAC4 and elevated levels of H3 acetylation (Figure 20). Therefore, we analyzed whether constitutively nuclear localized HDAC4 would interfere with CFA-induced histone acetylation. Expression constructions encoding lacZ, HDAC4 wt or HDAC4 3SA were delivered to the lumbar spinal cord *in vivo* via bilateral injection of rAAVs into the spinal parenchyma of adult mice (Simonetti et al., 2013, Litke et al., 2019). This technique provides stable gene transduction without causing persistent inflammation, tissue injury or glial scar formation (Tappe-Theodor et al., 2007, Litke et al., 2019). After a recovery period of three weeks, allowing for stable virus expression, mice received unilateral, intraplantar injections of CFA and were sacrificed for further analyses after 24 hours. Animals expressing lacZ or HDAC4 wt showed elevated levels of AcH3 in

dorsal horn neurons of the injected area at the ipsilateral side after CFA injection (Figure 22D-E), similar to previous experiments (Figure 20A, C). In contrast, CFA-mediated ipsilateral induction of AcH3 was completely blunted in mice expressing the nuclear HDAC4 mutant (rAAV-lacZ (CFA): 1.4 ± 0.24; rAAV-HDAC4 wt (CFA): 1.54 ± 0.1; rAAV-HDAC4 3SA (CFA): 0.81 ± 0.05; Figure 22D-E). Immunolabeling of HDAC4 in mice intra-spinally injected with rAAV-HDAC4 wt or -HDAC4 3SA confirmed that the 3SA mutant, in contrast to HDAC4 wt, remains localized in the nucleus even after intraplantar injection of CFA (Figure 22F) Thus, our results imply that HDAC4 subcellular localization regulates histone H3 acetylation in neurons of the spinal cord, *in vivo*.

Previous studies revealed that CFA-mediated inflammatory pain modulates the expression of genes in the spinal cord, important for nociceptive hypersensitivity, such as *ptgs2* and *c1q-c* (Simonetti et al., 2013). Moreover, it is known that the subcellular localization of HDAC4 regulates gene transcription via interaction with transcription factors or chromatin in neurons of the brain, playing an essential role for synaptic transmission and information processing (Sando et al., 2012, Schlumm et al., 2013, Litke et al., 2018). Therefore, we tested if the subcellular localization of HDAC4 in the spinal cord dorsal horn regulates the expression of pain relevant genes. Mice were intra-spinally injected with rAAV-constructs and, after recovery, received intraplantar CFA injections for 24 h. Messenger transcript levels of effector genes *ptgs2* and *c1q-c* were determined in corresponding spinal cord dorsal horn tissue using QRT-PCR. mRNA levels of *ptgs2* were significantly induced in the dorsal lumbar sections of mice expressing either lacZ or HDAC4 wt 24 h after CFA injection. However, *ptgs2* induction was blocked in mice expressing HDAC4 3SA (*ptgs2*: lacZ-Saline: 1 ± 0; lacZ-CFA: 1.74 ± 0.13; HDAC4 wt-Saline: 0.67 ± 0.15; HDAC4 wt-CFA: 1.68 ± 0.14; HDAC4 3SA-Saline: 0.53 ± 0.19; HDAC4 3SA-CFA: 1.16 ± 0.17; Figure 22G). Furthermore, expression levels of c1q-c, reportedly decreased under inflammatory pain (Simonetti et al., 2013), were decreased in rAAV-lacZ injected animals and unaltered in HDAC 4wt expressing mice. In contrast, mRNA levels of *c1q-c* were significantly increased in HDAC4 3SA injected animals, compared to CFA-injected, lacZ-expressing mice (*c1qc*: lacZ-Saline: 1 ± 0; lacZ-CFA: 0.71 ± 0.07; HDAC4 wt-Saline: 0.94 ± 0.15; HDAC4 wt-CFA: 1.04 ± 0.13; HDAC4 3SA-Saline: 1.42 ± 0.02; HDAC4 3SA-CFA: 1.18 ± 0.09; Figure 22G). These results are in line with previous observations made in hippocampal neurons (Schlumm et al., 2013).

Taken together, our data show that nuclear-localized HDAC4 affects CFA-mediated histone H3 acetylation in dorsal horn neurons and the expression of pain-related genes.

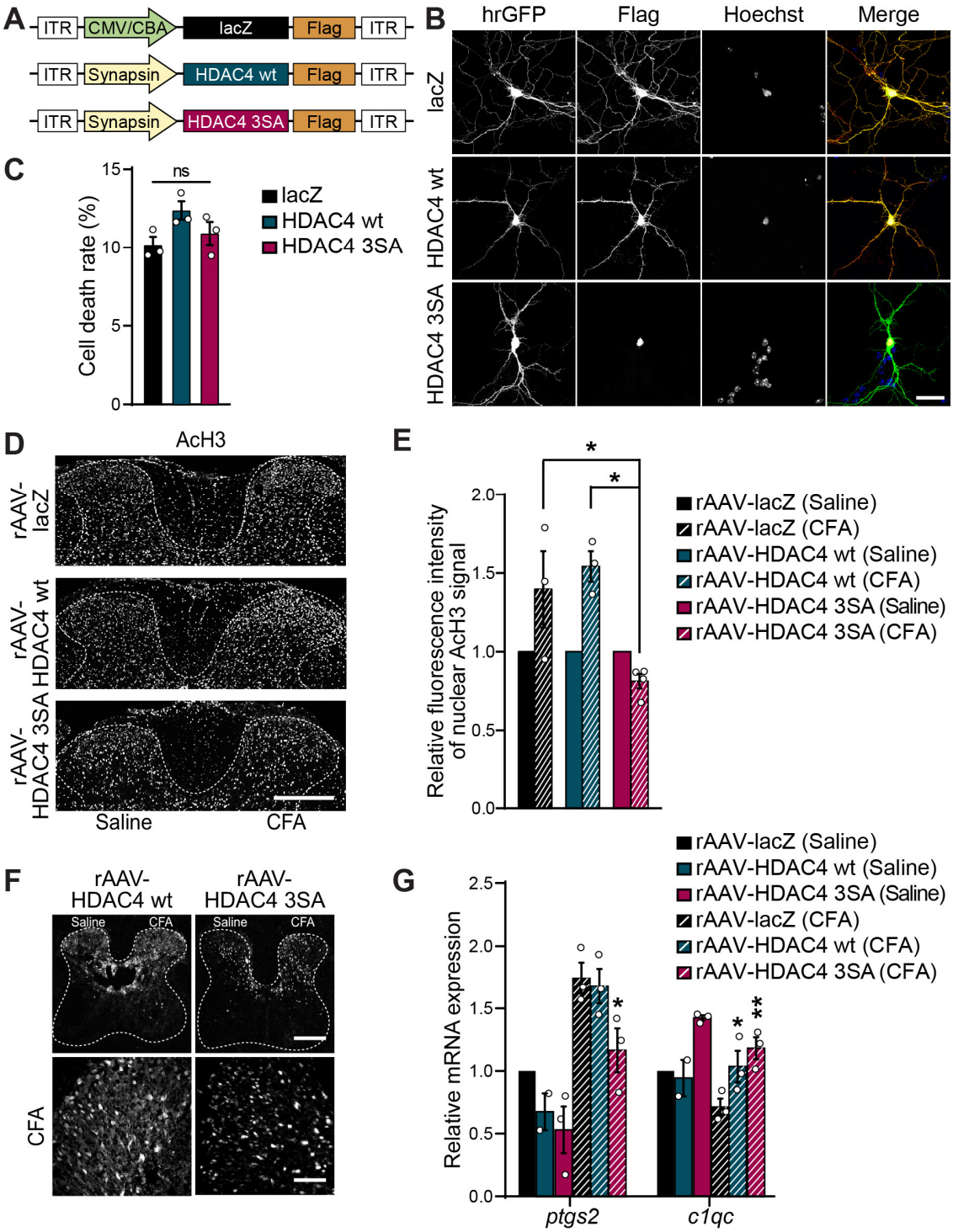

Figure 22: Nuclear HDAC4 regulates histone 3 acetylation and gene expression.

(A) Schematic representation of the rAAVs used for intraspinal injections. (B) Representative images of cultured spinal cord neurons at DIV 13, co-transfected with hrGFP and flag-tagged expression constructs for either lacZ, HDAC4 wt, or HDAC4 3SA. hrGFP fluorescence (green) reveals complete dendritic architecture and immunolabeling of flag tags (red) shows the subcellular localization of transgenes. Nuclei were labelled with Hoechst (blue). Scale bar is 40 µm. (C) Quantification of the average cell death rate of spinal cord cultured neurons transfected as in (B). 430 neurons (lacZ), 250 neurons (HDAC4 wt), and 209 neurons (HDAC4 3SA) from three independent experiments (n=3) were analyzed. (D) Representative images of dorsal sections of lumbar spinal cord L3-5, immunostained for acetylated histone H3-Lys9 (AcH3), intra-spinally injected with rAAV-lacZ, -HDAC4 wt, or -HDAC4 3SA, followed by unilateral intraplantar injections of CFA or saline for 24 h. Scale bar is 300 µm. (E) Quantification of relative fluorescence intensities of the nuclear signal of AcH3 in neurons of the dorsal horn (laminae I-V), following intraspinal rAAV delivery and intraplantar CFA and saline injections, as in (D), normalized to contralateral (saline) sides (n=3-4 mice per construct). (F) Representative images of lumbar spinal cord sections L3-5 (upper panels) and higher magnifications of the dorsal horn (lower panels), following intraspinal injections of rAAV-HDAC4 wt or -HDAC4 3SA, and CFA injection, revealing the presence of viral constructs and their subcellular localization. Scale bars are 300 µm (upper panels) and 100 µm (lower panels). (G) QRT-PCR analysis of *ptgs2* and *c1qc* in lumbar L3-5 spinal cord segments, 24 h after intraplantar injection of CFA or saline, in animals expressing lacZ, HDAC4 wt, or HDAC4 3SA (n=2-3 mice per condition). Expression values were normalized to rAAV-lacZ and saline-injected mice. Statistically significant differences were determined by one-way ANOVA followed by Tukey's post hoc test (C, E) or two-way ANOVA followed by Dunnett's post hoc test. **, $p < 0.01$; *, $p < 0.05$. In bar graphs, each point represents the mean value derived from one independent experiment (C) or animal (E, G). Graphs represent mean ± SEM.

3.3.7 Nuclear HDAC4 regulates pain hypersensitivity

Considering that persistent inflammatory pain induces nuclear export of HDAC4, whereas its subcellular localization regulates transcription of pain-associated genes, we investigated whether the subcellular localization of HDAC4 would affect behavioral hypersensitivity during inflammatory pain.

In collaboration with the lab of Prof. Rohini Kuner, mice were intra-spinally injected by Jianning Lu with rAAV-HDAC4 3SA, -HDAC4 wt, or saline as control and received, after three weeks, unilateral injections of CFA into one hind paw. Response thresholds to mechanical and thermal stimuli were assessed by Eszter Paldy, using the von Frey test and Hargreaves' method, respectively. Basal sensitivity was similar in all mice independent of the injected construct (Figure 23A-E). Upon CFA injection, all mice developed mechanical and thermal hypersensitivity, lasting up to ten days, expressed by an increase in the sum of all responses to stimulation with von Frey

filaments and reduced response latencies to thermal stimulation (Figure 23A, C). However, intraspinal expression of HDAC4 3SA significantly reduced mechanical hypersensitivity starting 24 hours after CFA-injection and lasted until nociceptive thresholds returned to basal levels (Figure 23A). In particular, rAAV-HDAC4 3SA injected mice showed significantly reduced allodynia in comparison to controls when stimulated by light touch filaments (0.04 g and 0.07 g), whereas hyperalgesia was not affected (Figure 23F-G). In contrast, thermal sensitivity was similar in all experimental groups (Figure 23C-D).
Taken together, these data suggest a regulatory role of HDAC4 subcellular localization in the induction of CFA-mediated mechanical hypersensitivity and spinal sensitization.

To dissect different temporal phases over which HDAC4 subcellular localization regulates pain behavior we investigated whether nuclear HDAC4 affects also acute nociception and early sensitization by applying the capsaicin and formalin tests in mice expressing HDAC4 3SA, HDAC4 wt or lacZ in the spinal cord dorsal horn. Intraplantar injection of capsaicin leads to acute activation of nociceptors, lasting for seconds to minutes. Within five minutes following capsaicin injection, durations of evoked acute nocifensive behaviors showed no significant differences between mice intra-spinally injected with rAAV-HDAC4 3SA and control animals (rAAV-lacZ: 25.84 s ± 3.29 s; rAAV-HDAC4 wt: 31.04 s ± 2.96 s; rAAV-HDAC4 3SA: 24.94 s ± 2.65 s; Figure 23H).
In contrast, the formalin test is characterized by a bi-phasic nociceptive response and bridges the aspect of acute nociceptor activation, as in the capsaicin model, and the early phase of inflammatory pain-mediated spinal sensitization of the CFA model (Coderre et al., 1990, Hunskaar and Hole, 1987, Tjolsen et al., 1992). During the acute phase (0-10 min after injection) intraplantar injections of formalin in mice expressing either lacZ, HDAC4 wt, or HDAC4 3SA in the lumbar spinal cord dorsal horn, evoked spontaneous nocifensive behaviors to a similar extend in all experimental groups (rAAV-lacZ: 67.5 s ± 4.28 s; rAAV-HDAC4 wt: 50.78 s ± 3.92 s; rAAV-HDAC4 3SA: 52.26 s ± 7.5 s; Figure 23I-J). However, during the second phase (10-60 min after injection), which is characterized by the induction of acute nociceptive hypersensitivity, thought to rely on plasticity-dependent changes in central neurons and on-going nociceptor activation (Coderre et al., 1990, Hunskaar

and Hole, 1987, Tjolsen et al., 1992), duration of nocifensive behaviors were significantly reduced in mice expressing HDAC4 3SA compared to both controls (rAAV-lacZ: 340.5 s ± 25.81 s; rAAV-HDAC4 wt: 275.7 s ± 24.61 s; rAAV-HDAC4 3SA: 155.1 s ± 16.38 s; Figure 23I-J).

Taken together, our data suggest that nuclear HDAC4 in dorsal horn neurons negatively affects the development of spinal sensitization without altering basal sensitivity or acute nociception.

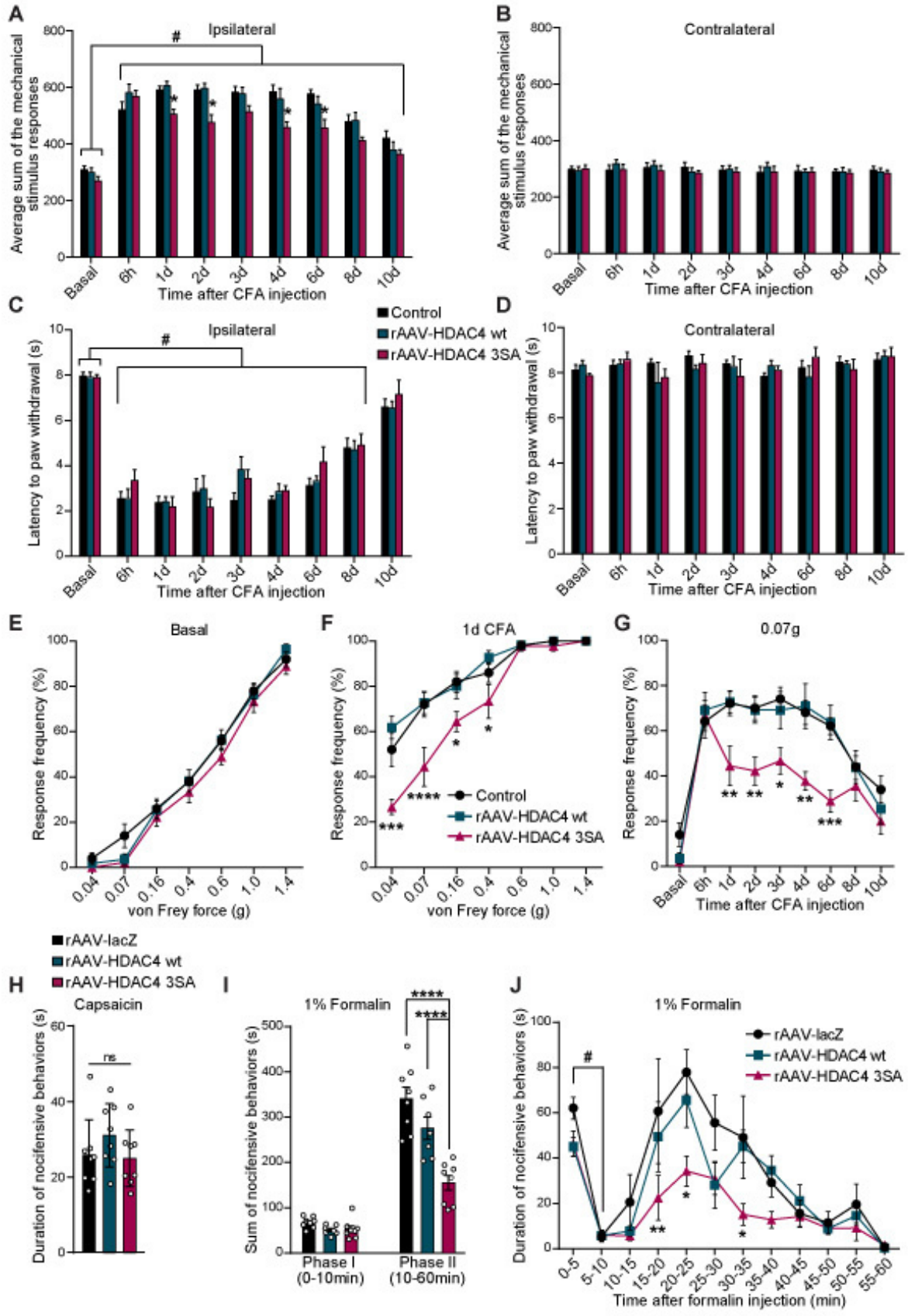

Figure 23: Nuclear HDAC4 regulates pain hypersensitivity.

(A-B) Mechanical hypersensitivity following plantar CFA injection is presented as the average sum of the von Frey stimulus responses at indicated timepoints of animals intra-spinally injected as indicated. (C-D) Thermal hypersensitivity following CFA-induced hind paw inflammation is presented as a drop in the paw withdrawal latency to a radiant heat light source at indicated timepoints of animals intra-spinally injected as indicated. (E-G) Stimulus intensity-response frequency curves of sensitivity to plantar von Frey mechanical stimulation in the same cohort of mice shown in (A-D). Shown are curves in the basal state (E) and at 24 h after intraplantar CFA injection (F) for all filaments. Panel (G) shows the response frequency to light touch (0.07 g filament) over time (n=9-11 mice per condition (A-G)). (H) Cumulative durations of acute nocifensive behaviors evoked by intraplantar injection of capsaicin in mice intra-spinally injected as indicated (n=8 mice per condition). (I-J) Cumulative durations of nocifensive behaviors evoked by intraplantar injection of formalin in mice intra-spinally injected as indicated. Bar graphs in panel (I) represent the sum of all nocifensive behaviors divided into early (Phase I) and late phase (Phase II) responses and panel (J) shows the response curves over time (n=7-8 mice per condition). Statistically significant differences were determined by one-way ANOVA followed by Tukey's post hoc test (H) or two-way ANOVA with repeated measures followed by Dunnett's post hoc test for comparisons to basal values and Tukey's post hoc test for comparisons between conditions (A-G, I-J). ****, $p < 0.0001$; ***, $p < 0.001$; **, $p < 0.01$; *, $p < 0.05$; #, $p < 0.05$. Asterisks (*) refer to statistical comparisons between conditions and hashtags (#) to comparisons relative to basal values. In bar graphs (H-I), each point represents the mean value derived from one animal. Graphs represent mean ± SEM. (Intraspinal injections of rAAV-constructs and behavioral assessments (A-G) were performed by Jianning Lu and Eszter Paldy from the lab of Prof. Kuner).

3.3.8 Infection control of primary afferent neurons

Immunohistological analysis of spinal cord sections of mice injected with rAAV-constructs showed a local distribution of infected cells in the spinal cord dorsal horn (Figure 22F). To exclude transduction of primary afferent neurons, which could contribute to the observed changes in behavioral hypersensitivity (Figure 23), dorsal root ganglia (DRGs) were screened for signs of viral infection (Figure 24). To enhance the visibility of infected tissue upon intraspinal injection, we utilized a rAAV construct that mediates strong expression of the green fluorescent protein (GFP) (rAAV-GFP). Following intraparenchymal injection of rAAV-GFP, GFP expression was limited to the area of the dorsal horn in spinal segments L3-5, as expected, whereas no signs of viral infection could be detected in sections of corresponding DRGs (Figure 24A). Moreover, DRGs of mice intra-spinally injected with rAAV-HDAC4 3SA or -HDAC4 wt did not show an overexpression of HDAC4 compared to control mice (rAAV-lacZ) (Figure 24B), confirming that the area of viral infection is restricted to the injection site within the dorsal horn.

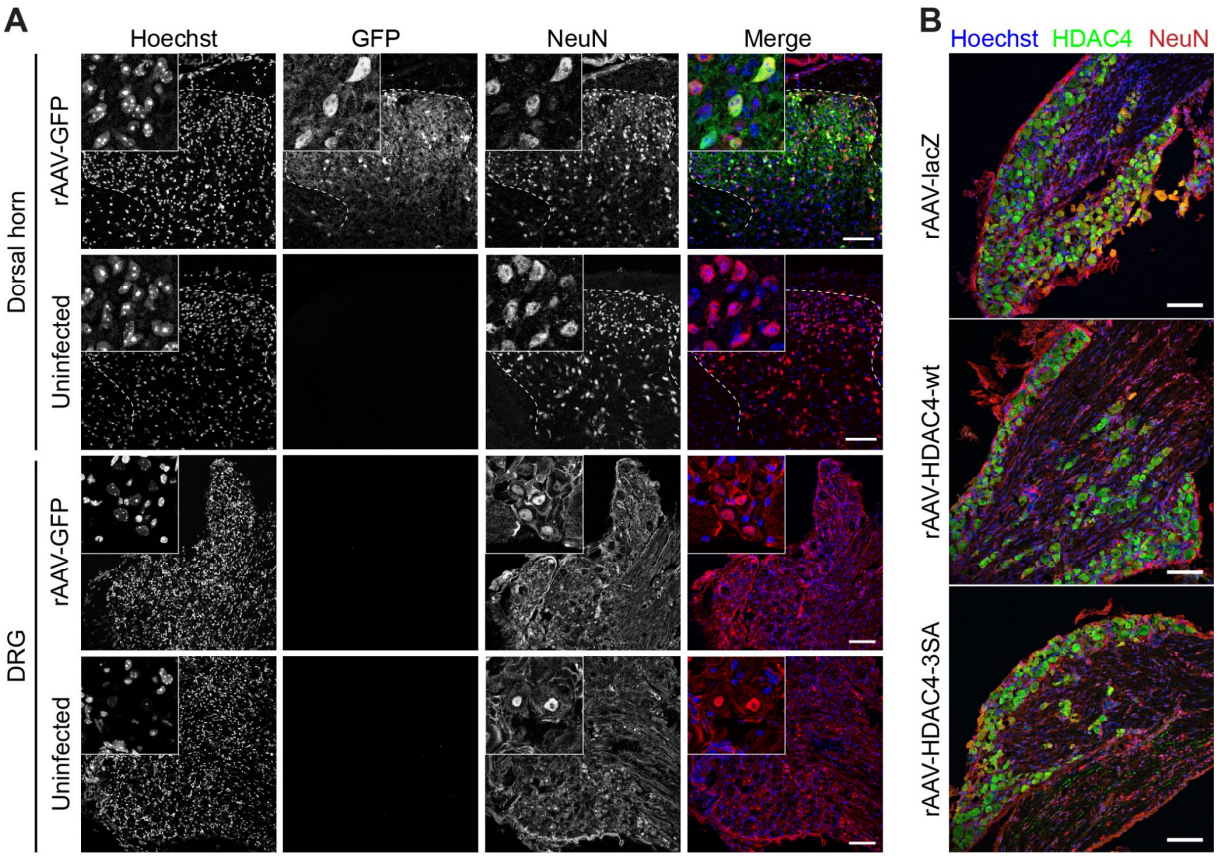

Figure 24: DRGs do not get infected by intraparenchymal injection of rAAV.

(A) Representative images of dorsal sections of lumbar spinal cord L3-5 (dorsal horn) and corresponding dorsal root ganglia (DRG), intra-spinally injected with rAAV-GFP (green) or uninfected. Nuclei were labelled with Hoechst (blue) and NeuN (red) as neuronal marker. Scale bars are 100 µm. (B) Representative images of DRG sections from the lumbar spinal cord (L3-5) of mice intra-spinally injected with rAAV-lacZ, -HDAC4 wt, or -HDAC4 3SA, immunostained for HDAC4 (green). Nuclei were labelled with Hoechst (blue) and NeuN (red) as neuronal marker. Scale bars are 100 µm.

3.3.9 HDAC4 shapes dendritic morphology of cultured spinal cord neurons

Structural adaptations and changes in the plasticity of central spinal cord neurons have been linked to central sensitization (Simonetti et al., 2013, Kuner, 2010). Given that the subcellular localization of HDAC4 controls dendritic morphology by regulating expression of VEGFD (Litke et al., 2018) and governs a transcriptional program essential for synaptic plasticity in hippocampal neurons (Sando et al., 2012), we sought to investigate whether morphology of spinal cord neurons is also regulated by HDAC4.

Spinal cord cultures were co-transfected on DIV 10 using expression vectors for either lacZ, HDAC4 wt, or HDAC4 3SA, in combination with hrGFP to reveal the entire dendritic arbor. Immunolabeling of the epitope tag revealed that HDAC4 wt was equally distributed between the nucleus and the cytosol, similar to lacZ-transfected cells, whereas HDAC4 3SA was exclusively localized in the nucleus, as expected (Figure 25A). Morphometric analyses at DIV 13 showed severe impairments of the total dendritic length (Figure 25B) and complexity of the dendritic arbor (Figure 25C-D), in HDAC4 3SA expressing neurons, compared to cells transfected with HDAC4 wt or lacZ (total dendritic length: lacZ, 1265 µm ± 306 µm; HDAC4 wt, 1314 µm ± 307 µm; HDAC4 3SA, 638 µm ± 216 µm; total number of intersections: lacZ, 186 ± 48; HDAC4 wt, 187 ± 46; HDAC4 3SA, 94 ± 28).

Thus, our data indicate that nuclear HDAC4 compromises the dendritic architecture of cultured spinal cord neurons.

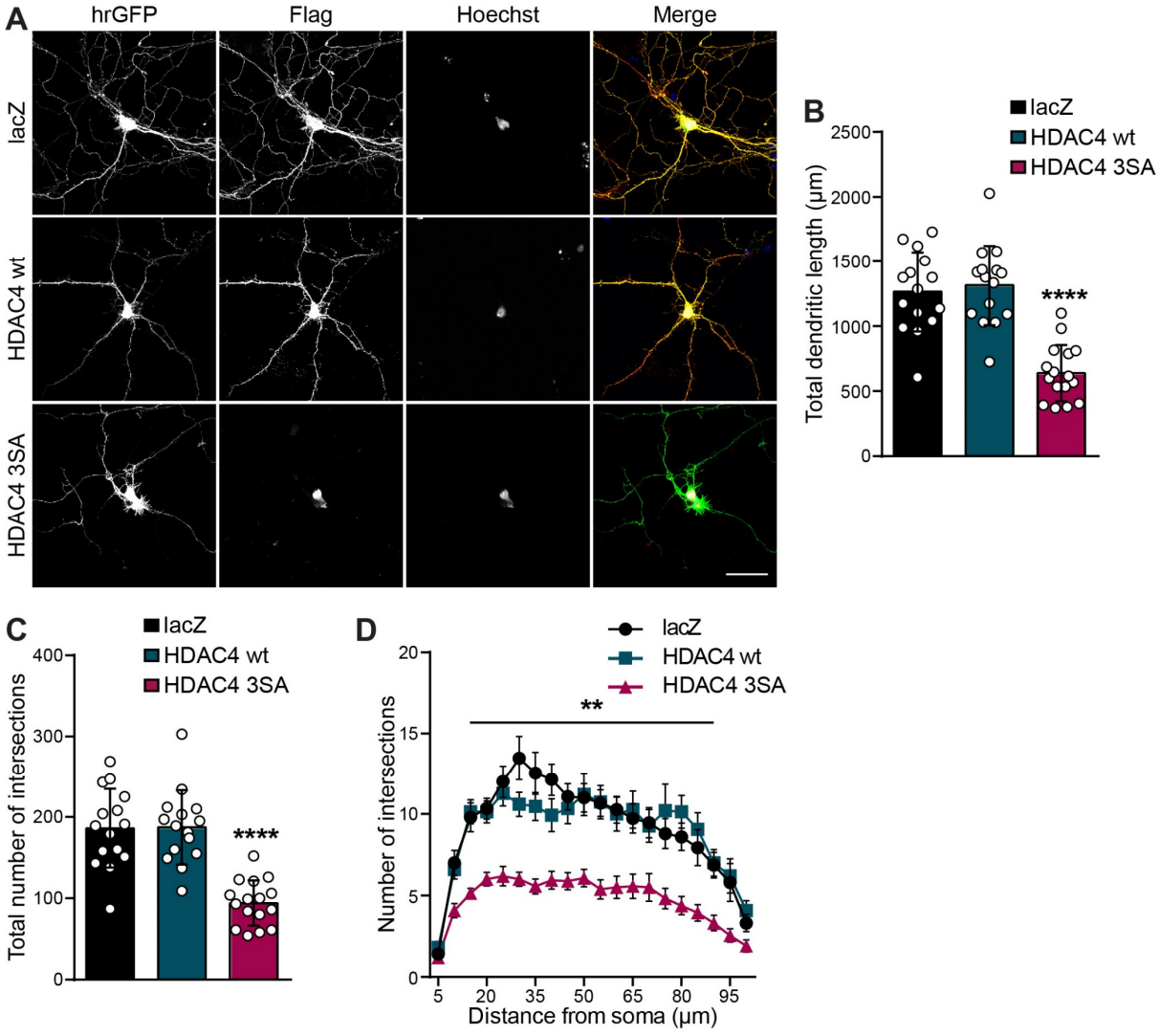

Figure 25: HDAC4 affects morphology of cultured spinal cord neurons.

(A) Representative images of cultured spinal cord neurons at DIV 13, co-transfected with hrGFP and flag-tagged constructs lacZ, HDAC4 wt, or HDAC4 3SA for 5 days. hrGFP fluorescence reveals complete dendritic architecture and immunolabeling of flag tags shows the subcellular localization of transgenes. Nuclei were labelled with Hoechst. Scale bar is 40 µm. (B) Quantification of the total dendritic length of spinal cord neurons transfected as indicated. (C) Total number of intersections derived from Sholl analysis (D). In total, 15 neurons (lacZ and HDAC4 wt) and 16 neurons (HDAC4 3SA) from three independent experiments (n=3) were analyzed for each construct. Statistically significant differences were determined by one-way ANOVA (B-C) and two-way ANOVA (D), followed by Tukey's post hoc test. ****, $p < 0.0001$; **, $p < 0.01$. In bar graphs, each point represents a value derived from one neuron (B-C). Graphs represent mean ± S.D.

3.3.10 Analysis of dendritic morphology in dorsal horn neurons

Prompted by the regulatory effects of nuclear HDAC4 on the dendritic structure of hippocampal and spinal cord neurons *in vitro* (Figure 8 andFigure 25), we investigated whether HDAC4 subcellular localization also mediates similar effects in dorsal horn neurons *in vivo*.

Spinal cord tissues of animals intra-spinally injected with either rAAV-lacZ, -HDAC4 wt or -HDAC4 3SA, were stained using the Golgi-Cox method in order to visualize the entire dendritic arbor of individual neurons. The method has been modified over the years but is still based on the "black reaction", originally described by Camillo Golgi in 1873. Cells were impregnated with potassium (di)chromate and mercuric chloride, forming black mercuric sulfide crystals that accumulate in neuronal membranes after alkalization, allowing visualization under a light microscope (Fregerslev et al., 1971, Das et al., 2013, Stean, 1974). Golgi-staining of spinal cord sections labeled neurons across dorsal horn laminae IV-VI and the ventral horn (Figure 26A).

Only neurons in lamina V, displaying a continuous labeling of primary, as well as higher order dendrites were used for quantifications (Figure 26B). However, morphological analyses revealed no significant changes in the total dendritic length between HDAC4 3SA expressing mice and controls (total dendritic length: lacZ, 853 µm ± 182 µm; HDAC4 wt, 886 µm ± 223 µm; HDAC4 3SA, 798 µm ± 254 µm; Figure 26C). Moreover, total number of intersections was not affected (lacZ, 128 ± 27; HDAC4 wt, 133 µm ± 34; HDAC4 3SA, 120 ± 38; Figure 26D). Only slight differences between HDAC4 3SA injected mice and controls could be identified in the number of intersections at 40 µm and 60 µm distance apart from the soma (Figure

26E). In summary, nuclear HDAC4 affects dendritic morphology of cultured spinal cord neurons but not in dorsal horn neurons of lamina V *in vivo*.

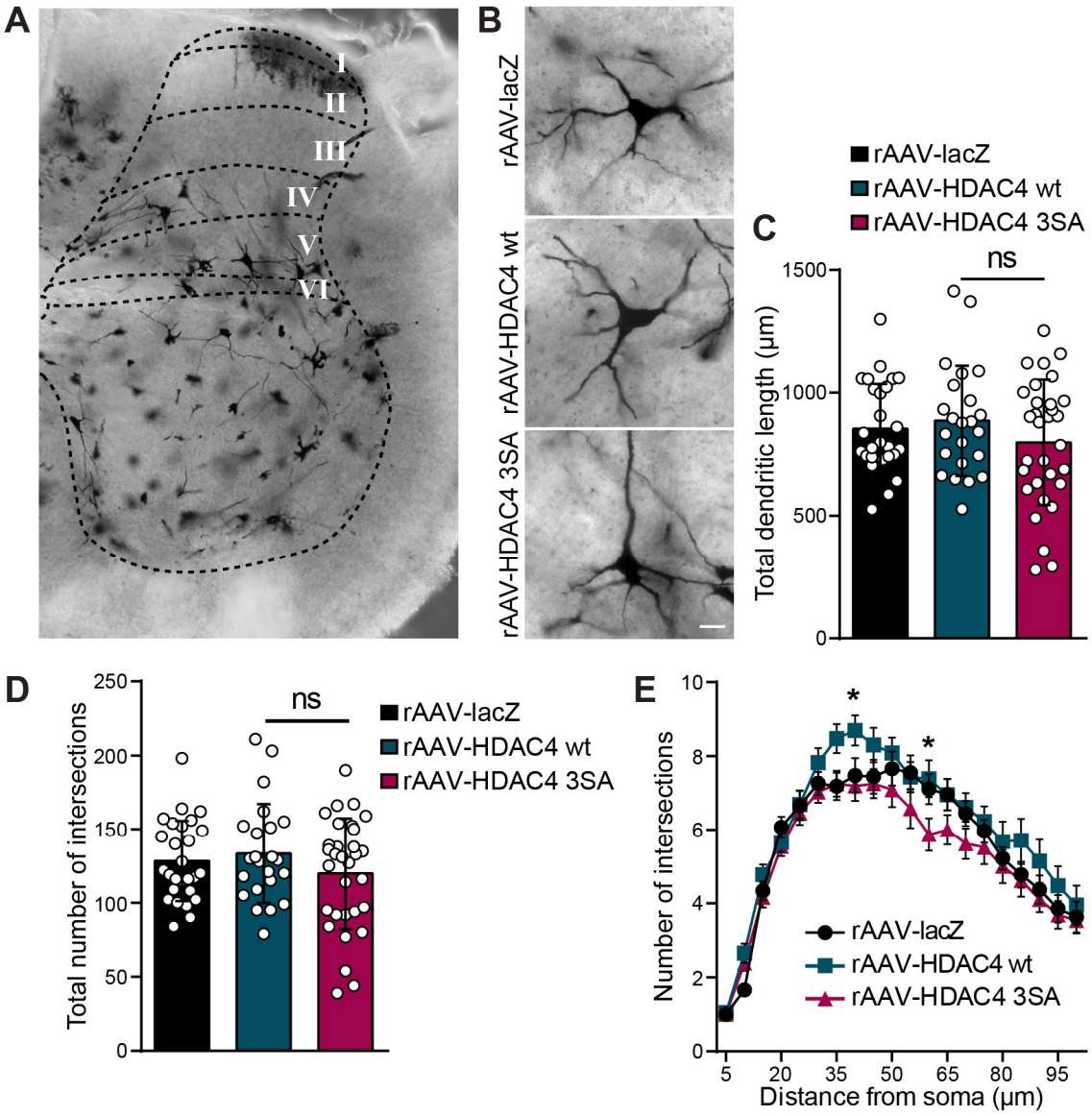

Figure 26: HDAC4 does not affect morphology of lamina V dorsal horn neurons.
(A) Representative image of Golgi staining on a spinal cord section with neurons labelled across dorsal horn laminae IV – VI and the ventral horn. (B) Typical examples of labeled neurons in dorsal horn lamina V from mice intra-spinally injected with rAAV-lacZ, -HDAC4 wt, or HDAC4 3SA. Scale bar is 20 µm. (C) Quantification of the total dendritic length of spinal cord neurons in lamina V from mice intra-spinally injected as indicated. (D) Total number of intersections derived from Sholl analysis (E). Ca. 30 neurons from four independent experiments (n=4) were analyzed in each condition. Statistically significant differences were determined by one-way ANOVA (C-D) and two-way ANOVA (E), followed by Tukey's post hoc test. *, $p < 0.05$. In bar graphs, each point represents a value derived from one neuron (C-D). Graphs represent mean ± S.D.

3.3.11 RNAseq analysis of HDAC4 regulated genes in inflammatory pain

HDAC4 regulates expression of pain and plasticity related genes (Figure 22G). Prompted by the effects of nuclear HDAC4 on hypersensitivity in inflammatory pain (Figure 23), as well as on dendritic structures of spinal cord neurons (Figure 25), we sought to identify underlying genetic down-stream targets of HDAC4 in the context of inflammatory pain.

A comprehensive transcriptome analysis was performed using next generation RNA sequencing (RNAseq) with samples derived from the lumbar dorsal horn of mice that received intraspinal injections of either rAAV-lacZ, -HDAC4 wt, or -HDAC4 3SA, followed by intraplantar injections of CFA or saline for 24 hours. RNAseq and differential gene expression analysis were performed by GATC Biotech AG. Due to the complexity and amount of generated data, we focused our analysis on genes that were differentially regulated upon CFA-induced inflammatory pain compared to saline-injected mice, in the respective condition (rAAV-lacZ, - HDAC4 wt, or HDAC4 3SA) (Figure 27A). Following CFA injection, we found 104 genes upregulated and nine genes downregulated in lacZ-expressing mice, whereas 47 genes were up- and five genes downregulated in HDAC4 wt expressing animals, and 252 up- and six genes downregulated in mice intra-spinally injected with HDAC4 3SA. Details on expression foldchanges and annotation of identified DEGs is given in supplementary tables (Table 11-Table 16).

Genes that were differentially regulated (FDR-adjusted p-value < 0.05) upon CFA injection in lacZ-expressing mice were analyzed for enrichment of gene ontology (GO) terms. Following CFA injection, identified biological processes (enrichment score > 5) indicated an inflammatory immune response, as expected (Figure 27B).

Expression foldchanges of identified and significantly regulated genes that were exclusively under the control of CFA (rAAV-lacZ; saline vs. CFA) were compared to the expression foldchanges of HDAC4 wt and HDAC4 3SA expressing mice (saline vs. CFA) (Figure 27C-D). Most DEGs that were upregulated in rAAV-lacZ injected mice under inflammatory pain, showed a relative decrease in their foldchange in HDAC4 wt and HDAC4 3SA expressing animals (Figure 27D).

However, to identify genes that possibly explain the ameliorating effect of nuclear HDAC4 on spinal sensitization (Figure 23), we focused our analysis on genes that were induced in both lacZ and HDAC4 wt expressing mice, following CFA injection, but not or less induced in rAAV-HDAC4 3SA injected mice. Respective expression

foldchanges of identified target genes are shown in Figure 27E. Transcriptional changes were confirmed using QRT-PCR analysis on an extended cohort of samples, including the ones used for RNAseq (Figure 27F). In line with our observations obtained from RNAseq analysis, relative mRNA levels of *slc22a6*, *slc26a7*, *prx*, *nov*, *lrg1*, *h19*, and *msln* were reduced in HDAC4 3SA expressing mice, compared to controls, in the context of inflammatory pain.

Our analysis identified several inflammatory pain-induced genes in the spinal cord, whose expression is under the control of the subcellular localization of HDAC4 in dorsal horn neurons and suggests their involvement in the development of early central sensitization.

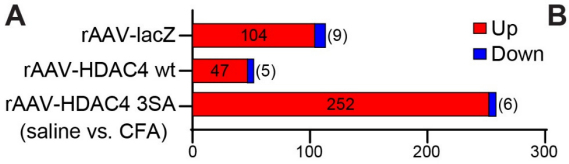

B

GO term	GO biological process	Fold enrichment	FDR
GO:0015816	Glycine transport	56.36	2.28E-02
GO:0002523	Leukocyte migration involved in inflammatory response	37.57	6.98E-03
GO:0007159	Leukocyte cell-cell adhesion	21.47	6.12E-03
GO:0019730	Antimicrobial humoral response	17.89	1.09E-02
GO:0071621	Granulocyte chemotaxis	15.66	1.56E-02
GO:0046942	Carboxylic acid transport	7.42	1.09E-02
GO:0015711	Organic anion transport	5.33	2.80E-02

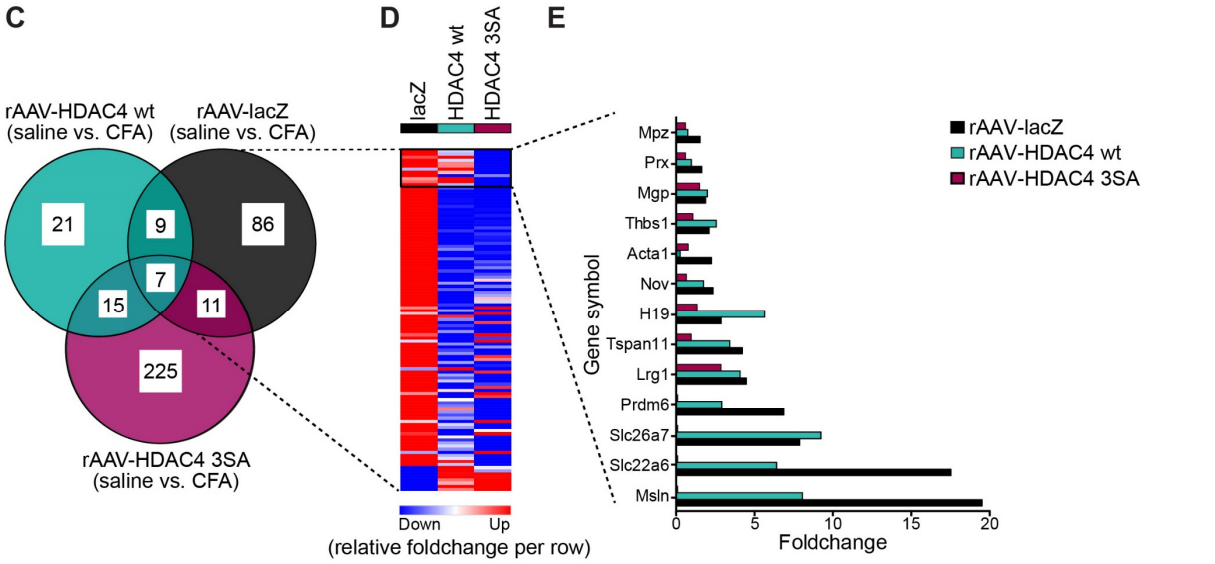

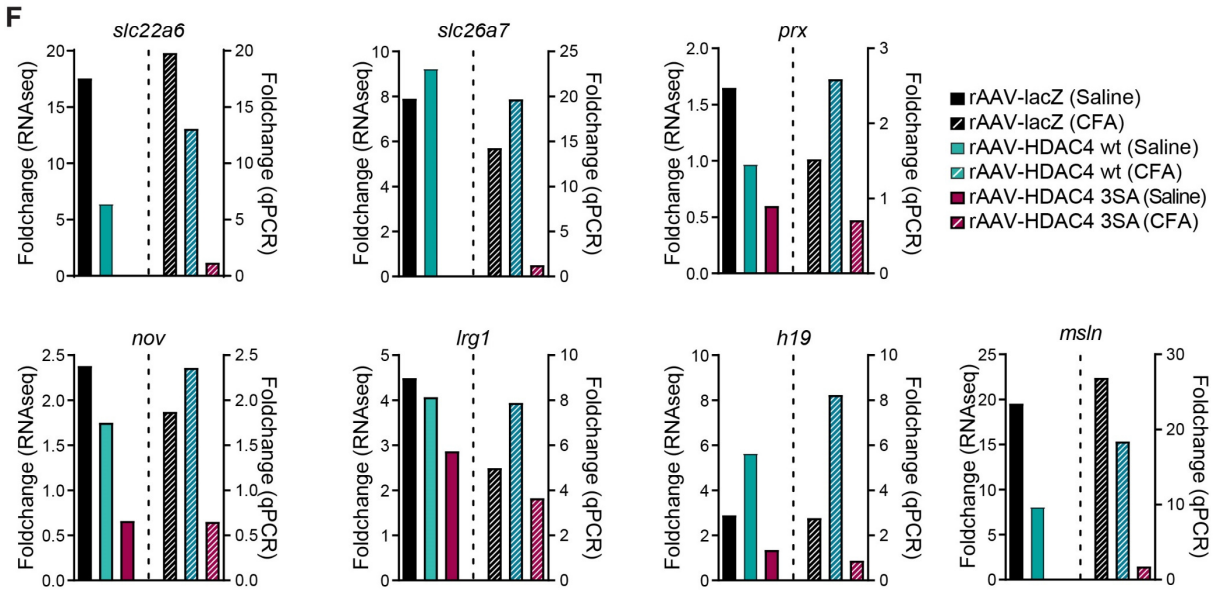

Figure 27: RNAseq analysis of HDAC4 regulated genes in inflammatory pain.
(A) Number of differentially expressed genes (DEGs) ($p_{adjusted} < 0.05$), identified by RNA-seq analysis, in the dorsal spinal cord (L3-5) of mice, intra-spinally injected with either rAAV-lacZ, -HDAC4 wt, or HDAC4 3SA that are significantly up- or downregulated following intraplantar injection of CFA (n=3 mice/group). (B) Gene ontology (GO) analysis of DEGs that are significantly up- or downregulated following CFA injection in lacZ-expressing mice, using the PANTHER overrepresentation test and database. Enriched GO terms with an enrichment score > 5 are listed. (C) Venn diagram illustrating

the number and overlap of significantly up- or downregulated DEGs following CFA injection, as in (A). (D) Heat map of the relative foldchange of significantly DEGs in lacZ expressing mice after CFA injection compared to the foldchanges of the same genes in rAAV-HDAC4 wt or -HDAC4 3SA injected mice. (E) Relative expression foldchanges of CFA-induced genes according to (C) that are not induced in HDAC4 3SA-expressing mice. (F) Comparison of relative expression foldchanges obtained from RNAseq analysis, according to (E), with relative expression foldchanges from QRT-PCR validation analysis using additional samples in combination with samples of the RNAseq experiment (*slc22a6*, *slc26a7*, *prx*, *nov* and *lrg1* (n=6), *h19* and *msln* (n=3).

3.3.12 Regulation of OAT1 in the spinal cord dorsal horn

Among the top CFA-induced genes whose transcription was strongly regulated by the subcellular localization of HDAC4, we identified members of the solute carrier (SLC) superfamily. S*lc22a6* (solute carrier family 22 member 6), encoding the organic anion transporter 1 (OAT1), is one of the best characterized members of the OAT family of transmembrane proteins and known to mediate the transport of a diverse range of low molecular weight substrates, including steroids, hormones, neurotransmitters, as well as numerous drugs and xenobiotics (Roth et al., 2012). OAT1 is primarily expressed in the kidney, where it has well-described functions in the renal clearance from organic anions, in exchange for α-ketoglutarate (Hosoyamada et al., 1999, Roth et al., 2012). While expression of OAT1 has also been detected in neurons of the CNS as well as in the ependymal cell layer of the choroid plexus (Roth et al., 2012, Bahn et al., 2005), a detailed understanding of its function in the nervous system is still missing.

Based on our findings that transcript levels of *slc22a6* were dramatically increased in the lumbar spinal cord of control mice, 24 hours after intraplantar injection of CFA (Figure 27E-F), we investigated whether an increase in the expression of OAT1 could also be observed at the protein level. Immunohistochemical analyses of lumbar spinal cord sections of wildtype mice that received intraplantar injections of either CFA or saline for 24 hours, showed a significant increase in the relative fluorescence intensity of the OAT1 signal throughout dorsal horn laminae I – V (Figure 28A-B). Accordingly, immunoblot analysis of dorsal spinal cord (L3-5) tissue of mice injected with CFA over a time course of 0.5; 2; 6, or 24 hours, showed a significant increase in the detected antibody signal of OAT1 at 24 hours post inflammation, compared to saline-injected controls (Figure 28C-D).

In contrast, mice that underwent sciatic nerve ligation according to the spared nerve injury (SNI) model (Richner et al., 2011), over a period of 21 days, eliciting long-lasting neuropathic pain, did not show a change in the fluorescent intensity of the OAT1 signal in the dorsal spinal cord (Figure 28E).

Immunohistochemical analyses of dorsal horn sections from an independent cohort of mice, showed that expression of HDAC4 3SA completely prevents the induction of OAT1 in CFA injected mice, compared to control conditions (Figure 28F). This confirms the results obtained from RNAseq analysis (Figure 27E-F) and further supports the hypothesis that nuclear accumulation of HDAC4 in neurons of the dorsal horn regulates OAT1 expression.

Given that all previous analyses were performed in tissue samples containing mixed cell populations, we performed a co-localization analysis in spinal sections, using NeuN as neuronal marker, to identify the cell type showing a change in expression of OAT1 upon inflammation. Quantifications revealed that the CFA-mediated increase in the expression of OAT1 is primarily taking place in neurons, whereas non-neuronal cells did not show a change in OAT1 levels (Figure 28G).

Taken together, our data indicate that the expression of OAT1 is specifically induced in neurons of the spinal cord dorsal horn by CFA-mediated inflammatory-, but not neuropathic pain, and under the control of HDAC4. Thus, OAT1 is a potential mediator of inflammatory pain that acts downstream of HDAC4.

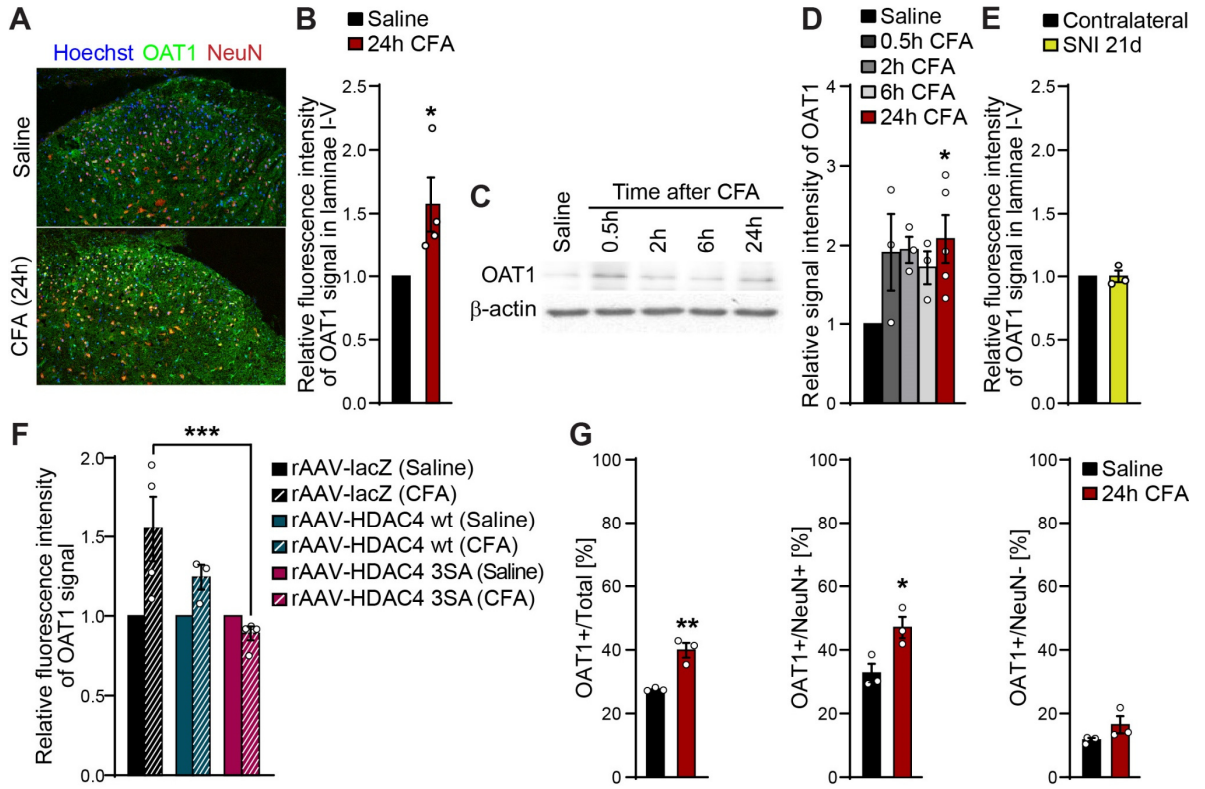

Figure 28: Regulation of OAT1 in the spinal cord dorsal horn.

(A) Representative images of dorsal horn sections of lumbar spinal segments L3-5 of wildtype mice at 24 h after saline or CFA injection, immunostained for OAT1 (green). Nuclei were labelled with Hoechst (blue) and NeuN (red) as neuronal marker. (B) Quantification of relative fluorescence intensities of the OAT1 signal in dorsal horn laminae I-V, following intraplantar CFA and saline injections, as in (A) (n=4 mice per condition). (C) Representative immunoblots of OAT1 and β-actin from dorsal horn tissue of the lumbar spinal cord segments L3-5, following saline or CFA injection, as indicated. (D) Quantification of the relative protein levels displayed in (C), normalized to saline injected control mice (n=3-5 mice per condition). (E) Quantification of relative fluorescence intensities of the OAT1 signal in dorsal horn laminae I-V, following spared nerve injury (SNI) for 21 days, normalized to contralateral sides (n=3 mice). SNI samples were provided by Dr. Anna Hertle. (F) Quantification of relative fluorescence intensities of the OAT1 signal in dorsal horn laminae I-V of mice intra-spinally injected with rAAV-lacZ, -HDAC4 wt, or -HDAC4 3SA, followed by intraplantar injections of CFA or saline for 24 h (n=3-4 mice per condition). (G) Co-localization analysis of OAT1 in the spinal cord dorsal horn following intraplantar injections of either CFA or saline for 24 h. Graphs from left to right represent the percentage of OAT1-postive cells within the total cell population (Hoechst), within the neuronal population (NeuN), or within non-neuronal cells (NeuN-negative) (n=3 mice per condition). Statistically significant differences were determined by two-tailed Student's t-test (B, E, G), one-way ANOVA followed by Dunnett's post hoc test (D), or two-way ANOVA followed by Tukey's post hoc test (F). ***, $p < 0.01$; *, $p < 0.05$. In bar graphs, each point represents the mean value derived from one independent animal. Graphs represent mean ± SEM.

3.3.13 Pharmacological inhibition of OAT1 ameliorates pain hypersensitivity

OAT1 has been shown to transport prostaglandins, which can mediate an inflammatory reaction (Roth et al., 2012). To investigate whether changes in CFA-induced hypersensitivity can be linked to the activity of OAT1 in neurons of the spinal cord, we sought to inhibit the activity of OAT1, specifically in the central nervous system. We made use of the uricosuric drug probenecid (PBN), a potent competitive inhibitor of OAT1 transport (Burckhardt and Burckhardt, 2011, Roth et al., 2012). Using minimally invasive intrathecal injections, probenecid was delivered into the subarachnoid space of the lumbar spine, allowing to bypass the blood-spinal cord barrier (BSCB) and assuring quick and easy delivery of the drug.

Mechanical and thermal hypersensitivity were assessed in mice that received unilateral injections of CFA (ipsilateral) and saline (contralateral), in combination with a single intrathecal injection of probenecid (16 µg) or vehicle as control. Intrathecal drug dose was calculated according to available literature (see 2.1.2). Six hours after CFA injection both experimental groups developed mechanical, as well as thermal hyperalgesia in the ipsilateral paw compared to basal levels, lasting until the end of the observation period of five days (Figure 29A-B). However, mice intrathecally injected with probenecid showed a temporary reduction in their responses to mechanical stimulation at six hours and one day after CFA treatment (Figure 29A). Analysis of single von Frey filaments ranging from 0.04 g up to 2 g showed that mice intrathecally injected with probenecid display a significant reduction in allodynia when stimulated with light touch filaments, as well as hyposensitivity towards large diameter filaments, at six and 24 hours after CFA injection, compared to controls (Figure 29D-E). Pain sensitivity of the contralateral paw was not affected and comparable to basal levels before intrathecal administration of probenecid (Figure 29C-E). Paw withdrawal latency to thermal stimulation was also not affected by probenecid at any measured time point post CFA injection (Figure 29B).

These data indicate a timely limited effect of probenecid in the CSF on the induction of mechanical hypersensitivity in a mouse model of persistent inflammatory pain.

To test whether probenecid has the capacity to affect pain behavior even after hypersensitivity has already been established, we repeated the experiment, injecting probenecid at a later timepoint, two days post CFA injection. Similar to previous

observations, mechanical hypersensitivity was significantly induced over the entire observation period in both experimental groups following CFA injection (Figure 29F). Nonetheless, intrathecal delivery of probenecid was sufficient to temporary ameliorate hypersensitivity to mechanical stimulation, up to one day, starting 54 hours after intraplantar CFA injection, without affecting the sensitivity of the contralateral paw (Figure 29F-H).

In summary, our data indicate that intrathecal administration of probenecid results in a temporary decrease in mechanical hypersensitivity, suggesting that inhibition of OAT1 in the central nervous system has the potential to mediate inflammatory pain behavior.

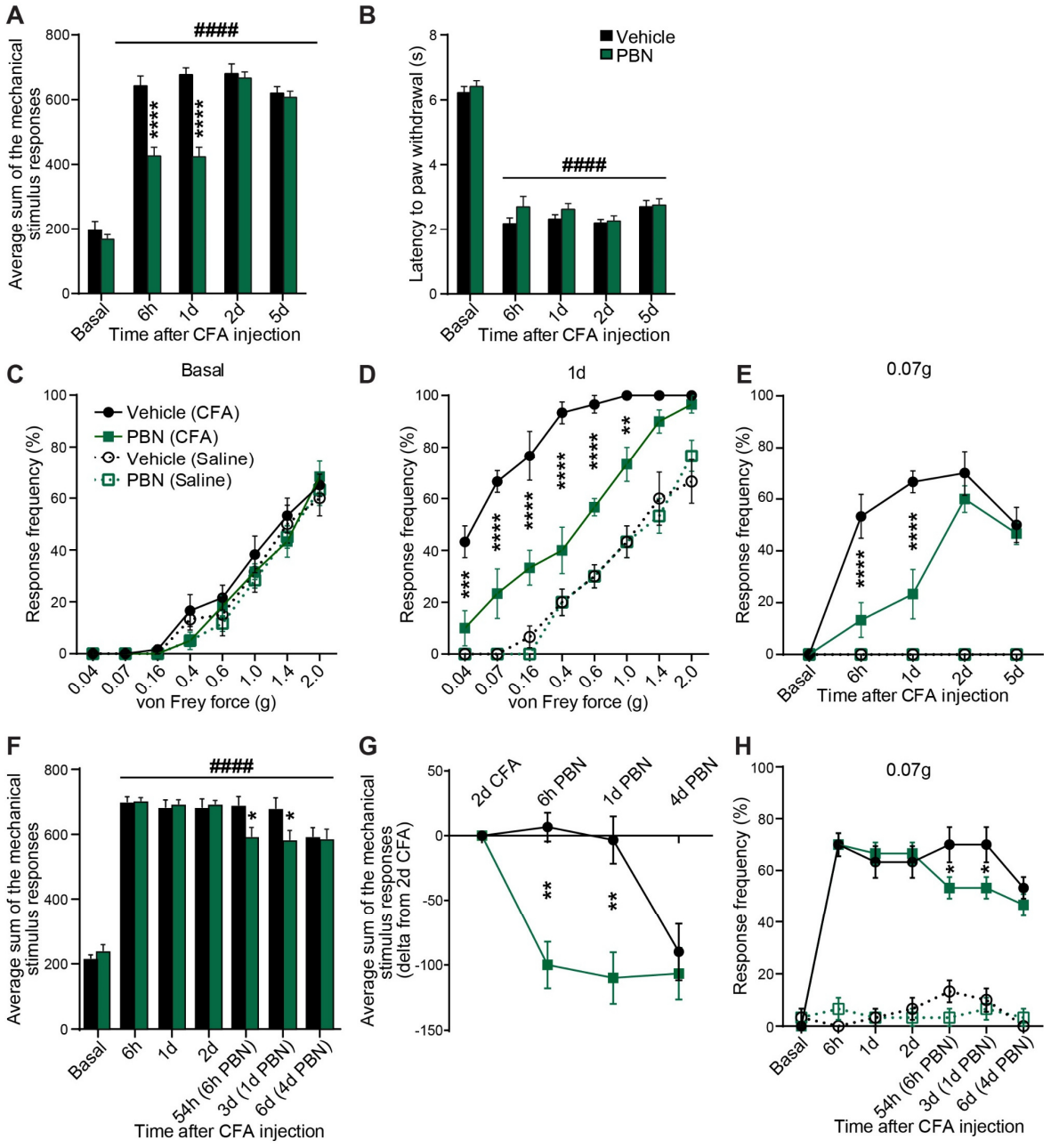

Figure 29: Pharmacological inhibition of OAT1 in the central nervous system.

(A) Mechanical hypersensitivity following plantar CFA injection, represented as the average sum of the von Frey stimulus responses at indicated timepoints of animals intrathecally injected with probenecid (PBN) or vehicle. (B) Thermal hypersensitivity following CFA-induced hind paw inflammation, represented as a drop in the paw withdrawal latency to a radiant heat light source at indicated timepoints of animals intrathecally injected as indicated. (C-E) Stimulus intensity-response frequency curves of sensitivity to plantar von Frey mechanical stimulation in the same cohort of mice shown in (A-B). Shown are curves in the basal state (C) and 24 h after intraplantar CFA injection (D) for all filaments. Panel (E) shows the response frequency to light touch (0.07 g filament) over time (n=6 mice per condition (A-E)). (F) Average sum of mechanical stimulus responses following plantar injection of CFA at indicated timepoints and intrathecal injection of probenecid (PBN) or vehicle with a delay of two days, in a new cohort of mice. (G) Average sum of mechanical stimulus responses at indicated timepoints, represented as delta from the day of intrathecal injection of PBN or vehicle, in the same cohort of mice as in (F). (H) Response frequency to light touch (0.07 g filament) stimulation at indicated timepoints (n=6 mice per condition (F-H)). Statistically significant differences were determined by two-way ANOVA with repeated measures followed by Dunnett's post hoc test for comparisons to basal values and multiple t-tests for comparisons between conditions (A-B, F-G). Two-way ANOVA with repeated measures followed by Tukey's post hoc test was used for comparisons between conditions in (C-E, H) (differences between CFA conditions are shown). ****, $p < 0.0001$; ***, $p < 0.001$; **, $p < 0.01$; *, $p < 0.05$; ####, $p < 0.0001$. Asterisks (*) refer to statistical comparisons between conditions and hashtags (#) to comparisons relative to basal values. Graphs represent mean ± SEM.

3.3.14 siRNA mediated knockdown of OAT1 in the CNS

As probenecid targets the function of OAT1, we addressed whether targeting the expression of OAT1 would also affect pain sensitivity. For this, we intrathecally injected siRNAs directed against OAT1 transcripts (siOAT1). Knockdown of OAT1 expression in the spinal cord *in vivo* could be confirmed using QRT-PCR analysis 24 h after the last siRNA injection (Figure 30A). Following intraplantar CFA injection all experimental groups developed mechanical and thermal hypersensitivity as expected (Figure 30B-C). Mice intrathecally injected with siOAT1 showed a significant reduction in mechanical hypersensitivity at six and 24 hours after CFA-treatment compared to siControl or vehicle-only injected mice (Figure 30B, F-H). In contrast, basal sensitivity as well as thermal nociceptive thresholds remained unchanged after intrathecal injections in all experimental groups (Figure 30C-E).

Taken together, these experiments provide further evidence that spinal OAT1 is a critical mediator of mechanical hypersensitivity in CFA-induced inflammatory pain.

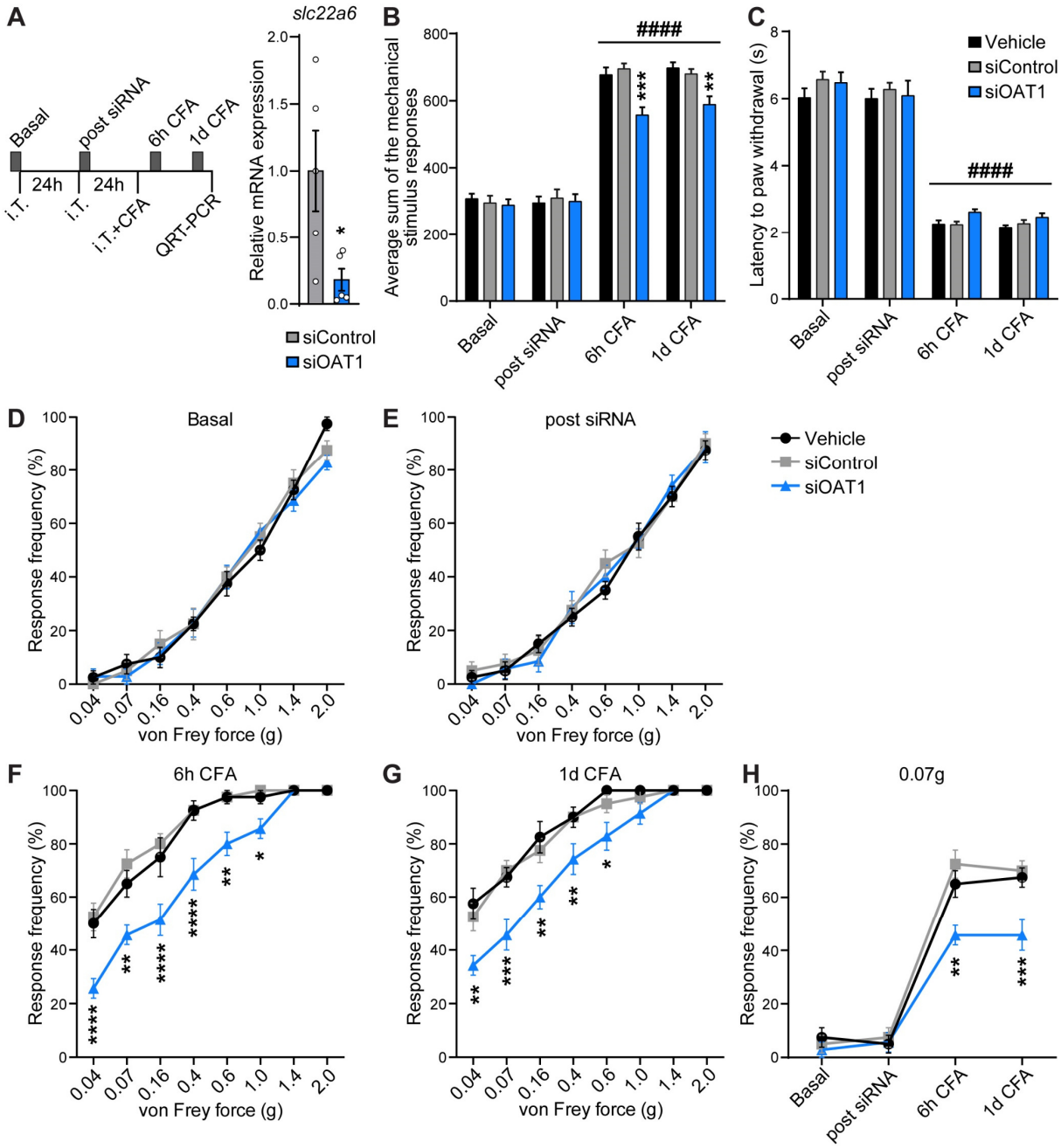

Figure 30: siRNA mediated knockdown of OAT1 in the CNS.

(A) Timeframe of the experiment and QRT-PCR validation of siRNA-mediated spinal knock down of OAT1 mRNA *in vivo* 24 h after the last of three consecutive intrathecal injections (every 24 h) of either siControl or siOAT1 (n=5 mice per condition). (B) Mechanical hypersensitivity following plantar CFA injection, represented as the average sum of the von Frey stimulus responses at indicated timepoints of animals intrathecally injected as indicated. (C) Thermal hypersensitivity following CFA-induced hind paw inflammation, represented as a drop in the paw withdrawal latency to a radiant heat light source at indicated timepoints of animals intrathecally injected as indicated. (D-H) Stimulus intensity-response frequency curves of sensitivity to plantar von Frey mechanical stimulation. Responses to all tested filaments (0.04 g – 2 g) are shown for the basal state, before (D) and after (E) intrathecal siRNA injection, as well as at 6 h (F) and 24 h (G) post intraplantar CFA and final i.T. injection.

Panel (H) shows the response frequency to light touch (0.07 g filament) over time (n=6 mice per condition (B-H)). Statistically significant differences were determined by two-tailed Student's t-test (A) or two-way ANOVA with repeated measures followed by Dunnett's post hoc test for comparisons to basal values and Tukey's post hoc test for comparisons between conditions (B-H) ****, $p < 0.0001$;***, $p < 0.001$; **, $p < 0.01$; *, $p < 0.05$; ####, $p < 0.0001$. Asterisks (*) refer to statistical comparisons between conditions and hashtags (#) to comparisons relative to basal values. In bar graphs, each point represents a value derived from one animal (A). Graphs represent mean ± SEM. (QRT-PCR analysis in panel (A) were performed by Dr. Daniela Mauceri).

3.3.15 shRNA mediated knockdown of OAT1 in the spinal cord dorsal horn

Given the limited time span of siRNA-mediated OAT1 knockdown, and that intrathecal delivery of siRNAs affects all cell types within the spinal cord canal and ventricular system of the brain, we decided to use rAAV- mediated shRNA to achieve temporal and spatial modulation of OAT1 expression.

Two different shRNAs, targeting different regions of the OAT1 mRNA sequence (rAAV-shOAT1-1 and -shOAT1-2), as well as a target-unspecific scrambled control (rAAV-shUNC), were generated and validated *in vitro* and *in vivo*. Cultured hippocampal neurons infected at DIV 3 showed a significant reduction in the mRNA levels of OAT1 by more than 50% at DIV 10 for both shOAT1 constructs, compared to control (51.4% rAAV-shOAT1-1; 71% rAAV-shOAT1-2, Figure 31A).

We found that intraspinal delivery of rAAV-shOAT1-1 and rAAV-shOAT1-2 administrated three weeks prior to intraplantar CFA injection was able to attenuate CFA-induced mechanical hypersensitivity starting at six hours after CFA treatment until the end of the observation period of ten days, as compared to mice intra-spinally injected with the shRNA-scramble control (Figure 31B, G-H). In particular, mice expressing shOAT1 displayed reduced allodynia to stimulation with light touch filaments over the entire observation period (Figure 31I), as well as an earlier decrease in hyperalgesia to noxious mechanical stimulation (Figure 31J).

Thermal sensitivity was partly affected in mice intra-spinally injected with rAAV-shOAT1-1 and -2, showing a trend towards increased paw withdrawal latencies at various timepoints (Figure 31C). In contrast, basal sensitivity, as well as acute inflammatory pain behavior, following intraplantar injection of capsaicin, was not affected in both experimental groups (Figure 31D-F) in comparison to shUNC-

injected mice. QRT-PCR analysis six weeks after injection of shRNA constructs into lumbar spinal cord segments L3-5 showed a 76.2% reduction of OAT1 mRNA in rAAV-shOAT1-1 injected mice, and 87.7% reduction in rAAV-shOAT1-2 treated animals (Figure 31K), confirming a successful *in vivo* knockdown.

In conclusion, knockdown of OAT1 expression in the spinal cord dorsal horn mediates long-lasting ameliorating effects on persistent but not acute inflammatory pain, suggesting a key role of OAT1 in the regulation of inflammatory processes in the spinal cord dorsal horn.

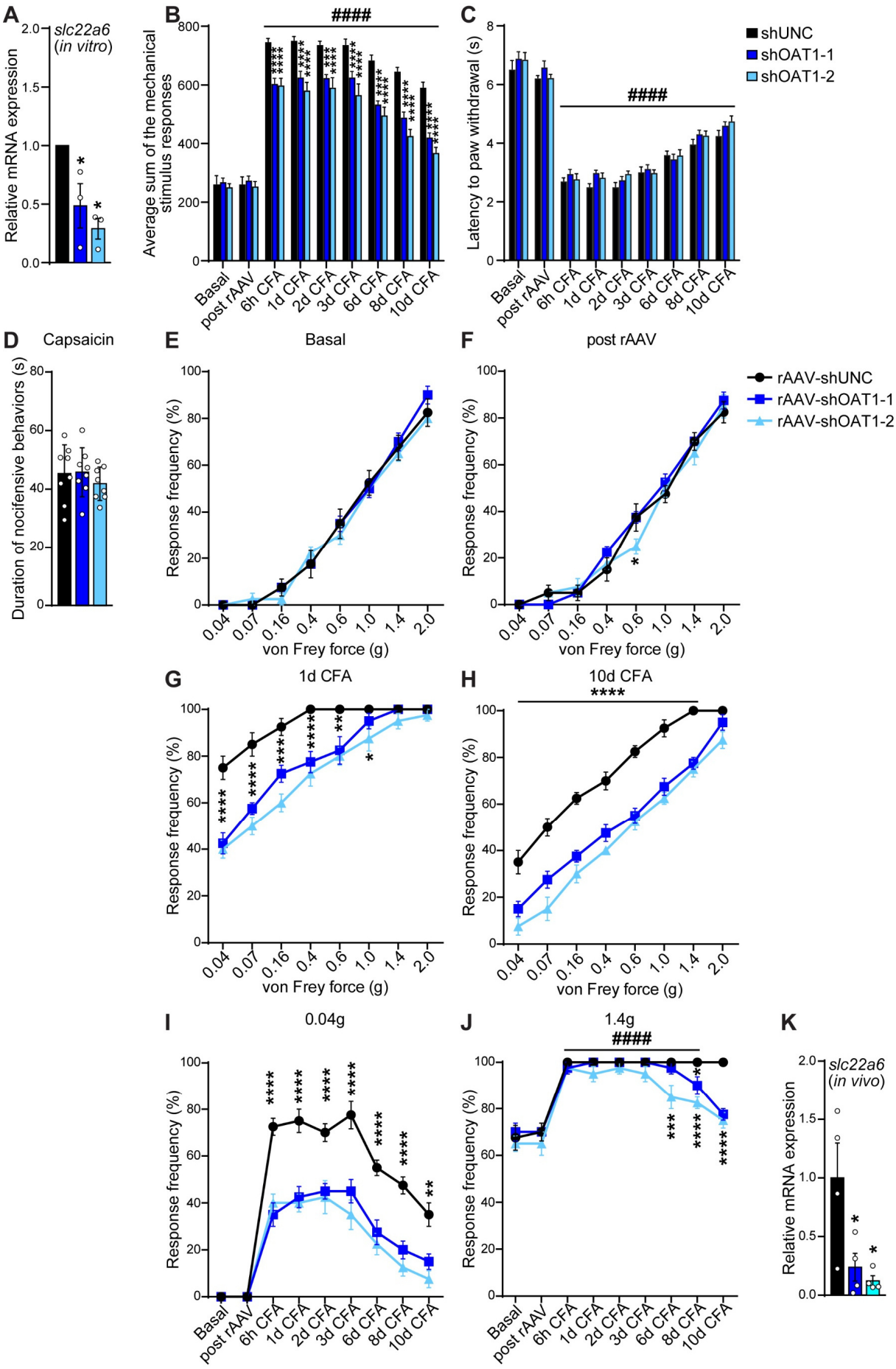

Figure 31: shRNA mediated knockdown of OAT1 in the spinal cord dorsal horn.

(A) QRT-PCR validation of shRNA-mediated knock down of OAT1 mRNA *in vitro* using cultured hippocampal neurons, infected as indicated at DIV 3 and analyzed after 10 days in culture (n=3 independent experiments per condition). (B) Mechanical hypersensitivity following plantar CFA injection, represented as the average sum of the von Frey stimulus responses at indicated timepoints of animals intra-spinally injected as indicated. (C) Thermal hypersensitivity following CFA-induced hind paw inflammation at indicated timepoints of animals intra-spinally injected as indicated. (D) Cumulative durations of acute nocifensive behaviors evoked by intraplantar injection of capsaicin in mice intra-spinally injected as indicated (n=8 mice per condition). (E-H) Stimulus intensity-response frequency curves of sensitivity to plantar von Frey mechanical stimulation. Responses to all tested filaments (0.04 g – 2 g) are shown for the basal state, before (E) and after (F) intraspinal shRNA injection, as well as at 24 h (G) and 10 d (H) post intraplantar CFA injection. Panels (I-J) show the response frequency to light touch (0.04 g filament) and noxious mechanical stimulation (1.4 g filament) over time (n=8 mice per condition). (K) QRT-PCR validation of shRNA-mediated spinal knock down of OAT1 mRNA *in vivo* ca. 6 weeks after intraspinal injections of indicated constructs (n=4 mice per condition). Statistically significant differences were determined by one-way ANOVA followed by Tukey's post hoc test (A, D, K) or two-way ANOVA with repeated measures followed by Dunnett's post hoc test for comparisons to basal values and Tukey's post hoc test for comparisons between conditions (B-C, E-J) ****, $p < 0.0001$;***, $p < 0.001$; **, $p < 0.01$; *, $p < 0.05$; ####, $p < 0.0001$. Asterisks (*) refer to statistical comparisons between conditions and hashtags (#) to comparisons relative to basal values. In bar graphs, each point represents a value derived from one independent experiment (A) or animal (D, K). Graphs represent mean ± SEM. (QRT-PCR analyses in panel (A, K) were performed by Dr. Daniela Mauceri).

3.3.16 Overexpression of OAT1 in the spinal cord dorsal horn

We proceeded to investigate possible effects of OAT1 overexpression in the spinal cord dorsal horn on inflammatory pain behavior. The template sequence encoding OAT1 was provided by Prof. Geckle and sub-cloned for virus production by Dr. Anna Hertle. Expression constructs have been validated in cultured neurons using Western blot analysis (data not shown). Three weeks after intraspinal injection of rAAV-OAT1 into the dorsal horn of spinal cord segments L3-5, mechanical sensitivity was significantly induced at basal levels compared to mice intra-spinally injected with rAAV-lacZ (Figure 32A-B, F-G). A similar trend was observed for thermal sensitivity (Figure 32C-D). Thus, it appears as increasing the levels of OAT1 affects central nociceptive processes. CFA-induced mechanical and thermal hypersensitivity were significantly elevated in mice intra-spinally injected with rAAV-OAT1 compared to controls (Figure 32A, C, H-I). In contrast, acute nocifensive behavior following intraplantar injection of capsaicin, was not affected in rAAV-OAT1 injected mice

(Figure 32E). Thus, our data indicate that elevated OAT1 expression levels promote central sensitization.

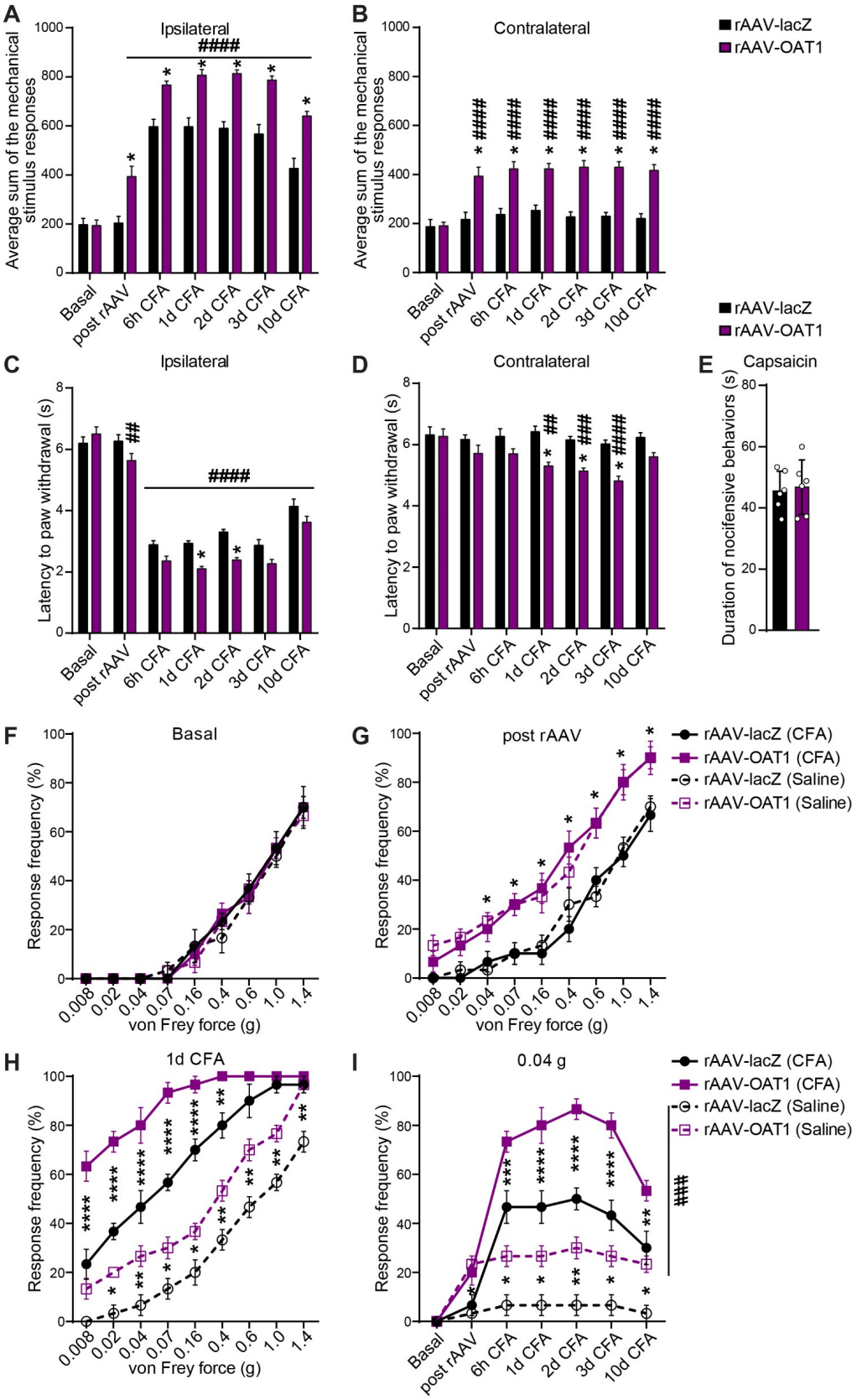

Figure 32: Overexpression of OAT1 in the spinal cord dorsal horn.

(A-B) Mechanical hypersensitivity, represented as the average sum of the von Frey stimulus responses at indicated timepoints of animals intra-spinally injected as indicated following plantar CFA (ipsilateral) and saline (contralateral) injections. (C-D) Thermal hypersensitivity of animals at indicated timepoints intra-spinally injected as indicated following plantar CFA and saline injections. (E) Cumulative durations of acute nocifensive behaviors evoked by intraplantar injection of capsaicin in mice intra-spinally injected as indicated (n=6 mice per condition). (F-I) Stimulus intensity-response frequency curves of sensitivity to plantar von Frey mechanical stimulation. Responses to all tested filaments (0.008 g – 1.4 g) are shown for the basal state, before (F) and after (G) intraspinal rAAV injection, as well as at 24 h (H) post intraplantar CFA and saline injection. Panel (I) shows the response frequency to light touch (0.04 g filament) over time (n=6 mice per condition). Statistically significant differences were determined by two-tailed Student's t-test (E) or two-way ANOVA with repeated measures followed by Dunnett's post hoc test for comparisons to basal values and Tukey's post hoc test for comparisons between conditions (A-D,F-I) ****, $p < 0.0001$;***, $p < 0.001$; **, $p < 0.01$; *, $p < 0.05$; ####, $p < 0.0001$; ###, $p < 0.001$; ##, $p < 0.003$. Asterisks (*) refer to statistical comparisons between conditions of the same paw and hashtags (#) to comparisons relative to basal values. In (E), each point represents a value derived from one animal. Graphs represent mean ± SEM.

In summary, our results show that the subcellular localization of HDAC4 in neurons of the spinal cord dorsal horn regulates histone H3 acetylation and gene expression of inflammatory pain-induced genes. We further demonstrate that nuclear HDAC4 in dorsal horn neurons ameliorates behavioral hypersensitivity in models of persistent but not acute inflammatory pain and that observed changes could be mediated by expression of the organic anion transporter OAT1 in spinal cord neurons, which we identified as a novel mediator of inflammatory pain and spinal sensitization.

4 Discussion

The presented work demonstrates that synaptic activity- and nuclear calcium-regulated epigenetic mechanisms, in particular the induction of Dnmt3a2 and the nucleo-cytoplasmic shuttling of class IIa HDAC4, regulate transcriptional changes in neurons that mediate morphological adaptations and contribute to spinal sensitization in mouse models of inflammatory pain. We identified the organic anion transporter OAT1, a target gene of HDAC4 in the spinal cord, as a new regulator of central sensitization.

4.1 HDAC4 shapes neuronal morphology

In the first part of this study, published in *The Journal of Biological Chemistry* (Litke et al., 2018), we showed that nuclear accumulation of HDAC4 results in a severe impairment of dendritic morphology, by decreasing the expression of VEGFD, a critical factor for dendrite stability, in hippocampal neurons.

Under basal levels of synaptic activity, HDAC4 is predominantly localized in the cytosol of neurons (Darcy et al., 2010, Schlumm et al., 2013), where it seems to have a critical function in regulating neuroprotective pathways during development and in mature neurons (Bolger and Yao, 2005, Chen and Cepko, 2009). Indeed, it has been shown that activity-induced nuclear calcium signaling (Lee et al., 2005, Papadia et al., 2005, Zhang et al., 2007, Zhang et al., 2009), known to promote neuronal survival, triggers nuclear export of HDAC4 (Schlumm et al., 2013). In contrast, toxic insults to the cells have been shown to result in HDAC4 nuclear accumulation (Chawla et al., 2003). In particular, we could show that activation of eNMDARs, which has been associated with excitotoxicity-dependent neurodegeneration and cell death (Hardingham et al., 2002, Parsons and Raymond, 2014, Bading, 2017, Hardingham and Bading, 2010) , results in HDAC4 nuclear accumulation (Figure 9). Nuclear accumulation of HDAC4 has also been detected in retinal ganglion cells (RGCs) upon NMDA-induced excitotoxicity *in vivo* (Schlüter et al., 2019), as well as in several neuronal pathologies, including stroke, Alzheimer's disease, Parkinson's disease and ataxia telangiectasia (Kassis et al., 2015, Shen et al., 2016, Wu et al., 2016, Yuan et al., 2016, Li et al., 2012), suggesting an involvement of HDAC4 subcellular localization in the diseases' progression and neurotoxicity.

Thus, an increase in nuclear HDAC4 localization, might be a suitable biomarker to indicate cell degeneration.

Our results show that nuclear accumulation of HDAC4 simplifies dendritic architecture by impairing the signals dedicated to its maintenance. Indeed, the neurodegenerative disorders mentioned above are characterized by a pathological alteration of neuronal morphology and often exhibit nuclear accumulation of HDAC4 (Baloyannis, 2009, Stephens et al., 2005), suggesting that both events could be functionally linked. Given that, depending on the brain region and cell type, dendritic architecture can be differentially regulated upon nuclear calcium signaling (Mellström et al., 2016), future experiments, analyzing HDAC4-mediated neuronal morphology must be extended *in vivo*. In the course of this doctoral thesis, we explored the effects of nuclear HDAC4 on neuronal morphology in neurons of the spinal cord *in vitro* and *in vivo* (Figure 25Figure 26).

Several HDACs of different classes have been linked to functional and developmental changes affecting neuronal architecture at the synaptic or dendritic level. Class I members HDAC1 and -2 have been shown to negatively regulate formation and maturation of excitatory synapses in developing neurons (Akhtar et al., 2009, Guan et al., 2009). Sando et al. showed that nuclear accumulation of HDAC4 in the neurons of mice expressing HDAC4 3SA or a truncated HDAC4 mutant, which lacks the nuclear export signal (NES) at its C-terminus, interferes with synaptic transmission and induces structural re-organization of excitatory synapses without affecting their number (Sando et al., 2012). Our data confirmed that spine density is not affected in neurons expressing HDAC4 3SA (Figure 8E, F). Moreover, activity of class IIa members HDAC5 and -9, as well as HDAC6 (class IIb) has been linked to the regulation of dendritogenesis during early neurodevelopment (Ageta-Ishihara et al., 2013, Gu et al., 2018, Sugo et al., 2010). Here, we demonstrated for the first time that HDAC4 affects the dendritic structure of neurons even in the post-developmental stage, where no further dendritogenesis is taking place and functional synaptic networks have been established. In contrast, increasing the expression of HDAC3 (class I) or HDAC11 (class IV) does not seem to affect the dendritic architecture of mature neurons, nor VEGFD expression, suggesting that dendritic arborization is primarily controlled by the subcellular shuttling of class IIa HDACs. This is supported by the observation that blocking synaptic activity causes both nuclear accumulation of HDAC4, while other HDAC classes are not affected (Schlumm et al., 2013), and

dendritic impairment (Segal, 2010). Moreover, VEGFD expression, which we found to be negatively regulated by nuclear HDAC4 (Figure 11), is also decreased in neurons upon blockade of synaptic transmission (Mauceri et al., 2011). Thus, proper maintenance of dendritic structures is supported by basal synaptic activity, as it promotes nuclear export of HDAC4 thereby ensuring sufficient levels of VEGFD expression.

In recent years, VEGFD has been identified as key for the maintenance of mature dendritic structure of pyramidal neurons (Mauceri et al., 2011, Mauceri et al., 2015), crucial for memory formation (Mauceri et al., 2011), as well as fear memory consolidation and extinction (Hemstedt et al., 2017). Moreover, excitotoxicity induced cell death of retinal ganglion cells could be linked to a decrease in VEGFD levels *in vivo*, while a supplementation strategy of VEGFD was successful in preserving structural and functional integrity of RGCs and neighboring cells after the excitotoxic insult (Schlüter et al., 2020). Several neurodegenerative disorders are characterized by both impairments of neuronal morphology and HDAC4 nuclear accumulation. Recently, it has been shown that VEGFD levels are significantly decreased in models of stroke, leading to dramatic loss of dendritic structures (Mauceri et al., 2020). Moreover, using the same middle cerebral artery occlusion (MCAO) model of stroke, nuclear retention of HDAC4 has been detected, whereas subcellular localization of HDAC5 was unaffected (Kassis et al., 2015), suggesting that HDAC4 might regulate VEGFD levels also *in vivo.*

Nevertheless, analysis of our RNAseq data suggests that nuclear accumulation of HDAC4 also affects additional genes with known functions in maintaining morphological structures, including cytoskeletal genes. Furthermore, we cannot exclude that downregulation of VEGFD might not directly be regulated by HDAC4 but via additional factors. Our study showed that overexpression of VEGFD or supplementation with recombinant VEGFD, but not VEGFC, is sufficient to prevent dendritic impairment triggered by nuclear HDAC4 and that rVEGFD can restore dendritic architecture even after it has already been compromised.

Since therapeutic effectiveness of VEGFD in preserving neuronal architecture has already been confirmed *in vivo,* by amelioration of stroke-induced damage (Mauceri et al., 2020, Schlüter et al., 2020, Schlüter et al., 2019), it will be interesting for future studies to investigate VEGFD expression and HDAC4 nuclear localization also in other neuronal pathologies and model systems.

4.2 Dnmt3a2 and inflammatory pain

It has been shown that the transition from physiological acute nociception to development of pathological chronic pain, referred to as central sensitization, shares many molecular mechanisms with learning and memory formation (Rahn et al., 2013). Epigenetic processes, like DNA methylation or histone acetylation/deacetylation, have been recognized as prime mediators of adaptive changes, facilitating long-lasting molecular adjustments by affecting chromatin structure and gene transcription and have frequently been linked to plasticity-dependent processes, including learning, memory and pain (Rahn et al., 2013, Denk and McMahon, 2012, Descalzi et al., 2015). Previous data already supported the role of Dnmt3a2 as a critical epigenetic regulator with the ability to modulate adaptive cognitive processes in the brain (Gulmez Karaca et al., 2020, Oliveira et al., 2012, Oliveira et al., 2016). Our recent study, which has been published in *Molecular Pain* (Litke et al., 2019), now extends this view, showing that the expression of *dnmt3a2* in the spinal cord plays a crucial role in central sensitization.

Using the CFA mouse model of inflammatory pain, we showed that nociceptive activity in the dorsal horn induces the expression of *dnmt3a2,* but not of its close transcript variant *dnmt3a1,* which contains an extended N-terminal domain. This observation is in line with previous experiments in hippocampal neurons, showing that transcription of *dnmt3a2* depends on synaptic activity, whereas expression of *dnmt3a1* is not activity-regulated (Oliveira et al., 2012). Previous studies have investigated the expression of DNA methyltransferases in models of neuropathic- and bone cancer pain in central neurons of the spinal cord and in primary sensory neurons at the DRGs and found mRNA levels of *dnmt3a* to be increased. However, none of the studies differentiated between the two isoforms and closer inspection revealed that they used antibodies specific to Dnmt3a1, and primers for QRT-PCR which would detect both transcript variants without distinction. (Miao et al., 2017, Pollema-Mays et al., 2014, Shao et al., 2017, Sun et al., 2017). Our study highlights that both DNMTs can be differentially regulated following pain stimulation and therefore should be analyzed individually. Moreover, the majority of studies investigating the expression of *dnmt3a* were focusing on models of neuropathic pain, whereas we were analyzing the effects of acute and chronic inflammatory pain.

Recent analysis of a sensory neuron-specific *dnmt3a*-knockout mouse line by Saunders et al. argues against a role of Dnmt3a in nociception (Saunders et al., 2018b). However, in the light of our results that rely on regulation of *dnmt3a2* expression in central cells of the spinal cord instead of peripheral DRGs, it can be suggested that regional and cell type-specific differences are important for the regulation of long-lasting hypersensitivity via Dnmt3a2.

Dnmt3a2 has been shown to act as an epigenetic regulator of expression of many plasticity-related genes in neurons of the hippocampus *in vitro* and *in vivo* (Oliveira et al., 2012, Oliveira et al., 2016), and in striatal neurons, where its regulatory effects come into play during dopamine D1 receptor signaling and cocaine stimulation (Cannella et al., 2018). Here we show that Dnmt3a2 regulates the expression of plasticity-related immediate early genes also in the spinal cord. In addition, we found transcriptional induction of *ptgs2,* key mediator of pain*,* to be regulated by Dnmt3a2 in the CFA model. This is in line with previous experiments, showing that *ptgs2* expression is activity-dependent in neurons of the spinal cord and hippocampus (Simonetti et al., 2013, Zhang et al., 2007). We observed that CFA-dependent induction of *arc*, *c-fos*, *bdnf*, and *ptgs2* occurs at the same time, or even precedes, CFA-dependent induction of Dnmt3a2. This indicates that, upon inflammatory pain, Dnmt3a2 may not regulate the expression of CFA-driven genes directly. Our current hypothesis suggests that Dnmt3a2 renders the genome more permissive towards stimulus-dependent gene transcription, similar to what previously described in the hippocampus and striatum (Cannella et al., 2018, Oliveira et al., 2012, Oliveira et al., 2016, Gulmez Karaca et al., 2020). Accordingly, activity-dependent induction of *dnmt3a2* expression is necessary to reinforce stimulus-dependent gene transcription, ensuring an adequate transcriptional response to upcoming stimuli. In turn, if Dnmt3a2 levels are reduced, the genome is less permissive for gene transcription, and activity-dependent gene expression upon CFA-stimulation is impaired.

DNA methylation has frequently been associated with transcriptional repression, which seems in contrast with the positive correlation between Dnmt3a2 expression and gene transcription that we observed. However, emerging evidence suggests that transcriptional regulation via DNA-methylation is a multifaceted process that can act both ways (Suzuki and Bird, 2008). The concept that DNA methylation primes the genome for external stimulus-evoked transcriptional responses in now widely

accepted (Baker-Andresen et al., 2013, Guo et al., 2011, Oliveira, 2016, Gulmez Karaca et al., 2020).

In vivo knockdown of *dnmt3a2* in the spinal cord dorsal horn ameliorated the induction of thermal and mechanical hypersensitivity in the CFA model of chronic inflammatory pain, whereas basal nociception and acute pain behavior, following capsaicin injection, were not affected, suggesting that Dnmt3a2 activity plays a role during early spinal sensitization.

With regard to the variability resulting from the use of both sexes, this study was limited to the use of male mice only. Therefore, we cannot exclude sex-related differences in the influence of Dnmt3a2 on hypersensitivity during inflammatory pain. However, sex-related qualitative differences in pain and analgesic sensitivity have been frequently demonstrated (Mogil, 2009), and represent a timely topic that needs to be addressed in future studies to improve the accuracy and relevance of obtained data with regard to epidemiological realities of clinical pain.

Our experiments exclusively covered models of inflammatory pain. In view of creating potential translational approaches using Dnmt3a2-mediated therapies, it will be necessary to analyze its role in different aspects of pain, including neuropathic-, arthritic, muscle-, or cancer pain. Indeed, epigenetic mediators represent emerging targets in search for novel pain treatment strategies and preclinical studies already showed that pharmacological modulation of histone acetylation/deacetylation can have ameliorating effects on hyperalgesia or allodynia (Crow et al., 2013, Niederberger et al., 2017). In contrast, fewer studies have tried interventional strategies targeting DNA methylation, as less is known about pharmacological modulation of DNMT function. Future studies are necessary to broaden our understanding about the activity and structure of the different DNMTs, that will help to specifically inhibit or induce their function. Along these lines, progress has recently been made by Guo et al., describing a novel inhibitory mechanism for Dnmt3a activity after determining its crystal structure and biochemical properties (Guo et al., 2015).

In conclusion, we identified Dnmt3a2 as a modulator of hypersensitivity in persistent inflammatory pain and as a potential new target for pain therapy.

4.3 The role of HDAC4 in spinal sensitization

The presented doctoral thesis establishes a role for spinal HDAC4 in the epigenetic regulation of expression of inflammatory pain-associated genes and identifies novel potential targets for future pain therapies.

Nuclear calcium regulates the nucleo-cytoplasmic shuttling of class IIa histone deacetylases in neurons of the hippocampus, where nuclear HDAC4 represses the expression of plasticity- and pain-related genes *arc*, *homer*, *ptgs2*, and *c1q-c* (Schlumm et al., 2013, Chawla et al., 2003). Here, we focused our efforts on the possible link between nociception, pain and HDAC4.

4.3.1 Neuronal activity drives nuclear export of HDAC4 and histone acetylation in spinal cord neurons *in vitro* and *in vivo*.

Upon synaptic stimulation of cultured spinal cord neurons or CFA-induced nociceptive activity *in vivo*, we found nuclear levels of HDAC4 to be specifically decreased in neurons of the spinal cord (Figure 16Figure 20). In contrast to hippocampal neurons (Schlumm et al., 2013), activity-dependent export seems to be specific for HDAC4, as other HDACs of class IIa and members of other classes did not change their subcellular localization *in vitro* and *in vivo* (Figure 16BFigure 20A). Yet, nucleo-cytoplasmic translocation of HDAC1, -3 (class I) and HDAC5 (class IIa) in neurons of the dorsal horn, after intraplantar CFA injection, cannot be completely excluded due to technical limitations hindering analyses. Based on our observations of cultured spinal cord neurons, we do not expect a nuclear export of these HDACs (Figure 16B).

Under basal conditions, cultured spinal cord neurons showed equally distributed HDAC4 between the cytosol and the nucleus. (Figure 16A). In contrast, hippocampal neurons display a predominantly cytoplasmic localization of HDAC4 (Schlumm et al., 2013, Litke et al., 2018). This could be explained by lower levels of basal synaptic activity in cultured spinal cord neurons, compared to hippocampal neurons, resulting in decreased nuclear export of HDAC4 (Schlumm et al., 2013). In addition, expression and subcellular localization of HDACs highly varies in-between cell types and regions of the CNS (Darcy et al., 2010).

Synaptic activity or nociception left total expression levels of HDACs unchanged (Figure 17 andFigure 20). Our results argue against a previous study, describing

induced expression of all class IIa HDAC members in the spinal cord, following CFA injection (Bai et al., 2010). These variations might be explained by the use of a distinct C57BL/6-substrain, which also shows behavioral differences in pain sensitivity (Bryant et al., 2008).

HDAC4 nuclear export and induced histone acetylation levels of H3-Lys9 in cultured spinal cord neurons upon synaptic stimulation appear to be correlated (Figure 18). This is true also in neurons of the dorsal horn following CFA injection (Figure 20Figure 22). Increased levels of global histone acetylation, following CFA-induced inflammatory pain, have also been reported in neurons of the nucleus raphe magnus (NRM), which plays a regulatory role in pain perception by modulating the descending feedback system (Zhang et al., 2011b). Moreover, increased levels of H3-Lys9 in the central amygdala (CeA) of rats have recently been associated with enhanced vulnerability to emotional disorders, like anxiety and depression, under chronic pain conditions (Zhou et al., 2020). On the other side, nuclear accumulation of HDAC4 has previously been associated with decreased acetylation of histone H3 and changes in gene expression in neurons of the cerebrum and cerebellum of mice (Li et al., 2012). Considering, however, that the deacetylation domain of class IIa HDACs has been evolutionary inactivated (Lahm et al., 2007, Schuetz et al., 2008), we cannot state that observed changes in histone acetylation are directly mediated by HDAC4. Since HDACs exert their gene regulatory effects also through non-epigenetic mechanisms (Crow et al., 2013), it is more likely that HDAC4 regulates histone acetylation by recruiting other interaction partners to the chromatin, such as the SMRT/NCoR-HDAC3 co-repressor complex (Fischle et al., 2001, Fischle et al., 2002, Guenther et al., 2001). Chromatin immunoprecipitation (ChIP) assays would be required to determine the levels and specific sites of histone acetylation at the promoter region of specific genes.

4.3.2 Nuclear HDAC4 in spinal cord neurons regulates inflammatory hypersensitivity

HDAC4 subcellular localization is affected by persistent inflammatory pain (Figure 20). Utilizing the nuclear dominant active mutant HDAC4 3SA, we have shown that nuclear HDAC4 in neurons of the dorsal horn not only hinders CFA-induced histone

H3 acetylation (Figure 22), but also regulates the expression of pain- and plasticity-related genes (Figure 22G andFigure 27), ameliorating pain hypersensitivity in models of persistent inflammatory pain (Figure 23). Interference with the shuttling of HDAC4 by inhibiting its nuclear export has also been successfully used to reduce allodynia in a rat model of neuropathic pain (Lin et al., 2015). Moreover, changes in the acetylation of histones in neurons have frequently been reported in different animal models of pain and pharmacological inhibition of HDACs has successfully been used to ameliorate the development and maintenance of chronic inflammatory and neuropathic pain (Crow et al., 2013, Bai et al., 2010, Zhang et al., 2011b, Shakespear et al., 2011, Chiechio et al., 2009, Denk et al., 2013). However, these studies relied on specific inhibition of class I HDACs or did not discriminate between different classes of HDACs. Since there are no suitable inhibitors available that are specific for class IIa, the role of HDAC4, -5, -7, and -9, in the modulation of central sensitization, requires further investigation.

We have shown that intraspinal rAAV-injections target central neurons of the spinal cord dorsal horn, without affecting primary sensory neurons (Figure 24). Indeed, acute nociception, during the early phase after formalin injection or following intraplantar delivery of capsaicin, is not affected by the subcellular localization of HDAC4 in neurons of the spinal cord dorsal horn (Figure 23H-I).

While our study is focusing on HDAC4-mediated transcriptional changes in central neurons of the spinal cord, it has been shown that conditional knockout of HDAC4, in primary sensory neurons of mice, affects peripheral sensitization and inflammatory hypersensitivity, following CFA-injection, by dysregulating the expression of *trpv1* and *calca* (CGRP), which are both crucial mediators of nociception (Crow et al., 2015). This highlights the important role of HDAC4 as key regulator of gene transcription in the context of inflammatory pain.

Nuclear calcium-dependent processes in central neurons do not become evident until hours after intense nociceptive activity (Simonetti et al., 2013). This is in line with our observation that capsaicin-induced acute inflammatory pain, in contrast to persistent nociceptive stimulation in the CFA model, was insufficient to induce changes in histone H3 acetylation (Figure 21). Nonetheless, mechanisms of central sensitization have also been described following hours to days after intradermal injection of capsaicin, resulting in secondary hyperalgesia and allodynia, subsequently after

acute sensitization of primary afferent nociceptors (Willis, 2009). Moreover, transcriptional regulation in central neurons has been observed upon long-term and systemic application of capsaicin over a period of two weeks (Wang et al., 2018).
The reason why nuclear HDAC4 in central neurons of the spinal cord affects only mechanical and not thermal hypersensitivity, remains unknown. It has been suggested that mechanical and thermal hyperalgesia rely on activation of two different intracellular signaling pathways within the spinal cord (Meller, 1994). Moreover, nuclear HDAC4 blocked the induction of *ptgs2* (Cox-2) in the spinal cord (Figure 22G), while previous studies could show that conditional knockout of Cox-2 in neural cells (Vardeh et al., 2009), as well as its selective knockdown in spinal excitatory neurons (Simonetti et al., 2013), results in a failure of the mice to develop mechanical pain hypersensitivity, evoked by peripheral inflammation, without affecting thermal nociception. This suggests that nuclear HDAC4 mediates specifically mechanical hypersensitivity by regulating the expression of Cox-2 in the spinal cord.

4.3.3 Nuclear HDAC4 and morphology of spinal cord neurons

Structural adaptations and changes in the plasticity of central spinal cord neurons are known to contribute to central sensitization (Simonetti et al., 2013, Kuner, 2010, Tan et al., 2008, Tappe et al., 2006). We and others showed that nuclear HDAC4 regulates dendritic morphology and synaptic plasticity in hippocampal neurons (Litke et al., 2018, Sando et al., 2012). Previous investigations indicated that hippocampal pyramidal neurons and spinal cord neurons share common mechanisms for gene regulation and morphological remodeling (Simonetti et al., 2013). We found that nuclear HDAC4 impairs dendritic morphology of cultured spinal cord neurons (Figure 25), as observed for hippocampal cultures (Figure 8). Using the Golgi-Cox method on spinal cord sections after intraspinal injection of rAAV-lacz, -HDAC4 wt, or -HDAC4 3SA, no changes in the dendritic structure of large pyramidal neurons in dorsal horn lamina V could be detected (Figure 26). Due to technical reasons neurons within the superficial dorsal horn laminae I – III, could not be labeled and analyzed. Therefore, possible effects of HDAC4 on dendritic morphology of neurons in the superficial dorsal horn cannot be evaluated. Moreover, in contrast to *in vitro*

experiments, Golgi-stained dorsal horn neurons had to be analyzed without knowing whether they were successfully transduced and indeed express the transgenes.

Neurons in lamina V, receiving nociceptive input via primary afferent fibers (Figure 7), have been shown to respond to CFA-induced inflammatory pain with adaptations in synaptic plasticity, which are regulated by changes in the expression of the synaptic pruning factor C1q-c (Simonetti et al., 2013). Interestingly, our QRT-PCR and RNAseq analyses have shown that nuclear HDAC4 upregulates *c1q-c* (Table 15), counteracting the downregulatory effect of CFA on *c1q-c*. This might contribute to the amelioration of CFA-induced hypersensitivity, in mice intra-spinally injected with HDAC4 3SA. To confirm this hypothesis, effects of nuclear HDAC4 on spine remodeling still need to be evaluated *in vivo*.

In hippocampal cultures, we demonstrated that HDAC4 shapes dendritic morphology by regulating the expression of *vegfd* (Litke et al., 2018), a key factor for the maintenance of dendritic structures (Mauceri et al., 2020, Mauceri et al., 2011, Mauceri et al., 2015). Whether VEGFD expression is also affected in spinal cord neurons, still needs to be evaluated. RNAseq analysis of dorsal spinal cord tissue failed to detect sufficient expression levels of *vegfd.* Therefore, we cannot yet draw any conclusions about possible regulatory effects of HDAC4 on VEGFD in the spinal cord.

RNAseq analysis revealed regulatory effects of nuclear HDAC4 on genes encoding for cytoskeletal elements, including members of the ERM (Ezrin/Radixin/Moesin) family, which are known to regulate morphogenesis of neurons and memory formation (Mangeat et al., 1999, Freymuth and Fitzsimons, 2017). Our results align with a previous study which found expression of *msn* (Moesin) significantly induced in cortical neurons of HDAC4 3SA-expressing mice (Sando et al., 2012).

4.3.4 HDAC4 regulates expression of inflammatory pain-induced genes

Given the complexity of network interactions by which HDACs can mediate several inflammatory and immune regulatory pathways (Shakespear et al., 2011), it is crucial for the development of future therapeutic interventions to identify HDAC-regulated genes that mediate structural and functional adaptations during central sensitization (Buchheit et al., 2012).

Performing a comprehensive transcriptome analysis using next generation RNA sequencing analysis, we identified candidate genes, whose expression is regulated by the subcellular localization of HDAC4 in the context of inflammatory pain (Figure 27). These genes might serve as potential targets for interventional strategies.

In the spinal cord of mice, injected with rAAV-HDAC4 wt or the nuclear mutant - HDAC4 3SA, we found most genes to be upregulated after intraplantar injection of saline (data not shown) and CFA (Figure 27A). Since HDAC4 is associated with negative regulation of gene transcription (Lee and Workman, 2007), it is reasonable to assume that HDAC4 modulates the expression of these genes indirectly by suppressing other negative regulators of gene transcription. Moreover, regulatory mechanisms in the cytosol, involving HDAC4-mediated effects on non-histone targets, cannot be ruled out (Wang et al., 2014).

In the search for target genes that are involved in early spinal sensitization, we focused our analysis primarily on DEGs that were induced following CFA injection, in lacZ and HDAC4 wt expressing mice, but not in rAAV-HDAC4 3SA injected animals (Figure 27C-E). We identified genes with reported functions in nociception, like *thbs1*, encoding thrombospondin 1 (Thbs1), a secreted glycoprotein that mediates cell-cell interactions and is involved in inflammatory responses (Adams, 2001, Wang et al., 2009). Thbs1 has been reported to induce behavioral hypersensitivity in rats upon intrathecal injection of the recombinant protein (Kim et al., 2012a). HDAC4-regulated targets also included the long non-coding RNA (lncRNA) H19, which has recently been linked to the development of neuropathic pain (Wu et al., 2019). Besides, we identified several downstream targets of HDAC4, which have not been associated with inflammatory pain before.

Among those, the organic anion transporter OAT1 (*slc22a6)* caught our attention, as it is, apart from its classical role in renal tubular cells (Roth et al., 2012), also expressed in neurons of the CNS (Bahn et al., 2005, Cousins and Wood, 2010), where its expression is temporarily increased during embryogenesis (Cousins and Wood, 2010, Pavlova et al., 2000). OAT1 has been shown to mediate the renal transport of prostaglandins, as well as of neurotransmitter metabolites (Alebouyeh et al., 2003, Bahn et al., 2005, Roth et al., 2012, Sauvant et al., 2006), suggesting a potential regulatory role for OAT1 in inflammatory and neuromodulatory processes. Indeed, there is evidence that OAT1-activity is critical for the distribution of prostaglandins and tryptophan metabolites within the CNS (Bahn et al., 2005,

Nakamura et al., 2018). We describe, for the very first time, that CFA-mediated inflammation induces the expression of OAT1, specifically in neurons of the spinal cord dorsal horn, and that this process can be regulated by the subcellular localization of HDAC4 (Figure 27 andFigure 28). However, the underlying regulatory mechanisms governing its transcription remain unknown. Using the Eukaryotic Promoter Database (EPD) and JASPAR library (Dreos et al., 2017, Sandelin et al., 2004), motif search for transcription factor binding sites within the putative promoter region of murine *slc22a6,* -1000 bp upstream to its transcription start site (TSS), revealed potential interaction with the transcription factor MEF2. Putative binding sites for MEF2 have also been identified in the human genes encoding OAT1 and -3 (Bhatnagar et al., 2006). MEF2 is highly expressed in neurons and known to suppress gene transcription by recruiting HDAC4 and associated co-repressor complexes to its binding side, whereas nuclear export of HDAC4 has been shown to promote MEF2 interaction with the coactivator p300, stimulating transcription of MEF2-targeted genes via local histone acetylation (McKinsey et al., 2002). This suggests that nuclear HDAC4 might negatively regulate the expression of OAT1 via MEF2 interaction. However, experimental evidence for this hypothesis is still missing and requires further investigations.

4.3.5 OAT1 – a mediator of central sensitization

Using intrathecal application of probenecid, a potent inhibitor of OAT1 activity, we linked CFA-induced changes in the expression of OAT1 and the development of pain hypersensitivity (Figure 29). Probenecid is considered a safe drug and it is already used in clinical praxis primarily for the treatment of hyperuricemic disorders, like gout (Stamp et al., 2007), by increasing renal excretion of uric acid or to extend the plasma levels of antibiotics or antiviral drugs via renal retention (Rayner et al., 2008, Cunningham et al., 1981). Intrathecal injection is a well-established and minimally invasive method that allows quick delivery of drugs, bypassing the BSCB, directly into the spinal cord canal, without triggering significant inflammation, even after consecutive injections on the same mouse (Njoo et al., 2014). However, in contrast to intraspinal injection, cell type-specific targeting of spinal cord neurons cannot be achieved. Moreover, probenecid is not only inhibiting OAT1 but also other organic anion transporters (Takeda et al., 2001, Cunningham et al., 1981). Therefore, we

cannot completely rule out off-target effects. Anti-inflammatory and -nociceptive properties have been reported in a model of trigeminal inflammatory pain using orofacial injection of formalin in rats after intraperitoneal delivery of PBN (Fejes-Szabó et al., 2015). It has been suggested that PBN acts by inhibiting MRP4 (multidrug resistance-associated protein 4), an organic anion transporter with an ATP-binding cassette (ABC), that plays a crucial role in the release of prostaglandin E2 (PGE2), which in turn contributes to inflammatory hyperalgesia (van Aubel et al., 2002, Reid et al., 2003). PGE2 is also a known substrate of OAT1 (Nigam et al., 2015). In the kidney, vectoral transport of various substrates across epithelial cells is achieved by the coupling of SLC- (OAT1) and ABC transporter (MRP4) activities (Nigam et al., 2015). But regulation of metabolites and signaling molecules via remote communication between OAT1 and other transporters of the SLC and ABC family, has also been suggested for other cell types and tissues (Nigam et al., 2015). Yet, their specific role in neurons of the spinal cord remains unknown.

Probenecid might also exert its anti-nociceptive function by inhibiting pannexin 1 (Silverman et al., 2008, Fejes-Szabó et al., 2015), a postsynaptic gap junction protein, which is primarily expressed in the spinal cord (Zoidl et al., 2007, Bruzzone et al., 2003) and known to play a crucial role in the release of pro-inflammatory IL-1β in neurons and astrocytes (Silverman et al., 2009). Furthermore, probenecid has been shown to mediate accumulation of kynurenic acid (KYNA), a neuroactive tryptophan metabolite (Sellgren et al., 2019), within the central nervous system (Vécsei et al., 1992). This can be achieved by inhibiting the organic anion transporter OAT1 and -3 (Perwitasari et al., 2013, Chiba et al., 2011), which have been shown to transport KYNA and other tryptophan metabolites, like xanthurenic acid (XA), as well as the serotonin metabolite 5-hdydroxyindol acetate (5-HIAA), away from the brain through the blood-brain-barrier (Colín-González and Santamaría, 2013, Bahn et al., 2005).

Interestingly, 5-HIAA was found to regulate CFA-induced hyperalgesia in mice (Chen et al., 2011), while kynurenic acid has also been linked to nociception (Mecs et al., 2009, Vécsei et al., 2013, Näsström et al., 1992, Fejes et al., 2011), probably acting by its known antagonistic effects on the glycine co-agonist site of the NMDA receptor, as well as on other ionotropic glutamate and α7 nicotinic receptors (Schwarcz et al., 2012, Kessler et al., 1989, Pereira et al., 2002). KYNA also acts on the G-protein

coupled receptor 35 (GPR35) (Wang et al., 2006), which plays a regulatory role in nociceptive pathways by mediating cAMP signaling in DRGs and the spinal cord (Ohshiro et al., 2008, Fejes et al., 2011).

Taken together, probenecid might mediate its analgesic effects in the CFA model by inhibiting the clearance of KYNA or other metabolites, like PGE2, via OATs within the spinal cord. However, PBN has also been shown to mediate anti-nociceptive effects that do not involve activity of organic anion transporters, like the inhibition of pannexin 1. Besides, PBN is not a specific inhibitor of OAT1 and interferes with the transport activity of OAT3 (*slc22a8*), its closest family member (Duan et al., 2012). Interestingly, it has been shown that PBN inhibits OAT3-mediated transport *in vitro* and *in vivo*, by reducing the expression of the antiporter itself (Perwitasari et al., 2013). By targeting the expression of OAT1 in the spinal cord, using intrathecal injection of specific siRNAs (Figure 30) and intraspinal injection of rAAV-shOAT1 (Figure 31), we could demonstrate that decreased expression of OAT1 exerts similar anti-nociceptive effects as PBN treatment (Figure 29), suggesting a critical role for OAT1 in central sensitization and that PBN exerts its ameliorating effects by inhibiting OAT1 function.

Owing to the transient spatial and temporal distribution of intrathecally delivered siRNAs (Rao et al., 2009), the anti-nociceptive effects diminished within 48 hours. In contrast, intraspinal injection of rAAV-delivered genetic constructs, which utilize the endogenous processing machinery for shRNA transcription (Rao et al., 2009), mediated sustainable ameliorating effects on pain hypersensitivity in the CFA model (Figure 31). Moreover, targeted injection into the superficial laminae of the dorsal horn is thought to result in less off-target effects in comparison to intrathecal injection of siRNAs (Rao et al., 2009). This highlights the critical role of OAT1 within the spinal cord dorsal horn (Figure 28), in the modulation of nociceptive processing.

In a gain of function experiment, increasing the expression of OAT1 within the spinal cord dorsal horn, we successfully induced allodynia under basal conditions and increased allodynia and hypersensitivity in the CFA model of persistent inflammatory pain, confirming the role of OAT1 as a mediator of spinal sensitization (Figure 32). Yet, the underlying molecular mechanisms by which spinal OAT1 mediates persistent inflammatory pain, still need to be evaluated.

Our current hypothesis implicates that OAT1 participates to the elimination of anti-nociceptive tryptophan metabolites, like kynurenic acid, from the spinal cord. While expression levels of OAT1 are relatively low under basal conditions, persistent inflammatory pain mediates the induction of OAT1, probably due to nuclear export of HDAC4, bringing hypersensitivity-promoting effects via OAT1 into play. This is in line with our observations following overexpression of OAT1 (rAAV-OAT1) which resulted in allodynia. In contrast, interfering with the function of OAT1 in terms of activity (PBN) or expression, using RNA interference or intraspinal expression of nuclear HDAC4 (HDAC4 3SA), results in an accumulation of KYNA, or other relevant metabolites, in the spinal cord, diminishing nociceptive activity.
However, to verify our hypothesis, it remains to be evaluated if and how the dynamics and intracellular concentrations of metabolites like KYNA are changed in the spinal cord dorsal horn upon inflammatory pain. Nevertheless, several human diseases, such as Huntington's disease, migraine or multiple sclerosis have already been associated with abnormalities in the metabolic route of tryptophan degradation in the kynurenine pathway (Vécsei et al., 2013).

Knockout mice for OAT1 have been generated by replacing a segment within the coding region of the first exon with a cassette encoding β-galactosidase (LacZ) instead (Eraly et al., 2006). OAT1 null mice are viable and fertile and show deficiencies in the transport of many endogenous metabolites in the kidneys and choroid plexus, as well as in the clearance of antiviral drugs (Eraly et al., 2006, Nigam et al., 2015). This animal model has been critical to determine the relative contribution of OAT1 in the transport of common drug substrates within the SLC transporter family and led to the identification of novel endogenous substrates of OAT1 (Eraly et al., 2006). Phenotypic analysis of KO mice, performed by Deltagen Inc, detected no significant changes in any tested behavioral parameters, including tests for activity, anxiety, depression, thermal analgesia, motor coordination, learning, auditory reflex, and seizure susceptibility (Mouse Genome Database (MGD), 2013). However, potential effects on mechanical analgesia, as suggested by our study, have not been analyzed yet.

Taken together, we have shown that OAT1 is expressed in neurons of the spinal cord dorsal horn and is transcriptionally regulated by the subcellular localization of HDAC4 and persistent inflammatory pain. Using gain and loss of function experiments, we identified OAT1 as a mediator of pain hypersensitivity in the CFA model, suggesting a critical role in central sensitization.

4.4 Outlook

Given the complexity of performed *in vivo* experiments and following the guiding principles for ethical use of laboratory animals, our experiments were so far restricted to the use of male mice. Thus, it will be interesting to extend experiments to incorporate female mice to further increase the clinical relevance of observed effects. In fact, our preliminary analyses indicated sex-specific differences in the expression of OAT1, at basal levels and after CFA treatment, suggesting a possible dimorphism in pain behavior due to differential regulation of OAT1 in the spinal cord.

In addition, we have so far focused our efforts on models of acute and chronic inflammatory pain, but it would be interesting to investigate the role of Dnmt3a2 and HDAC4 in models of neuropathic-, deep-, muscle-, or visceral pain. These rodent models try to closely resemble pathological pain conditions in human patients (Mogil, 2009, Mogil et al., 2010). Yet, our assessment of pain behavior relies on the measurement of stimulus-evoked responses, reflecting allodynia and hyperalgesia, and therefore only parts of the global pain experience. Future studies should also evaluate spontaneous pain behavior of mice using non-reflexive measures, like the conditioned place preference test (Mogil, 2009), that rely on voluntary decisions and provide a better translation of preclinical finings. Along these lines, potential consequences of the affective-emotional component of chronic pain, such as anxiety and depression, need to be considered, as they have been shown to further exacerbate the severity and chronicity of pain (Price, 2000).

Using RNA sequencing analysis, we identified a variety of inflammatory pain and HDAC4-regulated genes in the spinal cord dorsal horn. These data provide a solid repertoire of potential therapeutic targets, as demonstrated at the example of *slc22a6* (OAT1), that might be used for future pain therapies. Single cell sequencing or in situ hybridization will help to better understand the role of HDAC4-mediated

transcriptional regulation in the spinal cord, by providing information on individual cell populations.

We are currently establishing the OAT1 knockout mouse colony in our lab to validate previous findings and to further evaluate the role of OAT1 in spinal sensitization. KO mice will be subjected to different models of acute and chronic pain and behavior will be assessed using different nociceptive tests. Since OAT1 KO mice express LacZ under the control of the endogenous OAT1 promoter, we will use this mouse line as a reporter to better dissect the regulation of OAT1 expression in different cell types of the spinal cord dorsal horn in the context of pain. In collaboration with the Metabolomics Core Technology Platform (MCTP) of Heidelberg University, we will perform metabolomic analyses of spinal cord tissue and CSF from OAT1 KO mice to identify metabolites that are transported by OAT1 in the spinal cord and play a role in central sensitization.

In summary, we have shown that nociceptive activity induces nuclear calcium signaling-dependent epigenetic processes, namely the induction of Dnmt3a2 and the subcellular shuttling of HDAC4, in neurons of the spinal cord, which mediate early spinal sensitization by regulating the expression of pain and plasticity-related genes in the CFA model of chronic inflammatory pain. Our study identified spinal OAT1 as critical mediator of pain hypersensitivity and marks it as potential target for future therapeutically interventions in the treatment of chronic pain conditions.

References

ABRAIRA, V. E. & GINTY, D. D. 2013. The Sensory Neurons of Touch. *Neuron,* 79**,** 618-639.

ADAMS, J. C. 2001. Thrombospondins: multifunctional regulators of cell interactions. *Annu Rev Cell Dev Biol,* 17**,** 25-51.

AGETA-ISHIHARA, N., MIYATA, T., OHSHIMA, C., WATANABE, M., SATO, Y., HAMAMURA, Y., HIGASHIYAMA, T., MAZITSCHEK, R., BITO, H. & KINOSHITA, M. 2013. Septins promote dendrite and axon development by negatively regulating microtubule stability via HDAC6-mediated deacetylation. *Nat Commun,* 4**,** 2532.

AJAMIAN, F., SUURONEN, T., SALMINEN, A. & REEBEN, M. 2003. Upregulation of class II histone deacetylases mRNA during neural differentiation of cultured rat hippocampal progenitor cells. *Neurosci Lett,* 346**,** 57-60.

AKHTAR, M. W., RAINGO, J., NELSON, E. D., MONTGOMERY, R. L., OLSON, E. N., KAVALALI, E. T. & MONTEGGIA, L. M. 2009. Histone deacetylases 1 and 2 form a developmental switch that controls excitatory synapse maturation and function. *J Neurosci,* 29**,** 8288-97.

ALEBOUYEH, M., TAKEDA, M., ONOZATO, M. L., TOJO, A., NOSHIRO, R., HASANNEJAD, H., INATOMI, J., NARIKAWA, S., HUANG, X.-L., KHAMDANG, S., ANZAI, N. & ENDOU, H. 2003. Expression of Human Organic Anion Transporters in the Choroid Plexus and Their Interactions With Neurotransmitter Metabolites. *Journal of Pharmacological Sciences,* 93**,** 430-436.

ANDERSON, K. A., RIBAR, T. J., ILLARIO, M. & MEANS, A. R. 1997. Defective survival and activation of thymocytes in transgenic mice expressing a catalytically inactive form of Ca2+/calmodulin-dependent protein kinase IV. *Mol Endocrinol,* 11**,** 725-37.

APKARIAN, A. V., BUSHNELL, M. C., TREEDE, R. D. & ZUBIETA, J. K. 2005. Human brain mechanisms of pain perception and regulation in health and disease. *Eur J Pain,* 9**,** 463-84.

ARANY, Z., NEWSOME, D., OLDREAD, E., LIVINGSTON, D. M. & ECKNER, R. 1995. A family of transcriptional adaptor proteins targeted by the E1A oncoprotein. *Nature,* 374**,** 81-4.

ASHWELL, K. W. S. 2009. Chapter 2 - Development of the Spinal Cord. *In:* WATSON, C., PAXINOS, G. & KAYALIOGLU, G. (eds.) *The Spinal Cord.* San Diego: Academic Press.

ATZENI, F., TURIEL, M., CAPSONI, F., DORIA, A., MERONI, P. & SARZI-PUTTINI, P. 2005. Autoimmunity and anti-TNF-alpha agents. *Ann N Y Acad Sci,* 1051**,** 559-69.

AVANTAGGIATO, V., ORLANDINI, M., ACAMPORA, D., OLIVIERO, S. & SIMEONE, A. 1998. Embryonic expression pattern of the murine figf gene, a growth factor belonging to platelet-derived growth factor/vascular endothelial growth factor family. *Mech Dev,* 73**,** 221-4.

BACKS, J., SONG, K., BEZPROZVANNAYA, S., CHANG, S. & OLSON, E. N. 2006. CaM kinase II selectively signals to histone deacetylase 4 during cardiomyocyte hypertrophy. *J Clin Invest,* 116**,** 1853-64.

BADING, H. 2000. Transcription-dependent neuronal plasticity the nuclear calcium hypothesis. *Eur J Biochem,* 267**,** 5280-3.

BADING, H. 2013. Nuclear calcium signalling in the regulation of brain function. *Nat Rev Neurosci,* 14**,** 593-608.

BADING, H. 2017. Therapeutic targeting of the pathological triad of extrasynaptic NMDA receptor signaling in neurodegenerations. *J Exp Med,* 214**,** 569-578.

BADING, H., GINTY, D. D. & GREENBERG, M. E. 1993. Regulation of gene expression in hippocampal neurons by distinct calcium signaling pathways. *Science,* 260**,** 181-6.

BADING, H. & GREENBERG, M. E. 1991. Stimulation of protein tyrosine phosphorylation by NMDA receptor activation. *Science,* 253**,** 912-4.

BADING, H., SEGAL, M. M., SUCHER, N. J., DUDEK, H., LIPTON, S. A. & GREENBERG, M. E. 1995. N-methyl-D-aspartate receptors are critical for mediating the effects of glutamate on intracellular calcium concentration and immediate early gene expression in cultured hippocampal neurons. *Neuroscience,* 64**,** 653-64.

BAHN, A., LJUBOJEVIC, M., LORENZ, H., SCHULTZ, C., GHEBREMEDHIN, E., UGELE, B., SABOLIC, I., BURCKHARDT, G. & HAGOS, Y. 2005. Murine renal organic anion transporters mOAT1 and mOAT3 facilitate the transport of neuroactive tryptophan metabolites. *Am J Physiol Cell Physiol,* 289**,** C1075-84.

BAI, G., WEI, D., ZOU, S., REN, K. & DUBNER, R. 2010. Inhibition of class II histone deacetylases in the spinal cord attenuates inflammatory hyperalgesia. *Mol Pain,* 6**,** 51.

BAKER-ANDRESEN, D., RATNU, V. S. & BREDY, T. W. 2013. Dynamic DNA methylation: a prime candidate for genomic metaplasticity and behavioral adaptation. *Trends Neurosci,* 36**,** 3-13.

BALDWIN, M. E., CATIMEL, B., NICE, E. C., ROUFAIL, S., HALL, N. E., STENVERS, K. L., KARKKAINEN, M. J., ALITALO, K., STACKER, S. A. & ACHEN, M. G. 2001. The specificity of receptor binding by vascular endothelial growth factor-d is different in mouse and man. *J Biol Chem,* 276**,** 19166-71.

BALOYANNIS, S. J. 2009. Dendritic pathology in Alzheimer's disease. *Journal of the Neurological Sciences,* 283**,** 153-157.

BANNISTER, A. J. & KOUZARIDES, T. 1995. CBP-induced stimulation of c-Fos activity is abrogated by E1A. *EMBO J,* 14**,** 4758-62.

BASBAUM, A. I., BAUTISTA, D. M., SCHERRER, G. & JULIUS, D. 2009. Cellular and molecular mechanisms of pain. *Cell,* 139**,** 267-84.

BASSEL-DUBY, R. & OLSON, E. N. 2006. Signaling pathways in skeletal muscle remodeling. *Annu Rev Biochem,* 75**,** 19-37.

BERGER, I., BIENIOSSEK, C., SCHAFFITZEL, C., HASSLER, M., SANTELLI, E. & RICHMOND, T. J. 2003. Direct interaction of Ca2+/calmodulin inhibits histone deacetylase 5 repressor core binding to myocyte enhancer factor 2. *J Biol Chem,* 278**,** 17625-35.

BERGER, S. L. 2007. The complex language of chromatin regulation during transcription. *Nature,* 447**,** 407-12.

BERGER, S. L., KOUZARIDES, T., SHIEKHATTAR, R. & SHILATIFARD, A. 2009. An operational definition of epigenetics. *Genes Dev,* 23**,** 781-3.

BHATNAGAR, V., XU, G., HAMILTON, B. A., TRUONG, D. M., ERALY, S. A., WU, W. & NIGAM, S. K. 2006. Analyses of 5' regulatory region polymorphisms in human SLC22A6 (OAT1) and SLC22A8 (OAT3). *J Hum Genet,* 51**,** 575-580.

BISWAS, S. & RAO, C. M. 2018. Epigenetic tools (The Writers, The Readers and The Erasers) and their implications in cancer therapy. *European Journal of Pharmacology,* 837**,** 8-24.

BOLGER, T. A. & YAO, T. P. 2005. Intracellular trafficking of histone deacetylase 4 regulates neuronal cell death. *J Neurosci,* 25**,** 9544-53.

BREIVIK, H., COLLETT, B., VENTAFRIDDA, V., COHEN, R. & GALLACHER, D. 2006. Survey of chronic pain in Europe: prevalence, impact on daily life, and treatment. *Eur J Pain,* 10**,** 287-333.

BROIDE, R. S., REDWINE, J. M., AFTAHI, N., YOUNG, W., BLOOM, F. E. & WINROW, C. J. 2007. Distribution of histone deacetylases 1-11 in the rat brain. *J Mol Neurosci,* 31**,** 47-58.

BRUZZONE, R., HORMUZDI, S. G., BARBE, M. T., HERB, A. & MONYER, H. 2003. Pannexins, a family of gap junction proteins expressed in brain. *Proc Natl Acad Sci U S A,* 100**,** 13644-9.

BRYANT, C. D., ZHANG, N. N., SOKOLOFF, G., FANSELOW, M. S., ENNES, H. S., PALMER, A. A. & MCROBERTS, J. A. 2008. Behavioral differences among C57BL/6 substrains: implications for transgenic and knockout studies. *Journal of neurogenetics,* 22**,** 315-331.

BRYANT, D. T., LANDLES, C., PAPADOPOULOU, A. S., BENJAMIN, A. C., DUCKWORTH, J. K., ROSAHL, T., BENN, C. L. & BATES, G. P. 2017. Disruption to schizophrenia-associated gene Fez1 in the hippocampus of HDAC11 knockout mice. *Sci Rep,* 7**,** 11900.

BUCHHEIT, T., VAN DE VEN, T. & SHAW, A. 2012. Epigenetics and the transition from acute to chronic pain. *Pain Med,* 13**,** 1474-90.

BUCHTHAL, B., LAU, D., WEISS, U., WEISLOGEL, J. M. & BADING, H. 2012. Nuclear calcium signaling controls methyl-CpG-binding protein 2 (MeCP2) phosphorylation on serine 421 following synaptic activity. *J Biol Chem,* 287**,** 30967-74.

BURCKHARDT, G. & BURCKHARDT, B. C. 2011. In vitro and in vivo evidence of the importance of organic anion transporters (OATs) in drug therapy. *Handb Exp Pharmacol***,** 29-104.

BURGERING, B. M. & KOPS, G. J. 2002. Cell cycle and death control: long live Forkheads. *Trends Biochem Sci,* 27**,** 352-60.

BURKE, R. E. & O'MALLEY, K. 2013. Axon degeneration in Parkinson's disease. *Exp Neurol,* 246**,** 72-83.

CAMPBELL, J. N., RAJA, S. N., MEYER, R. A. & MACKINNON, S. E. 1988. Myelinated afferents signal the hyperalgesia associated with nerve injury. *Pain,* 32**,** 89-94.

CANNELLA, N., OLIVEIRA, A. M. M., HEMSTEDT, T., LISSEK, T., BUECHLER, E., BADING, H. & SPANAGEL, R. 2018. Dnmt3a2 in the Nucleus Accumbens Shell Is Required for Reinstatement of Cocaine Seeking. *J Neurosci,* 38**,** 7516-7528.

CAO, L., JIAO, X., ZUZGA, D. S., LIU, Y., FONG, D. M., YOUNG, D. & DURING, M. J. 2004. VEGF links hippocampal activity with neurogenesis, learning and memory. *Nat Genet,* 36**,** 827-35.

CAO, X. C., PAPPALARDO, L. W., WAXMAN, S. G. & TAN, A. M. 2017. Dendritic spine dysgenesis in superficial dorsal horn sensory neurons after spinal cord injury. *Molecular pain,* 13**,** 1744806916688016-1744806916688016.

CARRION, A. M., LINK, W. A., LEDO, F., MELLSTROM, B. & NARANJO, J. R. 1999. DREAM is a Ca2+-regulated transcriptional repressor. *Nature,* 398**,** 80-4.

CARVALHO, A. L., DUARTE, C. B. & CARVALHO, A. P. 2000. Regulation of AMPA Receptors by Phosphorylation. *Neurochemical Research,* 25**,** 1245-1255.

CATERINA, M. J., SCHUMACHER, M. A., TOMINAGA, M., ROSEN, T. A., LEVINE, J. D. & JULIUS, D. 1997. The capsaicin receptor: a heat-activated ion channel in the pain pathway. *Nature,* 389**,** 816-24.

CEYHAN, G. O., BERGMANN, F., KADIHASANOGLU, M., ALTINTAS, B., DEMIR, I. E., HINZ, U., MÜLLER, M. W., GIESE, T., BÜCHLER, M. W., GIESE, N. A. & FRIESS, H. 2009. Pancreatic neuropathy and neuropathic pain--a comprehensive pathomorphological study of 546 cases. *Gastroenterology,* 136**,** 177-186.e1.

CHAHROUR, M., JUNG, S. Y., SHAW, C., ZHOU, X., WONG, S. T., QIN, J. & ZOGHBI, H. Y. 2008. MeCP2, a key contributor to neurological disease, activates and represses transcription. *Science,* 320**,** 1224-9.

CHAO, M. V. 2003. Neurotrophins and their receptors: a convergence point for many signalling pathways. *Nat Rev Neurosci,* 4**,** 299-309.

CHAWLA, S., HARDINGHAM, G. E., QUINN, D. R. & BADING, H. 1998. CBP: a signal-regulated transcriptional coactivator controlled by nuclear calcium and CaM kinase IV. *Science,* 281**,** 1505-9.

CHAWLA, S., VANHOUTTE, P., ARNOLD, F. J., HUANG, C. L. & BADING, H. 2003. Neuronal activity-dependent nucleocytoplasmic shuttling of HDAC4 and HDAC5. *J Neurochem,* 85**,** 151-9.

CHEN, B. & CEPKO, C. L. 2009. HDAC4 regulates neuronal survival in normal and diseased retinas. *Science,* 323**,** 256-9.

CHEN, B. S. & ROCHE, K. W. 2007. Regulation of NMDA receptors by phosphorylation. *Neuropharmacology,* 53**,** 362-8.

CHEN, T., UEDA, Y., XIE, S. & LI, E. 2002. A novel Dnmt3a isoform produced from an alternative promoter localizes to euchromatin and its expression correlates with active de novo methylation. *J Biol Chem,* 277**,** 38746-54.

CHEN, W. G., CHANG, Q., LIN, Y., MEISSNER, A., WEST, A. E., GRIFFITH, E. C., JAENISCH, R. & GREENBERG, M. E. 2003. Derepression of BDNF transcription involves calcium-dependent phosphorylation of MeCP2. *Science,* 302**,** 885-9.

CHEN, Y. & GHOSH, A. 2005. Regulation of dendritic development by neuronal activity. *J Neurobiol,* 64**,** 4-10.

CHEN, Y., PALM, F., LESCH, K.-P., GERLACH, M., MOESSNER, R. & SOMMER, C. 2011. 5-hydroxyindolacetic acid (5-HIAA), a main metabolite of serotonin, is responsible for complete Freund's adjuvant-induced thermal hyperalgesia in mice. *Molecular pain,* 7**,** 21-21.

CHENG, L., DUAN, B., HUANG, T., ZHANG, Y., CHEN, Y., BRITZ, O., GARCIA-CAMPMANY, L., REN, X., VONG, L., LOWELL, B. B., GOULDING, M., WANG, Y. & MA, Q. 2017. Identification of spinal circuits involved in touch-evoked dynamic mechanical pain. *Nat Neurosci,* 20**,** 804-814.

CHENG, L., SAMAD, O. A., XU, Y., MIZUGUCHI, R., LUO, P., SHIRASAWA, S., GOULDING, M. & MA, Q. 2005. Lbx1 and Tlx3 are opposing switches in determining GABAergic versus glutamatergic transmitter phenotypes. *Nature Neuroscience,* 8**,** 1510-1515.

CHIANG, C.-Y., WANG, J., XIE, Y.-F., ZHANG, S., HU, J. W., DOSTROVSKY, J. O. & SESSLE, B. J. 2007. Astroglial glutamate-glutamine shuttle is involved in central sensitization of nociceptive neurons in rat medullary dorsal horn. *The*

Journal of neuroscience : the official journal of the Society for Neuroscience, 27**,** 9068-9076.

CHIBA, S., IKAWA, T., TAKESHITA, H., ICHIBA, K., SAGI, M., MUKAI, T. & ANZAI, N. 2011. Interactions of human organic anion transporter 1 (hOAT1) with substances associated with forensic toxicology. *Leg Med (Tokyo),* 13**,** 180-5.

CHIECHIO, S., ZAMMATARO, M., MORALES, M. E., BUSCETI, C. L., DRAGO, F., GEREAU, R. W. T., COPANI, A. & NICOLETTI, F. 2009. Epigenetic modulation of mGlu2 receptors by histone deacetylase inhibitors in the treatment of inflammatory pain. *Mol Pharmacol,* 75**,** 1014-20.

CHOW, F. A., ANDERSON, K. A., NOELDNER, P. K. & MEANS, A. R. 2005. The autonomous activity of calcium/calmodulin-dependent protein kinase IV is required for its role in transcription. *J Biol Chem,* 280**,** 20530-8.

CLINE, H. & HAAS, K. 2008. The regulation of dendritic arbor development and plasticity by glutamatergic synaptic input: a review of the synaptotrophic hypothesis. *J Physiol,* 586**,** 1509-17.

COBOS, E. J., GHASEMLOU, N., ARALDI, D., SEGAL, D., DUONG, K. & WOOLF, C. J. 2012. Inflammation-induced decrease in voluntary wheel running in mice: a nonreflexive test for evaluating inflammatory pain and analgesia. *Pain,* 153**,** 876-84.

CODERRE, T. J., VACCARINO, A. L. & MELZACK, R. 1990. Central nervous system plasticity in the tonic pain response to subcutaneous formalin injection. *Brain Res,* 535**,** 155-8.

COHEN, S., GABEL, H. W., HEMBERG, M., HUTCHINSON, A. N., SADACCA, L. A., EBERT, D. H., HARMIN, D. A., GREENBERG, R. S., VERDINE, V. K., ZHOU, Z., WETSEL, W. C., WEST, A. E. & GREENBERG, M. E. 2011. Genome-wide activity-dependent MeCP2 phosphorylation regulates nervous system development and function. *Neuron,* 72**,** 72-85.

COLÍN-GONZÁLEZ, A. L. & SANTAMARÍA, A. 2013. Probenecid: an emerging tool for neuroprotection. *CNS Neurol Disord Drug Targets,* 12**,** 1050-65.

CORTY, M. M., MATTHEWS, B. J. & GRUEBER, W. B. 2009. Molecules and mechanisms of dendrite development in Drosophila. *Development,* 136**,** 1049-61.

COULL, J. A., BEGGS, S., BOUDREAU, D., BOIVIN, D., TSUDA, M., INOUE, K., GRAVEL, C., SALTER, M. W. & DE KONINCK, Y. 2005. BDNF from microglia causes the shift in neuronal anion gradient underlying neuropathic pain. *Nature,* 438**,** 1017-21.

COUSINS, R. & WOOD, C. E. 2010. Expression of organic anion transporters 1 and 3 in the ovine fetal brain during the latter half of gestation. *Neurosci Lett,* 484**,** 22-5.

CROW, M., DENK, F. & MCMAHON, S. B. 2013. Genes and epigenetic processes as prospective pain targets. *Genome Med,* 5**,** 12.

CROW, M., KHOVANOV, N., KELLEHER, J. H., SHARMA, S., GRANT, A. D., BOGDANOV, Y., WOOD, J. N., MCMAHON, S. B. & DENK, F. 2015. HDAC4 is required for inflammation-associated thermal hypersensitivity. *Faseb j,* 29**,** 3370-8.

CRUZALEGUI, F. H., HARDINGHAM, G. E. & BADING, H. 1999. c-Jun functions as a calcium-regulated transcriptional activator in the absence of JNK/SAPK1 activation. *EMBO J,* 18**,** 1335-44.

CUNNINGHAM, R. F., ISRAILI, Z. H. & DAYTON, P. G. 1981. Clinical pharmacokinetics of probenecid. *Clin Pharmacokinet,* 6**,** 135-51.

DARCY, M. J., CALVIN, K., CAVNAR, K. & OUIMET, C. C. 2010. Regional and subcellular distribution of HDAC4 in mouse brain. *J Comp Neurol,* 518**,** 722-40.

DAS, G., REUHL, K. & ZHOU, R. 2013. The Golgi-Cox method. *Methods Mol Biol,* 1018**,** 313-21.

DEAN, W., SANTOS, F. & REIK, W. 2003. Epigenetic reprogramming in early mammalian development and following somatic nuclear transfer. *Semin Cell Dev Biol,* 14**,** 93-100.

DENK, F., HUANG, W., SIDDERS, B., BITHELL, A., CROW, M., GRIST, J., SHARMA, S., ZIEMEK, D., RICE, A. S. C., BUCKLEY, N. J. & MCMAHON, S. B. 2013. HDAC inhibitors attenuate the development of hypersensitivity in models of neuropathic pain. *PAIN,* 154.

DENK, F. & MCMAHON, S. B. 2012. Chronic pain: emerging evidence for the involvement of epigenetics. *Neuron,* 73**,** 435-44.

DESCALZI, G., IKEGAMI, D., USHIJIMA, T., NESTLER, E. J., ZACHARIOU, V. & NARITA, M. 2015. Epigenetic mechanisms of chronic pain. *Trends Neurosci,* 38**,** 237-46.

DESCALZI, G., MITSI, V., PURUSHOTHAMAN, I., GASPARI, S., AVRAMPOU, K., LOH, Y. E., SHEN, L. & ZACHARIOU, V. 2017. Neuropathic pain promotes adaptive changes in gene expression in brain networks involved in stress and depression. *Sci Signal,* 10.

DICKSTEIN, D. L., KABASO, D., ROCHER, A. B., LUEBKE, J. I., WEARNE, S. L. & HOF, P. R. 2007. Changes in the structural complexity of the aged brain. *Aging Cell,* 6**,** 275-84.

DONG, X.-X., WANG, Y. & QIN, Z.-H. 2009. Molecular mechanisms of excitotoxicity and their relevance to pathogenesis of neurodegenerative diseases. *Acta Pharmacologica Sinica,* 30**,** 379-387.

DREOS, R., AMBROSINI, G., GROUX, R., CAVIN PÉRIER, R. & BUCHER, P. 2017. The eukaryotic promoter database in its 30th year: focus on non-vertebrate organisms. *Nucleic Acids Res,* 45**,** D51-d55.

DRUMMOND, D. C., NOBLE, C. O., KIRPOTIN, D. B., GUO, Z., SCOTT, G. K. & BENZ, C. C. 2005. Clinical development of histone deacetylase inhibitors as anticancer agents. *Annu Rev Pharmacol Toxicol,* 45**,** 495-528.

DUAN, P., LI, S., AI, N., HU, L., WELSH, W. J. & YOU, G. 2012. Potent inhibitors of human organic anion transporters 1 and 3 from clinical drug libraries: discovery and molecular characterization. *Mol Pharm,* 9**,** 3340-6.

DUPONT, C., ARMANT, D. R. & BRENNER, C. A. 2009. Epigenetics: definition, mechanisms and clinical perspective. *Semin Reprod Med,* 27**,** 351-7.

ECKSCHLAGER, T., PLCH, J., STIBOROVA, M. & HRABETA, J. 2017. Histone Deacetylase Inhibitors as Anticancer Drugs. *Int J Mol Sci,* 18.

EDER, A. & BADING, H. 2007. Calcium signals can freely cross the nuclear envelope in hippocampal neurons: somatic calcium increases generate nuclear calcium transients. *BMC neuroscience,* 8**,** 57-57.

ERALY, S. A., VALLON, V., VAUGHN, D. A., GANGOITI, J. A., RICHTER, K., NAGLE, M., MONTE, J. C., RIEG, T., TRUONG, D. M., LONG, J. M., BARSHOP, B. A., KALER, G. & NIGAM, S. K. 2006. Decreased renal organic anion secretion and plasma accumulation of endogenous organic anions in OAT1 knock-out mice. *J Biol Chem,* 281**,** 5072-83.

ESLAMINEJAD, M. B., FANI, N. & SHAHHOSEINI, M. 2013. Epigenetic regulation of osteogenic and chondrogenic differentiation of mesenchymal stem cells in culture. *Cell journal,* 15**,** 1-10.

FANG, J. Y. 2005. Histone deacetylase inhibitors, anticancerous mechanism and therapy for gastrointestinal cancers. *J Gastroenterol Hepatol,* 20**,** 988-94.

FEJES-SZABÓ, A., BOHÁR, Z., NAGY-GRÓCZ, G., VÁMOS, E., TAR, L., PŐDÖR, B., TAJTI, J., TOLDI, J., VÉCSEI, L. & PÁRDUTZ, Á. 2015. Effect of probenecid on the pain-related behaviour and morphological markers in orofacial formalin test of the rat. *CNS Neurol Disord Drug Targets,* 14**,** 350-9.

FEJES, A., PÁRDUTZ, A., TOLDI, J. & VÉCSEI, L. 2011. Kynurenine metabolites and migraine: experimental studies and therapeutic perspectives. *Curr Neuropharmacol,* 9**,** 376-87.

FENG, J., CHANG, H., LI, E. & FAN, G. 2005. Dynamic expression of de novo DNA methyltransferases Dnmt3a and Dnmt3b in the central nervous system. *J Neurosci Res,* 79**,** 734-46.

FERRARA, N., GERBER, H. P. & LECOUTER, J. 2003. The biology of VEGF and its receptors. *Nat Med,* 9**,** 669-76.

FINNIN, M. S., DONIGIAN, J. R., COHEN, A., RICHON, V. M., RIFKIND, R. A., MARKS, P. A., BRESLOW, R. & PAVLETICH, N. P. 1999. Structures of a histone deacetylase homologue bound to the TSA and SAHA inhibitors. *Nature,* 401**,** 188-93.

FISCHLE, W., DEQUIEDT, F., FILLION, M., HENDZEL, M. J., VOELTER, W. & VERDIN, E. 2001. Human HDAC7 histone deacetylase activity is associated with HDAC3 in vivo. *J Biol Chem,* 276**,** 35826-35.

FISCHLE, W., DEQUIEDT, F., HENDZEL, M. J., GUENTHER, M. G., LAZAR, M. A., VOELTER, W. & VERDIN, E. 2002. Enzymatic activity associated with class II HDACs is dependent on a multiprotein complex containing HDAC3 and SMRT/N-CoR. *Mol Cell,* 9**,** 45-57.

FOGARTY, M. J., MU, E. W. H., LAVIDIS, N. A., NOAKES, P. G. & BELLINGHAM, M. C. 2017. Motor Areas Show Altered Dendritic Structure in an Amyotrophic Lateral Sclerosis Mouse Model. *Frontiers in neuroscience,* 11**,** 609-609.

FREGERSLEV, S., BLACKSTAD, T. W., FREDENS, K. & HOLM, M. J. 1971. Golgi potassium-dichromate silver-nitrate impregnation. *Histochemie,* 25**,** 63-71.

FREYMUTH, P. S. & FITZSIMONS, H. L. 2017. The ERM protein Moesin is essential for neuronal morphogenesis and long-term memory in Drosophila. *Molecular Brain,* 10**,** 41.

GALLINARI, P., DI MARCO, S., JONES, P., PALLAORO, M. & STEINKÜHLER, C. 2007. HDACs, histone deacetylation and gene transcription: from molecular biology to cancer therapeutics. *Cell Res,* 17**,** 195-211.

GAO, L., CUETO, M. A., ASSELBERGS, F. & ATADJA, P. 2002. Cloning and functional characterization of HDAC11, a novel member of the human histone deacetylase family. *J Biol Chem,* 277**,** 25748-55.

GÉRANTON, S. M., MORENILLA-PALAO, C. & HUNT, S. P. 2007. A role for transcriptional repressor methyl-CpG-binding protein 2 and plasticity-related gene serum- and glucocorticoid-inducible kinase 1 in the induction of inflammatory pain states. *J Neurosci,* 27**,** 6163-73.

GERANTON, S. M. & TOCHIKI, K. K. 2015. Regulation of gene expression and pain states by epigenetic mechanisms. *Prog Mol Biol Transl Sci,* 131**,** 147-83.

GILLETTE, T. G. & HILL, J. A. 2015. Readers, writers, and erasers: chromatin as the whiteboard of heart disease. *Circulation research,* 116**,** 1245-1253.

GOLDBERG, J. L. 2004. Intrinsic neuronal regulation of axon and dendrite growth. *Curr Opin Neurobiol,* 14**,** 551-7.

GOLDMAN, P. S., TRAN, V. K. & GOODMAN, R. H. 1997. The multifunctional role of the co-activator CBP in transcriptional regulation. *Recent Prog Horm Res,* 52**,** 103-19; discussion 119-20.

GOLL, M. G., KIRPEKAR, F., MAGGERT, K. A., YODER, J. A., HSIEH, C. L., ZHANG, X., GOLIC, K. G., JACOBSEN, S. E. & BESTOR, T. H. 2006. Methylation of tRNAAsp by the DNA methyltransferase homolog Dnmt2. *Science,* 311**,** 395-8.

GOTO, K., NUMATA, M., KOMURA, J. I., ONO, T., BESTOR, T. H. & KONDO, H. 1994. Expression of DNA methyltransferase gene in mature and immature neurons as well as proliferating cells in mice. *Differentiation,* 56**,** 39-44.

GREGORETTI, I. V., LEE, Y. M. & GOODSON, H. V. 2004. Molecular evolution of the histone deacetylase family: functional implications of phylogenetic analysis. *J Mol Biol,* 338**,** 17-31.

GREGORY, N. S., HARRIS, A. L., ROBINSON, C. R., DOUGHERTY, P. M., FUCHS, P. N. & SLUKA, K. A. 2013. An overview of animal models of pain: disease models and outcome measures. *The journal of pain : official journal of the American Pain Society,* 14**,** 1255-1269.

GRIFFITH, J. S. & MAHLER, H. R. 1969. DNA ticketing theory of memory. *Nature,* 223**,** 580-2.

GROZINGER, C. M., HASSIG, C. A. & SCHREIBER, S. L. 1999. Three proteins define a class of human histone deacetylases related to yeast Hda1p. *Proc Natl Acad Sci U S A,* 96**,** 4868-73.

GROZINGER, C. M. & SCHREIBER, S. L. 2000. Regulation of histone deacetylase 4 and 5 and transcriptional activity by 14-3-3-dependent cellular localization. *Proc Natl Acad Sci U S A,* 97**,** 7835-40.

GRUNSTEIN, M. 1997. Histone acetylation in chromatin structure and transcription. *Nature,* 389**,** 349-52.

GU, X., FU, C., LIN, L., LIU, S., SU, X., LI, A., WU, Q., JIA, C., ZHANG, P., CHEN, L., ZHU, X. & WANG, X. 2018. miR-124 and miR-9 mediated downregulation of HDAC5 promotes neurite development through activating MEF2C-GPM6A pathway. *J Cell Physiol,* 233**,** 673-687.

GUAN, J. S., HAGGARTY, S. J., GIACOMETTI, E., DANNENBERG, J. H., JOSEPH, N., GAO, J., NIELAND, T. J., ZHOU, Y., WANG, X., MAZITSCHEK, R., BRADNER, J. E., DEPINHO, R. A., JAENISCH, R. & TSAI, L. H. 2009. HDAC2 negatively regulates memory formation and synaptic plasticity. *Nature,* 459**,** 55-60.

GUENTHER, M. G., BARAK, O. & LAZAR, M. A. 2001. The SMRT and N-CoR corepressors are activating cofactors for histone deacetylase 3. *Mol Cell Biol,* 21**,** 6091-101.

GULMEZ KARACA, K., KUPKE, J., BRITO, D. V. C., ZEUCH, B., THOME, C., WEICHENHAN, D., LUTSIK, P., PLASS, C. & OLIVEIRA, A. M. M. 2020. Neuronal ensemble-specific DNA methylation strengthens engram stability. *Nature Communications,* 11**,** 639.

GUO, J. U., MA, D. K., MO, H., BALL, M. P., JANG, M. H., BONAGUIDI, M. A., BALAZER, J. A., EAVES, H. L., XIE, B., FORD, E., ZHANG, K., MING, G. L., GAO, Y. & SONG, H. 2011. Neuronal activity modifies the DNA methylation landscape in the adult brain. *Nat Neurosci,* 14**,** 1345-51.

GUO, X., WANG, L., LI, J., DING, Z., XIAO, J., YIN, X., HE, S., SHI, P., DONG, L., LI, G., TIAN, C., WANG, J., CONG, Y. & XU, Y. 2015. Structural insight into autoinhibition and histone H3-induced activation of DNMT3A. *Nature,* 517**,** 640-4.

HABERLAND, M., MONTGOMERY, R. L. & OLSON, E. N. 2009. The many roles of histone deacetylases in development and physiology: implications for disease and therapy. *Nature Reviews Genetics,* 10**,** 32-42.

HAGGARTY, S. J. & TSAI, L. H. 2011. Probing the role of HDACs and mechanisms of chromatin-mediated neuroplasticity. *Neurobiol Learn Mem,* 96**,** 41-52.

HAIGIS, M. C. & GUARENTE, L. P. 2006. Mammalian sirtuins--emerging roles in physiology, aging, and calorie restriction. *Genes Dev,* 20**,** 2913-21.

HARDINGHAM, G. E., ARNOLD, F. J. & BADING, H. 2001. Nuclear calcium signaling controls CREB-mediated gene expression triggered by synaptic activity. *Nat Neurosci,* 4**,** 261-7.

HARDINGHAM, G. E. & BADING, H. 2010. Synaptic versus extrasynaptic NMDA receptor signalling: implications for neurodegenerative disorders. *Nat Rev Neurosci,* 11**,** 682-96.

HARDINGHAM, G. E., CHAWLA, S., CRUZALEGUI, F. H. & BADING, H. 1999. Control of recruitment and transcription-activating function of CBP determines gene regulation by NMDA receptors and L-type calcium channels. *Neuron,* 22**,** 789-98.

HARDINGHAM, G. E., CHAWLA, S., JOHNSON, C. M. & BADING, H. 1997. Distinct functions of nuclear and cytoplasmic calcium in the control of gene expression. *Nature,* 385**,** 260-5.

HARDINGHAM, G. E., FUKUNAGA, Y. & BADING, H. 2002. Extrasynaptic NMDARs oppose synaptic NMDARs by triggering CREB shut-off and cell death pathways. *Nat Neurosci,* 5**,** 405-14.

HARRISON, M., O'BRIEN, A., ADAMS, L., COWIN, G., RUITENBERG, M. J., SENGUL, G. & WATSON, C. 2013. Vertebral landmarks for the identification of spinal cord segments in the mouse. *Neuroimage,* 68**,** 22-9.

HARVEY, R. J., DEPNER, U. B., WÄSSLE, H., AHMADI, S., HEINDL, C., REINOLD, H., SMART, T. G., HARVEY, K., SCHÜTZ, B., ABO-SALEM, O. M., et al. 2004. GlyR alpha3: an essential target for spinal PGE2-mediated inflammatory pain sensitization. *Science,* 304**,** 884-7.

HÄUSSER, M., SPRUSTON, N. & STUART, G. J. 2000. Diversity and dynamics of dendritic signaling. *Science,* 290**,** 739-44.

HEMSTEDT, T. J., BENGTSON, C. P., RAMIREZ, O., OLIVEIRA, A. M. M. & BADING, H. 2017. Reciprocal Interaction of Dendrite Geometry and Nuclear Calcium-VEGFD Signaling Gates Memory Consolidation and Extinction. *J Neurosci,* 37**,** 6946-6955.

HOLLIDAY, R. & PUGH, J. E. 1975. DNA modification mechanisms and gene activity during development. *Science,* 187**,** 226-32.

HOSOYAMADA, M., SEKINE, T., KANAI, Y. & ENDOU, H. 1999. Molecular cloning and functional expression of a multispecific organic anion transporter from human kidney. *Am J Physiol,* 276**,** F122-8.

HUANG, Y., MYERS, S. J. & DINGLEDINE, R. 1999. Transcriptional repression by REST: recruitment of Sin3A and histone deacetylase to neuronal genes. *Nat Neurosci,* 2**,** 867-72.

HUNSKAAR, S., FASMER, O. B. & HOLE, K. 1985. Acetylsalicylic acid, paracetamol and morphine inhibit behavioral responses to intrathecally administered substance P or capsaicin. *Life Sci,* 37**,** 1835-41.

HUNSKAAR, S. & HOLE, K. 1987. The formalin test in mice: dissociation between inflammatory and non-inflammatory pain. *Pain,* 30**,** 103-14.

IADAROLA, M. J., BRADY, L. S., DRAISCI, G. & DUBNER, R. 1988. Enhancement of dynorphin gene expression in spinal cord following experimental inflammation: stimulus specificity, behavioral parameters and opioid receptor binding. *Pain,* 35**,** 313-26.

IASP Task Force on TAXONOMY. 1994. Part III: Pain Terms, A Current List with Definitions and Notes on Usage. *In:* MERSKEY, H. & BOGDUK, N. (eds.) *Classification of Chronic Pain.* Seattle: IASP Press.

IMPEY, S., FONG, A. L., WANG, Y., CARDINAUX, J. R., FASS, D. M., OBRIETAN, K., WAYMAN, G. A., STORM, D. R., SODERLING, T. R. & GOODMAN, R. H. 2002. Phosphorylation of CBP mediates transcriptional activation by neural activity and CaM kinase IV. *Neuron,* 34**,** 235-44.

JAN, Y. N. & JAN, L. Y. 2003. The control of dendrite development. *Neuron,* 40**,** 229-42.

JI, R. R. & RUPP, F. 1997. Phosphorylation of transcription factor CREB in rat spinal cord after formalin-induced hyperalgesia: relationship to c-fos induction. *J Neurosci,* 17**,** 1776-85.

JI, R. R., SAMAD, T. A., JIN, S. X., SCHMOLL, R. & WOOLF, C. J. 2002. p38 MAPK activation by NGF in primary sensory neurons after inflammation increases TRPV1 levels and maintains heat hyperalgesia. *Neuron,* 36**,** 57-68.

JONES, P. L., VEENSTRA, G. J., WADE, P. A., VERMAAK, D., KASS, S. U., LANDSBERGER, N., STROUBOULIS, J. & WOLFFE, A. P. 1998. Methylated DNA and MeCP2 recruit histone deacetylase to repress transcription. *Nat Genet,* 19**,** 187-91.

JULIUS, D. & BASBAUM, A. I. 2001. Molecular mechanisms of nociception. *Nature,* 413**,** 203-10.

KANG, H., SUN, L. D., ATKINS, C. M., SODERLING, T. R., WILSON, M. A. & TONEGAWA, S. 2001. An important role of neural activity-dependent CaMKIV signaling in the consolidation of long-term memory. *Cell,* 106**,** 771-83.

KASSIS, H., SHEHADAH, A., CHOPP, M., ROBERTS, C. & ZHANG, Z. G. 2015. Stroke Induces Nuclear Shuttling of Histone Deacetylase 4. *Stroke,* 46**,** 1909-15.

KAUFMANN, W. E. & MOSER, H. W. 2000. Dendritic anomalies in disorders associated with mental retardation. *Cereb Cortex,* 10**,** 981-91.

KAWASHIMA, T., KITAMURA, K., SUZUKI, K., NONAKA, M., KAMIJO, S., TAKEMOTO-KIMURA, S., KANO, M., OKUNO, H., OHKI, K. & BITO, H. 2013. Functional labeling of neurons and their projections using the synthetic activity-dependent promoter E-SARE. *Nat Methods,* 10**,** 889-95.

KESSLER, M., TERRAMANI, T., LYNCH, G. & BAUDRY, M. 1989. A glycine site associated with N-methyl-D-aspartic acid receptors: characterization and identification of a new class of antagonists. *J Neurochem,* 52**,** 1319-28.

KHANGURA, R. K., BALI, A., JAGGI, A. S. & SINGH, N. 2017. Histone acetylation and histone deacetylation in neuropathic pain: An unresolved puzzle? *Eur J Pharmacol,* 795**,** 36-42.

KIM, D.-S., LI, K.-W., BOROUJERDI, A., PETER YU, Y., ZHOU, C.-Y., DENG, P., PARK, J., ZHANG, X., LEE, J., CORPE, M., SHARP, K., STEWARD, O.,

EROGLU, C., BARRES, B., ZAUCKE, F., XU, Z. C. & LUO, Z. D. 2012a. Thrombospondin-4 contributes to spinal sensitization and neuropathic pain states. *The Journal of neuroscience : the official journal of the Society for Neuroscience,* 32**,** 8977-8987.

KIM, H. C., CHOI, K. C., CHOI, H. K., KANG, H. B., KIM, M. J., LEE, Y. H., LEE, O. H., LEE, J., KIM, Y. J., JUN, W., JEONG, J. W. & YOON, H. G. 2010. HDAC3 selectively represses CREB3-mediated transcription and migration of metastatic breast cancer cells. *Cell Mol Life Sci,* 67**,** 3499-510.

KIM, M. S., AKHTAR, M. W., ADACHI, M., MAHGOUB, M., BASSEL-DUBY, R., KAVALALI, E. T., OLSON, E. N. & MONTEGGIA, L. M. 2012b. An essential role for histone deacetylase 4 in synaptic plasticity and memory formation. *J Neurosci,* 32**,** 10879-86.

KLOSE, R. J. & BIRD, A. P. 2006. Genomic DNA methylation: the mark and its mediators. *Trends Biochem Sci,* 31**,** 89-97.

KOUZARIDES, T. 2007. Chromatin modifications and their function. *Cell,* 128**,** 693-705.

KUKK, E., LYMBOUSSAKI, A., TAIRA, S., KAIPAINEN, A., JELTSCH, M., JOUKOV, V. & ALITALO, K. 1996. VEGF-C receptor binding and pattern of expression with VEGFR-3 suggests a role in lymphatic vascular development. *Development,* 122**,** 3829-37.

KUNER, R. 2010. Central mechanisms of pathological pain. *Nat Med,* 16**,** 1258-66.

KUNER, R. & FLOR, H. 2017. Structural plasticity and reorganisation in chronic pain. *Nature Reviews Neuroscience,* 18**,** 20-30.

LAHM, A., PAOLINI, C., PALLAORO, M., NARDI, M. C., JONES, P., NEDDERMANN, P., SAMBUCINI, S., BOTTOMLEY, M. J., LO SURDO, P., CARFí, A., et al. 2007. Unraveling the hidden catalytic activity of vertebrate class IIa histone deacetylases. *Proceedings of the National Academy of Sciences,* 104**,** 17335.

LANGMEAD, B., TRAPNELL, C., POP, M. & SALZBERG, S. L. 2009. Ultrafast and memory-efficient alignment of short DNA sequences to the human genome. *Genome Biology,* 10**,** R25.

LARSON, A. A. 2008. Immune and Glial Regulation of Pain. Edited by Joyce A. DeLeo, PhD; Linda S. Sorkin, PhD; Linda R. Watkins, PhD. *Journal of Musculoskeletal Pain,* 16**,** 358-359.

LATREMOLIERE, A. & WOOLF, C. J. 2009. Central sensitization: a generator of pain hypersensitivity by central neural plasticity. *The journal of pain : official journal of the American Pain Society,* 10**,** 895-926.

LE BRAS, B., BARALLOBRE, M.-J., HOMMAN-LUDIYE, J., NY, A., WYNS, S., TAMMELA, T., HAIKO, P., KARKKAINEN, M. J., YUAN, L., MURIEL, M.-P., CHATZOPOULOU, E., et al. 2006. VEGF-C is a trophic factor for neural progenitors in the vertebrate embryonic brain. *Nature Neuroscience,* 9**,** 340-348.

LEE, B., BUTCHER, G. Q., HOYT, K. R., IMPEY, S. & OBRIETAN, K. 2005. Activity-dependent neuroprotection and cAMP response element-binding protein (CREB): kinase coupling, stimulus intensity, and temporal regulation of CREB phosphorylation at serine 133. *J Neurosci,* 25**,** 1137-48.

LEE, J., GRAY, A., YUAN, J., LUOH, S. M., AVRAHAM, H. & WOOD, W. I. 1996. Vascular endothelial growth factor-related protein: a ligand and specific activator of the tyrosine kinase receptor Flt4. *Proc Natl Acad Sci U S A,* 93**,** 1988-92.

LEE, K. K. & WORKMAN, J. L. 2007. Histone acetyltransferase complexes: one size doesn't fit all. *Nat Rev Mol Cell Biol,* 8**,** 284-95.

LEIN, E. S., HAWRYLYCZ, M. J., AO, N., AYRES, M., BENSINGER, A., BERNARD, A., BOE, A. F., BOGUSKI, M. S., BROCKWAY, K. S., BYRNES, E. J., CHEN, L., et al. 2007. Genome-wide atlas of gene expression in the adult mouse brain. *Nature,* 445**,** 168-176.

LI, B., CAREY, M. & WORKMAN, J. L. 2007. The role of chromatin during transcription. *Cell,* 128**,** 707-19.

LI, J., CHEN, J., RICUPERO, C. L., HART, R. P., SCHWARTZ, M. S., KUSNECOV, A. & HERRUP, K. 2012. Nuclear accumulation of HDAC4 in ATM deficiency promotes neurodegeneration in ataxia telangiectasia. *Nat Med,* 18**,** 783-90.

LIMBACK-STOKIN, K., KORZUS, E., NAGAOKA-YASUDA, R. & MAYFORD, M. 2004. Nuclear calcium/calmodulin regulates memory consolidation. *J Neurosci,* 24**,** 10858-67.

LIN, T.-B., HSIEH, M.-C., LAI, C.-Y., CHENG, J.-K., CHAU, Y.-P., RUAN, T., CHEN, G.-D. & PENG, H.-Y. 2015. Modulation of Nerve Injury–induced HDAC4 Cytoplasmic Retention Contributes to Neuropathic Pain in Rats. *Anesthesiology: The Journal of the American Society of Anesthesiologists,* 123**,** 199-212.

LINGUEGLIA, E. 2007. Acid-sensing ion channels in sensory perception. *J Biol Chem,* 282**,** 17325-9.

LITKE, C., BADING, H. & MAUCERI, D. 2018. Histone deacetylase 4 shapes neuronal morphology via a mechanism involving regulation of expression of vascular endothelial growth factor D. *J Biol Chem,* 293**,** 8196-8207.

LITKE, C., OLIVEIRA, A. M., PALDY, E., HAGENSTON, A. M., LU, J., KUNER, R., BADING, H. & MAUCERI, D. 2019. Epigenetic control of hypersensitivity in chronic inflammatory pain by the de novo DNA methyltransferase Dnmt3a2. *Mol Pain,* 15**,** 1744806919827469.

LIU, Y., RANDALL, W. R. & SCHNEIDER, M. F. 2005. Activity-dependent and -independent nuclear fluxes of HDAC4 mediated by different kinases in adult skeletal muscle. *J Cell Biol,* 168**,** 887-97.

LOESER, J. D. & TREEDE, R. D. 2008. The Kyoto protocol of IASP Basic Pain Terminology. *Pain,* 137**,** 473-7.

LOHELA, M., BRY, M., TAMMELA, T. & ALITALO, K. 2009. VEGFs and receptors involved in angiogenesis versus lymphangiogenesis. *Curr Opin Cell Biol,* 21**,** 154-65.

LONGAIR, M. H., BAKER, D. A. & ARMSTRONG, J. D. 2011. Simple Neurite Tracer: open source software for reconstruction, visualization and analysis of neuronal processes. *Bioinformatics,* 27**,** 2453-4.

LU, J., LUO, C., BALI, K. K., XIE, R. G., MAINS, R. E., EIPPER, B. A. & KUNER, R. 2015. A role for Kalirin-7 in nociceptive sensitization via activity-dependent modulation of spinal synapses. *Nat Commun,* 6**,** 6820.

LUO, C., HAJKOVA, P. & ECKER, J. R. 2018. Dynamic DNA methylation: In the right place at the right time. *Science (New York, N.Y.),* 361**,** 1336-1340.

MA, W., ZHENG, W. H., POWELL, K., JHAMANDAS, K. & QUIRION, R. 2001. Chronic morphine exposure increases the phosphorylation of MAP kinases and the transcription factor CREB in dorsal root ganglion neurons: an in vitro and in vivo study. *Eur J Neurosci,* 14**,** 1091-104.

MANGEAT, P., ROY, C. & MARTIN, M. 1999. ERM proteins in cell adhesion and membrane dynamics. *Trends Cell Biol,* 9**,** 187-92.

MARIE, H., MORISHITA, W., YU, X., CALAKOS, N. & MALENKA, R. C. 2005. Generation of silent synapses by acute in vivo expression of CaMKIV and CREB. *Neuron,* 45**,** 741-52.

MARMORSTEIN, R. & TRIEVEL, R. C. 2009. Histone modifying enzymes: structures, mechanisms, and specificities. *Biochim Biophys Acta,* 1789**,** 58-68.

MARSHALL, P. & BREDY, T. W. 2016. Cognitive neuroepigenetics: the next evolution in our understanding of the molecular mechanisms underlying learning and memory? *npj Science of Learning,* 1**,** 16014.

MARTIN, M., KETTMANN, R. & DEQUIEDT, F. 2007. Class IIa histone deacetylases: regulating the regulators. *Oncogene,* 26**,** 5450-67.

MAUCERI, D., BUCHTHAL, B., HEMSTEDT, T. J., WEISS, U., KLEIN, C. D. & BADING, H. 2020. Nasally delivered VEGFD mimetics mitigate stroke-induced dendrite loss and brain damage. *Proceedings of the National Academy of Sciences,* 117**,** 8616-8623.

MAUCERI, D., FREITAG, H. E., OLIVEIRA, A. M., BENGTSON, C. P. & BADING, H. 2011. Nuclear calcium-VEGFD signaling controls maintenance of dendrite arborization necessary for memory formation. *Neuron,* 71**,** 117-30.

MAUCERI, D., HAGENSTON, A. M., SCHRAMM, K., WEISS, U. & BADING, H. 2015. Nuclear Calcium Buffering Capacity Shapes Neuronal Architecture. *J Biol Chem,* 290**,** 23039-49.

MAYER, M. L., WESTBROOK, G. L. & GUTHRIE, P. B. 1984. Voltage-dependent block by Mg2+ of NMDA responses in spinal cord neurones. *Nature,* 309**,** 261-3.

MCCLUNG, C. A. & NESTLER, E. J. 2008. Neuroplasticity Mediated by Altered Gene Expression. *Neuropsychopharmacology,* 33**,** 3-17.

MCCLURE, C., COLE, K. L. H., WULFF, P., KLUGMANN, M. & MURRAY, A. J. 2011. Production and Titering of Recombinant Adeno-associated Viral Vectors. *JoVE***,** e3348.

MCDONALD, N. Q. & HENDRICKSON, W. A. 1993. A structural superfamily of growth factors containing a cystine knot motif. *Cell,* 73**,** 421-4.

MCGHEE, J. D. & FELSENFELD, G. 1980. Nucleosome structure. *Annu Rev Biochem,* 49**,** 1115-56.

MCKINSEY, T. A., ZHANG, C. L. & OLSON, E. N. 2001. Identification of a signal-responsive nuclear export sequence in class II histone deacetylases. *Mol Cell Biol,* 21**,** 6312-21.

MCKINSEY, T. A., ZHANG, C. L. & OLSON, E. N. 2002. MEF2: a calcium-dependent regulator of cell division, differentiation and death. *Trends Biochem Sci,* 27**,** 40-7.

MECS, L., TUBOLY, G., NAGY, E., BENEDEK, G. & HORVATH, G. 2009. The Peripheral Antinociceptive Effects of Endomorphin-1 and Kynurenic Acid in the Rat Inflamed Joint Model. *Anesthesia & Analgesia,* 109**,** 1297-1304.

MELLER, S. T. 1994. Thermal and mechanical hyperalgesia: A distinct role for different excitatory amino acid receptors and signal transduction pathways? *APS Journal,* 3**,** 215-231.

MELLSTRÖM, B., KASTANAUSKAITE, A., KNAFO, S., GONZALEZ, P., DOPAZO, X. M., RUIZ-NUÑO, A., JEFFERYS, J. G. R., ZHUO, M., BLISS, T. V. P., NARANJO, J. R. & DEFELIPE, J. 2016. Specific cytoarchitectureal changes in hippocampal subareas in daDREAM mice. *Molecular brain,* 9**,** 22-22.

MELLSTRÖM, B. & NARANJO, J. R. 2001. Ca2+-dependent transcriptional repression and derepression: DREAM, a direct effector. *Seminars in cell & developmental biology,* 12**,** 59-63.

MEYER, R. A., RINGKAMP, M., CAMPBELL, J. & RAJA, S. Peripheral mechanisms of cutaneous nociception. 2006.

MGD, M. G. D. 2013. *Mouse Genome Informatics* [Online]. Bar Harbor, Maine. Available: http://www.informatics.jax.org/reference/J:101679.

MI, H., MURUGANUJAN, A., CASAGRANDE, J. T. & THOMAS, P. D. 2013. Large-scale gene function analysis with the PANTHER classification system. *Nat Protoc,* 8**,** 1551-66.

MIAO, X. R., FAN, L. C., WU, S., MAO, Q., LI, Z., LUTZ, B., XU, J. T., LU, Z. & TAO, Y. X. 2017. DNMT3a contributes to the development and maintenance of bone cancer pain by silencing Kv1.2 expression in spinal cord dorsal horn. *Mol Pain,* 13**,** 1744806917740681.

MILLER, C. A. & SWEATT, J. D. 2007. Covalent modification of DNA regulates memory formation. *Neuron,* 53**,** 857-69.

MIZUMURA, K. & MURASE, S. 2015. Role of nerve growth factor in pain. *Handb Exp Pharmacol,* 227**,** 57-77.

MOGIL, J. S. 2009. Animal models of pain: progress and challenges. *Nat Rev Neurosci,* 10**,** 283-94.

MOGIL, J. S., DAVIS, K. D. & DERBYSHIRE, S. W. 2010. The necessity of animal models in pain research. *Pain,* 151**,** 12-7.

MONSEY, M. S., OTA, K. T., AKINGBADE, I. F., HONG, E. S. & SCHAFE, G. E. 2011. Epigenetic alterations are critical for fear memory consolidation and synaptic plasticity in the lateral amygdala. *PLoS One,* 6**,** e19958.

MOORE, K. A., KOHNO, T., KARCHEWSKI, L. A., SCHOLZ, J., BABA, H. & WOOLF, C. J. 2002. Partial peripheral nerve injury promotes a selective loss of GABAergic inhibition in the superficial dorsal horn of the spinal cord. *J Neurosci,* 22**,** 6724-31.

MOORE, L. D., LE, T. & FAN, G. 2013. DNA methylation and its basic function. *Neuropsychopharmacology,* 38**,** 23-38.

MORGAN, D. & MORGAN, D. O. 2007. *The Cell Cycle: Principles of Control*, OUP/New Science Press.

MOTTIS, A., MOUCHIROUD, L. & AUWERX, J. 2013. Emerging roles of the corepressors NCoR1 and SMRT in homeostasis. *Genes & development,* 27**,** 819-835.

NAKAMURA, Y., NAKANISHI, T. & TAMAI, I. 2018. Membrane Transporters Contributing to PGE2 Distribution in Central Nervous System. *Biological and Pharmaceutical Bulletin,* 41**,** 1337-1347.

NAKAYAMA, A. Y., HARMS, M. B. & LUO, L. 2000. Small GTPases Rac and Rho in the maintenance of dendritic spines and branches in hippocampal pyramidal neurons. *J Neurosci,* 20**,** 5329-38.

NAN, X., NG, H. H., JOHNSON, C. A., LAHERTY, C. D., TURNER, B. M., EISENMAN, R. N. & BIRD, A. 1998. Transcriptional repression by the methyl-CpG-binding protein MeCP2 involves a histone deacetylase complex. *Nature,* 393**,** 386-9.

NÄSSTRÖM, J., KARLSSON, U. & POST, C. 1992. Antinociceptive actions of different classes of excitatory amino acid receptor antagonists in mice. *Eur J Pharmacol,* 212**,** 21-9.

NEUMANN, S., BRAZ, J. M., SKINNER, K., LLEWELLYN-SMITH, I. J. & BASBAUM, A. I. 2008. Innocuous, not noxious, input activates PKCgamma interneurons of the spinal dorsal horn via myelinated afferent fibers. *The Journal of neuroscience : the official journal of the Society for Neuroscience,* 28**,** 7936-7944.

NIEDERBERGER, E., RESCH, E., PARNHAM, M. J. & GEISSLINGER, G. 2017. Drugging the pain epigenome. *Nat Rev Neurol,* 13**,** 434-447.

NIGAM, S. K., BUSH, K. T., MARTOVETSKY, G., AHN, S.-Y., LIU, H. C., RICHARD, E., BHATNAGAR, V. & WU, W. 2015. The Organic Anion Transporter (OAT) Family: A Systems Biology Perspective. *Physiological Reviews,* 95**,** 83-123.

NJOO, C., HEINL, C. & KUNER, R. 2014. In vivo SiRNA transfection and gene knockdown in spinal cord via rapid noninvasive lumbar intrathecal injections in mice. *Journal of visualized experiments : JoVE***,** 51229.

NORTH, R. A. 2004. P2X3 receptors and peripheral pain mechanisms. *The Journal of Physiology,* 554**,** 301-308.

NOWAK, L. M., YOUNG, A. B. & MACDONALD, R. L. 1982. GABA and bicuculline actions on mouse spinal cord and cortical neurons in cell culture. *Brain Res,* 244**,** 155-64.

NUSINZON, I. & HORVATH, C. M. 2005. Histone Deacetylases as Transcriptional Activators? Role Reversal in Inducible Gene Regulation. *Science's STKE,* 2005**,** re11.

O'NEILL, J., BROCK, C., OLESEN, A. E., ANDRESEN, T., NILSSON, M. & DICKENSON, A. H. 2012. Unravelling the mystery of capsaicin: a tool to understand and treat pain. *Pharmacological reviews,* 64**,** 939-971.

OHSHIRO, H., TONAI-KACHI, H. & ICHIKAWA, K. 2008. GPR35 is a functional receptor in rat dorsal root ganglion neurons. *Biochem Biophys Res Commun,* 365**,** 344-8.

OKANO, M., BELL, D. W., HABER, D. A. & LI, E. 1999. DNA methyltransferases Dnmt3a and Dnmt3b are essential for de novo methylation and mammalian development. *Cell,* 99**,** 247-57.

OKANO, M., XIE, S. & LI, E. 1998. Dnmt2 is not required for de novo and maintenance methylation of viral DNA in embryonic stem cells. *Nucleic Acids Res,* 26**,** 2536-40.

OLIVEIRA, A. M. 2016. DNA methylation: a permissive mark in memory formation and maintenance. *Learn Mem,* 23**,** 587-93.

OLIVEIRA, A. M., HEMSTEDT, T. J. & BADING, H. 2012. Rescue of aging-associated decline in Dnmt3a2 expression restores cognitive abilities. *Nat Neurosci,* 15**,** 1111-3.

OLIVEIRA, A. M., HEMSTEDT, T. J., FREITAG, H. E. & BADING, H. 2016. Dnmt3a2: a hub for enhancing cognitive functions. *Mol Psychiatry,* 21**,** 1130-6.

ORLANDINI, M., MARCONCINI, L., FERRUZZI, R. & OLIVIERO, S. 1996. Identification of a c-fos-induced gene that is related to the platelet-derived growth factor/vascular endothelial growth factor family. *Proc Natl Acad Sci U S A,* 93**,** 11675-80.

ORPHANIDES, G. & REINBERG, D. 2000. RNA polymerase II elongation through chromatin. *Nature,* 407**,** 471-5.

PAPADIA, S., STEVENSON, P., HARDINGHAM, N. R., BADING, H. & HARDINGHAM, G. E. 2005. Nuclear Ca2+ and the cAMP response element-binding protein family mediate a late phase of activity-dependent neuroprotection. *J Neurosci,* 25**,** 4279-87.

PARONI, G., CERNOTTA, N., DELLO RUSSO, C., GALLINARI, P., PALLAORO, M., FOTI, C., TALAMO, F., ORSATTI, L., STEINKUHLER, C. & BRANCOLINI, C. 2008. PP2A regulates HDAC4 nuclear import. *Mol Biol Cell,* 19**,** 655-67.

PARRA, M. & VERDIN, E. 2010. Regulatory signal transduction pathways for class IIa histone deacetylases. *Curr Opin Pharmacol,* 10**,** 454-60.

PARSONS, M. P. & RAYMOND, L. A. 2014. Extrasynaptic NMDA receptor involvement in central nervous system disorders. *Neuron,* 82**,** 279-93.

PARVATHY, S. S. & MASOCHA, W. 2013. Gait analysis of C57BL/6 mice with complete Freund's adjuvant-induced arthritis using the CatWalk system. *BMC Musculoskelet Disord,* 14**,** 14.

PAVLOVA, A., SAKURAI, H., LECLERCQ, B., BEIER, D. R., YU, A. S. & NIGAM, S. K. 2000. Developmentally regulated expression of organic ion transporters NKT (OAT1), OCT1, NLT (OAT2), and Roct. *Am J Physiol Renal Physiol,* 278**,** F635-43.

PEREIRA, E. F. R., HILMAS, C., SANTOS, M. D., ALKONDON, M., MAELICKE, A. & ALBUQUERQUE, E. X. 2002. Unconventional ligands and modulators of nicotinic receptors. *Journal of Neurobiology,* 53**,** 479-500.

PERL, D. P. 2010. Neuropathology of Alzheimer's disease. *Mt Sinai J Med,* 77**,** 32-42.

PERL, E. R. 2007. Ideas about pain, a historical view. *Nature Reviews Neuroscience,* 8**,** 71-80.

PERWITASARI, O., YAN, X., JOHNSON, S., WHITE, C., BROOKS, P., TOMPKINS, S. M. & TRIPP, R. A. 2013. Targeting organic anion transporter 3 with probenecid as a novel anti-influenza a virus strategy. *Antimicrob Agents Chemother,* 57**,** 475-83.

PESERICO, A. & SIMONE, C. 2011. Physical and functional HAT/HDAC interplay regulates protein acetylation balance. *J Biomed Biotechnol,* 2011**,** 371832.

PITZER, C., KUNER, R. & TAPPE-THEODOR, A. 2016. Voluntary and evoked behavioral correlates in inflammatory pain conditions under different social housing conditions. *Pain reports,* 1**,** e564-e564.

POLGÁR, E., HUGHES, D. I., ARHAM, A. Z. & TODD, A. J. 2005. Loss of Neurons from Laminas I-III of the Spinal Dorsal Horn Is Not Required for Development of Tactile Allodynia in the Spared Nerve Injury Model of Neuropathic Pain. *The Journal of Neuroscience,* 25**,** 6658.

POLLEMA-MAYS, S. L., CENTENO, M. V., APKARIAN, A. V. & MARTINA, M. 2014. Expression of DNA methyltransferases in adult dorsal root ganglia is cell-type specific and up regulated in a rodent model of neuropathic pain. *Front Cell Neurosci,* 8**,** 217.

PORRECA, F., OSSIPOV, M. H. & GEBHART, G. F. 2002. Chronic pain and medullary descending facilitation. *Trends Neurosci,* 25**,** 319-25.

PRICE, D. D. 2000. Psychological and neural mechanisms of the affective dimension of pain. *Science,* 288**,** 1769-72.

PRICE, V., WANG, L. & D'MELLO, S. R. 2013. Conditional deletion of histone deacetylase-4 in the central nervous system has no major effect on brain architecture or neuronal viability. *J Neurosci Res,* 91**,** 407-15.

RACEY, L. A. & BYVOET, P. 1971. Histone acetyltransferase in chromatin. Evidence for in vitro enzymatic transfer of acetate from acetyl-coenzyme A to histones. *Exp Cell Res,* 64**,** 366-70.

RAHN, E. J., GUZMAN-KARLSSON, M. C. & DAVID SWEATT, J. 2013. Cellular, molecular, and epigenetic mechanisms in non-associative conditioning: implications for pain and memory. *Neurobiol Learn Mem,* 105**,** 133-50.

RAMÓN-MOLINER, E. 1970. The Golgi-Cox Technique. *In:* NAUTA, W. J. H. & EBBESSON, S. O. E. (eds.) *Contemporary Research Methods in Neuroanatomy.* Berlin, Heidelberg: Springer Berlin Heidelberg.

RAO, D. D., VORHIES, J. S., SENZER, N. & NEMUNAITIS, J. 2009. siRNA vs. shRNA: Similarities and differences. *Advanced Drug Delivery Reviews,* 61**,** 746-759.

RAYNER, C. R., CHANU, P., GIESCHKE, R., BOAK, L. M. & JONSSON, E. N. 2008. Population Pharmacokinetics of Oseltamivir When Coadministered With Probenecid. *The Journal of Clinical Pharmacology,* 48**,** 935-947.

REDMOND, L., KASHANI, A. H. & GHOSH, A. 2002. Calcium regulation of dendritic growth via CaM kinase IV and CREB-mediated transcription. *Neuron,* 34**,** 999-1010.

REID, G., WIELINGA, P., ZELCER, N., VAN DER HEIJDEN, I., KUIL, A., DE HAAS, M., WIJNHOLDS, J. & BORST, P. 2003. The human multidrug resistance protein MRP4 functions as a prostaglandin efflux transporter and is inhibited by nonsteroidal antiinflammatory drugs. *Proc Natl Acad Sci U S A,* 100**,** 9244-9.

REINER, A., DRAGATSIS, I. & DIETRICH, P. 2011. Genetics and neuropathology of Huntington's disease. *Int Rev Neurobiol,* 98**,** 325-72.

REN, K. & DUBNER, R. 1999. Inflammatory Models of Pain and Hyperalgesia. *ILAR Journal,* 40**,** 111-118.

REN, K. & DUBNER, R. 2008. Neuron-glia crosstalk gets serious: role in pain hypersensitivity. *Curr Opin Anaesthesiol,* 21**,** 570-9.

RENTHAL, W., MAZE, I., KRISHNAN, V., COVINGTON, H. E., 3RD, XIAO, G., KUMAR, A., RUSSO, S. J., GRAHAM, A., TSANKOVA, N., KIPPIN, T. E., KERSTETTER, K. A., NEVE, R. L., HAGGARTY, S. J., MCKINSEY, T. A., BASSEL-DUBY, R., OLSON, E. N. & NESTLER, E. J. 2007. Histone deacetylase 5 epigenetically controls behavioral adaptations to chronic emotional stimuli. *Neuron,* 56**,** 517-29.

RICCIO, A. 2010. Dynamic epigenetic regulation in neurons: enzymes, stimuli and signaling pathways. *Nature Neuroscience,* 13**,** 1330-1337.

RICHNER, M., BJERRUM, O. J., NYKJAER, A. & VAEGTER, C. B. 2011. The Spared Nerve Injury (SNI) Model of Induced Mechanical Allodynia in Mice. *JoVE***,** e3092.

RITTNER, H. L., MACHELSKA, H. & STEIN, C. 2008. 5.30 - Immune System, Pain and Analgesia. *In:* MASLAND, R. H., ALBRIGHT, T. D., ALBRIGHT, T. D., MASLAND, R. H., DALLOS, P., OERTEL, D., FIRESTEIN, S., BEAUCHAMP, G. K., CATHERINE BUSHNELL, M., BASBAUM, A. I., KAAS, J. H. & GARDNER, E. P. (eds.) *The Senses: A Comprehensive Reference.* New York: Academic Press.

RODRIGUEZ-RAECKE, R., NIEMEIER, A., IHLE, K., RUETHER, W. & MAY, A. 2009. Brain gray matter decrease in chronic pain is the consequence and not the cause of pain. *J Neurosci,* 29**,** 13746-50.

ROTH, M., OBAIDAT, A. & HAGENBUCH, B. 2012. OATPs, OATs and OCTs: the organic anion and cation transporters of the SLCO and SLC22A gene superfamilies. *British journal of pharmacology,* 165**,** 1260-1287.

SALZER, W., WIDEMANN, B., MCCULLY, C., ADAMSON, P. C. & BALIS, F. M. 2001. Effect of probenecid on ventricular cerebrospinal fluid methotrexate pharmacokinetics after intralumbar administration in nonhuman primates. *Cancer Chemotherapy and Pharmacology,* 48**,** 235-240.

SANDELIN, A., ALKEMA, W., ENGSTRÖM, P., WASSERMAN, W. W. & LENHARD, B. 2004. JASPAR: an open-access database for eukaryotic transcription factor binding profiles. *Nucleic Acids Res,* 32**,** D91-4.

SANDKÜHLER, J. 2009. Models and mechanisms of hyperalgesia and allodynia. *Physiol Rev,* 89**,** 707-58.

SANDO, R., 3RD, GOUNKO, N., PIERAUT, S., LIAO, L., YATES, J., 3RD & MAXIMOV, A. 2012. HDAC4 governs a transcriptional program essential for synaptic plasticity and memory. *Cell,* 151**,** 821-34.

SANMIGUEL, J. M. & BARTOLOMEI, M. S. 2018. DNA methylation dynamics of genomic imprinting in mouse development. *Biology of reproduction,* 99**,** 252-262.

SAUNDERS, A., MACOSKO, E. Z., WYSOKER, A., GOLDMAN, M., KRIENEN, F. M., DE RIVERA, H., BIEN, E., BAUM, M., BORTOLIN, L., WANG, S., GOEVA, A., NEMESH, J., KAMITAKI, N., BRUMBAUGH, S., KULP, D. & MCCARROLL, S. A. 2018a. Molecular Diversity and Specializations among the Cells of the Adult Mouse Brain. *Cell,* 174**,** 1015-1030.e16.

SAUNDERS, J., HORE, Z., GENTRY, C., MCMAHON, S. & DENK, F. 2018b. Negative Evidence for a Functional Role of Neuronal DNMT3a in Persistent Pain. *Front Mol Neurosci,* 11**,** 332.

SAUVANT, C., HOLZINGER, H. & GEKLE, M. 2006. Prostaglandin E2 Inhibits Its Own Renal Transport by Downregulation of Organic Anion Transporters rOAT1 and rOAT3. *Journal of the American Society of Nephrology,* 17**,** 46.

SCHINDELIN, J., ARGANDA-CARRERAS, I., FRISE, E., KAYNIG, V., LONGAIR, M., PIETZSCH, T., PREIBISCH, S., RUEDEN, C., SAALFELD, S., SCHMID, B., TINEVEZ, J. Y., WHITE, D. J., HARTENSTEIN, V., ELICEIRI, K., TOMANCAK, P. & CARDONA, A. 2012. Fiji: an open-source platform for biological-image analysis. *Nat Methods,* 9**,** 676-82.

SCHLUMM, F., MAUCERI, D., FREITAG, H. E. & BADING, H. 2013. Nuclear calcium signaling regulates nuclear export of a subset of class IIa histone deacetylases following synaptic activity. *J Biol Chem,* 288**,** 8074-84.

SCHLÜTER, A., AKSAN, B., DIEM, R., FAIRLESS, R. & MAUCERI, D. 2020. VEGFD Protects Retinal Ganglion Cells and, consequently, Capillaries against Excitotoxic Injury. *Mol Ther Methods Clin Dev,* 17**,** 281-299.

SCHLÜTER, A., AKSAN, B., FIORAVANTI, R., VALENTE, S., MAI, A. & MAUCERI, D. 2019. Histone Deacetylases Contribute to Excitotoxicity-Triggered Degeneration of Retinal Ganglion Cells In Vivo. *Mol Neurobiol,* 56**,** 8018-8034.

SCHMIDT, R., SCHMELZ, M., FORSTER, C., RINGKAMP, M., TOREBJÖRK, E. & HANDWERKER, H. 1995. Novel classes of responsive and unresponsive C nociceptors in human skin. *J Neurosci,* 15**,** 333-41.

SCHNELL, S. A., STAINES, W. A. & WESSENDORF, M. W. 1999. Reduction of lipofuscin-like autofluorescence in fluorescently labeled tissue. *J Histochem Cytochem,* 47**,** 719-30.

SCHUETZ, A., MIN, J., ALLALI-HASSANI, A., SCHAPIRA, M., SHUEN, M., LOPPNAU, P., MAZITSCHEK, R., KWIATKOWSKI, N. P., LEWIS, T. A., MAGLATHIN, R. L., et al. 2008. Human HDAC7 harbors a class IIa histone

deacetylase-specific zinc binding motif and cryptic deacetylase activity. *The Journal of biological chemistry,* 283**,** 11355-11363.

SCHWALLER, B. 2009. The continuing disappearance of "pure" Ca2+ buffers. *Cell Mol Life Sci,* 66**,** 275-300.

SCHWARCZ, R., BRUNO, J. P., MUCHOWSKI, P. J. & WU, H. Q. 2012. Kynurenines in the mammalian brain: when physiology meets pathology. *Nat Rev Neurosci,* 13**,** 465-77.

SEGAL, M. 2010. Dendritic spines, synaptic plasticity and neuronal survival: activity shapes dendritic spines to enhance neuronal viability. *European Journal of Neuroscience,* 31**,** 2178-2184.

SEGEV, I. & LONDON, M. 2000. Untangling dendrites with quantitative models. *Science,* 290**,** 744-50.

SELLGREN, C. M., GRACIAS, J., JUNGHOLM, O., PERLIS, R. H., ENGBERG, G., SCHWIELER, L., LANDEN, M. & ERHARDT, S. 2019. Peripheral and central levels of kynurenic acid in bipolar disorder subjects and healthy controls. *Translational Psychiatry,* 9**,** 37.

SEMINOWICZ, D. A., LABUS, J. S., BUELLER, J. A., TILLISCH, K., NALIBOFF, B. D., BUSHNELL, M. C. & MAYER, E. A. 2010. Regional gray matter density changes in brains of patients with irritable bowel syndrome. *Gastroenterology,* 139**,** 48-57.e2.

SHAKESPEAR, M. R., HALILI, M. A., IRVINE, K. M., FAIRLIE, D. P. & SWEET, M. J. 2011. Histone deacetylases as regulators of inflammation and immunity. *Trends Immunol,* 32**,** 335-43.

SHAO, C., GAO, Y., JIN, D., XU, X., TAN, S., YU, H., ZHAO, Q., ZHAO, L., WANG, W. & WANG, D. 2017. DNMT3a methylation in neuropathic pain. *J Pain Res,* 10**,** 2253-2262.

SHEN, X., CHEN, J., LI, J., KOFLER, J. & HERRUP, K. 2016. Neurons in Vulnerable Regions of the Alzheimer's Disease Brain Display Reduced ATM Signaling. *eNeuro,* 3.

SHENG, J., LIU, S., WANG, Y., CUI, R. & ZHANG, X. 2017. The Link between Depression and Chronic Pain: Neural Mechanisms in the Brain. *Neural Plast,* 2017**,** 9724371.

SHOLL, D. A. 1953. Dendritic organization in the neurons of the visual and motor cortices of the cat. *J Anat,* 87**,** 387-406.

SILVERMAN, W., LOCOVEI, S. & DAHL, G. 2008. Probenecid, a gout remedy, inhibits pannexin 1 channels. *Am J Physiol Cell Physiol,* 295**,** C761-7.

SILVERMAN, W. R., DE RIVERO VACCARI, J. P., LOCOVEI, S., QIU, F., CARLSSON, S. K., SCEMES, E., KEANE, R. W. & DAHL, G. 2009. The pannexin 1 channel activates the inflammasome in neurons and astrocytes. *J Biol Chem,* 284**,** 18143-51.

SIMONETTI, M., HAGENSTON, A. M., VARDEH, D., FREITAG, H. E., MAUCERI, D., LU, J., SATAGOPAM, V. P., SCHNEIDER, R., COSTIGAN, M., BADING, H. & KUNER, R. 2013. Nuclear calcium signaling in spinal neurons drives a genomic program required for persistent inflammatory pain. *Neuron,* 77**,** 43-57.

SIVILOTTI, L. & WOOLF, C. J. 1994. The contribution of GABAA and glycine receptors to central sensitization: disinhibition and touch-evoked allodynia in the spinal cord. *J Neurophysiol,* 72**,** 169-79.

SKENE, P. J., ILLINGWORTH, R. S., WEBB, S., KERR, A. R., JAMES, K. D., TURNER, D. J., ANDREWS, R. & BIRD, A. P. 2010. Neuronal MeCP2 is

expressed at near histone-octamer levels and globally alters the chromatin state. *Mol Cell,* 37**,** 457-68.

SLIWINSKI, C., NEES, T. A., PUTTAGUNTA, R., WEIDNER, N. & BLESCH, A. 2018. Sensorimotor Activity Partially Ameliorates Pain and Reduces Nociceptive Fiber Density in the Chronically Injured Spinal Cord. *J Neurotrauma,* 35**,** 2222-2238.

SMITH, S. S., KAPLAN, B. E., SOWERS, L. C. & NEWMAN, E. M. 1992. Mechanism of human methyl-directed DNA methyltransferase and the fidelity of cytosine methylation. *Proc Natl Acad Sci U S A,* 89**,** 4744-8.

SNIDER, W. D. & MCMAHON, S. B. 1998. Tackling pain at the source: new ideas about nociceptors. *Neuron,* 20**,** 629-32.

SODERLING, T. R. 1999. The Ca-calmodulin-dependent protein kinase cascade. *Trends Biochem Sci,* 24**,** 232-6.

SOUTH, S. M., KOHNO, T., KASPAR, B. K., HEGARTY, D., VISSEL, B., DRAKE, C. T., OHATA, M., JENAB, S., SAILER, A. W., et al. 2003. A conditional deletion of the NR1 subunit of the NMDA receptor in adult spinal cord dorsal horn reduces NMDA currents and injury-induced pain. *J Neurosci,* 23**,** 5031-40.

STACKER, S. A. & ACHEN, M. G. 2018. Emerging Roles for VEGF-D in Human Disease. *Biomolecules,* 8**,** 1.

STACKER, S. A., CAESAR, C., BALDWIN, M. E., THORNTON, G. E., WILLIAMS, R. A., PREVO, R., JACKSON, D. G., NISHIKAWA, S., KUBO, H. & ACHEN, M. G. 2001. VEGF-D promotes the metastatic spread of tumor cells via the lymphatics. *Nat Med,* 7**,** 186-91.

STACKER, S. A., STENVERS, K., CAESAR, C., VITALI, A., DOMAGALA, T., NICE, E., ROUFAIL, S., SIMPSON, R. J., MORITZ, R., KARPANEN, T., ALITALO, K. & ACHEN, M. G. 1999. Biosynthesis of vascular endothelial growth factor-D involves proteolytic processing which generates non-covalent homodimers. *J Biol Chem,* 274**,** 32127-36.

STAMP, L. K., O'DONNELL, J. L. & CHAPMAN, P. T. 2007. Emerging therapies in the long-term management of hyperuricaemia and gout. *Intern Med J,* 37**,** 258-66.

STEAN, J. P. B. 1974. Some evidence of the nature of the Golgi-Cox deposit and its biochemical origin. *Histochemistry,* 40**,** 377-383.

STEPHENS, B., MUELLER, A. J., SHERING, A. F., HOOD, S. H., TAGGART, P., ARBUTHNOTT, G. W., BELL, J. E., KILFORD, L., KINGSBURY, A. E., DANIEL, S. E. & INGHAM, C. A. 2005. Evidence of a breakdown of corticostriatal connections in Parkinson's disease. *Neuroscience,* 132**,** 741-754.

STÖSSER, S., AGARWAL, N., TAPPE-THEODOR, A., YANAGISAWA, M. & KUNER, R. 2010. Dissecting the functional significance of endothelin A receptors in peripheral nociceptors in vivo via conditional gene deletion. *PAIN,* 148**,** 206-214.

STUART, G. J. & SAKMANN, B. 1994. Active propagation of somatic action potentials into neocortical pyramidal cell dendrites. *Nature,* 367**,** 69-72.

SUETAKE, I., SHINOZAKI, F., MIYAGAWA, J., TAKESHIMA, H. & TAJIMA, S. 2004. DNMT3L stimulates the DNA methylation activity of Dnmt3a and Dnmt3b through a direct interaction. *J Biol Chem,* 279**,** 27816-23.

SUGO, N., OSHIRO, H., TAKEMURA, M., KOBAYASHI, T., KOHNO, Y., UESAKA, N., SONG, W. J. & YAMAMOTO, N. 2010. Nucleocytoplasmic translocation of

HDAC9 regulates gene expression and dendritic growth in developing cortical neurons. *Eur J Neurosci,* 31**,** 1521-32.

SUN, L., ZHAO, J. Y., GU, X., LIANG, L., WU, S., MO, K., FENG, J., GUO, W., ZHANG, J., BEKKER, A., ZHAO, X., NESTLER, E. J. & TAO, Y. X. 2017. Nerve injury-induced epigenetic silencing of opioid receptors controlled by DNMT3a in primary afferent neurons. *Pain,* 158**,** 1153-1165.

SUNG, B., LIM, G. & MAO, J. 2003. Altered expression and uptake activity of spinal glutamate transporters after nerve injury contribute to the pathogenesis of neuropathic pain in rats. *The Journal of neuroscience : the official journal of the Society for Neuroscience,* 23**,** 2899-2910.

SUZUKI, M. M. & BIRD, A. 2008. DNA methylation landscapes: provocative insights from epigenomics. *Nat Rev Genet,* 9**,** 465-76.

SVENSSON, C. I. & YAKSH, T. L. 2002. The spinal phospholipase-cyclooxygenase-prostanoid cascade in nociceptive processing. *Annu Rev Pharmacol Toxicol,* 42**,** 553-83.

SWEATT, J. D. 2013. The emerging field of neuroepigenetics. *Neuron,* 80**,** 624-632.

TAKAHASHI, H. & SHIBUYA, M. 2005. The vascular endothelial growth factor (VEGF)/VEGF receptor system and its role under physiological and pathological conditions. *Clin Sci (Lond),* 109**,** 227-41.

TAKEDA, M., NARIKAWA, S., HOSOYAMADA, M., CHA, S. H., SEKINE, T. & ENDOU, H. 2001. Characterization of organic anion transport inhibitors using cells stably expressing human organic anion transporters. *Eur J Pharmacol,* 419**,** 113-20.

TAN, A. M., STAMBOULIAN, S., CHANG, Y. W., ZHAO, P., HAINS, A. B., WAXMAN, S. G. & HAINS, B. C. 2008. Neuropathic pain memory is maintained by Rac1-regulated dendritic spine remodeling after spinal cord injury. *J Neurosci,* 28**,** 13173-83.

TAPPE-THEODOR, A., AGARWAL, N., KATONA, I., RUBINO, T., MARTINI, L., SWIERCZ, J., MACKIE, K., MONYER, H., PAROLARO, D., WHISTLER, J., KUNER, T. & KUNER, R. 2007. A Molecular Basis of Analgesic Tolerance to Cannabinoids. *The Journal of Neuroscience,* 27**,** 4165-4177.

TAPPE, A., KLUGMANN, M., LUO, C., HIRLINGER, D., AGARWAL, N., BENRATH, J., EHRENGRUBER, M. U., DURING, M. J. & KUNER, R. 2006. Synaptic scaffolding protein Homer1a protects against chronic inflammatory pain. *Nature Medicine,* 12**,** 677-681.

TELANO, L. N. & BAKER, S. 2020. Physiology, Cerebral Spinal Fluid (CSF). *StatPearls.* Treasure Island (FL): StatPearls Publishing. Copyright © 2020, StatPearls Publishing LLC.

THIAGALINGAM, S., CHENG, K. H., LEE, H. J., MINEVA, N., THIAGALINGAM, A. & PONTE, J. F. 2003. Histone deacetylases: unique players in shaping the epigenetic histone code. *Ann N Y Acad Sci,* 983**,** 84-100.

TJOLSEN, A., BERGE, O. G., HUNSKAAR, S., ROSLAND, J. H. & HOLE, K. 1992. The formalin test: an evaluation of the method. *Pain,* 51**,** 5-17.

TODD, A. J. 2010. Neuronal circuitry for pain processing in the dorsal horn. *Nature Reviews Neuroscience,* 11**,** 823-836.

TOGNINI, P., NAPOLI, D. & PIZZORUSSO, T. 2015. Dynamic DNA methylation in the brain: a new epigenetic mark for experience-dependent plasticity. *Frontiers in cellular neuroscience,* 9**,** 331-331.

TRAPNELL, C., PACHTER, L. & SALZBERG, S. L. 2009. TopHat: discovering splice junctions with RNA-Seq. *Bioinformatics,* 25**,** 1105-11.

TRAPNELL, C., WILLIAMS, B. A., PERTEA, G., MORTAZAVI, A., KWAN, G., VAN BAREN, M. J., SALZBERG, S. L., WOLD, B. J. & PACHTER, L. 2010. Transcript assembly and quantification by RNA-Seq reveals unannotated transcripts and isoform switching during cell differentiation. *Nat Biotechnol,* 28**,** 511-5.

TSUDA, M., SHIGEMOTO-MOGAMI, Y., KOIZUMI, S., MIZOKOSHI, A., KOHSAKA, S., SALTER, M. W. & INOUE, K. 2003. P2X4 receptors induced in spinal microglia gate tactile allodynia after nerve injury. *Nature,* 424**,** 778-83.

TUCKER, K. L. 2001. Methylated cytosine and the brain: a new base for neuroscience. *Neuron,* 30**,** 649-52.

UHLÉN, M., FAGERBERG, L., HALLSTRÖM, B. M., LINDSKOG, C., OKSVOLD, P., MARDINOGLU, A., SIVERTSSON, Å., KAMPF, C., SJÖSTEDT, E., ASPLUND, A., et al. 2015. Tissue-based map of the human proteome. *Science,* 347**,** 1260419.

USOSKIN, D., FURLAN, A., ISLAM, S., ABDO, H., LÖNNERBERG, P., LOU, D., HJERLING-LEFFLER, J., HAEGGSTRÖM, J., KHARCHENKO, O., KHARCHENKO, P. V., LINNARSSON, S. & ERNFORS, P. 2015. Unbiased classification of sensory neuron types by large-scale single-cell RNA sequencing. *Nature Neuroscience,* 18**,** 145-153.

VAN AUBEL, R. A., SMEETS, P. H., PETERS, J. G., BINDELS, R. J. & RUSSEL, F. G. 2002. The MRP4/ABCC4 gene encodes a novel apical organic anion transporter in human kidney proximal tubules: putative efflux pump for urinary cAMP and cGMP. *J Am Soc Nephrol,* 13**,** 595-603.

VAN OTTERDIJK, S. D. & MICHELS, K. B. 2016. Transgenerational epigenetic inheritance in mammals: how good is the evidence? *Faseb j,* 30**,** 2457-65.

VARDEH, D., WANG, D., COSTIGAN, M., LAZARUS, M., SAPER, C. B., WOOLF, C. J., FITZGERALD, G. A. & SAMAD, T. A. 2009. COX2 in CNS neural cells mediates mechanical inflammatory pain hypersensitivity in mice. *J Clin Invest,* 119**,** 287-94.

VÉCSEI, L., MILLER, J., MACGARVEY, U. & FLINT BEAL, M. 1992. Kynurenine and probenecid inhibit pentylenetetrazol- and NMDLA-induced seizures and increase kynurenic acid concentrations in the brain. *Brain Research Bulletin,* 28**,** 233-238.

VÉCSEI, L., SZALÁRDY, L., FÜLÖP, F. & TOLDI, J. 2013. Kynurenines in the CNS: recent advances and new questions. *Nat Rev Drug Discov,* 12**,** 64-82.

VEGA, R. B., MATSUDA, K., OH, J., BARBOSA, A. C., YANG, X., MEADOWS, E., MCANALLY, J., POMAJZL, C., SHELTON, J. M., RICHARDSON, J. A., KARSENTY, G. & OLSON, E. N. 2004. Histone deacetylase 4 controls chondrocyte hypertrophy during skeletogenesis. *Cell,* 119**,** 555-66.

VERDIN, E., DEQUIEDT, F. & KASLER, H. G. 2003. Class II histone deacetylases: versatile regulators. *Trends in Genetics,* 19**,** 286-293.

VO, N. & GOODMAN, R. H. 2001. CREB-binding protein and p300 in transcriptional regulation. *J Biol Chem,* 276**,** 13505-8.

WADDINGTON, C. H. 2012. The epigenotype. 1942. *Int J Epidemiol,* 41**,** 10-3.

WANG, A. H. & YANG, X. J. 2001. Histone deacetylase 4 possesses intrinsic nuclear import and export signals. *Mol Cell Biol,* 21**,** 5992-6005.

WANG, J., CAMPOS, B., JAMIESON, G. A., JR., KAETZEL, M. A. & DEDMAN, J. R. 1995. Functional elimination of calmodulin within the nucleus by targeted expression of an inhibitor peptide. *J Biol Chem,* 270**,** 30245-8.

WANG, J., SIMONAVICIUS, N., WU, X., SWAMINATH, G., REAGAN, J., TIAN, H. & LING, L. 2006. Kynurenic acid as a ligand for orphan G protein-coupled receptor GPR35. *J Biol Chem,* 281**,** 22021-8.

WANG, S. E., KO, S. Y., KIM, Y.-S., JO, S., LEE, S. H., JUNG, S. J. & SON, H. 2018. Capsaicin upregulates HDAC2 via TRPV1 and impairs neuronal maturation in mice. *Experimental & Molecular Medicine,* 50**,** e455-e455.

WANG, W. H., CHENG, L. C., PAN, F. Y., XUE, B., WANG, D. Y., CHEN, Z. & LI, C. J. 2011a. Intracellular trafficking of histone deacetylase 4 regulates long-term memory formation. *Anat Rec (Hoboken),* 294**,** 1025-34.

WANG, X., CHEN, W., LIU, W., WU, J., SHAO, Y. & ZHANG, X. 2009. The role of thrombospondin-1 and transforming growth factor-β after spinal cord injury in the rat. *Journal of Clinical Neuroscience,* 16**,** 818-821.

WANG, Y., LIU, C., GUO, Q. L., YAN, J. Q., ZHU, X. Y., HUANG, C. S. & ZOU, W. Y. 2011b. Intrathecal 5-azacytidine inhibits global DNA methylation and methyl-CpG-binding protein 2 expression and alleviates neuropathic pain in rats following chronic constriction injury. *Brain Res,* 1418**,** 64-9.

WANG, Z., QIN, G. & ZHAO, T. C. 2014. HDAC4: mechanism of regulation and biological functions. *Epigenomics,* 6**,** 139-150.

WATSON, C. & KAYALIOGLU, G. 2009. Chapter 1 - The Organization of the Spinal Cord. *In:* WATSON, C., PAXINOS, G. & KAYALIOGLU, G. (eds.) *The Spinal Cord.* San Diego: Academic Press.

WATT, F. & MOLLOY, P. L. 1988. Cytosine methylation prevents binding to DNA of a HeLa cell transcription factor required for optimal expression of the adenovirus major late promoter. *Genes Dev,* 2**,** 1136-43.

WEISLOGEL, J. M., BENGTSON, C. P., MULLER, M. K., HORTZSCH, J. N., BUJARD, M., SCHUSTER, C. M. & BADING, H. 2013. Requirement for nuclear calcium signaling in Drosophila long-term memory. *Sci Signal,* 6**,** ra33.

WESTENBROEK, R. E., AHLIJANIAN, M. K. & CATTERALL, W. A. 1990. Clustering of L-type Ca2+ channels at the base of major dendrites in hippocampal pyramidal neurons. *Nature,* 347**,** 281-4.

WIEGERT, J. S., BENGTSON, C. P. & BADING, H. 2007. Diffusion and not active transport underlies and limits ERK1/2 synapse-to-nucleus signaling in hippocampal neurons. *J Biol Chem,* 282**,** 29621-33.

WILLIAMS, S. R., ALDRED, M. A., DER KALOUSTIAN, V. M., HALAL, F., GOWANS, G., MCLEOD, D. R., ZONDAG, S., TORIELLO, H. V., MAGENIS, R. E. & ELSEA, S. H. 2010. Haploinsufficiency of HDAC4 causes brachydactyly mental retardation syndrome, with brachydactyly type E, developmental delays, and behavioral problems. *Am J Hum Genet,* 87**,** 219-28.

WILLIS, W. D. 2009. The role of TRPV1 receptors in pain evoked by noxious thermal and chemical stimuli. *Experimental Brain Research,* 196**,** 5-11.

WOLFFE, A. P. & GUSCHIN, D. 2000. Review: chromatin structural features and targets that regulate transcription. *J Struct Biol,* 129**,** 102-22.

WOOLF, C. J. 1983. Evidence for a central component of post-injury pain hypersensitivity. *Nature,* 306**,** 686-8.

WOOLF, C. J. & MA, Q. 2007. Nociceptors--noxious stimulus detectors. *Neuron,* 55**,** 353-64.

WOOLF, C. J. & SALTER, M. W. 2000. Neuronal plasticity: increasing the gain in pain. *Science,* 288**,** 1765-9.

WU, Q., YANG, X., ZHANG, L., ZHANG, Y. & FENG, L. 2016. Nuclear Accumulation of Histone Deacetylase 4 (HDAC4) Exerts Neurotoxicity in Models of Parkinson's Disease. *Mol Neurobiol*.

WU, S., BONO, J. & TAO, Y.-X. 2019. Long noncoding RNA (lncRNA): a target in neuropathic pain. *Expert opinion on therapeutic targets,* 23**,** 15-20.

YAKSH, T. L. 1989. Behavioral and autonomic correlates of the tactile evoked allodynia produced by spinal glycine inhibition: effects of modulatory receptor systems and excitatory amino acid antagonists. *Pain,* 37**,** 111-23.

YAMAZAKI, Y. & MORITA, T. 2006. Molecular and functional diversity of vascular endothelial growth factors. *Mol Divers,* 10**,** 515-27.

YAP, E. L. & GREENBERG, M. E. 2018. Activity-Regulated Transcription: Bridging the Gap between Neural Activity and Behavior. *Neuron,* 100**,** 330-348.

YOU, A., TONG, J. K., GROZINGER, C. M. & SCHREIBER, S. L. 2001. CoREST is an integral component of the CoREST- human histone deacetylase complex. *Proceedings of the National Academy of Sciences,* 98**,** 1454.

YOUN, H. D., GROZINGER, C. M. & LIU, J. O. 2000. Calcium regulates transcriptional repression of myocyte enhancer factor 2 by histone deacetylase 4. *J Biol Chem,* 275**,** 22563-7.

YUAN, H., DENTON, K., LIU, L., LI, X. J., BENASHSKI, S., MCCULLOUGH, L. & LI, J. 2016. Nuclear translocation of histone deacetylase 4 induces neuronal death in stroke. *Neurobiol Dis,* 91**,** 182-93.

ZARGHI, A. & ARFAEI, S. 2011. Selective COX-2 Inhibitors: A Review of Their Structure-Activity Relationships. *Iranian journal of pharmaceutical research : IJPR,* 10**,** 655-683.

ZEISEL, A., HOCHGERNER, H., LÖNNERBERG, P., JOHNSSON, A., MEMIC, F., VAN DER ZWAN, J., HÄRING, M., BRAUN, E., BORM, L. E., LA MANNO, G., et al. 2018. Molecular Architecture of the Mouse Nervous System. *Cell,* 174**,** 999-1014.e22.

ZHANG, C. L., MCKINSEY, T. A., LU, J. R. & OLSON, E. N. 2001. Association of COOH-terminal-binding protein (CtBP) and MEF2-interacting transcription repressor (MITR) contributes to transcriptional repression of the MEF2 transcription factor. *J Biol Chem,* 276**,** 35-9.

ZHANG, C. L., MCKINSEY, T. A. & OLSON, E. N. 2002. Association of class II histone deacetylases with heterochromatin protein 1: potential role for histone methylation in control of muscle differentiation. *Molecular and cellular biology,* 22**,** 7302-7312.

ZHANG, L. I. & POO, M. M. 2001. Electrical activity and development of neural circuits. *Nat Neurosci,* 4 Suppl**,** 1207-14.

ZHANG, S. J., BUCHTHAL, B., LAU, D., HAYER, S., DICK, O., SCHWANINGER, M., VELTKAMP, R., ZOU, M., WEISS, U. & BADING, H. 2011a. A signaling cascade of nuclear calcium-CREB-ATF3 activated by synaptic NMDA receptors defines a gene repression module that protects against extrasynaptic NMDA receptor-induced neuronal cell death and ischemic brain damage. *J Neurosci,* 31**,** 4978-90.

ZHANG, S. J., STEIJAERT, M. N., LAU, D., SCHUTZ, G., DELUCINGE-VIVIER, C., DESCOMBES, P. & BADING, H. 2007. Decoding NMDA receptor signaling: identification of genomic programs specifying neuronal survival and death. *Neuron,* 53**,** 549-62.

ZHANG, S. J., ZOU, M., LU, L., LAU, D., DITZEL, D. A., DELUCINGE-VIVIER, C., ASO, Y., DESCOMBES, P. & BADING, H. 2009. Nuclear calcium signaling

controls expression of a large gene pool: identification of a gene program for acquired neuroprotection induced by synaptic activity. *PLoS Genet,* 5**,** e1000604.

ZHANG, Z., CAI, Y. Q., ZOU, F., BIE, B. & PAN, Z. Z. 2011b. Epigenetic suppression of GAD65 expression mediates persistent pain. *Nat Med,* 17**,** 1448-55.

ZHAO, X., ITO, A., KANE, C. D., LIAO, T. S., BOLGER, T. A., LEMROW, S. M., MEANS, A. R. & YAO, T. P. 2001. The modular nature of histone deacetylase HDAC4 confers phosphorylation-dependent intracellular trafficking. *J Biol Chem,* 276**,** 35042-8.

ZHOU, C., WU, Y., DING, X., SHI, N., CAI, Y. & PAN, Z. Z. 2020. SIRT1 Decreases Emotional Pain Vulnerability with Associated CaMKIIα Deacetylation in Central Amygdala. *The Journal of Neuroscience,* 40**,** 2332-2342.

ZHOU, X., RICHON, V. M., WANG, A. H., YANG, X. J., RIFKIND, R. A. & MARKS, P. A. 2000. Histone deacetylase 4 associates with extracellular signal-regulated kinases 1 and 2, and its cellular localization is regulated by oncogenic Ras. *Proc Natl Acad Sci U S A,* 97**,** 14329-33.

ZHU, Y., HUANG, M., BUSHONG, E., PHAN, S., UYTIEPO, M., BEUTTER, E., BOEMER, D., TSUI, K., ELLISMAN, M. & MAXIMOV, A. 2019. Class IIa HDACs regulate learning and memory through dynamic experience-dependent repression of transcription. *Nature Communications,* 10**,** 3469.

ZIMMERMANN, K., LEFFLER, A., BABES, A., CENDAN, C. M., CARR, R. W., KOBAYASHI, J., NAU, C., WOOD, J. N. & REEH, P. W. 2007. Sensory neuron sodium channel Nav1.8 is essential for pain at low temperatures. *Nature,* 447**,** 855-8.

ZLATANOVA, J., LEUBA, S. H. & VAN HOLDE, K. 1998. Chromatin Fiber Structure: Morphology, Molecular Determinants, Structural Transitions. *Biophysical Journal,* 74**,** 2554-2566.

ZOIDL, G., PETRASCH-PARWEZ, E., RAY, A., MEIER, C., BUNSE, S., HABBES, H. W., DAHL, G. & DERMIETZEL, R. 2007. Localization of the pannexin1 protein at postsynaptic sites in the cerebral cortex and hippocampus. *Neuroscience,* 146**,** 9-16.

ZOVKIC, I. B., GUZMAN-KARLSSON, M. C. & SWEATT, J. D. 2013. Epigenetic regulation of memory formation and maintenance. *Learn Mem,* 20**,** 61-74.

Appendix

Table 11: Up-regulated DEGs in inflammatory pain by FC (Lacz-Sal/CFA)

RefSeq ID	Gene symbol	Full gene name	Log2 fold change	FDR adjusted p-value
NM_026862	Cd177	CD177 antigen	4.54	1.51E-02
NM_018857*	Msln	mesothelin	4.29	1.51E-02
NM_008766*	Slc22a6	solute carrier family 22 (organic anion transporter), member 6	4.13	1.51E-02
NM_010369	Gypa	glycophorin A	3.71	1.51E-02
NM_008694	Ngp	neutrophilic granule protein	3.56	1.51E-02
NM_001281852	S100a9	S100 calcium binding protein A9 (calgranulin B)	3.41	1.51E-02
NM_013650	S100a8	S100 calcium binding protein A8 (calgranulin A)	3.38	1.51E-02
NM_017370	Hp	haptoglobin	3.28	1.51E-02
NM_028770	Krt80	keratin 80	3.26	1.51E-02
NM_009921	Camp	cathelicidin antimicrobial peptide	3.15	1.51E-02
NM_008491	Lcn2	lipocalin 2	3.07	1.51E-02
NM_009264	Sprr1a	small proline-rich protein 1A	3.03	1.51E-02
NM_145947*	Slc26a7	solute carrier family 26, member 7	2.98	1.51E-02
NM_008522	Ltf	lactotransferrin	2.95	1.51E-02
NM_008685	Nfe2	nuclear factor, erythroid derived 2	2.95	3.79E-02
NM_001033281*	Prdm6	PR domain containing 6	2.78	1.51E-02
NM_011403	Slc4a1	solute carrier family 4 (anion exchanger), member 1	2.75	1.51E-02
NM_011410	Slfn4	schlafen 4	2.71	1.51E-02
NM_009892	Chil3	chitinase-like 3	2.65	1.51E-02
NM_008611	Mmp8	matrix metallopeptidase 8	2.62	1.51E-02
NM_008599	Cxcl9	chemokine (C-X-C motif) ligand 9	2.61	1.51E-02
NM_181596	Retnlg	resistin like gamma	2.43	1.51E-02
NM_001099217	Ly6c2	lymphocyte antigen 6 complex, locus C2	2.29	4.63E-02
NM_029796*	Lrg1	leucine-rich alpha-2-glycoprotein 1	2.17	1.51E-02
NM_026743*	Tspan11	tetraspanin 11	2.08	1.51E-02
NM_001080971	Tubb1	tubulin, beta 1 class VI	2.07	2.64E-02
NM_007759	Crabp2	cellular retinoic acid binding protein II	1.92	1.51E-02
NM_023785	Ppbp	pro-platelet basic protein	1.89	1.51E-02
NM_007655	Cd79a	CD79A antigen (immunoglobulin-associated alpha)	1.82	1.51E-02
NM_007876	Dpep1	dipeptidase 1	1.74	1.51E-02
NM_010855	Myh4	myosin, heavy polypeptide 4, skeletal muscle	1.67	1.51E-02
NR_130974*	H19	H19, imprinted maternally expressed transcript	1.53	1.51E-02
NM_010730	Anxa1	annexin A1	1.42	1.51E-02
NM_025806	Plbd1	phospholipase B domain containing 1	1.39	1.51E-02
NM_007962	Mpzl2	myelin protein zero-like 2	1.39	1.51E-02
NM_008339	Cd79b	CD79B antigen	1.35	4.63E-02
NM_010545	Cd74	CD74 antigen	1.29	1.51E-02
NM_001081117	Mki67	antigen identified by monoclonal antibody Ki 67	1.27	1.51E-02
NM_010930*	Nov	nephroblastoma overexpressed gene	1.25	1.51E-02
NM_013519	Foxc2	forkhead box C2	1.23	1.51E-02

NM_010382	H2-Eb1	histocompatibility 2, class II antigen E beta	1.20	1.51E-02
NM_011859	Osr1	odd-skipped related transcription factor 1	1.19	1.51E-02
NM_009606*	Acta1	actin, alpha 1, skeletal muscle	1.18	1.51E-02
NM_010378	H2-Aa	histocompatibility 2, class II antigen A, alpha	1.18	1.51E-02
NM_207105	H2-Ab1	histocompatibility 2, class II antigen A, beta 1	1.18	1.51E-02
NM_001253874	Itgal	integrin alpha L	1.17	2.64E-02
NM_008489	Lbp	lipopolysaccharide binding protein	1.16	1.51E-02
NM_008009	Fgfbp1	fibroblast growth factor binding protein 1	1.15	1.51E-02
NM_008147	Lilrb4a/b	leukocyte immunoglobulin-like receptor, subfamily B, member 4B	1.13	4.63E-02
NM_172479	Slc38a5	solute carrier family 38, member 5	1.09	1.51E-02
NM_001313914*	Thbs1	thrombospondin 1	1.08	1.51E-02
NM_198024	Ranbp3l	RAN binding protein 3-like	1.07	1.51E-02
NM_001033374	Gm694	steroid receptor associated and regulated protein	1.05	4.63E-02
NM_008963	Ptgds	prostaglandin D2 synthase (brain)	1.04	1.51E-02
NM_198095	Bst2	bone marrow stromal cell antigen 2	1.01	1.51E-02
NM_001177954	Rpgr	retinitis pigmentosa GTPase regulator	1.00	2.64E-02
NM_011255	Rbp4	retinol binding protein 4, plasma	0.99	1.51E-02
NM_001286502	Pdyn	prodynorphin	0.98	1.51E-02
NM_013706	Cd52	CD52 antigen	0.96	3.79E-02
NM_001145799	Ctla2a	cytotoxic T lymphocyte-associated protein 2 alpha	0.96	1.51E-02
NM_001276413	Fn1	fibronectin 1	0.96	1.51E-02
NM_172892	Slc13a4	solute carrier family 13 (sodium/sulfate symporters), member 4	0.94	1.51E-02
NM_008597*	Mgp	matrix Gla protein	0.93	1.51E-02
NM_010582	Itih2	inter-alpha trypsin inhibitor, heavy chain 2	0.92	2.64E-02
NM_009526	Wnt6	wingless-type MMTV integration site family, member 6	0.91	1.51E-02
NM_008344	Igfbp6	insulin-like growth factor binding protein 6	0.91	1.51E-02
NM_009008	Rac2	Rac family small GTPase 2	0.91	1.51E-02
NM_001143689	H2-Q4	histocompatibility 2, Q region locus 4	0.89	1.51E-02
NM_010728	Lox	lysyl oxidase	0.88	1.51E-02
NM_001201391	Hbb-bs	hemoglobin, beta adult s chain	0.88	1.51E-02
NM_139142	Slc6a20a	solute carrier family 6 (neurotransmitter transporter), member 20A	0.87	1.51E-02
NM_010260	Gbp2	guanylate binding protein 2	0.86	1.51E-02
NM_153170	Slc36a2	solute carrier family 36 (proton/amino acid symporter), member 2	0.85	1.51E-02
NM_008036	Fosb	FBJ osteosarcoma oncogene B	0.85	4.63E-02
NM_009378	Thbd	thrombomodulin	0.83	1.51E-02
NM_016907	Spint1	serine protease inhibitor, Kunitz type 1	0.82	3.79E-02
NM_007486	Arhgdib	Rho, GDP dissociation inhibitor (GDI) beta	0.82	2.64E-02
NM_001168318	Scara5	scavenger receptor class A, member 5	0.81	1.51E-02
NM_011355	Spi1	spleen focus forming virus (SFFV) proviral integration oncogene	0.81	4.63E-02
NM_011708	Vwf	Von Willebrand factor	0.77	1.51E-02
NM_009864	Cdh1	cadherin 1	0.76	1.51E-02
NM_010118	Egr2	early growth response 2	0.74	1.51E-02
NM_019412*	Prx	periaxin	0.72	1.51E-02
NM_148927	Plekha4	pleckstrin homology domain containing, family A, member 4	0.71	1.51E-02
NM_172604	Scara3	scavenger receptor class A, member 3	0.70	2.64E-02
NM_001013741	Ddn	dendrin	0.70	1.51E-02

NM_007857	Dhh	desert hedgehog	0.68	1.51E-02
NM_027957	Fam178b	family with sequence similarity 178, member B	0.67	1.51E-02
NM_001001892	H2-K1	histocompatibility 2, K1, K region	0.67	1.51E-02
NM_015776	Mfap5	microfibrillar associated protein 5	0.67	1.51E-02
NM_001291539	Sema3b	semaphorin 3B	0.66	1.51E-02
NM_012043	Islr	immunoglobulin superfamily containing leucine-rich repeat	0.64	2.64E-02
NM_009369	Tgfbi	transforming growth factor, beta induced	0.63	1.51E-02
NM_008623*	Mpz	myelin protein zero	0.63	1.51E-02
NM_010078	Drp2	dystrophin related protein 2	0.63	1.51E-02
NM_007557	Bmp7	bone morphogenetic protein 7	0.63	1.51E-02
NM_007742	Col1a1	collagen, type I, alpha 1	0.63	1.51E-02
NM_008885	Pmp22	peripheral myelin protein 22	0.59	1.51E-02
NM_153105	Cldn19	claudin 19	0.59	2.64E-02
NM_010380	H2-D1	histocompatibility 2, D region locus 1	0.59	1.51E-02
NM_080553	Itpr3	inositol 1,4,5-triphosphate receptor 3	0.54	1.51E-02
NM_008760	Ogn	osteoglycin	0.53	2.64E-02
NM_027907	Etnppl	ethanolamine phosphate phospholyase	0.51	4.63E-02
NM_008305	Hspg2	perlecan (heparan sulfate proteoglycan 2)	0.50	4.63E-02

* less induced or down-regulated in HDAC4-3SA expressing mice

Table 12: Down-regulated DEGs in inflammatory pain by FC (LacZ-Sal/CFA)

RefSeq ID	Gene symbol	Full gene name	Log2 fold change	FDR adjusted p-value
NM_028735	Ttc21a	tetratricopeptide repeat domain 21A	-0.95	2.64E-02
NM_001081369	Ccdc153	coiled-coil domain containing 153	-1.21	1.51E-02
NM_030187	Ak7	adenylate kinase 7	-1.21	1.51E-02
NM_001163638	Cfap70	cilia and flagella associated protein 70	-1.33	4.63E-02
NM_177922	Mapk15	mitogen-activated protein kinase 15	-1.44	1.51E-02
NM_177629	Fam216b	family with sequence similarity 216, member B	-1.50	1.51E-02
NM_001164669	Dnah6	dynein, axonemal, heavy chain 6	-1.54	1.51E-02
NM_198660	Ccdc180	coiled-coil domain containing 180	-1.59	4.63E-02
NM_029122	Iqca	IQ motif containing with AAA domain	-1.70	1.51E-02

Table 13: Up-regulated DEGs in inflammatory pain by FC (4wt-Sal/CFA)

RefSeq ID	Gene symbol	Full gene name	Log2 fold change	FDR adjusted p-value
NM_026183	Slc47a1	solute carrier family 47, member 1	4.99	1.26E-02
NM_001168680	Tspan8	tetraspanin 8	3.87	1.26E-02
NM_016685	Comp	cartilage oligomeric matrix protein	3.79	1.26E-02
NM_145947	Slc26a7	solute carrier family 26, member 7	3.21	1.26E-02
NM_018857	Msln	mesothelin	3.01	1.26E-02
NM_008766	Slc22a6	solute carrier family 22 (organic anion transporter), member 6	2.68	1.26E-02
NR_130974	H19	H19, imprinted maternally expressed transcript	2.50	1.26E-02

NM_029796	Lrg1	leucine-rich alpha-2-glycoprotein 1	2.02	1.26E-02
NM_170727	Scgb3a1	secretoglobin, family 3A, member 1	1.99	3.47E-02
NM_009854	Cd7	CD7 antigen	1.78	1.26E-02
NM_026743	Tspan11	tetraspanin 11	1.77	1.26E-02
NM_008491	Lcn2	lipocalin 2	1.66	1.26E-02
NM_011910	Uts2	urotensin 2	1.44	1.26E-02
NM_021712	Slc18a3	solute carrier family 18 (vesicular monoamine), member 3	1.36	1.26E-02
NM_001313914	Thbs1	thrombospondin 1	1.36	1.26E-02
NM_013639	Prph	peripherin	1.31	1.26E-02
NM_029568	Mfap4	microfibrillar-associated protein 4	1.26	1.26E-02
NM_173403	Slc10a4	solute carrier family 10 (sodium/bile acid cotransporter family), member 4	1.25	1.26E-02
NM_009504	Vdr	vitamin D (1,25-dihydroxyvitamin D3) receptor	1.24	2.45E-02
NM_009264	Sprr1a	small proline-rich protein 1A	1.12	4.53E-02
NM_139134	Chodl	chondrolectin	1.11	1.26E-02
NM_145963	Kcnj14	potassium inwardly-rectifying channel, subfamily J, member 14	1.09	1.26E-02
NM_008489	Lbp	lipopolysaccharide binding protein	1.08	1.26E-02
NM_022025	Slc5a7	solute carrier family 5 (choline transporter), member 7	1.05	1.26E-02
NM_008597	Mgp	matrix Gla protein	1.00	1.26E-02
NM_010846	Mx1	MX dynamin-like GTPase 1	0.95	1.26E-02
NM_013653	Ccl5	chemokine (C-C motif) ligand 5	0.84	1.26E-02
NM_010930	Nov	nephroblastoma overexpressed gene	0.81	3.47E-02
NM_021487	Kcne1l	potassium voltage-gated channel, Isk-related family, member 1-like	0.81	1.26E-02
NM_013560	Hspb1	heat shock protein 1	0.80	1.26E-02
NM_001276413	Fn1	fibronectin 1	0.78	1.26E-02
NM_001289444	Calca	calcitonin/calcitonin-related polypeptide, alpha	0.76	4.53E-02
NM_001161845	Sgk1	serum/glucocorticoid regulated kinase 1	0.74	1.26E-02
NM_021384	Rsad2	radical S-adenosyl methionine domain containing 2	0.73	2.45E-02
NM_011426	Siglec1	sialic acid binding Ig-like lectin 1, sialoadhesin	0.73	1.26E-02
NM_146007	Col6a2	collagen, type VI, alpha 2	0.73	3.47E-02
NM_025734	Kcng4	potassium voltage-gated channel, subfamily G, member 4	0.69	1.26E-02
NM_011708	Vwf	Von Willebrand factor	0.69	1.26E-02
NM_001252601	Irf7	interferon regulatory factor 7	0.67	1.26E-02
NM_010904	Nefh	neurofilament, heavy polypeptide	0.67	1.26E-02
NM_053110	Gpnmb	glycoprotein (transmembrane) nmb	0.64	1.26E-02
NM_009778	C3	complement component 3	0.62	1.26E-02
NM_013723	Podxl	podocalyxin-like	0.59	1.26E-02
NM_009252	Serpina3n	serine (or cysteine) peptidase inhibitor, clade A, member 3N	0.56	1.26E-02
NM_008630	Mt2	metallothionein 2	0.55	2.45E-02
NM_011854	Oasl2	2'-5' oligoadenylate synthetase-like 2	0.52	4.53E-02
NM_013602	Mt1	metallothionein 1	0.52	1.26E-02

Table 14: Down-regulated DEGs in inflammatory pain by FC (4wt-Sal/CFA)

RefSeq ID	Gene symbol	Full gene name	Log2 fold change	FDR adjusted p-value
NM_008694	Ngp	neutrophilic granule protein	-1.24	3.47E-02
NM_009606	Acta1	actin, alpha 1, skeletal muscle	-1.95	1.26E-02
NM_001013767	Capn11	calpain 11	-2.07	1.26E-02
NM_001163669	Tnnt3	troponin T3, skeletal, fast	-2.56	1.26E-02
NM_013697	Ttr	transthyretin	-4.67	1.26E-02

Table 15: Up-regulated DEGs in inflammatory pain by FC (3SA-Sal/CFA)

RefSeq ID	Gene symbol	Full gene name	Log2 fold change	FDR adjusted p-value
NM_009690	Cd5l	CD5 antigen-like	2.50	1.47E-02
NM_009608	Actc1	actin, alpha, cardiac muscle 1	2.46	2.79E-02
NM_053188	Srd5a2	steroid 5 alpha-reductase 2	2.20	8.50E-03
NM_011315	Saa3	serum amyloid A 3	2.09	2.79E-02
NM_134160	Mcoln3	mucolipin 3	2.04	8.50E-03
NM_001199940	Serpina3i	serine (or cysteine) peptidase inhibitor, clade A, member 3l	1.98	2.79E-02
NM_011910	Uts2	urotensin 2	1.96	8.50E-03
NM_175406	Atp6v0d2	ATPase, H+ transporting, lysosomal V0 subunit D2	1.87	8.50E-03
NM_019944	Mnx1	motor neuron and pancreas homeobox 1	1.86	8.50E-03
NM_011426	Siglec1	sialic acid binding Ig-like lectin 1, sialoadhesin	1.85	8.50E-03
NM_145226	Oas3	2'-5' oligoadenylate synthetase 3	1.76	8.50E-03
NM_018729	Cd244	CD244 molecule A	1.72	3.13E-02
NM_207244	Cd200r4	CD200 receptor 4	1.65	8.50E-03
NM_024406	Fabp4	fatty acid binding protein 4, adipocyte	1.65	3.54E-02
NM_008491	Lcn2	lipocalin 2	1.63	8.50E-03
NM_001310331	Ms4a4a	membrane-spanning 4-domains, subfamily A, member 4A	1.62	8.50E-03
NM_010819	Clec4d	C-type lectin domain family 4, member d	1.56	3.54E-02
NM_001164327	Phf11b	PHD finger protein 11B	1.55	8.50E-03
NM_008486	Anpep	alanyl (membrane) aminopeptidase	1.53	8.50E-03
NM_011407	Slfn1	schlafen 1	1.53	8.50E-03
NM_029796	Lrg1	leucine-rich alpha-2-glycoprotein 1	1.52	8.50E-03
NM_152803	Hpse	heparanase	1.50	8.50E-03
NM_001277944	Apoc2	apolipoprotein C-II	1.49	3.13E-02
NM_145209	Oasl1	2'-5' oligoadenylate synthetase-like 1	1.49	8.50E-03
NM_013639	Prph	peripherin	1.48	8.50E-03
NM_008372	Il7r	interleukin 7 receptor	1.48	1.47E-02
NM_009977	Cst7	cystatin F (leukocystatin)	1.47	8.50E-03
NM_001204203	Spp1	secreted phosphoprotein 1	1.44	8.50E-03
NM_001165932	Ucma	upper zone of growth plate and cartilage matrix associated	1.44	1.47E-02
NM_144955	Nkx6-1	NK6 homeobox 1	1.43	8.50E-03
NM_145227	Oas2	2'-5' oligoadenylate synthetase 2	1.43	8.50E-03
NM_009890	Ch25h	cholesterol 25-hydroxylase	1.43	1.47E-02

NM_001177350	Pydc4	interferon activated gene 213	1.42	2.79E-02
NM_001081957	Wfdc17	WAP four-disulfide core domain 17	1.41	4.55E-02
NM_001113326	Msr1	macrophage scavenger receptor 1	1.39	8.50E-03
NM_010705	Lgals3	lectin, galactose binding, soluble 3	1.38	8.50E-03
NM_027397	Isl2	insulin related protein 2 (islet 2)	1.38	3.91E-02
NM_001204910	AI607873	interferon activated gene 207	1.37	8.50E-03
NM_001004174	AA467197	expressed sequence AA467197	1.37	1.96E-02
NM_017372	Lyz2	lysozyme 2	1.36	8.50E-03
NM_021384	Rsad2	radical S-adenosyl methionine domain containing 2	1.36	8.50E-03
NM_001024230	Gm5431	predicted gene 5431	1.34	4.55E-02
NM_011819	Gdf15	growth differentiation factor 15	1.34	1.96E-02
NR_110993	Cd68	CD68 antigen	1.32	8.50E-03
NM_009891	Chat	choline acetyltransferase	1.31	3.91E-02
NM_010846	Mx1	MX dynamin-like GTPase 1	1.31	8.50E-03
NM_008147	Lilr4b, Lilrb4a	leukocyte immunoglobulin-like receptor, subfamily B, member 4B	1.31	8.50E-03
NM_029499	Ms4a4c	membrane-spanning 4-domains, subfamily A, member 4C	1.31	8.50E-03
NM_001276398	Ms4a7	membrane-spanning 4-domains, subfamily A, member 7	1.30	1.47E-02
NM_009264	Sprr1a	small proline-rich protein 1A	1.30	4.94E-02
NM_175026	Pyhin1	interferon activated gene 209	1.29	8.50E-03
NM_018866	Cxcl13	chemokine (C-X-C motif) ligand 13	1.29	8.50E-03
NM_021394	Zbp1	Z-DNA binding protein 1	1.29	1.96E-02
NM_145211	Oas1a	2'-5' oligoadenylate synthetase 1A	1.28	8.50E-03
NM_021718	Ms4a4b	membrane-spanning 4-domains, subfamily A, member 4B	1.27	1.96E-02
NM_021712	Slc18a3	solute carrier family 18 (vesicular monoamine), member 3	1.26	1.96E-02
NM_001252601	Irf7	interferon regulatory factor 7	1.23	8.50E-03
NM_001163256	Fblim1	filamin binding LIM protein 1	1.23	8.50E-03
NM_026835	Ms4a6d	membrane-spanning 4-domains, subfamily A, member 6D	1.22	8.50E-03
NM_007807	Cybb	cytochrome b-245, beta polypeptide	1.21	8.50E-03
NM_030707	Fcrls	Fc receptor-like S, scavenger receptor	1.21	8.50E-03
NM_144830	Tmem106a	transmembrane protein 106A	1.20	8.50E-03
NM_009403	Tnfsf8	tumor necrosis factor (ligand) superfamily, member 8	1.19	3.13E-02
NM_008873	Plau	plasminogen activator, urokinase	1.19	8.50E-03
NM_010821	Mpeg1	macrophage expressed gene 1	1.19	8.50E-03
NM_026829	Mthfs	5, 10-methenyltetrahydrofolate synthetase	1.18	2.44E-02
NM_009635	Avil	advillin	1.18	4.26E-02
NM_177337	Arl11	ADP-ribosylation factor-like 11	1.18	2.44E-02
NM_001167743	Slfn8	schlafen 8	1.17	8.50E-03
NM_001276413	Fn1	fibronectin 1	1.17	8.50E-03
NM_009845	Cd22	CD22 antigen	1.17	1.96E-02
NM_008329	Ifi204	interferon activated gene 204	1.16	1.47E-02
NM_153098	Cd109	CD109 antigen	1.16	8.50E-03
NM_001291066	Adam8	a disintegrin and metallopeptidase domain 8	1.16	2.79E-02
NM_001286610	Arhgap25	Rho GTPase activating protein 25	1.15	8.50E-03
NM_021334	Itgax	integrin alpha X	1.15	8.50E-03
NM_170758	Cd300a	CD300A molecule	1.15	2.44E-02
NM_001038654	Slc16a3	solute carrier family 16 (monocarboxylic acid transporters), member 3	1.15	2.44E-02

NM_011662	Tyrobp	TYRO protein tyrosine kinase binding protein	1.15	8.50E-03
NM_011198	Ptgs2	prostaglandin-endoperoxide synthase 2	1.14	4.26E-02
NM_010871	Naip6	NLR family, apoptosis inhibitory protein 6	1.14	3.91E-02
NR_003508	Mx2	MX dynamin-like GTPase 2	1.14	3.13E-02
NM_011408	Slfn2	schlafen 2	1.13	8.50E-03
NM_007781	Csf2rb2	colony stimulating factor 2 receptor, beta 2	1.13	1.96E-02
NM_172796	Slfn9	schlafen 9	1.13	1.47E-02
NM_001302650	Ifi203	interferon activated gene 203	1.12	1.96E-02
NM_008489	Lbp	lipopolysaccharide binding protein	1.12	3.13E-02
NM_031254	Trem2	triggering receptor expressed on myeloid cells 2	1.11	8.50E-03
NM_206536	AB124611	cDNA sequence AB124611	1.11	4.55E-02
NM_010186	Fcgr1	Fc receptor, IgG, high affinity I	1.10	8.50E-03
NM_008404	Itgb2	integrin beta 2	1.10	8.50E-03
NM_031159	Apobec1	apolipoprotein B mRNA editing enzyme, catalytic polypeptide 1	1.10	1.47E-02
NM_008533	Cd180	CD180 antigen	1.10	8.50E-03
NM_013560	Hspb1	heat shock protein 1	1.10	8.50E-03
NM_001290758	Tlr7	toll-like receptor 7	1.10	8.50E-03
NM_008369	Il3ra	interleukin 3 receptor, alpha chain	1.10	4.26E-02
NM_011909	Usp18	ubiquitin specific peptidase 18	1.10	8.50E-03
NM_013653	Ccl5	chemokine (C-C motif) ligand 5	1.10	3.13E-02
NM_031376	Pik3ap1	phosphoinositide-3-kinase adaptor protein 1	1.10	8.50E-03
NM_013489	Cd84	CD84 antigen	1.09	8.50E-03
NM_010501	Ifit3	interferon-induced protein with tetratricopeptide repeats 3	1.08	8.50E-03
NM_009099	Trim30a	tripartite motif-containing 30A	1.08	8.50E-03
NM_001277968	Ly9	lymphocyte antigen 9	1.08	8.50E-03
NM_023380	Samsn1	SAM domain, SH3 domain and nuclear localization signals, 1	1.08	3.13E-02
NM_173403	Slc10a4	solute carrier family 10 (sodium/bile acid cotransporter family), member 4	1.08	3.13E-02
NM_019738	Nupr1	nuclear protein transcription regulator 1	1.08	4.55E-02
NM_008153	Cmklr1	chemokine-like receptor 1	1.08	2.44E-02
NM_019984	Tgm1	transglutaminase 1, K polypeptide	1.08	4.26E-02
NM_008353	Il12rb1	interleukin 12 receptor, beta 1	1.07	4.26E-02
NM_011723	Xdh	xanthine dehydrogenase	1.07	8.50E-03
NM_007498	Atf3	activating transcription factor 3	1.06	8.50E-03
NM_013706	Cd52	CD52 antigen	1.06	8.50E-03
NM_020008	Clec7a	C-type lectin domain family 7, member a	1.06	8.50E-03
NM_001081123	Arhgap36	Rho GTPase activating protein 36	1.06	8.50E-03
NM_008332	Ifit2	interferon-induced protein with tetratricopeptide repeats 2	1.06	8.50E-03
NM_001190161	Psrc1	proline/serine-rich coiled-coil 1	1.05	8.50E-03
NM_030150	Dhx58	DEXH (Asp-Glu-X-His) box polypeptide 58	1.05	1.96E-02
NM_009779	C3ar1	complement component 3a receptor 1	1.05	8.50E-03
NM_011539	Tbxas1	thromboxane A synthase 1, platelet	1.05	2.79E-02
NM_205820	Tlr13	toll-like receptor 13	1.05	8.50E-03
NM_007574*	C1qc	complement component 1, q subcomponent, C chain	1.05	8.50E-03
NM_022964	Lat2	linker for activation of T cells family, member 2	1.04	1.96E-02
NM_001308535	Gm20489, Il2rg	interleukin 2 receptor, gamma chain	1.04	1.47E-02
NM_145509	Rab7b	RAB7B, member RAS oncogene family	1.04	8.50E-03

NM_009777	C1qb	complement component 1, q subcomponent, beta polypeptide	1.04	8.50E-03
NM_011176	St14	suppression of tumorigenicity 14 (colon carcinoma)	1.04	8.50E-03
NM_183201	Slfn5	schlafen 5	1.03	8.50E-03
NM_009139	Ccl6	chemokine (C-C motif) ligand 6	1.03	2.79E-02
NM_013482	Btk	Bruton agammaglobulinemia tyrosine kinase	1.03	3.54E-02
NM_019388	Cd86	CD86 antigen	1.03	2.44E-02
NM_130449	Colec12	collectin sub-family member 12	1.02	8.50E-03
NM_008528	Blnk	B cell linker	1.02	3.13E-02
NM_007645	Cd37	CD37 antigen	1.02	2.44E-02
NM_001146022	Wdfy4	WD repeat and FYVE domain containing 4	1.02	1.47E-02
NM_001033767	Gm4951	predicted gene 4951	1.02	1.47E-02
NM_007806	Cyba	cytochrome b-245, alpha polypeptide	1.02	8.50E-03
NM_133871	Ifi44	interferon-induced protein 44	1.01	8.50E-03
NM_001146275	Iigp1	interferon inducible GTPase 1	1.01	8.50E-03
NM_013612	Slc11a1	solute carrier family 11 (proton-coupled divalent metal ion transporters), member 1	1.01	1.47E-02
NM_008175	Grn	granulin	1.01	8.50E-03
NM_011815	Fyb	FYN binding protein	1.01	8.50E-03
NM_011150	Lgals3bp	lectin, galactoside-binding, soluble, 3 binding protein	1.01	8.50E-03
NM_007780	Csf2rb	colony stimulating factor 2 receptor, beta, low-affinity (granulocyte-macrophage)	1.01	1.96E-02
NM_001039530	Parp14	poly (ADP-ribose) polymerase family, member 14	1.00	8.50E-03
NM_015783	Isg15	ISG15 ubiquitin-like modifier	1.00	3.13E-02
NM_010686	Laptm5	lysosomal-associated protein transmembrane 5	1.00	8.50E-03
NM_001005858	Ifit3b	interferon-induced protein with tetratricopeptide repeats 3B	1.00	1.47E-02
NM_009911	Cxcr4	chemokine (C-X-C motif) receptor 4	1.00	2.79E-02
NM_053214	Myo1f	myosin IF	0.99	8.50E-03
NM_013820	Hk2	hexokinase 2	0.99	1.96E-02
NM_134250	Havcr2	hepatitis A virus cellular receptor 2	0.99	2.44E-02
NM_001099634	Myof	myoferlin	0.98	3.91E-02
NM_022325	Ctsz	cathepsin Z	0.98	8.50E-03
NM_001033308	Themis2	thymocyte selection associated family member 2	0.98	4.55E-02
NM_021281	Ctss	cathepsin S	0.98	8.50E-03
NM_178785	Rasal3	RAS protein activator like 3	0.98	1.47E-02
NM_007572	C1qa	complement component 1, q subcomponent, alpha polypeptide	0.98	8.50E-03
NM_013792	Naglu	alpha-N-acetylglucosaminidase (Sanfilippo disease IIIB)	0.97	8.50E-03
NM_153564	Gbp5	guanylate binding protein 5	0.96	1.47E-02
NM_198095	Bst2	bone marrow stromal cell antigen 2	0.96	8.50E-03
NM_021451	Pmaip1	phorbol-12-myristate-13-acetate-induced protein 1	0.95	2.44E-02
NM_134158	Cd300c2	CD300C molecule 2	0.95	1.96E-02
NM_001145960	Slc37a2	solute carrier family 37 (glycerol-3-phosphate transporter), member 2	0.95	1.96E-02
NM_011355	Spi1	spleen focus forming virus (SFFV) proviral integration oncogene	0.95	1.47E-02
NM_174857	Mamdc2	MAM domain containing 2	0.95	4.55E-02
NM_001162500	Parvg	parvin, gamma	0.95	8.50E-03
NM_008320	Irf8	interferon regulatory factor 8	0.95	8.50E-03
NM_001033207	Nlrc5	NLR family, CARD domain containing 5	0.94	1.96E-02
NM_153505	Nckap1l	NCK associated protein 1 like	0.94	8.50E-03

NM_001313712	Sp100	nuclear antigen Sp100	0.94	3.54E-02
NM_010368	Gusb	glucuronidase, beta	0.94	1.47E-02
NM_007651	Cd53	CD53 antigen	0.94	8.50E-03
NM_001253874	Itgal	integrin alpha L	0.94	4.26E-02
NM_013470	Anxa3	annexin A3	0.93	8.50E-03
NM_010156	Samd9l	sterile alpha motif domain containing 9-like	0.93	1.96E-02
NM_011019	Osmr	oncostatin M receptor	0.93	1.47E-02
NM_001126182	Naip2	NLR family, apoptosis inhibitory protein 2	0.93	3.13E-02
NM_013545	Ptpn6	protein tyrosine phosphatase, non-receptor type 6	0.92	1.96E-02
NM_183162	Helz2	helicase with zinc finger 2, transcriptional coactivator	0.92	8.50E-03
NM_009252	Serpina3n	serine (or cysteine) peptidase inhibitor, clade A, member 3N	0.91	8.50E-03
NM_001005508	Arhgap30	Rho GTPase activating protein 30	0.91	1.96E-02
NM_010745	Ly86	lymphocyte antigen 86	0.91	8.50E-03
NM_001033342	Cdc42bpg	CDC42 binding protein kinase gamma (DMPK-like)	0.91	8.50E-03
NM_001247984	Lcp1	lymphocyte cytosolic protein 1	0.91	8.50E-03
NM_008161	Gpx3	glutathione peroxidase 3	0.90	8.50E-03
NM_175088	Mdfic	MyoD family inhibitor domain containing	0.90	4.55E-02
NM_009778	C3	complement component 3	0.89	8.50E-03
NM_008225	Hcls1	hematopoietic cell specific Lyn substrate 1	0.89	3.13E-02
NM_001142952	Fam46c	terminal nucleotidyltransferase 5C	0.89	8.50E-03
NM_007801	Ctsh	cathepsin H	0.89	8.50E-03
NM_001190830	Jak3	Janus kinase 3	0.88	4.94E-02
NM_010130	Adgre1	adhesion G protein-coupled receptor E1	0.88	1.47E-02
NM_027521	Hmha1	Rho GTPase activating protein 45	0.88	1.47E-02
NM_008401	Itgam	integrin alpha M	0.88	8.50E-03
NM_010493	Icam1	intercellular adhesion molecule 1	0.87	2.44E-02
NM_001161111	Pqlc3	PQ loop repeat containing	0.87	4.55E-02
NM_010398	H2-T23	histocompatibility 2, T region locus 23	0.87	8.50E-03
NM_028195	Cyth4	cytohesin 4	0.86	8.50E-03
NM_010833	Msn	moesin	0.86	8.50E-03
NM_011854	Oasl2	2'-5' oligoadenylate synthetase-like 2	0.85	8.50E-03
NM_001289848	Cox6b2	cytochrome c oxidase subunit 6B2	0.85	4.55E-02
NM_028785	Dock8	dedicator of cytokinesis 8	0.85	1.47E-02
NM_010658	Mafb	v-maf musculoaponeurotic fibrosarcoma oncogene family, protein B (avian)	0.85	8.50E-03
NM_027835	Ifih1	interferon induced with helicase C domain 1	0.85	2.79E-02
NM_172285	Plcg2	phospholipase C, gamma 2	0.84	4.55E-02
NM_010260	Gbp2	guanylate binding protein 2	0.84	1.47E-02
NM_010240	Ftl1	ferritin light polypeptide 1	0.84	8.50E-03
NM_172689	Ddx58	DEAD (Asp-Glu-Ala-Asp) box polypeptide 58	0.83	2.79E-02
NM_010421	Hexa	hexosaminidase A	0.83	8.50E-03
NM_001163815	Vav1	vav 1 oncogene	0.83	4.55E-02
NM_007408	Plin2	perilipin 2	0.82	1.96E-02
NM_008331	Ifit1	interferon-induced protein with tetratricopeptide repeats 1	0.82	2.79E-02
NM_138672	Stab1	stabilin 1	0.82	2.44E-02
NM_001161730	Tap1	transporter 1, ATP-binding cassette, sub-family B (MDR/TAP)	0.82	3.54E-02
NM_010188	Fcgr3	Fc receptor, IgG, low affinity III	0.82	1.47E-02

NM_010422	Hexb	hexosaminidase B	0.82	8.50E-03
NM_001287514	Cebpa	CCAAT/enhancer binding protein (C/EBP), alpha	0.81	3.54E-02
NM_023141	Tor3a	torsin family 3, member A	0.80	2.79E-02
NM_001143689	H2-Q4	histocompatibility 2, Q region locus 4	0.80	1.47E-02
NM_001001892	H2-K1	histocompatibility 2, K1, K region	0.80	1.47E-02
NM_019449	Unc93b1	unc-93 homolog B1, TLR signaling regulator	0.80	3.54E-02
NM_009546	Trim25	tripartite motif-containing 25	0.79	4.55E-02
NM_008326	Irgm1	immunity-related GTPase family M member 1	0.79	1.96E-02
NM_178911	Pld4	phospholipase D family, member 4	0.78	2.79E-02
NM_001110192	Inpp5d	inositol polyphosphate-5-phosphatase D	0.78	3.13E-02
NM_018738	Igtp, Irgm2	interferon gamma induced GTPase	0.78	2.79E-02
NM_001162366	Ptk2b	PTK2 protein tyrosine kinase 2 beta	0.78	2.79E-02
NM_025378	Ifitm3	interferon induced transmembrane protein 3	0.77	4.26E-02
NM_011610	Tnfrsf1b	tumor necrosis factor receptor superfamily, member 1b	0.77	3.91E-02
NM_010380	H2-D1	histocompatibility 2, D region locus 1	0.77	8.50E-03
NM_001083312	Gbp7	guanylate binding protein 7	0.76	1.96E-02
NM_011609	Tnfrsf1a	tumor necrosis factor receptor superfamily, member 1a	0.76	1.96E-02
NM_011708	Vwf	Von Willebrand factor	0.76	1.96E-02
NM_009982	Ctsc	cathepsin C	0.75	2.79E-02
NM_007669	Cdkn1a	cyclin-dependent kinase inhibitor 1A (P21)	0.75	2.79E-02
NM_001271446	Ly6a	lymphocyte antigen 6 complex, locus A	0.75	4.26E-02
NM_009735	B2m	beta-2 microglobulin	0.75	2.79E-02
NM_010764	Man2b1	mannosidase 2, alpha B1	0.73	1.47E-02
NM_023409	Npc2	NPC intracellular cholesterol transporter 2	0.73	3.91E-02
NM_001164036	Ly6e	lymphocyte antigen 6 complex, locus E	0.73	3.91E-02
NM_026428	Dcxr	dicarbonyl L-xylulose reductase	0.73	3.13E-02
NM_007798	Ctsb	cathepsin B	0.71	4.55E-02
NM_001190974	Axl	AXL receptor tyrosine kinase	0.71	2.79E-02
NM_013454	Abca1	ATP-binding cassette, sub-family A (ABC1), member 1	0.71	2.44E-02
NM_010145	Ephx1	epoxide hydrolase 1, microsomal	0.70	3.91E-02
NM_010580	Itgb5	integrin beta 5	0.69	2.44E-02
NM_008630	Mt2	metallothionein 2	0.68	4.94E-02
NM_011701	Vim	vimentin	0.68	3.54E-02
NM_009987	Cx3cr1	chemokine (C-X3-C motif) receptor 1	0.68	3.13E-02
NM_029364	Gns	glucosamine (N-acetyl)-6-sulfatase	0.67	3.13E-02
NM_013602	Mt1	metallothionein 1	0.66	3.54E-02
NM_009831	Ccng1	cyclin G1	0.66	4.94E-02

* Exclusively upregulated in HDAC4 3SA expressing mice and implicated in inflammatory pain (Simonetti et al., 2013)

Table 16: Down-regulated DEGs in inflammatory pain by FC (3SA-Sal/CFA)

RefSeq ID	Gene symbol	Full gene name	Log2 fold change	FDR adjusted p-value
NM_008623*	Mpz	myelin protein zero	-0.74	2.79E-02
NM_019412*	Prx	periaxin	-0.75	8.50E-03
NM_145555*	Ncmap	noncompact myelin associated protein	-0.91	3.13E-02
NM_009135*	Scn7a	sodium channel, voltage-gated, type VII, alpha	-1.17	8.50E-03
NM_028572*	Vgll3	vestigial like family member 3	-1.19	2.79E-02
NM_008694	Ngp	neutrophilic granule protein	-1.30	2.44E-02

* Exclusively downregulated in HDAC4 3SA expressing mice